Performance of Thermal Protective Clothing upon Exposure to Hot Liquid Splash

by

Farzan Gholamreza

A thesis submitted in partial fulfillment of the requirements for the degree of

Doctor of Philosophy

Department of Human Ecology
University of Alberta

ABSTRACT

This study mainly involved an experimental evaluation of transient heat transfer through thermal protective fabric systems, in particular the convection heat transfer between hot water and the fabric systems. The main objective of this thesis was to gain a fundamental understanding of the heat and mass transfer mechanisms associated with protective clothing systems when exposed to hot water and other fluids and during the cooling period immediately afterwards. For this purpose, five interrelated studies were performed. The fabric systems selected for this thesis represent thermal protective garments worn by firefighters and other workers. In this study, the thermal protective performance of the fabric system was evaluated upon exposure to hot water, drilling fluid, canola oil steam and high-level radiation. In addition, an instrumented spray mannequin was used in order to see the effect of fabric system's properties, garment design and hot water flow on the thermal performance of the garments. A detailed study of the hydrodynamics of the hot water flow on the surface of the fabric, in-depth water penetration through the fabric system, the parameters which influence heat and mass transfer through the fabric system and their effects on thermal performance of the fabric was also conducted.

The results indicate that stored thermal energy contributes significantly to second degree burns and can reduce the level of protection expected from the studied fabrics. In hot water exposures, the liquid starts spreading radially from the stagnation point until there is a sudden increase in the fluid height. This phenomenon is termed a hydraulic jump. The position of the hydraulic jump on the surface of the fabric and the area of the supercritical region are a function of experimental variables as well as physical properties of the fabric system. This affects the thermal performance of the fabric systems.

Among the studied physical properties of fabrics, air permeability and fabric surface energy are dominant factors in the effective protection against hot liquid since resistance to mass transfer is shown to be the key factor for reducing the amount of transmitted and discharged thermal energy to the skin in bench-scale and full-scale tests. The results from the full-scale tests also show that garment fit and garment style, such as pocket style, have a great influence on the performance of the garments during the cooling period.

Also, this study suggests possible modifications to the existing bench top and full-scale test methods and equipment. These modifications could be used in the

existing standards, in order to better predict the thermal protection provided by thermal protective clothing systems considering the stored energy effects and the hydrodynamics of hot liquid flow. In order to address the contribution of the stored energy in a bench-scale fabric and a full-scale garment test, new predictive parameters were introduced. These parameters reveal the thermal response of protective clothing during the cooling period of the garment where heat transfer is influenced by the garment/fabric properties and/or the liquid flow. In addition, a predictive stored energy model and a burn evaluation model were proposed in order to determine the minimum exposure time for prediction of second degree burn in the cooling period. The proposed stored energy model calls for the use of only one test to predict the minimum exposure time to second degree burn. The findings obtained from this research will enable the engineering of textile materials to provide improved safety for firefighters and industrial workers under a wider range of conditions.

PREFACE

This thesis is an original work by Farzan Gholamreza. A portion of Chapter 4 has been published as: Gholamreza, F., & Song, G. (2013). Laboratory evaluation of thermal protective clothing performance upon hot liquid splash. Annals of Occupational Hygiene, 57(6), 805-822. The author was responsible for the data collection, analysis as well as manuscript composition. G. Song was the supervisory author and provided critical review of the manuscript.

Other portions of chapters 4, 5 and 6 were presented at the following conferences:

- Gholamreza, F., Song, G., & Ackerman, M. (2012). Thermal protective clothing performance: hot liquid splash and its flow effect on skin burn. Paper presented at the 5th European Conference on Protective Clothing and Nokobetef 10. Future of Protective Clothing: Intelligent or not, Valencia, Spain. The author was responsible for the data collection, analysis as well as manuscript composition. G. Song and M. Ackerman were the supervisory authors.

- Gholamreza, F., Song, G., & Ackerman, M. (2012). *Analyzing the discharged energy and its contribution to thermal performance of protective clothing upon hot liquid splash.* Paper presented at the Fiber Society Conference, Spring, St. Gallen, Switzerland.

- Gholamreza, F., Song, G., & Ackerman, M. (2012). *Thermal protective performance of protective clothing upon steam and hot liquid splash.* Paper presented at the Fiber Society Conference, Fall Boston, MA.

- Gholamreza, F., Song, G., & Ackerman, M. (2013). *Stored energy and thermal protective performance of protective clothing upon steam and hot liquid.* Paper presented at the 13th Autex World Textile Conference, Dresden, Germany.

- Gholamreza, F., Song, G., & Ackerman, M. (2014). Thermal stored energy and protective performance upon various hazards. Paper presented at the Fiber Society Conference, Spring, Liberec, Czech Republic.

- Gholamreza, F., Song, G., & Ackerman, M. (2014). Thermal stored energy and protective performance of protective clothing upon radiant heat. Paper presented at the 14th Autex World Textile Conference, Bursa, Turkey.

- Gholamreza, F., Song, G., & Lu, Y. (2015). Analyzing the discharged energy and its contribution to thermal performance of protective clothing upon hot water exposure using instrumented spray manikin. Paper presented at the Fiber Society Conference, Spring, Shanghai, China. The author was responsible for the analysis as well as manuscript composition. G. Song was the supervisory author and provided critical review of the manuscript. Y. Lu was responsible for the data collection.

- Gholamreza, F., Torvi, D., Kerr, N., Ackerman, M. & Song, G. (2016). A new protocol to characterize thermal protective performance of garments using instrumented flash fire and spray mannequin. Paper presented at the 7th European Conference on Protective Clothing and Nokobetef 12. Innovative Protective Clothing in a Changing World: Protective, Comfortable, Intelligent, Integrated, Ecological and Economical, Izmir, Turkey. The author was responsible for the analysis as well as manuscript composition. D. Torvi and N. Kerr were the supervisory authors and provided critical review of the manuscript. M. Ackerman assisted with the data collection and test method. G. Song was involved with concept formation.

- Gholamreza, F., Torvi, D., Dale, D., Kerr, N., & Ackerman, M. (2017). Laboratory evaluation of thermal protective clothing using instrumented flash fire and spray mannequin. Paper presented at the 17th Autex World Textile Conference, Corfu, Greece. The author was responsible for the analysis as well as manuscript composition. D. Torvi and N. Kerr were the supervisory authors and provided critical review of the manuscript. M. Ackerman assisted with the data collection and test method. D. Dale also assisted with the test method.

DEDICATION

I would like to dedicate this thesis to my loving mother, Fataneh Balalaey, my father, Hamidreza Gholamreza, my grandmother, Shahrbanou Ohamriz, My uncle, Homayoun Balalaey and my beloved sister, Nazanin, for their unconditional love and inspiration throughout my entire education. Thank you for all of your sacrifices and for allowing me to pursue my dreams. I love you all.

ACKNOWLEDGEMENTS

The author gratefully acknowledges and thanks his supervisors, Prof. David Torvi and Prof. Nancy Kerr, for their encouragement, support, patience, invaluable insights and guidance which helped lead to completion of this research. The author would like to thank Dr. Jane Batcheller and Prof. Hongbo Zeng for their help as members of the supervisory committee.

Gratitude is extended to many others who have contributed to the success of this research:

- Prof. Guowen Song who dedicated his expertise to help with the first three studies in this thesis (described in Chapters 4-6).
- Prof Douglas Dale who dedicated his time and expertise with the fundamentals of heat and mass transfer and mannequin studies.
- Dr. Jane Bacheller, Mark Ackerman and Stephen Paskaluk for their guidance and assistance setting up the test facilities and their continued support through the testing phase of the research.
- Prof. Betty Crown, Dr. Berna Skrypnek, Dr. Deanna Williamson, Dr. Arlene Oak, Dr. Megan Strickfadan, Angie Chenier, Linda Mirans, Judy Forsland, Michael Abley and Tahereh Attar for providing advice and assistance along the way.
- Stedfast Inc., Martin Filteau and Todd Jarand for providing moisture barriers and expressing interest in this research.
- The Department of Human Ecology and Protective Clothing and Equipment Research Facility Center (PCERF) for financial supports and teaching and research assistantship.
- My parents, Fataneh Balalaey and Hamidreza Gholamreza for their support, encouragement and inspiration during my studies.
- To the many individuals who have extended friendship and hospitality during my stay in Edmonton.

TABLE OF CONTENTS

LIST OF TABLES

LIST OF FIGURES

LIST OF ABBREVIATIONS

ASTM:	American Society for Testing and Materials
ETPP:	Effective thermal protective performance
ISO:	International Organization for Standardization
MET:	Minimum exposure time
NFPA:	National Fire Protection Association
R_{ct}:	Fabric thermal insulation
R_{et}:	Fabric evaporative resistance
SEC:	Total stored energy coefficient
SEI:	Stored energy index
STE rating	Stored thermal energy rating
TPP:	Thermal protective performance
TDE:	Total discharged energy
TAE:	Total absorbed energy
TTE:	Total transmitted energy

CHAPTER 1 INTRODUCTION

Stored Thermal Energy and Challenges in Engineering

Firefighters are often the first responders to emergencies. They may sustain burn injuries which can be caused by exposure to thermal hazards such as flash fires, radiant exposures, hot liquid splashes, impingement of hot gases and steam, hot surface contact, or any combination thereof. Thermal protective clothing is designed to provide protection from thermal hazardous environments. A multilayer construction of thermal protective clothing for firefighters typically consists of a series of protective layers such as an outer shell fabric, a moisture barrier and a thermal liner. There is also potential for air gaps between the individual layers, and between the clothing and the skin. This firefighter ensemble slows down the heat transfer to the firefighters' skin. However, while working in thermal exposures, the clothing is heated and may store thermal energy. Depending on the thermal intensity and the fabric systems, a large amount of stored energy during exposure can be discharged to the skin after the termination of the thermal exposure and can contribute to burn injuries (Song, Cao, & Gholamreza, 2011).

The discharge of stored energy may occur without any changes to the air spaces between the fabric and skin. In this dissertation, this discharge of stored energy will be referred to as ordinary discharge. The discharge of stored energy may also be enhanced by compression of the garment to the skin, which will be referred to as compressive discharge. This compression of fabric to the skin may be due to firefighter movements such as leaning, squatting or crawling. This phenomenon can reduce the level of protection expected from the protective clothing (Barker, Guerth, Behnke, & Bender, 2000).

A considerable amount of research has been done in order to understand the mechanisms and the relevant factors associated with the thermal protective performance of clothing systems and to develop standards for the evaluation of the clothing systems' performance. However, there have been few systematic studies on thermal stored energy in the fabric systems and the level of performance expected from these fabrics. Most of the studies on stored energy have focused on the thermal performance of fabric systems against radiation and convective-radiant exposures (e.g., (Song, Paskaluk, et al., 2011; Song, Cao, & Gholamreza, 2011; He,

& Li, 2016a, 2016b; Zhang, Song, Gu, Ren, & Cao, 2017; He, Chen, Wang, & Li, 2017; He, Lu, Chen, & Li, 2017)). Less attention has been paid to the role of stored energy in fabric systems and its contribution to burn injury for thermal hazards such as steam and hot liquids. Also, the current standard test methods used for thermal performance evaluation, such as NFPA 1971 and 2112, exclude the contribution of stored energy in their test method and performance requirements (NFPA, 2012, 2013). In addition, the current standard test method for measuring the transmitted and discharged energy to the skin (ASTM F 2731-10), is limited to low levels of convective radiant thermal exposures. This test method employs a relatively time-consuming iterative method as a burn evaluation approach.

Thermal Performance of Clothing upon Hot Liquid Splash

In spite of the significant amount of attention to exposures to heat and flame, there are some relatively unexplored hazards such as exposures to hot liquids and pressurized steam, which are used extensively in the oil and gas industry. Firefighters may also be exposed to hot liquid splashes and steam (Sati, Crown, Ackerman, Gonzalez, & Dale, 2008). Protective clothing is the only barrier between the skin and these thermal hazards. The thermal energy generated from these hazards can be transferred through the protective clothing and may cause skin burn injuries. Statistics show that approximately 34% of the burn injuries during 2004 to 2013 were scald burns (ABA, 2014). In 59,099 cases of scald burn injuries, 6,025 cases (11.0%) were work related scald injuries and 3,286 cases were related to industrial workers. According to a study of patients who were admitted to University of Alabama at Birmingham University Hospital, 69% of occupational burn patients from 1994 to 1999 were industrial workers (Taylor et al., 2002). Among them, flame burns were the most common type (33.3%) and 15% of burn injuries were scald injuries. As hot liquid splashes are a common occupational hazard for workers, the performance of protective clothing should be evaluated considering these hazards. Therefore, the characteristics of hot liquid splash and steam need to be described and the performance requirements of protective clothing need to be outlined (as well as the factors affecting protective performance upon these hazards).

Statement of Problem

Studies on stored energy have primarily focused on the thermal performance of fabric systems against convective-radiant heat exposures. Fewer studies have investigated thermal stored energy in exposures to hazards such as hot liquid splash and steam. Pressurized steam and hot liquids, which are being used extensively for material processing or enhanced in-situ recovery of bitumen from oil sands, commonly pose a threat to health of workers. During firefighting and industrial operations, workers may be exposed to steam from high pressure which is typically at pressures of 100~4000 kPa with temperatures of 100~300ºC (Ackerman, Crown, Dale, Paskaluk, & Song, 2011). Oils have higher viscosity than water and they may stay on the garment surface longer, increasing the potential for a scald injury. However, it has been found that the traditional materials used for protection against a hydrocarbon flash fire provide little protection against steam and hot liquid hazards (Ackerman et al., 2011; Murtaza, 2012). It has also been realized that there is significant stored thermal energy within the fabric system upon small splashes of hot liquid which may lower the thermal performance of the fabric systems as will be shown later in the thesis.

In the abovementioned research, some methods were introduced in order to capture the effects of thermal energy stored in the fabric and how it is discharged to the skin. The proposed methods helped to understand the mechanisms and the relevant factors associated with thermal protection provided by clothing specifically during the cooling period after an exposure.

Research Question and Purpose

The research question of this study is:

Is it possible to determine and predict the thermal response of protective fabric systems upon hot liquid splash by taking into account the transmitted and stored thermal energy developed in the fabric system during the exposure and cooling periods of the fabric?

The purpose of this research is to gain a fundamental understanding of the heat and mass transfer mechanisms associated with firefighters' and industrial workers' protective clothing systems when exposed to hot liquid splash (during an exposure and cooling after an exposure). This will aid in the development of

effective thermal protective clothing systems which have the ability to minimize skin burn injuries.

Significance

The understanding of the amount of thermal energy transmitted and discharged (stored energy) to the skin obtained from this research will enable the engineering of textile materials that can be used in thermal protective clothing systems that provide improved safety for firefighters and industrial workers under a wider range of conditions. Also, this work will help to identify key factors related to thermal stored energy and its contribution to skin burn injuries for different types of hazards. The findings from this study will also result in modifications to existing bench top test methods, which will improve the ability of these tests to evaluate the protection fabrics provide over a wider range of hazards.

Objectives

The overall goal of the research is to gain a fundamental understanding of the heat and mass transfer mechanisms associated with protective clothing systems when exposed to hot liquid and during the cooling period immediately afterwards. This goal relates to the understanding of the amount of thermal energy transmitted and discharged to the skin and thermal response of fabrics during the exposure and the cooling phase. As such, in the proposed research, it is intended to investigate the thermal stored energy developed in the fabric system upon hot liquid splash exposure and its contribution to burn injuries.

This study involves an experimental evaluation of transient heat transfer through thermal protective fabric systems, in particular the convection heat transfer between the hot liquid or steam and the fabric surface. Possible modifications to the existing bench top test methods and equipment will also be investigated in order to better predict the thermal protection provided by thermal protective clothing systems considering the stored energy effects.

Dissertation Overview

Research in the field of thermal protective clothing in the last 70 years is reviewed in Chapter 2. This ranges from early studies on burn injuries and the development of burn criteria, thermal hazards, thermal protective clothing and the interactions between them. In addition, hydrodynamics of the hot water flow on the surface of horizontal and inclined surfaces are summarized.

Chapter 3 describes fabric and garment systems used in this research for the evaluation of thermal protective fabric and garment systems exposed to various thermal hazards. The thermal hazards were exposures to hot liquids (hot water, drilling fluid and canola oil), steam and thermal radiation in bench-scale tests. A full-scale mannequin test is also used to evaluate thermal performance of the garments when exposed to hot water.

In Chapter 4, fabrics systems were exposed to hot water, drilling mud, and canola oil to examine the effects of liquid properties on effective thermal performance of the fabric systems. In order to quantify the amount of stored thermal energy in the fabric system, a stored energy coefficient (ψ) is introduced. Also in this chapter, the effect of fabric properties and the experimental variables such as non-dimensional displacement of the sensors from the stagnation point (y/d) and the impingement angle (β) on the effective thermal performance ETPP of the fabric system (second degree burn time and the stored energy coefficient) will be explored.

Chapter 5 analyzes performance of thermal protective fabrics exposed to hot liquids, steam, and thermal radiation with a focus on the stored thermal energy accumulated in the fabric system during the exposure to the hazards. The objective of this part relates to the development of a stored energy model which can predict the minimum exposure time to cause a second degree burn without using iterative tests. The effect of compression is also incorporated. Analysis of the results from this approach contributes to the development of a stored energy model. A series of iterative tests are conducted to validate the proposed stored energy model. The application of the stored energy model in evaluation of thermal performance of fabric systems and testing method development is explored. Also, the application of the new test method is investigated by using the instrumented flash fire and spray mannequins in the next chapter.

In Chapter 6, the contribution of stored energy to the thermal performance of the garment systems is investigated. The new predictive parameters such as total discharged energy (TDE) and the stored thermal energy rating (STE rating) are introduced. In addition, the effects of the fabric properties and garment design on the proposed predictive parameters are analyzed.

In Chapter 7, different experimental settings are employed to evaluate hot water transport properties of the fabric systems. The flow patterns created by the impingement of a circular jet of water on the surface of horizontal and inclined (45-degree) single layer fabric systems are studied. The effect of water temperature on the contact angle in horizontal single layer fabrics, and the relation between the contact angle and flow pattern are examined. In addition, the effect of experimental variables on impact penetration of water are investigated. Moreover, the effect of fabric properties on impact penetration of water is explored. The findings from the analyses of the flow patterns and moisture transfer properties are used to evaluate the thermal protective fabric systems in Chapter 8.

Chapter 8 includes the experimental studies which relate to the impingement of the skin simulant plate by hot water considering different experimental variables. It is also intended to investigate the influence of the flow pattern of hot water and liquid transfer properties (water surface resistance and water penetration resistance) of the fabrics on the transmitted and discharged thermal energy received by the skin simulant. As such, additional experimental work is done considering the experimental variables of interest. In addition, the thermal behavior of (a) the skin simulant plate and (b) the fabric systems-skin simulant plate is analyzed considering the transmitted energy, the discharged energy and their contributions to skin burn injury upon hot water splash will be analyzed.

Chapter 9 summarizes the important results presented in this thesis, as well as some topics for future work that may be done in the area of thermal protective clothing.

Limitations and Delimitations

- This research was limited to a small number of typical thermal protective fabrics used in garments worn by firefighters and other workers.
- In the bench-scale testing, the air gap between the fabric system and the skin is not considered.
- A simplified heat transfer model was used in this study to predict skin temperatures and burn injuries. Blood perfusion and metabolic heat production effect were not considered in order to simplify the mathematical calculations.
- Other limitations such as the testing apparatus and mathematical equations are addressed in corresponding chapters.

Definitions

For the purpose of this research the applicable terms are defined as follows:

Air permeability: is "the rate of air flow passing perpendicularly through a known area under a prescribed pressure differential between the two surfaces of a material" (American Society for Testing and Materials, 1996, p. 236).

Comfort: is "a pleasant state of physiological, psychological and physical harmony between a human being and the environment" (Slater, 1985).

Evaporative resistance: is the resistance of a material or a clothing ensemble to the flow of moisture vapor from a surface with a higher vapor pressure to an environment with a lower vapor pressure (American Society for Testing and Materials, 2009).

Froude number: "the ratio of inertial force to gravitational force" (Çengel, 2005, p. 274).

Heat flux: "thermal intensity indicated by the amount of energy transmitted per unit area and per unit time; kW/m^2" (ASTM, 2010).

Protective Clothing System: "any combination of materials which when used as a composite can, under certain conditions, permit a measured level of heat transfer to occur; or, under other conditions, prevent a measured level of heat transfer to occurt" (ASTM, 2010).

Reynolds number: "the ratio of inertial force to viscous force" (Çengel, 2005, p. 324).

Stored energy: "Energy stored in a fabric/composite after the heating source is removed" (ASTM, 2010).

The predicted area of second degree burn: "the sum of the weighted area corresponds to the heat flux sensors that predicts a second-degree burn" (ISO, 2017).

The predicted area of third degree burn: "the sum of the weighted area corresponds to the heat flux sensors that predicts a third-degree burn" (ISO, 2017).

Total absorbed energy throughout test: “total energy received by all sensors as the average of the weighted total energy transferred to each heat flux sensor over the data sampling period; (kJ/m^2)” (ISO, 2017).

Weber number: “the ratio of inertial force to surface tension force” (Çengel, 2005, p. 288).

CHAPTER 2 REVIEW OF LITERATURE

Thermal protective clothing

Human tissue reacts to increases in temperature (Moritz & Henriques, 1947). Once the human skin reaches a critical temperature, burn injuries may occur, which can result in severe medical problems. The environments of firefighters and industrial workers represent some of the most complicated sets of thermal exposure and intensity. Firefighters and industrial workers may be exposed to conduction, convection or radiation heat transfer, or any other combination of these modes.

Thermal protective clothing is designed to provide protection from thermal hazardous environments. In some applications such as firefighters protective clothing, a multilayer construction of thermal protective clothing is used, which consists of a series of protective layers such as an outer shell fabric, a moisture barrier and a thermal liner. The primary objective of thermal protective clothing is to minimize the rate of heat transfer from the environment to the skin.

The effectiveness of the protective clothing depends on the characteristics of this clothing and the thermal hazard. On one hand, the level and characteristics of the thermal exposure should be understood in order to know the magnitude of thermal energy which is delivered to the clothing. On the other hand, the thermal properties of clothing and their changes with different exposure conditions are required to be known. As such, the boundary conditions of the thermal hazard at the surface of the fabric, in depth absorption of thermal hazards, energy transfer between the fabric and skin (or test sensor in the case of standard tests or experiments) and how the thermal hazard causes second degree burn and deeper damages need to be understood for the evaluation of the performance of protective clothing (Torvi, 1997).

Thermal protective clothing should reduce heat transfer to the skin and provide enough insulation for the wearer who needs time to avoid thermal injuries (Hoschke, 1981). A thermal protective garment should not cause an extra hazard (such as a flammable garment) and should not melt or form brittle chars. It also needs to remain intact during and after a thermal exposure. If the clothing does not remain intact, it may break open and expose the wearer (Bajaj & Sengupta, 1992). In addition, thermal protective clothing should minimize hot liquid penetration

through the fabric. Resisting mass transfer stops the liquid from penetrating through the fabric and directly contacting the skin (Murtaza, 2012). The fabric system also needs to minimize the discharge of thermal energy to the skin and should not store hot liquid in its system as will be shown later in the thesis.

In addition to the highest level of protection, the goal of protective clothing is to offer the best possible comfort to its wearer. Body comfort is comprised of thermal comfort, sensorial comfort, body movement comfort as well as psychological comfort. Working with uncomfortable clothing may increase heat stress of the wearer and may cause a reduction in cognitive and physical performance (Hancock & Vasmatzidis, 2003). However, the demands for providing protection and maintaining comfort are often contradictory. More details on comfort and the contradictory requirements of thermal comfort and protection of protective clothing can be found in Song (2011) and Rossi (2005), respectively.

Skin burn injury

Human skin consists of three layers. The epidermis is the outermost layer which is approximately 60 to 800 μm thick, depending on its location on the body (Diller, 1985). The epidermis has no blood vessels and is nourished from the underlying layer, the dermis. The dermis is typically thicker than the epidermis (e.g. almost 25 times) and provides strength and elasticity to the skin. It also contains blood vessels, nerves, hair follicles and glands. The subcutaneous layer is the layer of the skin which consists of fat and connective tissues to muscles and bones.

Human skin tissue is a very sensitive to temperature fluctuations (Choudhury, Majumdar, & Datta, 2011). Once temperature increases, the body strives to regulate its temperature using components such as lungs and the respiratory tracts, autonomic nervous system, sympathetic nervous system and peripheral blood vessels. Heat sensors, located in the hypothalamus, the body's thermostat, send signals when the skin temperature is higher than 37°C. The flow of blood thorough the venular tissues of the thermally exposed areas can regulate body temperature via convection processes. By controlling the flow of blood to the skin by constricting (vasoconstriction) or expanding (vasodilatation) the blood vessels within the skin, the veins and arteries that are embedded in the skin in pairs throughout the body, act like a counter-flow heat exchanger. Blood has very high

thermal conductivity and gains thermal energy from the exposed areas (Weinbaum, Jiji, & Lemons, 1984). The arteriolar blood in the locally exposed areas exchange thermal energy with the cooler venular blood via the intervening solid tissues. These tissues also regulate their temperature through natural convection or any endothermic phenomenon such as sweating or evaporation of perspiration (Kiling-Balci, 2011). When the components fail to regulate the temperature change due to the amount and rate of heat transfer to the locally exposed areas, the total energy gained may result in a sensation of pain or burn injuries (Stoll & Greene, 1959). In addition, the increase in the rate of perspiration may accelerate the metabolic rate (Diller, 1985). If the body fails to regulate the thermal energy generated by the metabolic rate and the moisture generated through perspiration, the body core temperature may alter and result in heat stress. This hazard may also disturb individuals' health and comfort (Choudhury et al., 2011).

First degree burn injury

Any exposure and temperature that is sufficient to harm the upper layers of epidermal cells and fails to cause deeper burns (Moritz, 1947) is characterized as the first degree burn. This type of burn produces visible reddening which is caused by vasodilation of the subpapillary vessels often followed by edema, the puffy swelling cause by accumulation of serum. First degree burn is potentially reversible and the healing is quick with no permanent scaring or discoloration (Diller, 1985, pp. 85-134).

Second degree burn injury

When the thermal exposures result in a complete destruction of the epidermis and a fraction of the cells in the dermis, second degree burn occurs. Deeper second degree burns result in the destruction of a significant fraction of the dermal base. The first visible change in the dermis is the constriction of superficial blood vessels which is followed by vasodilatation in deeper parts where the temperature is less extreme. Then, vasodilatation increases vascular permeability and forms edema. The presence of aqueous edema in the dermis and the basal layer increases thermal conductivity of the dermis and enhances the heat delivery for a more rapid thermal regulation (Henriques & Moritz, 1947). This phenomenon collects a sufficient amount of edema underneath the epidermis and causes vesication which is the other second degree burn symptom. The thermal exposure is sometimes enough to impair the epidermis-dermis attachment.

Third degree burn injury

When the thermal energy exceeds the thermal tolerance of the dermis, the injury will be deeper (Moritz, 1947). In this type of burn all epidermal elements and the supporting dermal structures are destroyed as well as the blood vessels in the burned regions. With no blood flow, the cells in the region of full thickness burn eventually die. The full thickness injury also causes large volumes of extravascular fluid to be lost. As such, there is no possibility for spontaneous healing and skin grafting is required. Further details on skin burn injuries can be found in Moritz (1947) and Shitzer et al. (1985).

Skin burn research

There are two different methods which can be used to estimate the time to thermal injury. These methods will be described in the following section.

Henriques burn model

Henriques and Moritz conducted a series of studies to investigate and quantify skin burn injury and were among the first to publish in this area (Henriques, 1947; Henriques & Moritz, 1947; Moritz, 1947; Moritz & Henriques, 1947; Moritz, Henriques, Dutra, & Weisiger, 1947). Their experiments were performed on human volunteers (forearms and fronts of thorax) and pigs. Pigs were used since their skin is anatomically closest to human skin. The only major difference is that the pigs do not perspire. By exposing the skin to hot water, they maintained the surface at an elevated temperature. They investigated the time-temperature relation to the occurrence of cutaneous (skin) burns and compared the severity of burns for different surface temperatures and times of exposure. They discovered that the destruction of the skin cells at the epidermis-dermis interface in human skin starts once the temperature of the skin surface rises above 44°C. This temperature was found to be the threshold temperature for the onset of thermal damage (Moritz & Henriques, 1947).

Since the causation of a burn is a time-dependant process, the production of burns is a rate process (Henriques, 1947). The rate equation obtained from this study enabled the evaluation of the time dependence of the temperature of the basal epidermal layer which can be used to develop a mathematical equation with which the time-temperature threshold of the skin injury can be predicted. More details can be found in Henriques (1947).

Henriques modeled the cell destruction by the first order of chemical reaction rate equation (Henriques, 1947). Equation 2.1 was used to determine the rate of tissue damage, defined as the thermal death of the epithelium (skin tissue).

$$\frac{d\Omega}{dt} = Pe^{\frac{-\Delta E}{RT}} \tag{2.1}$$

Where:

$\partial\Omega/\partial t$: is the rate of damage or the rate of production of injury,

P: is the pre-exponential factor (s^{-1}),

ΔE: is the activation energy for reaction (J/mol),

R: is the universal gas constant (8.315 J/kg.mol.°C),

T_t: is the temperature at epidermis-dermis interface (basal layer) or at any depth in the dermis (°C).

This equation can be integrated to Equation 2.2 as follows:

$$\Omega = \int_0^t Pe^{\frac{-\Delta E}{RT}}\, dt \tag{2.2}$$

In equation 2.2, Ω is the quantitative measurement of the burn at the epidermis-dermis interface or deeper depth in the dermis. In Henriques study, two threshold values for epidermal injury were obtained:

"A" is the shortest time required to produce trans-epidermal necrosis (second degree burn) at the predetermined skin surface temperature ($\Omega \geq 1$).

"B" is the longest time that skin can tolerate, before first degree burn occurs, at the predetermined skin surface temperature ($\Omega < 0.53$).

The numerical evaluation of the pre-exponential factor (P) and the activation energy (ΔE) for the destruction of the skin through heating (denaturation of proteins such as keratin in the epidermis) were obtained for thresholds A and B (onset of first degree and second degree burn respectively) in Henriques study (3.1×10^{98} and 150 000 cal/mol respectively). These values were used in Equation

2.2 to predict first and second degree burns at the basal layer or at any depth in the dermis.

Henriques burn model can be applied to any depth of the skin provided the appropriate values of pre-exponential factor (P) and the activation energy (ΔE). Takata et al. (1973) obtained the values for the pre-exponential factor (P) and the activation energy (ΔE) for predicting dermal damage. The values were used in Henriques' burn model in the dermis-subcutaneous interface or any depth in the subcutaneous layer (Equation 2.2) to predict third degree burns.

However, Stoll et al. found that Henriques et al.'s values for the pre-exponential factor (P) and the activation energy (ΔE) were incorrect (Stoll & Greene, 1959; Weaver & Stoll, 1969). The data set used to develop Henriques's burn model did not contain data on short duration high level thermal exposures. Also the energies related to the cooling period of skin were not included in the model. The values for the pre-exponential factor (P) and the activation energy (ΔE) were modified by Stoll et al. and were applied to the original equation.

Stoll et al. studies and their criteria

Later, Stoll et al. developed a criterion for the estimation of second degree skin burn injury (Stoll & Chianta, 1969; Stoll & Greene, 1959; Weaver & Stoll, 1969). In this research, tissue damage rates were obtained empirically with respect to temperature. The volar surface of the forearms was blackened with India ink and exposed to thermal radiation (4.2 to 16.8 kW/m^2). Recording of the skin temperature was not interrupted and the cooling of the skin was measured after the exposure was terminated. By using a mathematical equation and the extrapolation of the data, the time-temperature history in higher levels of radiation, where obtaining empirical data is not feasible (16.8 to 41.9 kW/m^2), was predicted (Weaver & Stoll, 1969). Stoll et al. found that the results from their experiments can be predicted by Henriques burn model by employing the appropriate pre-exponential factor and the activation energy values which will be shown in Chapter 3.

Thermal hazards

At the environmental level, the total thermal energy delivered to the clothing boundaries, which depends on the nature, magnitude and duration of the thermal

hazards, is very important. The magnitude of the hazard is defined using the temperature and/or the heat flux, and duration of exposure. Among thermal hazards, there are some relatively unexplored/newly explored hazards such as hot liquid splash and pressurized steam. Studies show that traditional materials used for protection against hydrocarbon flash fire provide little protection upon hot liquid and steam hazards (Ackerman et al., 2011; Murtaza, 2012). Indeed, these hazards may apply pressure to the garment and skin. These hazards may also penetrate through the garment, contact the skin directly and deliver more thermal energy to the skin (Ackerman et al., 2011). As such, these hazards demand new criteria which have not been sufficiently addressed by the current standards and test methods. They also need to be better understood in order to have more realistic simulated laboratory test methods to evaluation thermal protective clothing.

Steam and hot liquid splash

Increasingly, hot liquids are being used for material processing or enhanced in-situ recovery of bitumen from oil sands (Ackerman et al., 2011). Firefighters are commonly exposed to hot liquid splashes and steam (Sati et al., 2008), and industrial workers have been injured in the oil industry by steam exposures. For example, one fatality was reported for a power boiler operator who was exposed to steam (150 kPa) and hot water (Enform, 2004). In a well site in North Dakota, another worker fell into steam-heated water and sustained second and third degree burns to his leg (Enform, 2006b). In Northern Alberta, steam, hot water and silicate were sprayed uncontrollably on a derrick-worker's foot and caused severe burn injuries (Enform, 2006a). Additionally, there are some reports that show that pressurized water (up to 13 100 kPa) and steam have caused severe burn injuries for industrial workers (Enform, 2010, 2011). There were two fatalities at Brookhaven National Laboratory when industrial workers' bodies were exposed to water hammer and high pressurized steam (Kirsner, 1999).

Characteristics (features) of hot liquid splash and steam

Hot water in individual processes can range from 90 to 200°C (70<P<1555 kPa) and have an energy content of almost 375 to 850 kJ/kg (Ackerman et al., 2011). Hot water may also impinge on the skin with different pressures due to breaks in pipelines and cause scald burns (Enform, 2010). For bare skin, exposure to water at 44°C may cause a second degree burn in 6 hours while a second burn injury may occur within 1 s for water at 70°C (Huyer & Corkum, 1997). Canola oil

and drilling fluid at 85°C also cause second degree burn in less than a second when exposed to a bare skin (Lu, Song, Ackerman, Paskaluk, & Li, 2013).

A steam hazard will typically include temperatures in the range of 100 to 300°C with pressures from 100 kPa to 4 MPa which may carry 2750 kJ/kg of thermal energy at 150 °C (Ackerman et al., 2011). Steam is extensively used in both oil extraction and processing which causes the worker to be exposed to up to 800 kPa pressurized steam with temperatures over 100°C (Crown & Dale, 2005) .

Typically, steam is more dangerous than hot water due to the energies associated with phase changes. Condensed steam at 150°C is able to release almost 2100 kJ/kg thermal energy (Cengel & Boles, 2008). A jet of leaking pressurized steam through a crack of small orifice at initial high velocity expands in the surrounding air which dilutes and cools the temperature of the jet of steam if the ambient contains cool air. In a study by Armstrong and Harris (1966), 150°C steam (450 kPa) and 88°C water were sprayed from a nozzle with 3 mm diameter. The steam temperature dropped significantly as the distance from the nozzle increased. For instance, at a distance of 14 cm from the nozzle, the steam temperature dropped from 150°C to 65°C and the temperature of hot water from 150°C to 92°C (Table 2.1). On the other hand, the temperature of water that exited the nozzle at 910 kPa and 88°C did not change as the distance from the nozzle increased to 44 cm.

Table 2.1 Maximum Temperature in jet of water and steam at distance from nozzle (Armstrong & Harris, 1966)

Distance from nozzle (cm)	Water at 910 kPa and 88°C (°C)	Water at 910 kPa and 150°C (°C)	Steam at 450 kPa and 150°C (°C)
14	88	92	65
25	88	90	50
32	88	86	45
38	88	80	41
44	88	75	40

When the volume of steam is 12% in the steam-air mixture, the condensing temperature of saturated steam is reported to be 48°C (Armstrong & Harris, 1966). As the volumetric percentage of steam in the air exceeds 12%, especially in the confined spaces such as air gaps, the steam can condense at higher temperatures (T>48°C) which may cause burn injuries. Also, due to the penetrating characteristics of steam, it can penetrate further into the fabric system, closer to the

skin and be condensed. Condensed steam has a high heat transfer coefficient and can cause severe burn injuries (Incropera & DeWitt, 2007; Murtaza, 2012).

Protective clothing requirements (hot liquid and steam)

Understanding heat and mass transfer through a fabric system is necessary for understanding the mechanisms required for preventing burn injuries to the skin. Once the pressurized steam and hot liquids contact the clothing, energy is transferred by conduction and convection on the surface and through the fabric (mass transfer). The heated fabric may also transfer thermal radiation which may be negligible in hot water and steam and for other hot liquids at low temperatures. The water vapor in steam, condensed steam and hot liquids at high temperatures may transfer thermal radiation to the skin. The hot liquid and condensed steam can be entrapped and stored in the fabric system even after an exposure has ended. Stored thermal energy in the fabric system can be discharged to human skin due to the physical activities of firefighters and industrial workers. Therefore, the most essential requirement for protective clothing exposed to pressurized steam and hot liquids is blocking or minimizing liquid penetration as well as decreasing liquid absorption into the fabric system.

As will be shown later in the thesis, fabric surface finishing is essential to reduce mass transfer and improve protective performance of clothing. Embedding a moisture barrier within the fabric system is the other effective method to prevent liquid penetration and mass transfer to the inner layers and the skin. Better insulating properties of clothing are also necessary to reduce the amount of heat transfer to the skin. Maintaining integrity of the protective clothing is also crucial to provide protection from hot liquid and pressurized steam. Once hot liquid and steam impinge upon the fabric, they may compress the fabric and result in changes in the fabric structure and reduction in the fabric thickness during exposure as will be shown in Chapter 5.

Factors influencing the protective performance against liquids

Once a fabric is contacted with a droplet of liquid, it may stay on the fabric or penetrate into the fabric's capillaries. The shape of the droplet is characteristic of the fabric's wettability and is measured by contact angle (Figure 2.1). In Equation 2.3, which is based on a force balance, γ_{LA} is the liquid-air tension, γ_{LS} is

the liquid and solid tension, γ_{SA} is the solid-air tension and θ is the liquid-solid (static) contact angle (Li & Shan, 2013).

$$\gamma_{LA} \cdot Cos(\theta) + \gamma_{LS} = \gamma_{SA} \qquad (2.3)$$

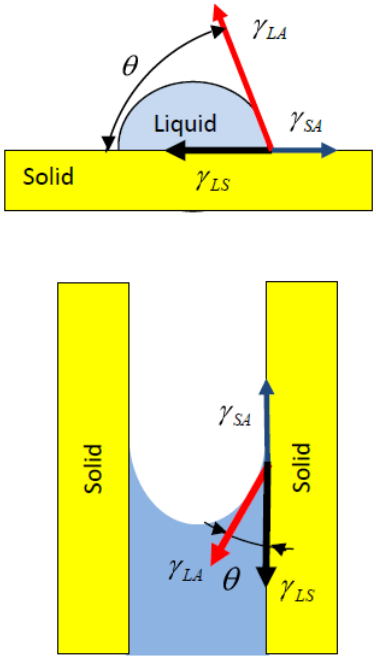

Figure 2.1 Contact angle and wetting (Çengel, 2005, pp. 53-55)

When the contact angle of the liquid with the fabric is below 90°, the fabric tends to have hydrophilic properties. For the values of contact above 90°, the fiber has hydrophobic surface properties which means a higher resistance to water spreading and surface wetting (Olderman, 1984). As such, the surface finishing of the outer shell in protective fabric systems is a crucial factor in decreasing mass transfer and liquid penetration (Lu, Song, Ackerman, et al., 2013).

There are few studies which address contributing factors to the performance of thermal protective fabrics upon exposure to hot liquid splash and steam. Some of the results of these studies will be discussed. In a study by Sati et al. (2008), it is shown that laminated and coated fabrics show better performance against steam than those without such treatments. They showed that the distance between the steam nozzle and the fabric, and the steam pressure have significant effects on thermal performance of the fabrics. Rossi et al. (2004) demonstrated that impermeable fabrics exhibited better performance against steam than permeable

ones. Also, adding a spacer material behind impermeable fabrics increases the thermal performance of the fabrics upon exposure to steam (Rossi, Indelicato, & Bolli, 2004). The position of the moisture barrier affects the thermal protection of the fabric system against hot water due to the fact that it minimizes mass transfer to inner layers. Fabric air permeability is also considered as a critical factor which improves the performance of protective clothing against hot water (Jalbani, Ackerman, Crown, van Keulen, & Song, 2011). Impermeable fabrics provide better protection than permeable fabrics from hot liquid splashes (Lu, Song, Zeng, Zhang, & Li, 2014).

Minimizing mass transfer is the most important factor to reduce heat transfer to the skin by keeping hot fluids away from the skin (Mandal, Song, Ackerman, Paskaluk, & Gholamreza, 2013; Murtaza, 2012). Therefore, keeping penetrating hot fluids at a greater distance from the skin is crucial to reduce heat transfer to clothing subjected to penetrating hot fluids.

A change in the hot liquid impingement angle results in changes to the liquid flow on the surface of the fabric and affects the liquid penetration (Lu et al., 2013). A horizontal configuration of the fabric system perpendicular to the stream of hot liquids provides lower protective performance than a fabric at an inclined angle (45°) as it will be shown in Chapter 4.

Distilled water and drilling fluid have different thermal properties. It is demonstrated that distilled water penetrates further than drilling fluid through a permeable fabric due to its lower viscosity (Lu et al, 2013). It is also shown that the air gap between a test sensor (or skin) and an impermeable fabric significantly improves the protective performance of clothing (Lu, Song, Li, & Paskaluk, 2013). However, vapor transfer through a permeable fabric and its condensation on the sensor eliminates the positive effect of the air gap on a fabric's performance.

Impingement of a circular liquid jet on a flat surface

Using an impinging jet on surfaces is a common technique for providing high local heat and mass transfer rates in many industrial applications (Kate, Das, & Chakraborty, 2007a; Liu & Linehard, 1993). Due to their high heat transfer coefficient, water jets have been widely used for cooling in internal combustion engines, controlled cooling in the metal and glass industries, and controlling of high performance computer components such as VLSI (very-large-scale integration)

circuits (Baonga, Louahlia-Gualous, & Imbert, 2006; Stevens & Webb, 1991). In liquid jet impingement heat transfer, the hydraulic jump is an important issue. Hydraulic jump was first noticed by Rayleigh when a vertical stream of water from a 6-mm diameter tap struck a shallow dish (Rayleigh, 1914). The water expanded into a thin sheet which suddenly increased in thickness after a certain distance and created a bore and a wave on a small scale. Normal impingement of a circular liquid jet on a horizontal flat surface leads in an axisymmetric circular jump. However, if the angle of the liquid jet is not perpendicular to the surface, a non-circular hydraulic jump occurs.

Impingement of liquid jet on the surface of fabric and challenges in engineering

It is also well-known that the hydraulic jump is a consequence of impingement of a liquid jet on a flat surface (Kate et al., 2007a). As such, hydraulic jump can be observed in the hot water splash phenomenon when a jet of water leaving the nozzle hits the fabric and flows on the surface of the fabric.

The determination of flow patterns, including the position of the hydraulic jump, is very important because heat transfer decreases significantly at the location of the hydraulic jump and in the flow downstream of the jump (Passandideh-Fard, Teymourtash, & Khavari, 2011; Stevens & Webb, 1991). Hydraulic jump may occur as the result of the impingement of a fluid jet on a plate at high Reynolds numbers and deceleration of the liquid as it expands radially (Watson, 1964). The sudden change in the liquid height and the location of the jump depend on a local balance between fluid momentum and hydrostatic and surface tension forces. As such, surface roughness will directly affect the shape and location of the jump (Johnson, Maynes, Vanderhoff, & Webb, 2012). Hydraulic jump is also affected by experimental variables such as liquid flow rate and temperature, and nozzle-to-plate separation (Kate, Das, & Chakaraborty, 2007b). The increase in the height of the liquid downstream of the hydraulic jump is accompanied by a significant loss of energy and affects the rate of heat transfer (Mikielewicz & Mikielewicz, 2009).

Therefore, it is very important to identify the hydrodynamics of hot liquid flow and physical properties of fabric systems that influence liquid flow patterns on the fabric surface. In this thesis, the characteristics of a vertical hot water jet impinging on the surface of horizontal and inclined fabric systems are investigated. Some of the literature regarding the hydrodynamics of the flow patterns as the result

of impingement of a liquid jet on horizontal and inclined flat surfaces are briefly reviewed.

Characteristics of circular hot water jet on the horizontal flat surface of single layer fabrics

The flow field due to a normal impingement of jet can be divided into three main regions (Figure 2.2): the free jet region, the impingement region, and the wall jet region (Abramovich, 1963; Glauert, 1956; Watson, 1964). Kate et al. (2007a) also divided the wall jet zone into five sub-regions that are illustrated in Figure 2.2 (Kate et al., 2007a).

Figure 2.2 shows regions of an impinging jet of liquid on a horizontal flat surface. Since this phenomenon is axisymmetric, only half of the flow is illustrated. When the fluid hits the plate, it spreads radially outward. Region “WJ 1” refers to the boundary-layer-type flow region where there is a transition of the vertical fluid flow at the stagnation region to a fully developed flow of the fluid “WJ 2” (Kate et al.,2007). The surface tension is the direct result of the thickness of the fluid film in the fully developed region (Liu & Lienhard, 1993). In this region, the layer of the fluid is typically thin until reaching a critical radius where the level of the fluid starts rising at WJ 3, the region immediately before the hydraulic jump. In Figure 2.2,” WJ 4” and “WJ 5” refer to the hydraulic jump region and the region downstream of the jump, respectively. However, in a latter study by Baonga et al, the wall jet region was divided into a parallel flow zone (zones WJ 1, WJ 2 and WJ 3) and the hydraulic jump zone (WJ 4 and WJ 5) (Baonga et al., 2006). They also added that heat transfer coefficient depends on the liquid flow rate and inertial forces in each zone.

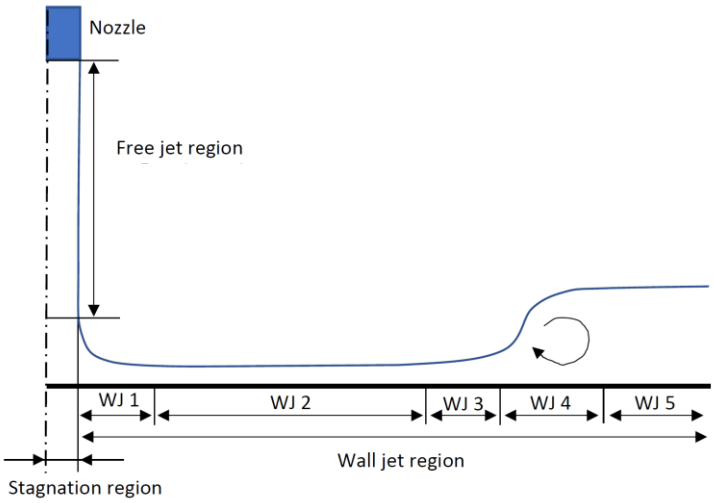

Figure 2.2. Regions of an impinging jet of liquid on a horizontal flat surface: transition of the vertical fluid flow at the stagnation region (WJ 1) to a fully developed flow of the fluid (WJ 2); the region immediately before the hydraulic jump (WJ 3), the hydraulic jump region (WJ 4), the region downstream of the jump (WJ 5) (Kate et al., 2007a) .

According to a study by Bowles and Smith (1992), the downstream conditions play an important role in determining the position of the jump. The hydraulic jump is controlled by the interaction between surface tension and viscosity forces upstream of the jump. The conditions downstream of the jump are governed by the interaction between gravitational pressure gradient and viscosity (Bowles & Smith, 1992; Watson, 1964). Rayleigh (1914) confirmed that surface tension plays a considerable role in this phenomenon. Liu and Lienhard (1993) realized that surface tension is the dominant factor which forms the shape of the jump. The study of local convective heat transfer coefficient for a round liquid jet impinging on a flat surface with uniform heat flux confirmed that increasing the Reynolds number caused an increase in the radial distance to the location of the hydraulic jump. On the other hand, nozzle-to-plate separation of the nozzle has a minor effect on magnitude of the local convective heat transfer coefficient (Stevens & Webb, 1991).

The shape and position of the hydraulic jump on a horizontal surface

Early research on the position of the hydraulic jump shows that the jump position depends on the upstream Reynolds and Froude numbers and the downstream Froude number (Watson, 1964). Froude number is a dimensionless

number which is the ratio of inertial force to gravitational force (Çengel, 2005, p. 287). In an open channel flow, similar to the flow of an impinging water jet on a flat surface, Froude number is a ratio of the average liquid velocity to the surface wave speed (Equation 2.4)

$$Fr = \frac{V}{\sqrt{gl}} \tag{2.4}$$

Where:

V = the average liquid velocity

l = the flow depth

g = the gravitational acceleration.

The Froude number is equal to 1 when the inertial and gravitational forces are equal. For a value of the Froude number less than one, the flow of water is referred to as subcritical or tranquil, while supercritical or rapid flow corresponds to values of Froude number larger than one (Çengel, 2005, p. 287).

The upstream Froude number at radius r_j (Fr_h) and downstream Froude number at radius r_s (Fr_s) are determined according to Equations 2.5 and 2.7 (Liu & Lienhard, 1993).

$$Fr_h = \frac{\overline{V_h}}{\sqrt{gh}} \tag{2.5}$$

$$\overline{V_h} = \frac{1}{h}\int_0^h u(r_j, y)dy = \frac{u_f d^2}{8r_j\sqrt{gh^3}} \tag{2.6}$$

$$Fr_s = \frac{\overline{V_s}}{\sqrt{gs}} \tag{2.7}$$

$$\overline{V_s} = \frac{u_f d^2}{8r_s\sqrt{gs^3}} \tag{2.8}$$

In these equations, $\overline{V_h}$ (Equation 2.6) and $\overline{V_s}$ (Equation 2.8) are the average velocity for the local thickness of liquid sheet upstream and downstream, respectively. The term u_f in Equations 2.6 and 2.8 is the velocity of the impinging jet and d is the diameter of the nozzle. In Equation 2.6, $u(r_j, y)$ is the radial velocity distribution in the liquid film.

The ratio of the downstream depth (subcritical depth) to upstream depth (supercritical depth) can be determined employing Equation 2.9 (Liu & Lienhard, 1993).

$$\frac{s}{h} = \frac{1}{2}\left(\sqrt{1 + 8Fr_h^2} - 1\right) \tag{2.9}$$

In Equation 2.9 and Figure 2.3, h and s are the height of the liquid sheet before and after the hydraulic jump. The radius at which subcritical depth equals s, is r_s (Figure 2.3).

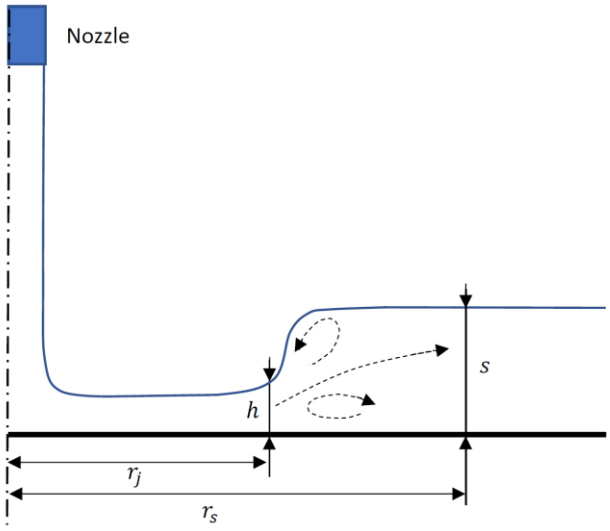

Figure 2.3. A schematic illustration of the subcritical film depth, s, and supercritical film depth, h, in a circular hydraulic jump.

Forms and instability of circular hydraulic jump

According to a study by Liu and Lienhard (1993), several forms of hydraulic jump occur when the downstream depth (s) increases (Equation 2.9). For a small difference between the downstream and upstream depth, a smooth jump occurs. In this type of hydraulic jump, the depth of the stream increases slightly and gradually (Figure 2.4 (a)). As the depth of the downstream flow increases, the hydrostatic pressure along the sloped jump causes a backward flow of the liquid which results in a single roller jump (Figure 2.4 (b)). The sudden transition in the liquid depth due to the liquid flow causes an eddy in the roller and another on the wall which forces the main flow to move between the two vortices. With a further increase in the depth of the downstream flow, the roller becomes lower than the surface of the stream. The distance between the roller and the surface creates a double roller

effect. The jump with a double roller creates unsteady variations on the surface (Figure 2.4 (c)). By further increasing the downstream depth, the double roller hydraulic jump turns into an unstable jump. This type of hydraulic jump has a turbulent surface which entrains a large amount of air and entrapped air bubbles. In addition, the jump loses its circular and axisymmetric shape (Figure 2.4 (d)).

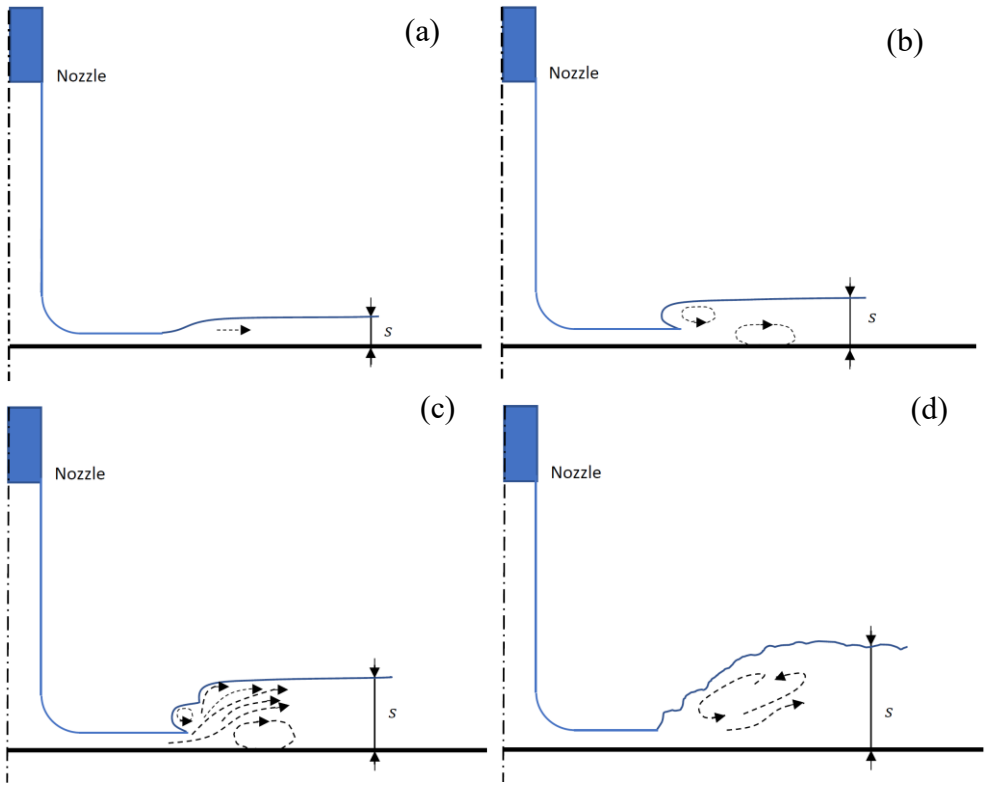

Figure 2.4. Schematic illustration of the increase in the instabilities of the hydraulic jump from (a) to (d): (a) jump with no roller, (b) jump with single roller (c) double roller hydraulic jump and (d) unstable hydraulic jump (Liu & Lienhard, 1993).

The role of surface tension and hydrostatic forces in determining the shape and stability of the hydraulic jump can be shown using the Weber number (Equation 2.10) (Liu & Lienhard, 1993).

$$We = s\sqrt{\frac{\rho g}{\sigma}} \tag{2.10}$$

where ρ is the liquid density, σ is surface tension, g is gravitational acceleration and s is the liquid sheet thickness after the hydraulic jump.

Liu and Lienhard (1993) found that the shape of the hydraulic jump is a function of the Weber number and the jump radius. Figure 2.5 shows the regions corresponding to different circular hydraulic jump forms as a function of the Weber number and the dimensionless jump radius for different Froude number values. An increase in the adverse pressure gradient (decelerating flow speed and positive pressure gradient) along the wall surface causes a more stable jump due to the fact that the deceleration of the flow decreases the Weber number. The single roller jump occurs only in the range of the smallest Weber numbers.

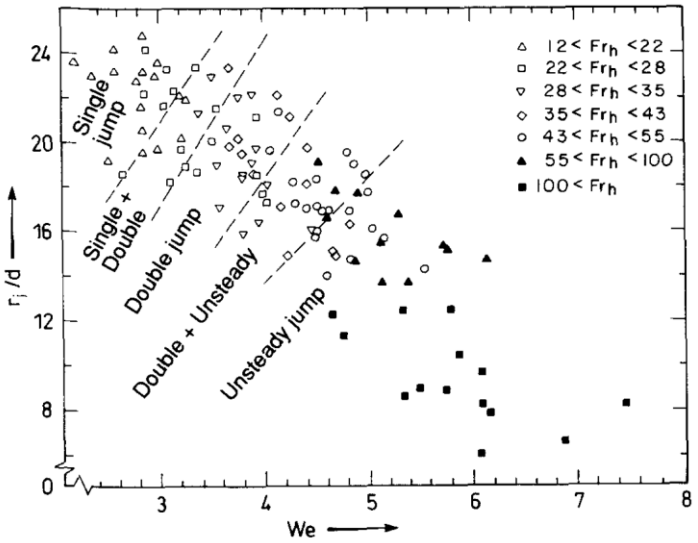

Figure 2.5. The relationship between dimensionless jump radius, Weber number and shape of the jump (Liu & Lienhard, 1993). Reprinted with permission.

For the initial conditions at the jet nozzle, Liu and Lienhard stated that the dimensionless hydraulic jump is a function of the jet Reynolds, Froude and Weber numbers (Equations 2.11, 2.12 and 2.13 respectively).

$$Re_d = \frac{u_f d}{v} \tag{2.11}$$

$$Fr_d = \frac{u_f}{\sqrt{gd}} \tag{2.12}$$

$$We_d = \frac{\rho {u_f}^2 d}{\sigma} \tag{2.13}$$

The dimensionless hydraulic jump is also a function of the jump Weber number which governs the shape of the jump. Moreover, the hydraulic jump is a function of the dimensionless downstream depth and the dimensionless radius at which the depth is determined (Liu & Lienhard, 1993).

Characteristics of a circular hot water jet on the inclined flat surface of single layer fabrics

In the previous section, it was mentioned that an axisymmetric hydraulic jump occurs when a jet of liquid is impinging on a horizontally oriented flat surface. When the angle of liquid stream is not perpendicular to the horizontal surface, the shape of the jump deviates from the circular form and creates non-circular hydraulic jumps (Beltaos, 1976; Kate et al., 2007b; Mertens, Putkaradze, & Vorobieff, 2005).

In a non-circular hydraulic jump, the jump resembles the onset of the rims on the outer boundaries of the flow and encompasses the supercritical stream of the liquid. Figure 2.6 shows a schematic illustration of a liquid flow on a hydrophobic inclined surface. Once a vertical liquid jet impinges on an inclined surface or an inclined jet of liquid impinges on a horizontal surface, different types of behaviour are observed based on the liquid and surface properties as well as the jet velocity (P. Kate et al., 2007; R. P. Kate et al., 2007; Kibar, Karabay, Yiğit, Ucar, & Erbil, 2010). On hydrophobic ($90°<\theta<150°$, (Kibar et al., 2010)) and super hydrophobic surfaces ($\theta>150°$, (Kibar et al., 2010)), the water starts spreading but the extent of spreading is limited to a certain distance. A thin sheet of liquid spreads in all directions and the hydraulic jump is created as a rim at the boundaries of the flow. Along the flow of the liquid on the surface, the thin sheet and the rim expand until the surface properties of the liquid and the surface beneath the liquid bring the outer boundaries of the flow back together which creates a braiding effect (Figure 2.6 (a)) (Kibar et al., 2010). Depending on the jet velocity, the liquid may expand again on the surface and create rims. The rims may also flow back together and create a second braiding on the surface. This phenomenon may repeat and create a chain effect on the surface (Figure 2.6 (a)) (Bush & Hasha, 2004). According to Merten et al. (2005), the liquid kinematic viscosity, density, surface tension, liquid flow rate and the component of the acceleration due to gravity in the direction of the acceleration are five dimensional parameters that determine how liquid flows on an inclined surface.

The dimension of the braid depends on the viscosity and the jet flow rate (Clanet, 2007; Mertens et al., 2005). An increase in the viscosity and decrease in the flow rate create smaller braids which may eventually disappear with further decrease in the flow rate. An increase in the flow rate also increases the braid's length. In hydrophobic and superhydrophobic surfaces, the liquid sheet may not remain confined on the surface and may bounce back from the surface. This effect is named reflection (Figure 2.6 (b)). The magnitude of the jump on the surface creates an angle called the reflection angle (γ). The reflection angle depends on the angle between the liquid jet and the surface, the velocity of impinging jet, Weber number (Equation 2.13) and the contact angle (Kibar et al., 2010).

In surfaces with hydrophilic properties, the outer boundaries do not flow back and the thin sheet of liquid expands along the width of the flow until it is rolls off the surface. Under this situation, the flow resembles a bell-shaped type of flow (Clanet, 2007). In addition, in high jet velocities, the inertial forces of the liquid sheet may overcome the surface tension of liquid. Under this circumstance, the braided and bell shaped liquid flow may be unstable and distorted and may cause splashing-type flow (Kibar et al., 2010). According to Kibar et al. (2010), the magnitude of the area that water spreads over increases as the water contact angle decreases. The area of the water on the surface also increases with an increase in Reynolds and Weber numbers.

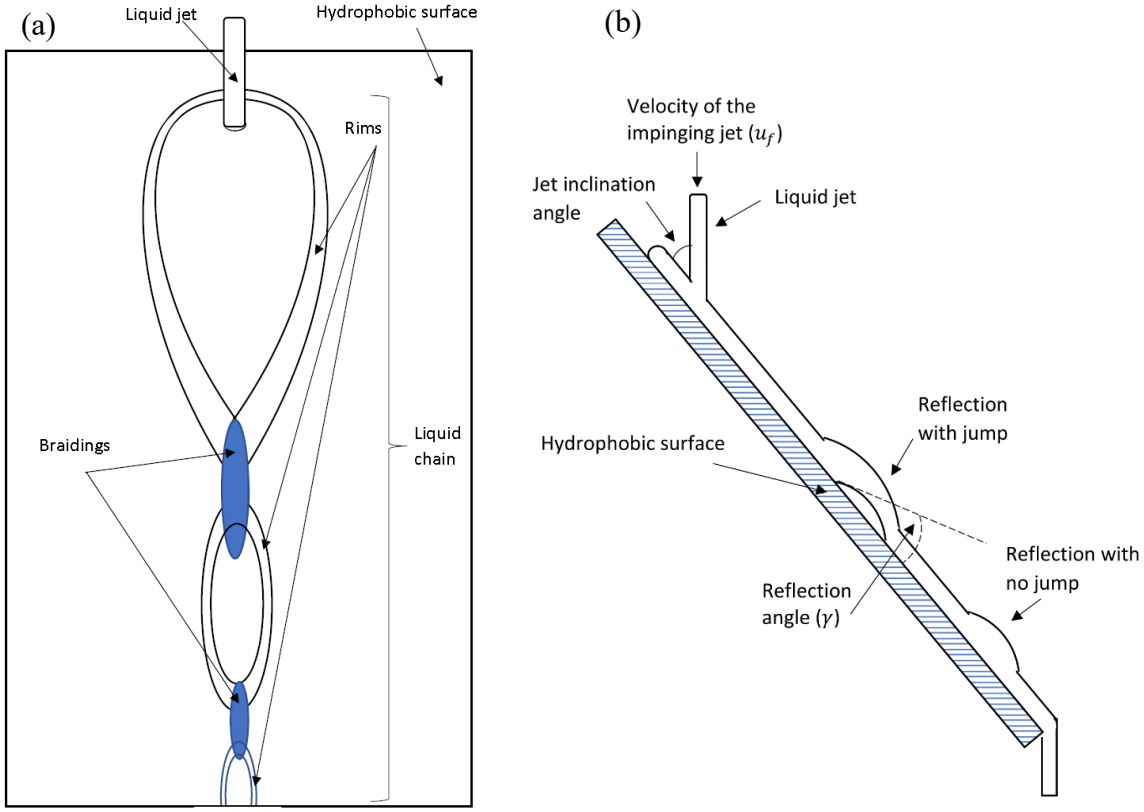

Figure 2.6. Schematic illustration of a non-circular hydraulic jump on a hydrophobic surface (a) front view (b) side view.

Stored thermal energy

Heat transfer to firefighters and industrial workers may occur due to stored thermal energy that was accumulated in the fabric/garment systems during the heating and cooling periods (G. Song, Cao, et al., 2011). Regular activities may cause clothing to be compressed against the skin. Stored thermal energy could be discharged to the skin in two ways: ordinary and compressive discharge.

Ordinary Discharge

The discharge of stored thermal energy will often occur without any changes to the air spaces between the fabric and skin. An ordinary discharge (OD) often occurs when firefighters and industrial workers are in static positions. Mah (2010b) found that there is a significant amount of stored thermal energy in a garment exposed to a flash fire particularly during the seven minutes after the exposure ends. In one of the studies in this area, Torvi and Threlfall (2006) developed a numerical model to include the effect of ordinary discharge of thermal

stored energy in a fabric system exposed to a flame, and the energy transfer between the fabric and heat sensor. They also gained a fundamental understanding of the heat transfer associated with ordinary discharge of stored thermal energy. Their model included radiation, natural convection and conduction heat transfer between the fabric and sensor. In a recent work, Su et al. (2016) introduced a numerical simulation for heat transfer in a multilayer fabric system under low-level thermal radiation (8.5 kW/m^2). Their model was used to analyze the relationship between the transmitted heat during exposure and the discharged heat during the cooling period and obtain the distribution of stored energy and its contribution to burn injuries. The model was also applied to examine the effect of air gap and the ambient temperature on stored thermal energy. Although there were some limitations to these models, they provided a fundamental understanding of this phenomenon.

Compressive Discharge

The compression of fabric to the skin may be due to a garment's weight (Allen, Corrado, Cox, & Dale, 2008). Compressive discharge may also be caused by an individual's movements. Regular activities such as squatting, leaning, sitting, crawling and rolling may cause clothing to be compressed against the skin. There are almost 206 bones in an adult human body and most of them are connected to the movable joints which create multitude of discrete positions (Hewes, 1957). When an industrial worker or a firefighter moves, his skin stretches, elongates and recovers due to the fact that skin is highly elastic material. However, thermal protective clothing barely stretches over a bent area (Guowen Song, 2011). As such, movement of the body during and after the thermal exposure may cause compression of the heated garment to the individual's skin and can reduce the level of protection expected from the thermal protective clothing (Barker et al., 2000). Compression of the heated fabric may also decrease its thickness and enhance heat conduction to the skin (Song, Cao, et al., 2011). Compression of the garment may also reduce the air volume in the fabric structure, between the individual layers of fabric, enhancing compressive discharge of stored thermal energy.

Previous Research and Its Limitations

Some research has been conducted to analyze stored energy and its contribution to thermal burn injuries (e.g., (Song, Paskaluk, et al., 2011; Song, Cao, & Gholamreza, 2011; He, & Li, 2016a, 2016b; Zhang, Song, Gu, Ren, & Cao, 2017;

He, Wang, & Li, 2015)). These studies are associated with the effect of discharged energy during the cooling period in thermal protective clothing materials under low radiant exposures (6.3, 7.5 and 8.3 kW/m^2) and under simulated flash fire conditions (24, 42, 84 kW/m^2). They indicated that the amount of energy stored in the fabric reduces the predicted time to produce second degree burns.

A minimum exposure time (MET) to cause a second degree burn was also introduced (Song, Cao, & Gholamreza, 2011). The minimum exposure time to second degree burn is the exposure time for which a second degree burn is predicted to occur at the end of the cooling period. In other words, for exposure times shorter than MET values, a second degree burn is not predicted. Song, Cao, et al. (2011) employed the approach to determine the minimum exposure time to cause a second degree burn. This is a reliable criterion for rating the thermal performance of protective clothing since the method includes the energies in the cooling period. However, this approach is based on iterative testing to determine the minimum exposure time and it is not time and cost effective. Although Song and coworkers analyzed stored thermal energy in the fabric system during convective and radiant thermal exposures of different intensities using a modified thermal protective performance (TPP) tester (ASTM, 1999), other thermal hazards were not considered.

The ASTM Committee F23 on Personal Protective Clothing and Equipment developed a standard test method (ASTM 2731-10) for measuring the transmitted and discharged energy of firefighter protective clothing exposed to low levels of radiation, 8.5 ±0.5 kW/m^2 (ASTM, 2010). In the test method, the TPP apparatus with a 6.4 mm (0.25 in) air gap is employed. In the compression test, specimens are compressed with a pressure of 13.8 kPa (2 psi) to simulate the discharge of the thermal stored energy to firefighter's clothing caused by some of their regular activities. This test method employs two procedures. The first is a time consuming iterative approach to determine transmitted and discharged energy, while the second is based on a fixed duration radiant exposure followed by compression of the fabric for 60 s. Although, the Standard Test Method ASTM F 2731-10 is a very good procedure for the evaluation of fabric systems considering the discharge of the stored energy to the skin, it nevertheless has some limitations.

According to the test method, the pressure of 13.8 kPa is applied to the heated specimen in order to simulate a firefighter leaning against a wall, squatting

or sitting down (ASTM, 2010). The test method employs a compressor block with an equivalent thermal conductivity of 0.12 (W/m°C) and provides the same conditions for the heated fabric to be compressed for the abovementioned simulated activities. However, leaning against a wall or sitting down where a heated garment is compressed between the skin and an external surface such as a wall creates different thermal boundary conditions than the case when the garment is compressed to the skin only due to squatting or similar activities. For example, when a heated garment is compressed by leaning against a wall, the heated garment is sandwiched between skin and the wall. Depending on the wall's thermal conditions, the garment may lose or gain thermal energy which cannot be simulated according to the test method. In addition, this test method is limited to low level convective-radiant thermal exposures. This test does not simulate all scenarios by which fabrics can be compressed in the field. In addition, this approach is based on iterative testing and it is not time and cost effective.

There are also other limitations in the existing standard test methods such as NFPA 1971 and 2112 (NFPA, 2012, 2013). In these standard test methods, the TPP rating is used as the thermal threshold index of materials. This rating employs the predicted time to second degree burn multiplied by the heat flux in calories per square centimeter per second (Behnke, 1977). The average reported value of the TPP rating can be used to rank fabrics and compare to a performance requirement for the materials. The TPP value is obtained by a continuous exposure time until burn injury is predicted and excludes the contribution of stored energy during the cooling period (NFPA, 2012, 2013). Therefore, it can be concluded that the TPP rating may not completely address the actual thermal performance of the fabric systems.

Stored thermal energy and evaluation of thermal performance of protective clothing using bench-scale tests

Some research has been conducted to analyze stored energy and its contribution to thermal burn injuries. These studies are associated with the effect of discharged energy during the cooling period in thermal protective clothing materials under simulated bench-scale thermal exposures and fire ground conditions.

Thermal stored energy upon exposure to convective-radiant heating

Song, Paskaluk, et al. (2011) tested some fabric systems corresponding to thermal protective garments worn by firefighters, under low level radiant exposures (6.3, 7.5 and 8.3 kW/m^2). They indicate that the amount of thermal stored energy in the fabric could be discharged to the skin during the cooling period and thus reduce the time required to produce a predicted second degree burn. The intent of the study was to provide information on the potential for burn injury of firefighters as a result of prolonged exposures. As such, the study was limited to low level radiant exposures.

In a later paper, Song, Cao, et al. (2011) used different heat intensities (24, 42 and 84 kW/m^2) to analyze stored energy and the thermal performance of firefighters' protective clothing under simulated flash fire conditions. They observed that stored energy may contribute a large portion of the total energy that is required for the prediction of a second degree burn.

Recently He et al., analyzed the transmitted and stored energy through protective fabric systems (He, & Li, 2016a, 2016b; He, Chen, Wang, & Li, 2017; He, Lu, Chen, & Li, 2017; He, Wang, & Li, 2015). They proposed several indices to evaluate the impact of heat storage within the fabric and the heat discharge from different layers of fabrics to skin using natural and forced heat discharge processes (He, Lu, Chen, & Li, 2017; He, Chen, Wang, & Li, 2017). Although they provided an understanding of the energy storage process within the fabric and the discharged energy to the sensor, their evaluation was limited to low level radiant heat and the contributions of the stored thermal energy to thermal performance of the fabric were not investigated.

He and Li (2016a) proposed a method to determine the thermal performance estimate (TPE) in ASTM F 2703-08 using regression equations. The equations were obtained for exposures to 84 kW/m^2 and a limited number of fabrics. This method was used to evaluate the role of air gaps on the stored energy effect using the Stoll Criterion. According to Holcombe and Hoschke (1986), the presence of air gaps and any distortion or movement of the fabric causes the measured heat flux to be far from a rectangular shape. As such, the Stoll criterion may not be an appropriate method in stored energy studies since the Stoll criterion is limited to a rectangular heat pulse shape for the thermal energy reaching the skin (Holcombe &

Hoschke, 1986). Similar attempts have been made in order to develop indices for quantitatively assessing the effect of exposure time on the grade of thermal protection in bench scale and full scale tests for exposures 84 kW/m^2 using Stoll Criterion (He, & Li, 2016b; He, Wang, & Li, 2015). On the other hand, the current standard test method for measuring the transmitted and discharged energy to the skin (ASTM F 2731-10) and the standard test methods for evaluation of thermal protective clothing for prediction against flash fire simulations using an instrumented mannequin employ Henriques et al.'s method for the estimation of tissue burn injuries (ASTM, 2017; ISO, 2017).

According to the previous studies on thermal stored energy in clothing, researchers proposed test methods for measuring the combination of transmitted and discharged energy that occurs in thermal protective clothing as the result of thermal exposure. In a study by Barker et al., a stored energy test was developed to show the potential of the heated garment to generate burn injuries when the firefighter is flexing parts of the body or compressing the garment against a wall or other surface (Barker et al., 2000). However, they employed the Stoll criterion for the burn evaluation. The Stoll criterion is valid for square wave heat flux (Weaver & Stoll, 1969). The heat flux behind the fabric is not rectangular especially when compression is applied to the specimen (Holcombe & Hoschke, 1986). As such, the Stoll criterion may not be the most appropriate method to calculate burn injury in stored energy tests.

Thermal stored energy upon exposure to steam and hot liquid

Few studies have been conducted to study and measure the stored energy in other thermal hazards such as steam and hot liquids. These studies have shown that like flame and heat, stored energy exists for hot liquid and steam and can contribute to skin burn (Ackerman et al., 2011). The results of these studies indicate that stored thermal energy contributes significantly to second degree burns and can reduce the level of protection expected from wearing protective clothing. Hot liquid penetration is the primary mode of heat transfer that increases the stored thermal energy and contributes to burn injuries upon exposure to liquid splash and steam. In steam exposure, the penetrated steam was condensed on the skin and delivered a considerable amount of thermal energy to the skin due to the released latent heat of condensation.

In hot liquid splash and steam exposure, compression of the fabric system during the cooling period enhances the heat transfer from the system to skin as will be shown later in Chapter 5. In multilayer fire fighter's protective clothing, the porous structure of the thermal liner traps hot liquid, condensed steam and sweat in its structure and creates more stored heat. Therefore, during exposure to hot water splash and steam, increasing the thickness for a permeable fabric system may lower its thermal performance. An analysis of the transmitted energy to the sensors when exposed to hot water and steam hazards confirms that the thickest fabric with no air permeability has displayed superior performance in resisting heat and mass transfer. However, a large amount of discharged energy was developed. As such, thickness and permeability of the system are the other key factors in studying the performance of thermal protective clothing considering the stored energy. In addition, when a fabric system is exposed to hot liquid horizontally, more water is trapped in the fabric system, and the trapped water enhances the thermal conductivity of the system, and increases the thermal energy stored in the fabric which will be shown later in the thesis.

However, the focus of these studies was limited to the areas where the fabric system was directly exposed to hot liquid and steam. In addition, these studies were performed only for hot water at a constant flow rate and temperature as well as a constant nozzle-to-sensor board separation (z/d).

Stored thermal energy and evaluation of thermal performance of protective clothing using instrumented mannequins

Instrumented manikins have been shown to be very helpful tools to characterize the performance of full-scale garments. Using a mannequin provides an opportunity to test the size, fit, ease, drape of garments as well as features such as collars, cuffs, pockets and closure (Crown, Ackerman, Dale, & Tan, 1998; Kirkpatrick, Curtis, & Adelgran, 1982; Lu, Song, &Li, 2013; Mah &Song, 2010b)

Crown et al. (1998) tested eight different flight suits which are typically worn by the Canadian Forces flight personnel. The flight suits were exposed to an average heat flux of 75-80 kW/m^2 for 3.5 s to simulate a flash fire from a plane crash. The four parameters of interests were style, fit, closure and seam type. Two-piece garments provided better thermal performance upon exposure to flash fire and had fewer second degree burn areas than a single piece garment. The overlapping parts of the two-piece garment provide a double layer fabric in the mentioned areas

with an extra air layer between the fabrics that may enhance the thermal protective performance of the two-piece garment. The cuff closures hinder the air circulation inside the garment and reduce the convective heat transfer in comparison to the zipped closure.

Crown et al. (1998) also noted that the loose fitting garment provided better thermal performance on the upper torso than the close fitted garment. The controlled looseness in this study enhanced the thermal protection due to the fact that more trapped air would be present. On the contrary, if the looseness of the garment is not controlled, it may be expected to have a low thermal performance due to the chimney effect that may occur inside the loose fit clothes. In a study by Kirkpatrick (1982), it was shown that the style of the trousers has a great influence on the performance of protective clothing and that tight fitting clothing decreases the thermal performance of clothing. It is also confirmed that the exposure conditions such as the intensity and exposure duration affect the thermal performance of the thermal protective clothing (Dale, Crown, Ackerman, Leung, & Rigakis, 1992).

Flash fire mannequins are useful tools for predicting and characterizing the performance of full scale thermal protective garments. This has inspired researchers to use instrumented mannequins to evaluate protective performance of the garments for other hazards such as steam and hot liquid (Ackerman et al., 2011; Lu, Song, & Li, 2013).

A copper mannequin was used for evaluation of protective performance in exposure to steam in a steam climate chamber (Desruelle & Schmid, 2004). The results confirmed that there is a positive correlation between the fabric thickness and its protective performance. Also, water vapor impermeable garments offered better thermal protection in steam exposures. A loose fitted impermeable garment was shown to have superior thermal performance in exposures to steam.

Protective performance of thermal protective clothing in exposures to hot water was also investigated by use of instrumented spray mannequin (Ackerman et al., 2011; Lu, Song, & Li, 2013). The results were consistent with the results obtained from bench-top tests which show that minimizing mass transfer is the critical factor for protection from hot liquid splash, and that impermeable garments provide better protection from hot water spray. The reflective tapes at the waist and

back of the garment provide extra protection. Adding layers also has a positive effect on the level of protection clothing can provide when exposed to hot liquid and steam spray in the mannequin tests (Ackerman et al., 2011; Desruelle & Schmid, 2004; Lu, Song, & Li, 2013). In a study by Lu, Song & Li (2013), minimizing mass transfer is the critical factor in protection from hot water, and the effect of the garment weight and garment size on the transmitted thermal energy to the manikin were insignificant.

A significant amount of attention has been paid to exposures to heat and flame, and the evaluation of the thermal performance of fabric systems against convective-radiant heat using an instrumented mannequin. On the other hand, there is limited research using a spray mannequin, in order to investigate the effect of clothing design features and fabric properties on protective performance of coveralls (Ackerman et al., 2011; Lu, Song, & Li, 2013). In addition, the studies do not completely investigate the effect of body geometry and garment design on stored thermal energy developed in the garment during exposure and its discharge to the skin in the cooling phase of the garment. In the existing full-scale mannequin studies, the average of total absorbed energy (TAE) and the percentage of second and third degree burn have been used as parameters to evaluate the thermal performance of the garment. These parameters do not completely address the contribution of the stored thermal energy to thermal performance of the garment.

Summary

The traditional materials used for protection against hydrocarbon flash fire provided little protection upon exposure to unexplored/newly explored hazards such as hot liquid and steam. In addition, the recent studies on hot liquid and steam did not completely address the contribution of stored thermal energy in the prediction of burn injuries. Also, the evaluation of thermal performance of fabric systems exposed to thermal hazards such as radiant heat, steam and hot liquid demand new criteria which have not been sufficiently addressed by the current bench-scale and full-scale standards and test methods.

In hot liquid exposure, it is very important to identify the hydrodynamics of the hot liquid flow and physical properties of the fabric systems that influence liquid flow patterns on the fabric surface. The hydraulic jump is a consequence of the impingement of a liquid jet on a flat surface. The determination of the flow patterns,

including the position of hydraulic jump, is very important because heat transfer decreases significantly at the location of the hydraulic jump and in the flow downstream of the jump. This phenomenon may affect the rate of heat transfer to the fabric and skin.

Therefore, the formation of the hydraulic jump on the surface of the fabric and its effects on the thermal performance of the fabric system need to be explored. The inherently rough surface and the hydrophobic surface finish of the fabrics which are typically used in firefighters' and industrial workers' garments may affect the sudden change in the liquid height and the location of the jump. Other experimental factors such as hot liquid momentum and surface tension forces, and the orientation of the fabric may also affect the shape and location of the hydraulic jump.

CHAPTER 3 MATERIALS AND METHODS

Introduction

The fabric and garment systems as well as the test methods under which the fabric and the garment system were evaluated in this thesis are explained in this chapter.

Fabric systems

The fabric systems selected for this study represent thermal protective garments worn by firefighters and other workers. Several protective fabric systems were constructed with different levels of protective performance including single layer, double layer and multilayer systems. High performance fabrics were used for each layer which provided a range of different fiber contents, fabric structures, and fabric physical and thermal properties.

Fabric systems used in Chapter 4 and Chapter 5

The structure and properties of the selected fabrics that were used in the fabric systems are provided in Table 3.1 The construction of each fabric system is also depicted in Table 3.2.

Table 3.1. Characteristic features of the fabrics used in Chapters 4 and 5.

Fabrics	Fiber content	Fabric Structure	Surface Property
Fabric AA	60% Kevlar®aramid/ 40% polybenzimidazole	Plain weave, rip-stop	Water resistant surface
Fabric BB	100% Nomex®aramid	Plain weave	No finish
Fabric CC	Kermel® (polyamide-imide)	Plain weave	Water resistant surface
Fabric DD	12% HT nylon+88% cotton	Twill weave	Water resistant surface (encapsulated fibers)
Moisture Barrier AA	Vapro® fabric: 85% Nomex®IIIA+ 15% FR polyurethane	Plain weave	Vapro® water resistant surface, vapor permeable coating
Thermal Liner AA	100% aramid (Nomex®IIIA)	Plain weave, Nomex® layer quilted to a thin Nomex® oriented webs	No finish
Thermal Liner BB	100% aramid (Nomex®IIIA)	Plain weave, Nomex® layer quilted to Nomex® needle felted batt	No finish

Table 3.2. Construction of the fabric systems used in Chapters 4 and 5.

Assembly Code	Assembly Description
SS-1	Fabric AA
SS-2	Fabric BB
SS-3	Fabric CC
SS-4	Fabric DD
DD-1	Fabric AA+ Thermal Liner AA
DD-2	Fabric AA+ Thermal Liner BB
DD-3	Fabric AA+ Moisture Barrier AA
DD-4	Moisture Barrier AA+ Fabric AA
MM-1	Fabric AA+ Moisture Barrier A+ Thermal Liner AA
MM-2	Fabric AA+ Moisture Barrier AA+ Thermal Liner BB

Inherently flame retardant fabrics such as Kevlar®/PBI (Fabric AA) and Nomex® (fabric BB and fabric CC) as well as a fabric with a fire retardant finish (fabric DD), all of which can be used in single layer firefighting coveralls were used as single layer fabric systems. Fabrics CC and DD were cut from thermal protective coveralls. Fabrics such as the moisture barrier were used in order to investigate their role in double layer and multilayer fabric systems. Two thermal liners are used so that the double layer (DD-1 and DD-2) and multilayer layer (MM-1 and MM-2) fabric systems have the same fiber content and construction but different masses and thicknesses. The effect of the position of the moisture barrier on the thermal protection and the stored energy effect in double layer systems (DD-3 and DD-4) were analyzed by positioning the moisture barrier from the outermost to the innermost layer of the fabric.

The fabric systems selected for the work reported in this Chapter 5 are similar to the fabric systems used in Chapter 4, which represent thermal protective garments worn by firefighters and other workers. However, only fabric systems S-1 and S-4 have been used for the single layer fabric system in the study in Chapter 5. Fabric system S-1 is used since this fabric is typically used in single layer and multilayer firefighting ensembles. Fabric system S-4 is also used because this fabric showed a superior thermal performance among the single layer fabric systems studied in the hot liquid exposure described in Chapter 4.

Fabrics used in Chapter 7 and Chapter 8

The fabrics in Table 3.3 were used in order to investigate and understand the hydrodynamics of the hot water flow patterns on the surface of horizontal and inclined fabrics. These fabrics were also used in order to explore the surface wetting and in-depth penetration in thermal protective fabric systems (Chapter 7). The effects of the hydrodynamics of the hot water flow patterns on the surface of horizontal and 45-degree angled fabrics and in-depth penetration on thermal performance of the selected fabrics were investigated in Chapter 8.

The structure and properties of the selected fabrics used in the fabric systems are provided in Table 3.3. The construction of each fabric system is also depicted in Table 3.4.

Please note that some of the fabrics used in Chapters 7 and 8 are the same as those used in Chapters 4 and 5:

- fabric D is the same as fabric CC, and
- fabric E is the same as fabric DD.

Two of the fabrics used in Chapters 7 and 8 are the same fabrics used in Chapter 4 and 5, but from different lots:

- fabric A is the same as fabric AA, and
- thermal liner A is the same as thermal liner AA.

Table 3.3. Fiber content and Structural features of the fabrics used in Chapters 7 and 8.

Fabrics	Fiber content	Fabric Structure	Surface Property	Fabric count (yarns/cm)
Moisture Barrier A	Nomex®aramid +2%carbon + underlying polytetrafluoroethylene coating	Plain weave, rip-stop	Water resistant surface, vapor permeable coating	85 × 70
Moisture Barrier B	Kevlar®/PBI +2%carbon + underlying polytetrafluoroethylene coating	Plain weave, rip-stop	Water resistant surface, vapor permeable coating	80 × 74
Moisture Barrier C	85% Nomex®aramid + 15% underlying polyurethane coating	Plain weave	Water resistant surface, vapor permeable coating	66 × 45
Fabric A	60% Kevlar®/ 40% polybenzimidazole	Plain weave, rip-stop	Water resistant surface	43 × 37
Fabric B	100% Nomex®IIIA	Plain weave	No finish	68 × 44
Fabric C	100% Nomex®IIIA	Plain weave	Water resistant surface	68 × 40
Fabric D	Kermel® (polyamide-imide)	Plain weave	Water resistant surface	70 × 50
Fabric E	88% cotton+ 12% HT nylon	Twill weave	Water resistant surface	98 × 48
Fabric F	Nomex®IIIA+ Neoprene coating	Plain weave, rip-stop	Water resistant surface	88 × 60
Thermal Liner A	100% Nomex®aramid	Plain weave, Nomex® layer quilted to a thin Nomex® oriented webs	No finish	
Thermal Liner B	100% Nomex®aramid	Plain weave, Nomex® layer quilted to two thin Nomex® oriented webs	No finish	
Thermal Liner C	100% Nomex®aramid	Plain weave, Nomex® layer quilted to Nomex® needle felted batt	No finish	
Thermal Liner D	100% Nomex®aramid	Plain weave, Nomex® layer quilted to Nomex® needle felted batt	No finish	

Table 3.4. Construction of the fabric systems used in Chapters 7 and 8.

Assembly Code	Assembly Description
S-1	Moisture Barrier A
S-2	Moisture Barrier B
S-3	Moisture Barrier C
S-4	Fabric A
S-5	Fabric B
S-6	Fabric C
S-7	Fabric D
S-8	Fabric E
S-9	Fabric F
D-1	Fabric A+ Thermal Liner A
D-2	Fabric A+ Thermal Liner B
D-3	Fabric A+ Thermal Liner C
D-4	Fabric A+ Thermal Liner D
D-5	Fabric A+ Moisture Barrier A
D-6	Moisture Barrier A+ Fabric A
M-1	Fabric A+ Moisture Barrier A+ Thermal Liner A
M-2	Fabric A+ Moisture Barrier A+ Thermal Liner B
M-3	Fabric A+ Moisture Barrier A+ Thermal Liner C
M-4	Moisture Barrier A+ Fabric A+ Thermal Liner C
M-5	Fabric A+ Thermal Liner C+ Moisture Barrier A
M-6	Fabric A+ Moisture Barrier A+ Thermal Liner D

In this study, moisture barriers A (S-1), B (S-2) and C (S-3) were tested as single layer fabrics in order to understand their individual performance and role in double layer and multilayer fabric systems. The selected moisture barriers A, B and C are constructed from a woven fabric laminated to a water resistant vapor permeable coating. Moisture barrier A and moisture barrier B are constructed from Nomex® and Kevlar®/PBI, respectively with water resistant properties and an underlying expanded polytetrafluoroethylene coating. The purpose of employing moisture barrier A and B in the fabric system was to investigate the effect of moisture barriers with different fiber content on the thermal performance of the fabric system when exposed to hot water. Moisture barrier C is constructed from Nomex®IIIA fabric with a water resistant vapor permeable surface film and an

underlying polyurethane coating. Moisture barrier C is Nomex® with a polyurethane underlying coating. Including moisture barrier C in the fabric system enables the comparison of the moisture barriers with different properties.

Inherently flame retardant fabrics such as Kevlar®/PBI and Nomex® that are typically used in single layer firefighting coveralls were used as a single layer or a thin fabric system. Fabric A is made from Kevlar®/PBI fibers with a water-resistant finish used as a single layer fabric system (S-4) and as a shell fabric in double layer (D-1 to D-6) and multilayer (M-1 to M-6) fabric systems. Shell fabric B (S-5), Fabric C (S-6) and Fabric D (S-7) are made from Nomex® fibers. Shell fabric S-5 has no finish while fabrics S-6 and S-7 have water resistant finishes. Employing fabric systems S-5, S-6 and S-7 enabled the evaluation of fabric system from the same fiber content with different physical properties.

Thermal liners with different thicknesses were used so that the double layer (D-1, D-3 and D-4) and multilayer layer (M-1, M-3 and M-6) fabric systems contained the same fiber content and construction, but had different thicknesses. Thermal liner B is constructed from two thin Nomex® oriented webs with mass of 256.4 g/m^2. Thermal liner C has one Nomex® oriented web which has a mass of 254.6 g/m^2. These two thermal liners have relatively close masses but different fabric structures. As such, analyses of the data obtained from fabric systems D-2 and D-3 as well as M-2 and M-3 may show the effect of the structure of the thermal liner on the performance of the fabric systems.

The effect of the position of the moisture barrier on the thermal protection and the stored energy effect in double layer (D-5 and D-6) and multilayer fabric systems (M-3, M-4 and M-5) was analyzed by positioning the moisture barrier from the outermost to the innermost layer of the fabric systems.

Fabric physical properties

Fabric physical properties such as mass, thickness, density and air permeability, thermal resistance as well as water vapor diffusion were measured under standard conditions (20±2°C, 65±5% RH) as follow:

Mass

The conditioned mass of each fabric was determined according to CAN/CGSB-42 No.5.1-M90 (CGSB, 2004). The mass was calculated in grams per unit area (g/m^2).

Thickness

The fabric thickness was tested according to ASTM D 1777-96 under pressure of 1 kPa (ASTM, 2011). Ten specimens of each sample were tested.

The fabric thickness was also measured under pressure of 13.8 ± 0.7 kPa (Chapter 5) a possible compression pressure which is indicative of the compression caused by individuals' regular activities such as leaning, squatting or sitting according to ASTM standard F 2731 (ASTM, 2010).

Air permeability

The fabric air permeability was tested according to ASTM D 737-04 (ASTM, 2012a). The air pressure differential was adjusted to 12.7 mm (0.5 inch) of water which was relatively low (approximately 125 Pa). Ten specimens of each sample were tested.

Fabric density

The density of the fabric (g/cm^3) was determined by dividing the mass of the fabric (g/m^2) by the thickness (m) at the two different pressures (1kPa and 13.8 kPa) and applying a conversion factor.

Fabric Count

Fabric count was determined according to ASTM D3775-12 (ASTM, 2012b). The average number of five specimens of warp yarns and filling yarns per 25 mm of the fabric were calculated, (fabric count (yarn/cm)= warp count× weft count).

Heat and moisture transfer properties

Fabric heat and moisture properties such as steady state heat transmission, water vapor diffusion and the liquid penetration through the fabric were determined.

Thermal resistance (R_{ct})

The thermal resistance R_{ct} of each fabric system was determined according to ISO 11092 (ISO, 2014) under standard environmental conditions (20°C and 65% relative humidity). Three specimens were tested.

Water vapor diffusion

Resistance of material to water vapor diffusion was determined according to CAN/CGSB-4.2 No. 49-99 (CGSB, 1999). Because the resistance of the fabric system exposed to hot water splash was to be determined, the resistance to water vapor diffusion was measured from the face of the fabric to the back side of the fabric. As such, the face of the fabric was placed next to the water cell and the back side of the fabric to the dry air flow. The air flow was adjusted to 4± 0.5 L/min. The average diffusion resistance of the sample tested in millimeter equivalent thickness of still air was reported as the resistance of the test specimen to water vapor diffusion. Only one specimen was tested for each fabric system.

Liquid penetration test

Liquid penetration through the fabric was tested using a blotter paper which is recommended in Standard AATCC 42 (AATCC, 2000). This method was used to capture the penetrated liquid through the fabric system. The weight of the blotter paper was measured before and after the test and the difference was used as the impact penetration of the liquid. The amount of water stored in the fabric was also measured by weighing the fabric before and after the test. This can be used to estimate the stored liquid within the structure of the fabric system.

Detailed construction and physical properties of the fabric systems used in Chapters 4 and 5 are depicted in Tables 3.5, and the the fabric systems used in Chapters 7 and 8 are shown in Table 3.6. The numbers shown in Tables 3.5 and 3.6 have low standard deviations and typically the standard deviation values were within 5% of the mean.

Table 3.5. Construction and physical properties of the fabric systems used in Chapters 4 and 5.

Assembly code and description		Mass (g/m^2)	Thickness (mm)[a]		Density (g/cm^3)		Air permeability ($cm^3/cm^2/s$)	R_{ct} ($m^2.°C/W$)	Chapter
			Pressure: 1 (kPa)[a]	Pressure: 13.8 (kPa)	Pressure: 1 (kPa)	Pressure: 13.8 (kPa)			
SS-1	Fabric AA	211	0.51	0.48	0.41	0.44	17.1	0.070	4 & 5
SS-2	Fabric BB	255	0.66	---	0.39	---	14.1	0.075	4
SS-3	Fabric CC	229	0.51	---	0.45	---	1.65	0.076	4
SS-4	Fabric DD	412	0.67	0.57	0.61	0.72	0	0.074	4 & 5
DD-1	Fabric AA+ Thermal Liner AA	382	1.54	1.16	0.248	0.329	13.9	0.1174	4 & 5
DD-2	Fabric AA+ Thermal Liner BB	544	4.03	2.63	0.135	0.207	12.5	0.1687	4 & 5
DD-3	Fabric AA+ Moisture Barrier AA	397	1.54	1.09	0.257	0.364	0	0.0946	4 & 5
DD-4	Moisture Barrier AA+ Fabric AA	397	1.54	1.09	0.257	0.364	0	0.0930	4 & 5
MM-1	Fabric AA+ Moisture Barrier AA+ Thermal Liner AA	568	2.22	1.80	0.255	0.316	0	0.1255	4 & 5
MM-2	Fabric AA+ Moisture Barrier AA+ Thermal Liner BB	730	4.78	3.40	0.152	0.215	0	0.1835	4 & 5

"---" means that thickness and density under 13.8 kPa was not measured for the fabrics.

Table 3.6. Construction and physical properties of the fabric systems used in Chapter 7 and 8.

Assembly code (description)	Mass (g/m^2)	Thickness (mm)	Density (g/cm^3)	Air permeability ($cm^3/cm^2/s^1$)	Rct ($m^2.°C/W$)	Diffusion resistance (mm still air)
S-1 (Moisture Barrier A)	214	0.41	0.52	0	0.074	92.00
S-2 (Moisture Barrier B)	188	0.31	0.61	0	0.074	62.66
S-3 (Moisture Barrier C)	272	0.63	0.43	0	0.084	38.04
S-4 (Fabric A)	246	0.54	0.45	10.06	0.077	6.06
S-5 (Fabric B)	213	0.61	0.35	25.62	0.080	3.47
S-6 (Fabric C)	204	0.55	0.37	33.80	0.074	3.61
S-7 (Fabric D)	229	0.51	0.45	0.98	0.076	22.15
S-8 (Fabric E)	412	0.67	0.61	0	0.073	118.57
S-9 (Fabric F)	503	0.38	1.32	0	0.062	938.03
D-1 (Fabric A+ Thermal Liner A)	421	1.43	0.29	8.77	0.109	---
D-2 (Fabric A+ Thermal Liner B)	503	1.84	0.27	8.23	0.120	---
D-3 (Fabric A+ Thermal Liner C)	500	2.54	0.20	8.64	0.136	---
D-4 (Fabric A+ Thermal Liner D)	552	3.13	0.18	8.26	0.167	---
D-5 (Fabric A+ Moisture Barrier A)	459	0.91	0.50	0	0.092	---
D-6 (Moisture Barrier A+ Fabric A)	459	0.91	0.50	0	0.118	---
M-1 (Fabric A+ Moisture Barrier A+ Thermal Liner A)	635	1.88	0.34	0	0.119	---
M-2 (Fabric A+ Moisture Barrier A+ Thermal Liner B)	718	2.29	0.31	0	0.125	---
M-3 (Fabric A+ Moisture Barrier A+ Thermal Liner C)	714	3.02	0.24	0	0.145	---
M-4 (Moisture Barrier A+ Fabric A+ Thermal Liner C)	714	3.02	0.24	0	0.148	---
M-5 (Fabric A+ Thermal Liner C+ Moisture Barrier A)	714	3.02	0.24	0	0.141	---
M-6 (Fabric A+ Moisture Barrier A+ Thermal Liner D)	765	3.62	0.21	0	0.166	---

The "----"means that the diffusion resistance was not determined.

Contact angle

Contact angle, which is a direct characterization of the fabric wettability, was determined using a Ramé-hart contact angle goniometer (Ramé-hart Instrument Co., Succasunna, New Jersey). A sessile drop technique was used to measure contact angles of water on the fabric systems' surfaces. A 3 μL distilled water droplet was placed onto the surface of the fabrics using a microsyringe. The contact angles were obtained by the goniometer software by the analysis of the drop profile. The apparatus is equipped with a high-speed camera (100 frames per second). Three specimens of each sample were tested. Each specimen contained different warp and weft yarns. More details on the fabric systems used in this thesis can be found in Appendix A.

Garment system

The garments selected for this study in Chapter 6 were thermal protective garment systems which are commercially available in the market and typically worn by industrial workers which are commercially available in the market. The details of the coveralls are presented in Table 3.7. Garments G-1 to G-10 are single layer coveralls. Garment G-11 is a double layer coverall with G-10 as the outer layer plus a FR cotton quilted Arcxel^{TM} lining. Garments G-12 and G-13 have bib pants and a separate jacket. The coveralls G-7, G-8 and G-9 were chosen to represent close-fitting, fitted and loose-fitting size, respectively, in order to investigate the effect of garment fit on the thermal performance of the coveralls exposed to hot water spray. The pockets consist of in-seam pockets, rear patch pockets and chest patch pockets with a flap. Garments G-1, G-3, G-10, G-11 and G-13 also have reflective tape. The garments have a top fly at the center of the garment as well as a double-folded collar.

Please note that Garments G-2 and G-6 were constructed using fabrics used in Chapters 4-5 and 7-8:

- Garment G-2 was constructed using fabric CC (Chapter 4-5)/ D (Chapter 7-8), and
- Garment G-6 was constructed using fabric DD (Chapter 4-5)/ E (Chapter 7-8).

Table 3.7. Specification of the thermal protective garments.

Garment code	Garment System	Fiber Content	Size	Density (g/cm^3)	Thickness[a] (mm)	Mass[b] (g/m^2)	Air Permeability[c] ($cm^3/cm^2/s$)	Average Air gap (mm)
G-1	Single layer	100% Nomex® IIIA	42	0.28	0.60	169	25.8	25.1
G-2	Single layer	100% Nomex® IIIA	42	0.45	0.51	229	1.65	---
G-3	Single layer	88% cotton and 12% nylon	42	0.38	0.62	237	26.9	26.1
G-4	Single layer	88% cotton and 12% nylon	42	0.47	0.65	305	18.3	27.1
G-5	Single layer	88% cotton and 12% nylon with polymer finishing	42	0.49	0.66	322	0	29.7
G-6	Single layer	88% cotton and 12% HT nylon with polymer finishing	42	0.61	0.67	412	0	27.8
G-7	Single layer	88% cotton and 12% nylon	40	0.44	0.69	305	5.62	25.5
G-8	Single layer	88% cotton and 12% nylon	42	0.44	0.69	305	5.62	28
G-9	Single layer	88% cotton and 12% nylon	44	0.44	0.69	305	5.62	31
G-10	Single layer	100% cotton	42	0.54	0.67	360	2.97	33.7
G-11	Double layer	FR cotton/quilted lining Arcxel™	42	0.38	1.91	730	2.16	38.5
G-12	Bib pants and a separate jacket	Polyvinyl chloride-coated cotton	42	0.92	0.49	450	0	---
G-13	Bib pants and a separate jacket	Polyurethane-coated Nomex®IIIA knit	42	0.22	1.19	260	0	---

[a] The fabric thickness was tested according to ASTM D 1777-96 under the pressure of 1kPa with a Coefficient of Variation (CV) of 1-1.5%. [b] Measured according to ASTM D 3776 with a Coefficient of Variation (CV) of 1–1.5%. [c] The fabric air permeability was tested according to ASTM D 737-04 with a Coefficient of Variation (CV) of 1–1.5% (Lu, Song, & Li, 2013).

The air gap sizes for Garments G-12 and G-13 were not measured because each garment consists of bib pants and a separate jacket and determination of air gap was difficult. A Vitus 3-D whole body scanner (Human Solutions GmbH, Kaiserslautern, Germany) was used for the determination of air gap between the clothing and the manikin surface. A motionless male manikin was used, scanned nude and dressed with each thermal protective coverall. A minimum of three tests were conducted for each ensemble. In order to provide as much as possible the same air gap distribution in the spray manikin and the scanned manikin, the same procedures were used to dress the spray and the scanned manikins. In addition, the same static position as the spray mannequin was chosen for the scanned mannequin to reproduce the air gap as accurately as possible in both manikins (Lu, Song, & Li, 2013; Mah & Song, 2010a).

Hot liquid splash apparatus

To assess the protection provided by a fabric when exposed to a hot liquid, a modified apparatus (based on ASTM F 2701-08, Evaluating Heat Transfer through Materials for Protective Clothing upon Contact with a Hot Liquid Splash) was used (Figure 3.1).

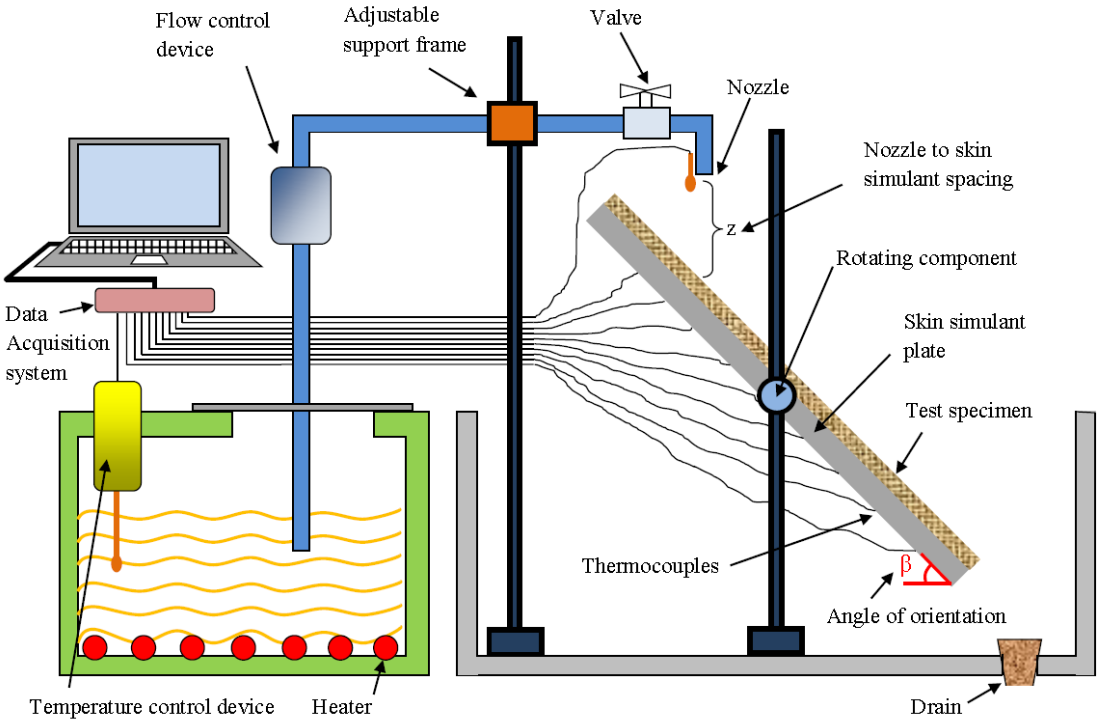

Figure 3.1. The hot liquid splash test apparatus used in Chapters 7 and 8.

The apparatus monitors the liquid temperature by a temperature control device and heats the liquid up to 150 °C. The apparatus is equipped with a liquid reservoir with a capacity of 8 L. The nozzle has a circular shape with 10 mm diameter which sprays the liquid onto a flat skin simulant plate. A thermocouple is installed near the spout to record the temperature of the liquid flow. A flow control device is used which gives the capability to regulate the flow of the liquid up to 90 mL/s. The height of the nozzle from the skin simulant sensor board is adjustable to a desirable nozzle-to-plate spacing (z). The apparatus is also equipped with a valve to control the exposure time manually. The skin simulant plate is mounted on a rotating component in order to regulate the angle of the sensor board with respect to the fluid stream. This angle is introduced as the angle of orientation β and can be varied between 0° to 70° (Figure 3.1).

The skin simulant material

The material is an inorganic material, colerceran, made of calcium, aluminum, silicate, asbestos and a binder (Crown, Rigakis, & Dale, 1989; Dale et al., 1992) . The thermal inertia ($k\rho c$) of this material closely simulates the thermal inertia of the skin. Therefore, this material can be used to simulate human skin in this study. This material is the same as the material which has been used for the skin simulant sensors in the University of Alberta thermal mannequin (Dale et al., 1992). The thermocouple wire used was 30-gauge copper constantan. A hole was drilled along the depth of the skin simulant at three locations shown in Figure 3.2. the thermocouple wire was rolled flat prior to installation and was mounted at the surface of the skin simulant board. The wire was held on the surface of the skin simulant plate with a special high temperature epoxy-phenolic adhesive. More detail on the skin simulant material and heat flux sensor installation can be found in Crown and Dale (1992). The surface mounted thermocouple on the skin simulant plate is referred to as skin simulant sensor or heat flux sensor in this thesis.

The skin simulant plate used in Chapters 4 and 5

The skin simulant board is square with dimensions of 404×253 mm and a thickness of 21 mm. A schematic illustration of the board can be seen in Figure 3.2. The radial locations are referred to as y/d locations for convenience, based on the ratio of distance from the stagnation point (y), where the jet of hot liquid hits the board, to the nozzle diameter (d) of 10 mm. One thermocouple is mounted at the center of the board and the other two thermocouples are mounted along the

longitudinal axes y^--y^+, 100 mm from the center point. Another thermocouple was mounted at the nozzle in order to monitors the temperature of the hot liquid at the nozzle exit. Table 3.8 shows non-dimensional displacement of each heat flux sensor. In 45-degree orientation, thermocouple (a) and in horizontal orientation, thermocouple (b) is exposed to hot water jet directly. The locations of the sensors are also illustrated in Figures 3.2.

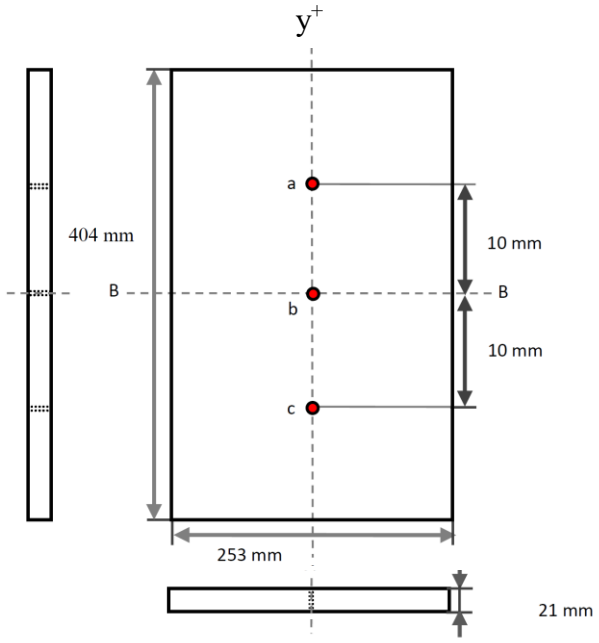

Figure 3.2 Skin simulant sensor and radial locations of the sensors a, b and c.

Table 3.8. Non-dimensional displacement of sensors and the corresponding thermocouples in 45-degree and horizontal orientation.

45-degree Orientation			Horizontal Orientation		
sensor	Thermocouple	Non-dimensional displacement, y/d	sensor	Thermocouple	Non-dimensional displacement, y/d
Upper*	a	0	Side	a	-10±1
Middle	b	10±1	Middle*	b	0
Lower	c	20±1	Side	c	+10±1

* Sensor at stagnation point.

The skin simulant plate used in Chapters 7 and 8

In the skin simulant used in Chapter 4, the three sensors were able to measure the transmitted and the discharged energy at the impingement point as well

as the energies at 10 and 20 nozzle diameters from the impingement point in the 45-degree orientation (β=45°) and 10 nozzle diameters from the stagnation point in the horizontal orientation (β=0°). However, when the water jet hits the surface of the fabric, it spreads on the fabric. As such, 29 heat flux sensors , which were spread on the skin simulant plate, were considered for this study (Table 7.1). The large number of thermocouples (29) provides more data in comparison to skin simulate plate used in Chapter 4. The hot liquid flow pattern is expected to be symmetrical with respect to y-axis when the impingement angle is not zero. Also, in horizontal orientation of the skin simulant board, the flow of the hot liquid is assumed to be symmetrical with respect to x-axis and y-axis. As such, half of the skin simulant flat plate was instrumented (Figure 3.3).

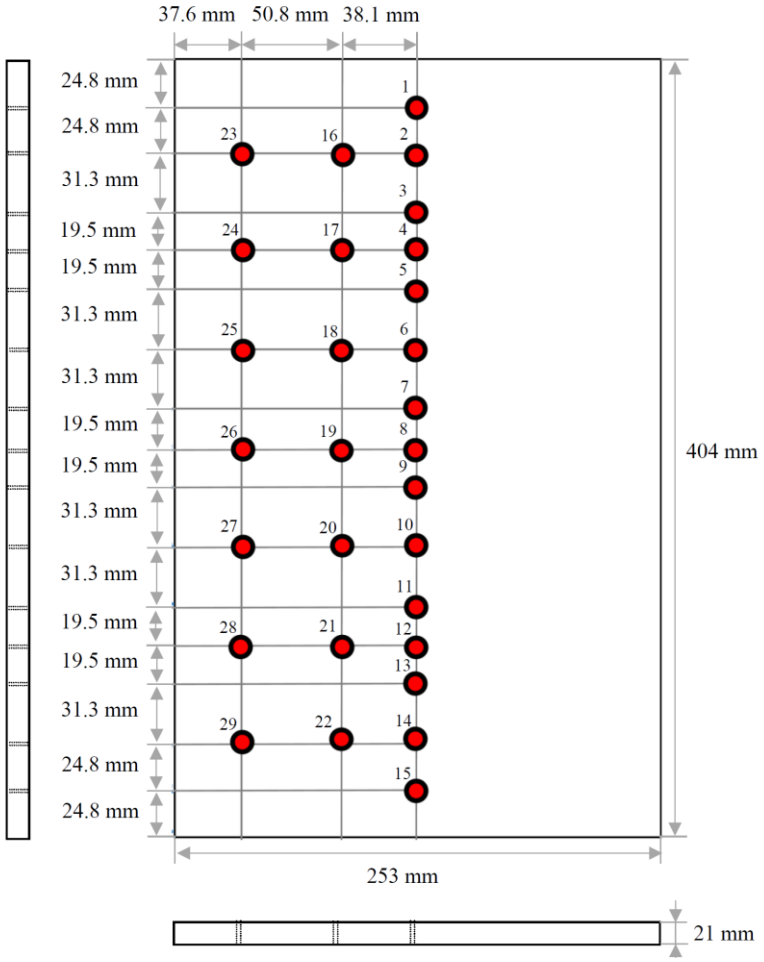

Figure 3.3. Schematic illustration of the skin simulant plate.

Thermocouple 4 is located at the impingement point for an orientation angle of 45 degrees (Figure 3.4 (a)). The flow of the liquid is assumed to be symmetric with respect to y-axis and is in the negative y direction in 45-degree orientation. The locations of the thermocouples (x, y) for 45 degrees are shown in Figure 3.4 (a) and Table 3.9. In Figure 3.4 (a), the intersection of x- and y-axis is the stagnation point and the origin of the coordinates. The dimensionless displacement for the thermocouples in the 45-degree orientation is defined as (±x/d) and (y/d) where d represents nozzle diameter (10 mm). The negative y/d refers to the thermocouples affected by the main direction of hot liquid flow from the origin of the coordinates in the negative y direction. The main flow is in accordance to the component of the acceleration due to gravity in the direction of the acceleration. The positive y/d refers to the thermocouples that are affected opposite to the main direction of the hot liquid flow (positive y-axis). The non-dimensional displacements in 45-degree orientation are also shown in Table 3.4.

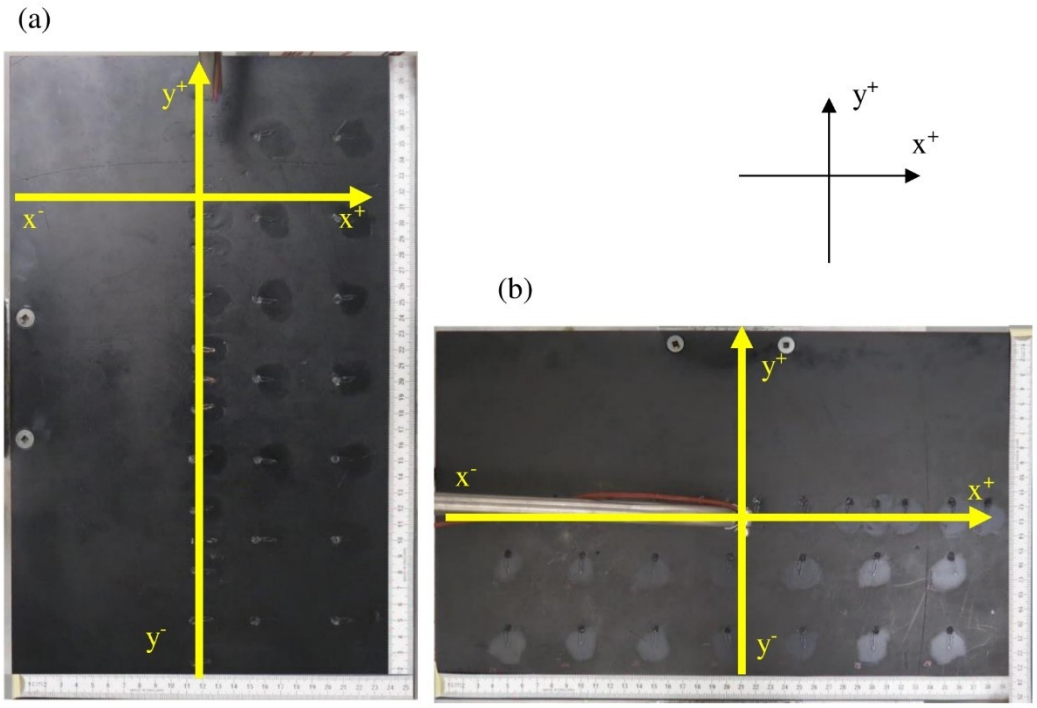

Figure 3.4. Skin simulant plate with 29 thermocouples and the x-axis and y-axis in (a) inclined orientation (β=45°) and (b) horizontal orientation (β=0°).

Table 3.9. Location of the thermocouples relative to the stagnation point in inclined orientation of the skin simulant plate (β=45°). x/d and y/d are non-dimensional displacement of the sensors in x and y direction with respect to the impingement point.

	Sensor Number	x (mm)	y (mm)	x/d	y/d
	1	0.0	75.6	0.0	7.6
	2	0.0	50.8	0.0	5.1
	3	0.0	19.5	0.0	2.0
Impingement point	**4**	**0.0**	**0.0**	**0.0**	**0.0**
	5	0.0	-19.5	0.0	-2.0
	6	0.0	-50.8	0.0	-5.1
	7	0.0	-82.1	0.0	-8.2
	8	0.0	-101.6	0.0	-10.2
	9	0.0	-121.1	0.0	-12.1
	10	0.0	-152.4	0.0	-15.2
	11	0.0	-183.7	0.0	-18.4
	12	0.0	-203.2	0.0	-20.3
	13	0.0	-222.7	0.0	-22.3
	14	0.0	-254.0	0.0	-25.4
	15	0.0	-278.8	0.0	-27.9
	16	38.1	-50.8	3.8	-5.1
	17	38.1	0.0	3.8	-0.0
	18	38.1	-50.8	3.8	-5.1
	19	38.1	-101.6	3.8	-10.2
	20	38.1	-152.4	3.8	-15.2
	21	38.1	-203.2	3.8	-20.3
	22	38.1	-254	3.8	-25.4
	23	50.8	-50.8	5.1	-5.1
	24	50.8	0	5.1	-0.0
	25	50.8	-50.8	5.1	-5.1
	26	50.8	-101.6	5.1	-10.2
	27	50.8	-152.4	5.1	-15.2
	28	50.8	-203.2	5.1	-20.3
	29	50.8	-254.0	5.1	-25.4

In horizontal orientation, thermocouple 8 is exposed to hot water jet at the stagnation point. The location of the thermocouples (x, y) from the stagnation point for orientation angle of 0° are shown in Figure 3.4 (b) and Table 3.10. In Figure 3.4 (b), the intersection of x- and y-axis is the stagnation point and the origin of the coordinates. The flow of hot liquid is assumed symmetric with respect to x-axis and y-axis. The non-dimensional displacement in horizontal orientation is defined as (x/d) and (y/d) for horizontal orientation for x-axis and y-axis respectively. The non-dimensional displacements in 45-degree orientation are also shown in Table

3.10. More thermocouples were installed near the impingement points (thermocouples 4 and 8) in order to observe the effect of flow in the areas immediately after the stagnation region.

Table 3.10. Location of the thermocouples relative to the stagnation point in horizontal orientation of the skin simulant plate (β=0°). x/d and y/d are non-dimensional displacement of the sensors in x and y direction with respect to the impingement point.

	Sensor Number	x (mm)	y (mm)	x/d	y/d
	1	-177.2	0.0	-17.7	0.0
	2	-152.4	0.0	-15.2	0.0
	3	-121.1	0.0	-12.1	0.0
	4	-101.6	0.0	-10.2	0.0
	5	-82.1	0.0	-8.2	0.0
	6	-50.8	0.0	-5.1	0.0
	7	-19.5	0.0	-2.0	0.0
Impingement point	**8**	**0.0**	**0.0**	**0.0**	**0.0**
	9	19.5	0.0	2.0	0.0
	10	50.8	0.0	5.1	0.0
	11	82.1	0.0	8.2	0.0
	12	101.6	0.0	10.2	0.0
	13	121.1	0.0	12.1	0.0
	14	152.4	0.0	15.2	0.0
	15	177.2	0.0	17.7	0.0
	16	-152.4	-38.1	-15.2	-3.8
	17	-101.6	-38.1	-10.2	-3.8
	18	-50.8	-38.1	-5.1	-3.8
	19	0.0	-38.1	0.0	-3.8
	20	50.8	-38.1	5.1	-3.8
	21	101.6	-38.1	10.2	-3.8
	22	152.4	-38.1	15.2	-3.8
	23	-152.4	-50.8	-15.2	-5.1
	24	-101.6	-50.8	-10.2	-5.1
	25	-50.8	-50.8	-5.1	-5.1
	26	0.0	-50.8	0.0	-5.1
	27	50.8	-50.8	5.1	-5.1
	28	101.6	-50.8	10.2	-5.1
	29	152.4	-50.8	15.2	-5.1

The larger number of thermocouples were employed to observe the effects of the flow of hot liquid on thermal performance of the fabric systems. A schematic illustration of the distribution of the sensors is shown in Figure 3.5. Each heat flux sensor was associated with an area on the skin simulant plate. The area of each heat

flux sensor was determined by location points approximately equidistant to the surrounding heat flux sensors.

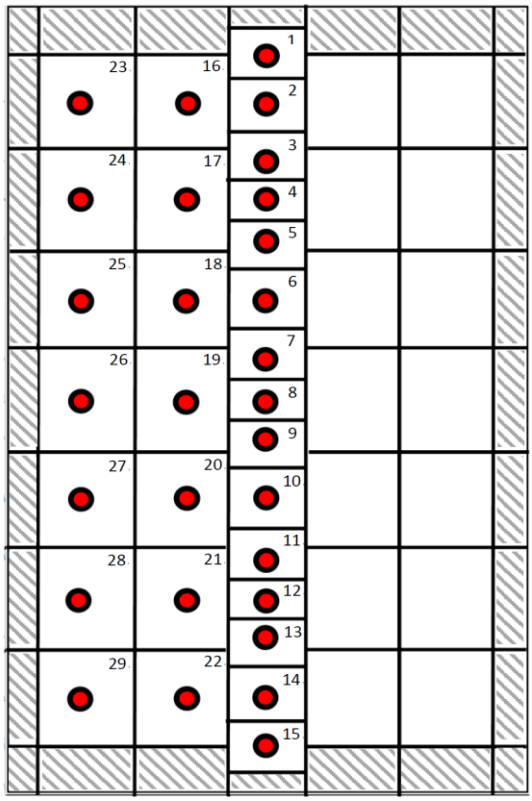

Figure 3.5. Sensor area and their corresponding numbers on the skin simulant plate.

The points were joined by straight lines and the area of each heat flux sensor encompassed by the straight lines corresponds to the area that the sensor represents. In order to determine the areas of the heat flux sensors closer to the edges of the skin simulant board (sensors 1, 16, 23 to 29, 22 and 15), the equidistance between the heat flux and the edge of the sensor board is considered. As such, the areas shown with diagonal stripes in Figure 3.5. are not considered in the percentage of the weighted area of the abovementioned sensors (24.5%). Therefore, the maximum skin simulant area that was considered for the measurement is 75.5%. Based on (1) the area each heat flux sensor represented and (2) the total area of the skin simulant plate, the percentage of the weighted area each sensor represents (A_i) on the surface was measured and shown in Table 3.11.

Table 3.11. Sensor weighted area

Sensor Number	Sensor weighted area (A_i)		Sensor Number	Sensor weighted area (A_i)
1	0.92		16	2.18
2	1.05		17	2.21
3	0.95		18	2.21
4	0.72		19	2.21
5	0.95		20	2.21
6	1.17		21	2.21
7	0.95		22	2.18
8	0.72		23	2.17
9	0.95		24	2.20
10	1.17		25	2.20
11	0.95		26	2.20
12	0.72		27	2.20
13	0.95		28	2.20
14	1.05		29	2.17
15	0.92			
Total				75.5

In this study, the skin simulant plate was exposed to a sudden heat flux which results in a temperature rise at the surface of the skin simulant plate. The skin simulant plate was assumed to be at an initially uniform temperature. As such, a 30 minute time interval was chosen between the tests in order to have uniform initial temperatures within the sensors (Crown & Dale, 1992).

A sudden heat flux exposure causes a non-linear temperature gradient within the plate. The transient heat conduction through a flat plate can be described by the heat diffusion equation. In order to solve this equation, it was assumed the thermo-physical properties of the skin simulant remained constant during and after the exposure of hot liquids. It was also assumed that heat flows in one direction into a semi-infinite skin-simulant board (transient one-dimensional heat transfer into a semi-infinite plate). As such, the temperature at the backside of the skin simulant plate is required not to be affected by the sudden rise in front side temperature in order to fulfill the semi-infinite solid theory. On the other hand, the length of the time for which the condition is valid depends on the thickness of the skin simulant provided that the thermal properties are known and assumed to be constant. Therefore, the length of the hot water exposure on the skin simulant plate needs to be determined so that the temperature rise at the surface does not affect the

back temperature of the plate and skin simulant plate behaves like a semi-infinite solid.

Equation 3.1 shows the condition under which the skin simulant as a semi-infinite solid to a step change of surface heat (Lawton, 1996, pp. 55-57).

$$\begin{cases} \theta \geq 2 \\ \theta = \dfrac{L}{2\sqrt{t(k/\rho c_p)}} \end{cases} \tag{3.1}$$

Where:

k = skin simulant thermal conductivity,

ρ = skin simulant density,

c_p = skin simulant specific heat,

t = the time that the skin simulant plate behaves like a semi-infinite solid,

L = the skin simulant plate thickness.

Solving for time t in Equation 3.1 employing the thermal properties of the skin simulant shown in Table 3.12 (Crown & Dale, 1992), the time that the skin simulant plate behaves like a semi-infinite solid can be determined. Therefore, after exposure to a sudden change in surface heat flux, the skin simulant will behave like a semi-infinite solid for approximately 150 s as an exposure at the surface is not expected to affect the temperature at the back of the skin simulant during this time period. In this thesis, the duration of most thermal exposures (including cooling period) was chosen to be less than 150 s. However, in a few cases in Chapter 4, where the TPP approach were employed in order to predict second degree burn for some thick fabrics exposed to hot water, the thermal exposures were longer than 150 s, which may affect the semi-infinite solid approximation. In these cases, the changes from semi-infinite solid behavior are expected to be relatively minor since the values of the heat flux incident on the sensor will be low at the end of these longer exposures.

Table 3.12. Skin simulant thermal properties (Crown & Dale, 1992) .

Thermal Property	Skin Simulant
Thermal conductivity, k $(W/m \cdot K)$	0.97
Density, ρ (kg/m^3)	1877
Specific heat, c_p $(J/kg \cdot K)$	1205
Thermal diffusivity, α (m^2/s)	4.29 x 10^{-7}
Thermal inertia, $k\rho c$ $(J^2/m^4 \cdot °C^2 \cdot s)$	2.2 x 10^6

The fabric systems were evaluated by exposure to radiant heat, steam and hot water. The equipment and test methods provide the opportunity to explore the behavior of the fabric systems under various thermal hazards. For the thermal exposures in this study, the skin-simulant sensors that were used are known to respond to heat transfer as closely as possible to human skin (Dale et al., 1992).

Steam apparatus

The thermal performance of protective clothing exposed to steam is tested via a steam/hot water splash apparatus developed at the University of Alberta (Ackerman et al., 2011). The steam apparatus is equipped with a Teflon-plated sample holder which is equipped with a skin stimulant sensor (Figure 3.6). The steam was generated in a 3 kW boiler. The generated steam is able to impinged upon the skin simulant vertically up to a pressure of 250 kPa. The fabric systems were exposed to steam at 150°C. The test specimen for a given fabric system were cut to 200 mm by 200 mm and were conditioned at 20 ± 2°C with 65% relative humidity for at least 24 hours prior to the testing. The specimen was placed on a Teflon-plated sample holder equipped with a skin stimulant sensor. The generated steam impinged on the fabric specimen at a pressure of 200 kPa. In this study, it was intended to expose the fabric and let it cool by natural convection. As such, an open jet spacing with a nozzle-to-sensor spacing of 5 cm was used to expose the fabric systems to steam. The nozzle-to-sensor spacing was the maximum spacing possible in this apparatus in order to provide enough space for the compression of the specimen during the cooling period.

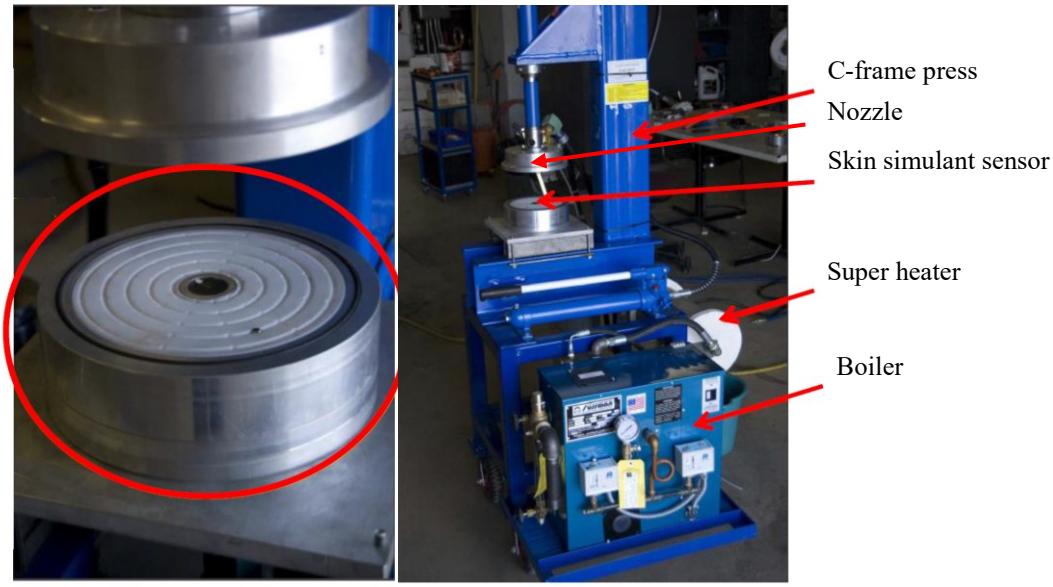

Figure 3.6. Steam apparatus.

Cone calorimeter apparatus

To measure the fabric's protective performance against radiant-heat exposure, a cone calorimeter test was conducted with a modified ASTM E 1354 testing approach. A truncated cone-shaped electrically heated coil (5000 W, 240 V) is controlled to deliver a heat flux of 50 kW/m^2. The specimens were cut to 15 cm by 15 cm and mounted on a 10 cm by 10 cm sensor board horizontally below the heated coil. There was no air gap between the fabric and the test sensor. The exposed area of the fabric was 10 cm by 10 cm. The heat flux is expected to be uniform within the central 50 mm by 50 mm area of the specimen (Rezazadeh, 2013). Therefore, the portion of the fabric in contact with the skin simulant, which has a diameter of 19 mm, is expected to receive a uniform heat flux. A transverse shutter was used to protect the specimen from the heat source before the test and during the cooling period (Figure 3.7).

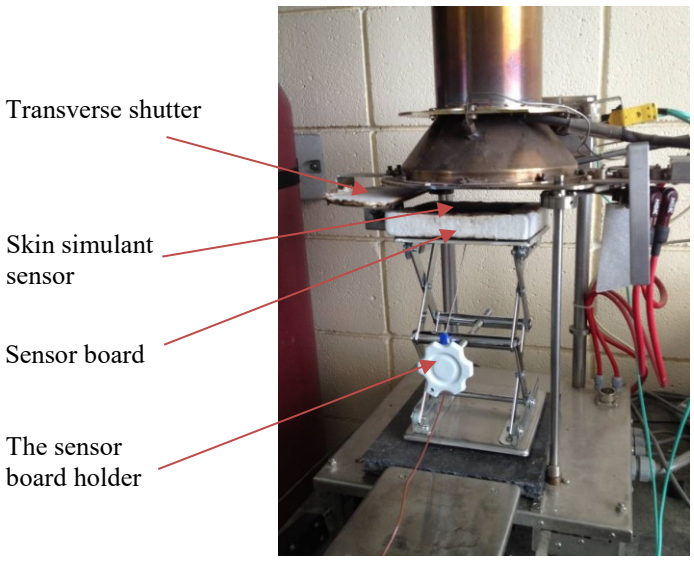

Figure 3.7. Cone calorimeter apparatus.

The experimental procedures for the selected fabric and garment systems will be explained later in each chapter.

Fabric compressor

Test methods in this research in Chapter 5, were modified for the stored energy study. In order to apply the compressive discharge to the fabric systems, a compressor assembly was made to provide the pressure of 13.8 ± 0.7 kPa (2.0 ± 0.1 psi) in order to simulate an individual's regular activities such as leaning, squatting or sitting (ASTM, 2010). The compressors are shown in Figure 3.8.

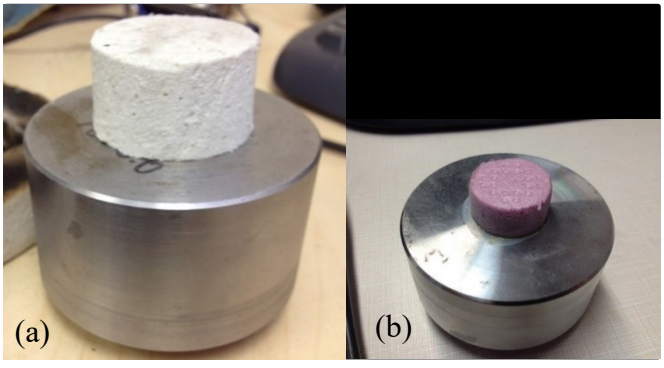

Figure 3.8. Compressors with (a) Kaowool block and (b) polystyrene block.

The compressors were constructed of bodies made from steel and two different compressor blocks. Compressor (a) was equipped with a Kaowool board

block with thermal conductivity of 0.06 W/m°C. Compressor (a) was used to compress the specimens which were exposed to radiant heat. Compressor (b) has a block made of polystyrene with an equivalent thermal conductivity (0.06 W/m°C). Compressor (b) was used in steam and hot liquid experiments. The small size of compressor (b) makes it possible to compress the fabric in steam tests where the nozzle to fabric spacing is 5 cm. In addition, polystyrene has a low water absorption (less than 2%) which made it suitable for water tests. In this research, where compressive approach was employed, the specimens were compressed manually by simply leaving the compressor on the fabric 5 s after the termination of the exposure. Based on the area of the compressor block and the weight of the attached steel, a total pressure of 13.8 ± 0.7 kPa was applied to the fabric.

Instrumented spray mannequin

The performance of the garments exposed to hot water splash was measured by the instrumented spray male mannequin developed by The University of Alberta Protective Clothing and Equipment Research Facility (Ackerman et al., 2011). The mannequin with size of 40R was equipped with 110 skin simulant sensors uniformly distributed over its surface (Crown & Dale, 1992). Four groups of cylinder spray jets, with a set of three-automatically-controlled-valve-bottom-up-nozzle assembly in each group, were employed to spray the mannequin. Hot water at 85°C and was ejected from the 12 nozzles with a pressure of 250 kPa in order to simulate hot water splash in an industrial occupational environment. Hot liquid can be sprayed simultaneously by the twelve nozzles. A computer-controlled data acquisition system is set to read the temperature every 0.1 s and the in-house software was used to obtain the skin burn distribution over the body, the transmitted and the discharge energy during and after exposure. A bio-heat transfer skin model in conjunction with Henriques Burn Integral was employed to predict second and third degree burn time. More detail on the burn evaluation criteria can be found in Crown and Dale (1992) and (ISO, 2017).

According to ISO 13506: 2008, the test results can be based on the following two measurements: the total surface area of the manikin receiving second and third degree burns, and the total energy transferred to the surface of the manikin during data acquisition. Each heat flux sensor is associated with an area on the manikin surface. The area of each heat flux sensor is determined by location points equidistant to the surrounding heat flux sensors. The points are joined by straight

lines and corresponds to the area that the sensor represents on the surface of the manikin (Figure 3.9). The hands and the feet are not equipped with heat flux sensors. The surface areas that hands and feet represent on the test manikin are 5 and 7%, respectively. Therefore, the maximum manikin surface area that is considered for the measurement is 88%. Based on the area each heat flux sensor represents and the total area of the manikin, the percentage of the area each sensor represents on the surface of the manikin is measured and shown in Appendix B.

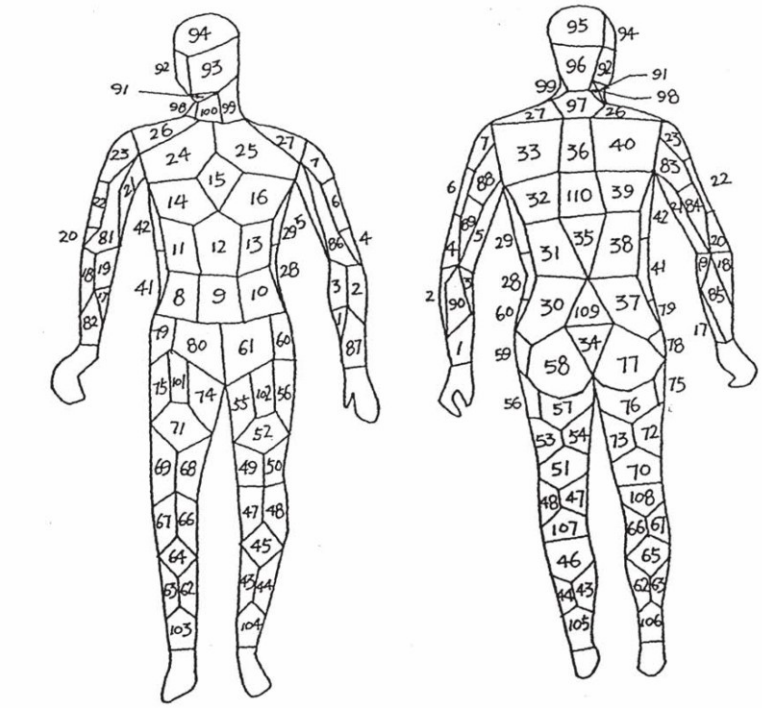

Figure 3.9. Sensor areas on the manikin and the corresponding heat flux sensor numbers (Crown & Dale, 1992). Reprinted with permission.

Data acquisition system

The apparatuses in this thesis are equipped with input cards with analogue-to-digital converters whose channels were assigned to the thermocouples mounted on the surface of the skin simulant sensors. The converter translates voltage input to temperature for copper-constantan thermocouples. The data acquisition system is set to read the temperature at one tenth of a second by employing DASYLab® software.

Burn evaluation criteria

The burn evaluation is used in Chapter 3 as well as Chapters 4, 5 and 7: the data acquisition system records the temperature at one tenth of a second, and Microsoft Excel software was employed to use the following steps in order to obtain the second and third degree burn times (Crown & Dale, 1992) (Figure 3.10).

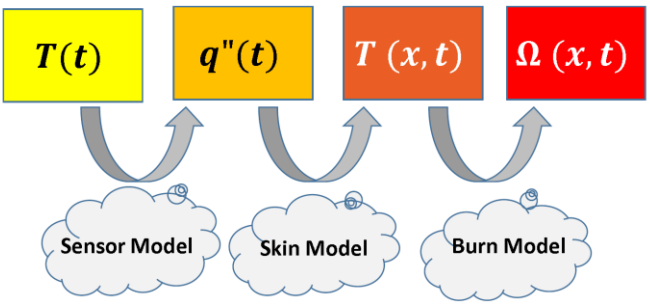

Figure 3.10 Experimental test setting.

Sensor model

Duhamel's theorem (Equation 3.2) was used in this study to calculate heat flux history from the surface temperature history recorded by the data acquisition system.

$$q_n(t) = \sqrt{\frac{k\rho c_p}{\pi}} \left[\sum_{i=1}^{n-1} \left(\frac{T_s(t_n) - T_s(t_i)}{(t_n - t_i)^{1/2}} - \frac{T_s(t_n) - T_s(t_{i-1})}{(t_n - t_{i-1})^{1/2}} + 2\frac{T_s(t_i) - T_s(t_{i-1})}{(t_n - t_i)^{1/2} + (t_n - t_{i-1})^{1/2}} \right) + \frac{T_s(t_n)}{t_n^{1/2}} + \frac{T_s(t_n) - T_s(t_{n-1})}{(\Delta t)^{1/2}} \right] \quad (3.2)$$

Where k = the thermal conductivity of the stimulant, W m°C^{-1}

ρ = the density of the stimulant, kg m^{-3}

c_P = the specific heat of the simulant, J kg^{-1} °C^{-1}

T_s= is the surface temperature of the simulant, °C

t = time, s.

The data acquisition system records the temperature and Microsoft Excel software was employed to convert the recorded temperatures to heat fluxes employing Duhamel's theorem as shown in Equation 3.2 (Torvi, 1997). In this model, it is assumed that the skin simulant plate is initially at uniform temperature. It is also assumed that the skin simulant is a semi-infinite solid with constant thermal properties and the heat transfer is one-dimensional. Based on the measured surface temperature, the surface heat flux was calculated by employing Equation 3.2. More details can be found in Crown and Dale (1992).

Skin model

A three-layer skin model and Henriques burn model is employed to predict the skin burn injury. The governing equation for heat transfer in skin model is described according to Equation 3.3 developed by Metha and Wong (Metha & Wong, 1973).

$$c_p \frac{\partial T}{\partial t} = k \frac{\partial^2 T}{\partial x^2} - \left(c_p\right)_b G(T - T_b) \qquad (3.3)$$

Where:

c_p = volumetric heat capacity of human tissue,

k = thermal conductivity of human tissue,

$(c_p)_b$ = volumetric heat capacity of blood,

G = the rate of blood perfusion,

T = the tissue temperature,

T_b = the perfusing blood temperature.

In this equation, it is assumed that the skin is opaque and the absorption of penetrating radiation by the tissue is negligible. In the epidermal layer, the blood perfusion (G) is zero due to its non-vascularity. The initial and the boundary conditions are as follows (Crown & Dale, 1992) :

$$\begin{cases} (1) t = 0, T = T_0(x) \\ (2)\ t > 0, x = 0 \\ -k_e \frac{\partial T}{\partial x} = q(t) - h(T - T_\infty) \text{ for opaque skin} \\ (3)\ t > 0, x = \delta_3, T = T_b \\ (4) \text{ Continuity of temperature and heat flux at the two interfaces at all times.} \end{cases} \quad (3.4)$$

where:

k_e= thermal conductivity of the epidermis,

$q(t)$ = radiation heat flux at the surface of the skin,

h = the overall surface heat loss coefficient,

T_∞ = the ambient temperature,

δ_3 = the distance of the deepest subcutaneous layer from the surface,

T_b = normal body temperature.

In order to investigate the performance of the thermal protective fabrics upon exposure to hot liquids in this thesis, different exposure times followed by more than 60 s cooling period were used. The range of exposure time in this thesis is from a second to more than two minutes of exposure. The prolonged exposure gives the blood the opportunity to regulate the imposed thermal energy prior to skin damage (Lipkin & Hardy, 1954; Weinbaum et al., 1984). As such, blood perfusion may have a positive effect in decreasing the skin temperature and prevention of burn injuries. In order to solve Equation 3.4 with the effect of the blood perfusion, it is necessary to assume that the temperature of the skin at basal layer is the same temperature as the blood (37°C). However, the temperature of the skin at basal layer is not 37°C. Therefore, it is assumed that the skin is at 33.5°C and the effect of blood flow is not considered in the analysis of the skin model (Crown & Dale, 1992).

The properties of the skin was used in this study are based on parameters reported in Crown and Dale (1992) and (ISO, 2017). In the Crown and Dale study,

which used body wide average properties, the results and the time to achieve second degree burn agreed with the experimental results obtained by Stoll et al. for the human forearm. As such, forearm skin properties are used in the skin model in order to provide a better fit to the experimental data originally obtained by Stoll et al. for the human forearm. The skin properties are shown in Table 3.13.

Table 3.13. Skin location, layers and their corresponding parameters.

Skin location		Parameters			
		Overall thickness of layer, $x\ (m)$	Thermal conductivity, $k\ (W/m \cdot ℃)$	Volumetric heat capacity, $c_P\ (J/m^3 \cdot ℃)$	Blood Perfusion rate, $G\ (m^3/s/m^3_{tissue})$
Body wide	Epidermis	0.00008	0.000255	4317.6	---
	Dermis	0.002	0.000523	3866.4	1.25×10^{-3}
	Subcutaneous	0.01	0.000167	2760	1.25×10^{-3}
	Blood	---	---	3996.2	---
forearm	Epidermis	0.000075	0.000628	4400	---
	Dermis	0.001125	0.000582	4184	---
	Subcutaneous	0.003885	0.000293	2600	---
	Blood	---	---	3996.2	---

Finite difference solution is employed to solve Equation 3.3 in order to predict temperature distribution and temperature history in the skin. More detail on the numerical solution method and calculation can be found in Crown and Dale (1992).

Burn Model

Once the temperature at basal layer and dermis-subcutaneous interface is predicted, Henriques burn criterion can be employed to predict the total damage by determining Ω value (Equation 2.2, Chapter 2, page 14). Henriques burn criterion reveals that when Ω value is less than 0.53, there is no damage at the basal layer. For the Ω value between 0.5 and 1.0 first degree burn occurs and for Ω values more than unity, second degree burn occurs (Henriques, 1947). This criterion can be used at any depth of the skin by employing an appropriate frequency factor (P) and activation energy (ΔE) for skin. Morse et al. compared predictions made using different values of the activation energy and pre-exponential factor with

experimental data, and determined that the Stoll values should be used for the epidermis (and second degree burn predictions) and that the Takata values should be used for the dermis (and third degree burn predictions) (Morse, Ticker, & Brown, 1975). These values are shown in Table 3.6.

Third degree burn was said to occur when the value of Henriques burn integral is equal to unity from the temperature history at the base of the dermis layer of skin. As such, by employing the appropriate use of the activation energy for skin, ΔE and P (Table 3.14), the Henriques burn integral was used to predict third degree burn at the base of dermal layer of skin.

Table 3.14. Frequency factor (P) and activation energy for skin (ΔE).

	Stoll et al. (2^{nd} degree burn)	Takata (3^{rd} degree burn)
$44℃ \leq T \leq 50℃$	$P = 2.1850 \times 10^{+124}$ $\Delta E/R = 93534.9$	$P = 4.322 \times 10^{+64}$ $\Delta E/R = 50000$
$T \geq 50℃$	$P = 1.8230 \times 10^{+51}$ $\Delta E/R = 39109.8$	$P = 9.389 \times 10^{+104}$ $\Delta E/R = 80000$

CHAPTER 4 EVALUATION OF THERMAL PROTECTIVE CLOTHING PERFORMANCE UPON EXPOSURE TO HOT LIQUID SPLASH[1]

Introduction

In this chapter, the effective thermal performance of the fabric system upon exposure to hot liquid splash is investigated. The effective thermal performance of the fabric system is comprised of two parts: (1) the prediction of the time to second degree burn and (2) the amount of stored thermal energy in the fabric system at the areas where a fabric system is exposed to an impinging jet. These areas include the area directly exposed to hot liquid (stagnation region) and the adjacent areas that are exposed to flow of hot liquid. The effective thermal protection provided by a fabric when exposed to hot liquid splashes has been investigated using a modified hot liquid splash apparatus, based on ASTM F 2701-08 (ASTM, 2008a). Also, the angle of orientation was varied between 0 (horizontal) and 45 degrees to determine the fabric system's effective protection performance under different exposure configurations.

In order to quantify the amount of stored thermal energy in the fabric system, a stored energy coefficient (ψ) is introduced. Also in this chapter, the effect of fabric properties, hot liquid properties and the experimental variables such as non-dimensional displacement of the sensors from the stagnation point (y/d) and the angle of orientation (β) on the effective thermal performance (ETPP) of the fabric system (second degree burn time and the stored energy coefficient) are explored.

---

[1] This chapter is an original work by the author. A portion of this chapter has been published in the Journal of Annals of Occupational Hygiene:

- Gholamreza, F., & Song, G. (2013). Laboratory evaluation of thermal protective clothing performance upon hot liquid splash. *Annals of Occupational Hygiene, 57*(6), 805-822. The author was responsible for the data collection, analysis as well as manuscript composition. G. Song was the supervisory author and provided critical review of the manuscript.

Other portions of this chapter were also presented at the following conference:

- Gholamreza, F., Song, G., & Ackerman, M. (2012). *Thermal protective clothing performance: hot liquid splash and its flow effect on skin burn.* Paper presented at the 5th European Conference on Protective Clothing and Nokobetef 10. Future of Protective Clothing: Intelligent or not, Valencia, Spain. The author was responsible for the data collection, analysis as well as manuscript composition. G. Song and M. Ackerman were the supervisory authors.

Experimental procedure

Selected fabrics (Table 3.1) and fabric systems (Table 3.2) were exposed to hot water, drilling mud, and canola oil at 85°C to examine the effects of liquid properties on effective thermal performance of the fabric systems. The hot liquid flow rate was adjusted to provide 1 L of liquid per 30 s.

The physical properties of the hot liquids are shown in Table 4.1. The drilling mud (SAGDRIL) is water based and manufactured by Schlumberger, Houston, Texas. Canola oil was the typical canola oil used for cooking available at the local supermarket.

The dynamic viscosity of the liquids was measured using a rheometer with a shear rate of 1.0 s^{-1} (Lu, Song, Ackerman, et al., 2013). It was found that the drilling mud was a non-Newtonian fluid with shear thinning behavior. Surface tension of the liquids was measured with a Krüss drop shape analysis system (DSA 10-MK2, Germany). Properties of the drilling fluid and canola oil were obtained by Lu et al. (2013).

Table 4.1. Properties of the hot liquids at 85°C

Liquid	Density (kg/m^3)	Dynamic Viscosity (Pa·s)	Specific Heat (kJ/kg·°C)	Thermal Conductivity (W/m·°C)	Surface Tension (N/m)
Distilled Water*	960	3.34×10^{-4}	4.19	0.61	0.062
Drilling mud**	900-920	1.0	2.5-3.5	0.5-0.6	0.029
Canola oil**	870	0.08	2.3	0.23	0.027

*(Cengel & Ghajar, 2011, p. 854)
** (Lu, Song, Ackerman, et al., 2013)

The specimens were first conditioned at 20±2°C with 65±5% relative humidity for at least 24 hours prior to the testing. For the first phase of experiments, the TPP approach was employed. In order to obtain the exposure time for this approach, the specimen was first exposed to the hot liquids until the second degree burn was predicted for the directly exposed sensor. The exposure time for the specimen were chosen as the second degree burn time plus 30 s in order to obtain the second degree burn for all of the sensors. After the termination of liquid exposure, the data acquisition continued recording the heat flux sensor output. The data acquisition was stopped 60 s after the termination of the exposure. The

measured heat flux as a function of time from the sensor was obtained for the entire test. Based on the time and the corresponding heat flux, the energies such as q_{2nd} (the energy required to generate the second degree burn), $q_{cooling}$ (the energy discharged to the sensor during the cooling period) and total absorbed energy during the test q_{total} were determined. Figure 4.1 is a schematic illustration of sensor surface heat flux history during exposure and cooling periods. Using the abovementioned steps, the following thermal performance predictive parameters are introduced. For convenience, these parameters, equations and abbreviations are described as follows:

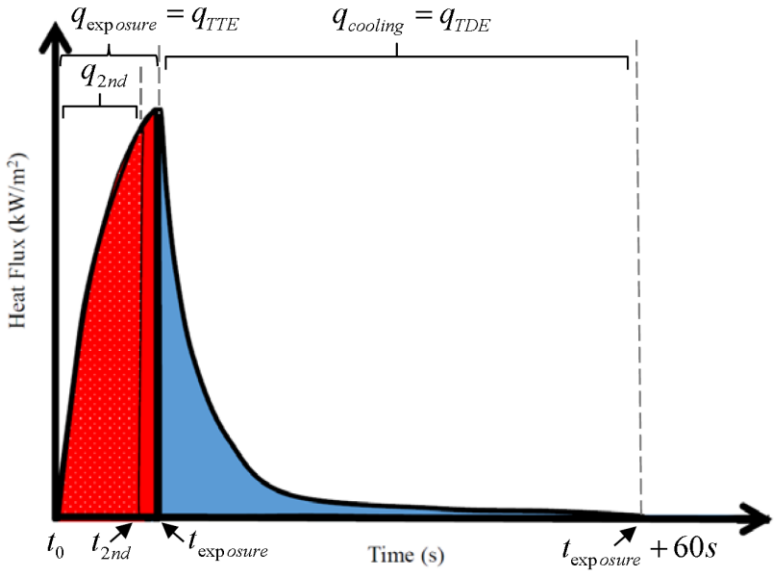

Figure 4.1. Schematic illustration of sensor surface heat flux history during exposure and cooling period.

Temperature history, $T(t)$: refers to the change in the temperature of the surface of the skin simulant with time t during exposure and cooling period. In this study, the cooling period ends 60 s after termination of exposure.

Heat flux history, $q"(t)$*:* the change in thermal intensity indicated by the amount of energy transmitted or discharged per unit area per unit time during the exposure and post-exposure; kW/m^2. The surface heat flux was calculated by using Duhamel's method employing Equation 3.1.

Absorbed energy history: the change in the transmitted and the discharged thermal energy with time during the exposure and post-exposure; kJ/m^2. In this

study, the data acquisition was recorded for 60 s after the exposure ended ($t_{exposue} + 60s$).

Second degree burn time (t_{2rd}): predicted time required for a complete destruction of the epidermis during and after the termination of thermal energy to the skin; s.

Third degree burn time (t_{3rd}): predicted time to when the thermal energy exceeds the supra-threshold and all epidermal element and the supporting dermal structure are predicted to be destroyed; s (Moritz, 1947).

Total absorbed energy, TAE (q_{total}): total thermal energy absorbed by the heat flux sensor during the exposure and post-exposure periods (Equation 4.1); (kJ/m^2).

$$q_{total} = \int_{t_0}^{t_{exposure}+60} q"(t)dt \tag{4.1}$$

Total energy absorbed at onset of second degree burn, TAE$_{2nd}$ (q_{2nd}): total energy absorbed by the heat flux sensor at the time during the time required for second degree burn to occur (Equation 4.2); (kJ/m^2).

$$q_{2nd} = \int_{0}^{t_{2nd}} q"(t)dt \tag{4.2}$$

Total transmitted energy, TTE (q_{TTE}): total energy absorbed by the heat flux sensor during the exposure (Equation 4.3); (kJ/m^2).

$$q_{TTE} = \int_{0}^{t_{exposure}} q"(t)dt \tag{4.3}$$

Total discharged energy, TDE (q_{TDE}): total energy absorbed by the heat flux sensor during the cooling period (Equation 4.4); (kJ/m^2).

$$q_{TDE} = \int_{t_{exposure}}^{t_{exposure}+60} q"(t)dt \tag{4.4}$$

Stored energy index (φ): the discharged energy's contribution to the generation of second degree burn injury (Equation 4.5).

$$\varphi = \frac{q_{TDE}}{q_{2nd}} \tag{4.5}$$

Stored energy coefficient (ψ): the discharged energy's contribution to the total absorbed energy (Equation 4.6).

$$\psi = \frac{q_{TDE}}{q_{TAE}} \tag{4.6}$$

These parameters can be used to explain the transmission and the discharge of thermal energy phenomenon through the fabric system to skin when evaluating the performance of protective clothing. In addition, the stored energy index and stored energy coefficient are introduced as predictive parameters to quantify the stored thermal energy in fabric systems. The abovementioned parameters were used in the following chapters in the analyses and the discussions.

The fabric specimens were cut to same size as the sensor board (404 mm x 253 mm) and were mounted on the sensor board. In the 45-degree orientation, the upper sensor position was exposed directly to the hot liquid, and the middle and lower sensors were used to measure the energy transfer due to the liquid flow (Figure 4.2). In the horizontal position, the middle sensor was exposed directly to the liquid source and the adjacent sensors were used to measure the energy transfer due to the liquid flow (Figure 4.3).

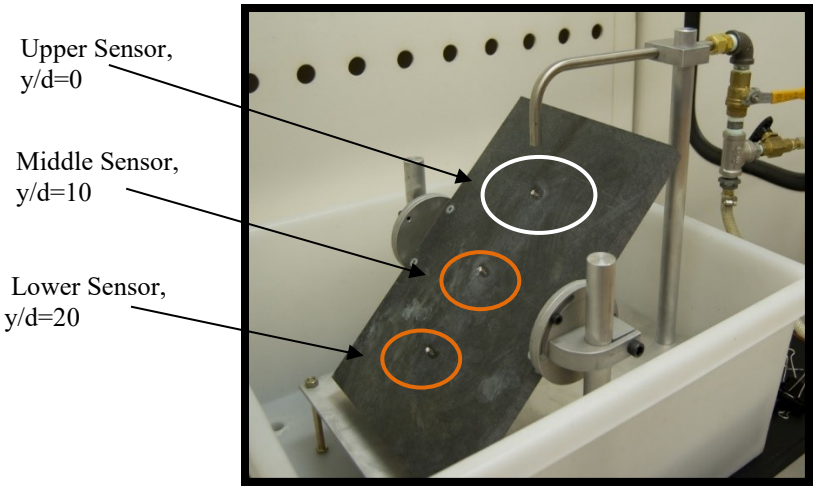

Figure 4.2. The exposed sensors in the 45-degree orientation.

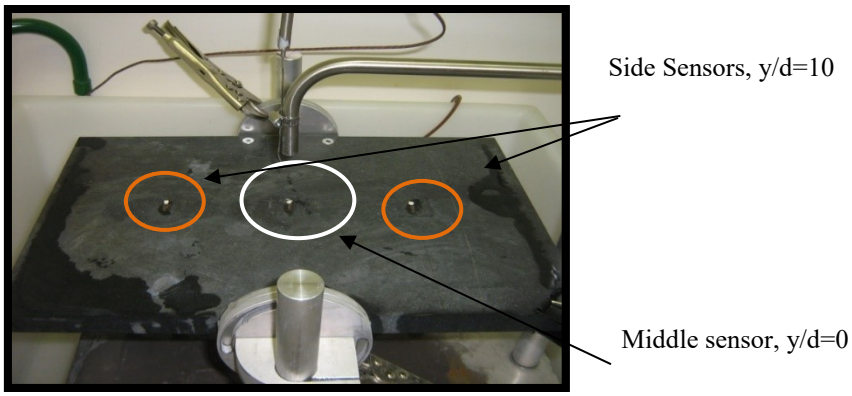

Figure 4.3. The exposed sensors in horizontal orientation.

Results and discussion

The predicted second degree burn time, predicted third degree burn time, total absorbed energy, total absorbed energy at onset of second degree burn, stored energy coefficient and stored energy index for the fabric systems exposed to the three liquids at an angle of inclination of 45 degrees are listed in Appendix C, Tables C.1 to C.8. The values in these tables are the average values of a minimum of three specimens tested for each fabric.

General observations

Hot liquid splash is a phenomenon that causes heat and mass transfer once the hot liquid splashes on clothing, and it may cause skin burn injuries. The splashed hot liquid may run off or stay on the surface of the fabric. Hot liquid that flows on

the surface of the fabric results in convection heat transfer to the surface of the fabric. Conduction heat transfer will then occur through the fabric. More details about the hydrodynamics of external flow of an impinging hot liquid on the surface of a flat fabric will be discussed in Chapter 7.

The liquid may also penetrate through the porous structure of the fabrics and be stored in the fabric. The penetration of hot liquid through the fabric delivers heat closer to the skin and causes more severe burn injuries. The hot liquid may also be transferred to the inside surface of the fabric and contact the skin. This skin contact with hot liquid is even more damaging since it delivers the thermal energy directly to the skin. Figures 4.4 and 4.5 are schematic illustrations of a fabric during exposure to hot liquid in horizontal and inclined orientation respectively. The phenomena shown in these figures were observed during the experiments.

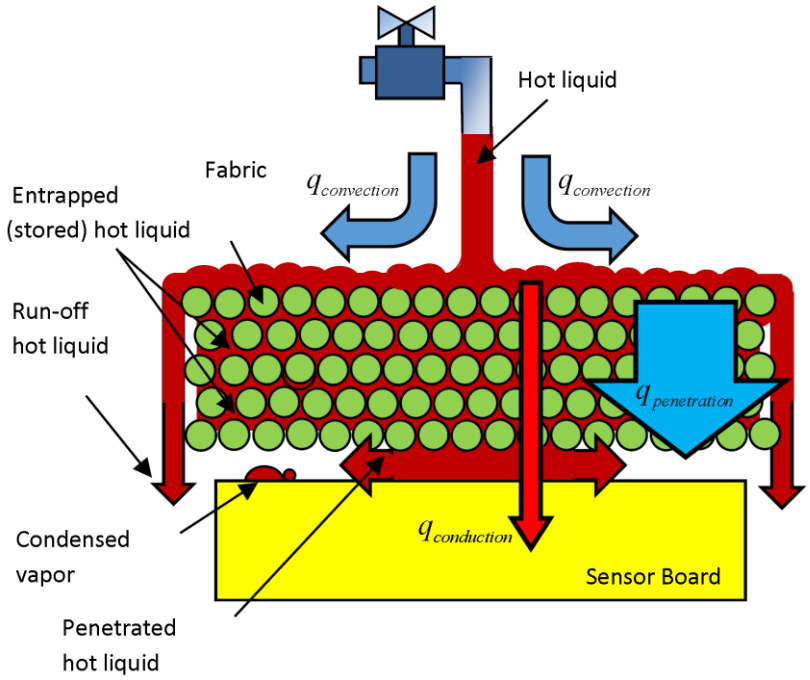

Figure 4.4. Schematic illustration of fabric exposed to hot liquid in horizontal orientation.

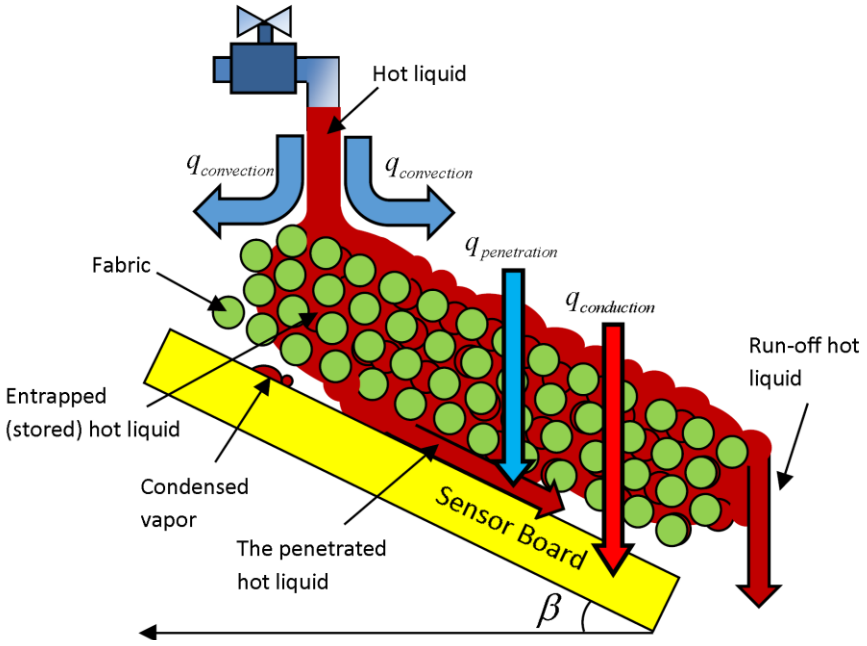

Figure 4.5. Schematic illustration of fabric exposed to hot liquid in an inclined orientation

The flow of hot liquid on the surface or through the fabric system creates convection heat transfer. The external convective heat transfer, that caused by flow of the hot liquid on the external surface of the fabric, determines the boundary conditions ($q_{convection}$). The convective heat transfer, caused by flow of hot liquid through the fabric structure, is defined in this thesis as $q_{penetration}$. When hot liquid stays on the fabric, or penetrates but is trapped within the fabric structure, it creates conduction heat transfer to the skin ($q_{conduction}$). It can also enhance conductive heat transfer by an increase in the thermal conductivity of the fabric system. During the cooling period after the exposure, hot liquid may also stay at the surface of the fabric and causes beading or pooling effects. In the horizontal configuration, the accumulated hot liquid may cause pooled hot liquid at the surface of the fabric (Figure 4.6). The pooled hot liquid may stay on the surface due to the surface finishing of the fabric and cause conduction heat transfer to the fabric. The pooled hot liquid may also penetrate into the fabric with time during the cooling period (Figure 4.7). This phenomenon may enhance bulk fluid motion and convection heat transfer ($q_{convection}$). The beading effect may also happen during post exposure period due to the fabric surface finishing (Figures 4.6 and 4.8). Similar to the pooled hot liquid, the beaded hot liquids may also enhance the overall heat transfer to the skin and cause additional injury.

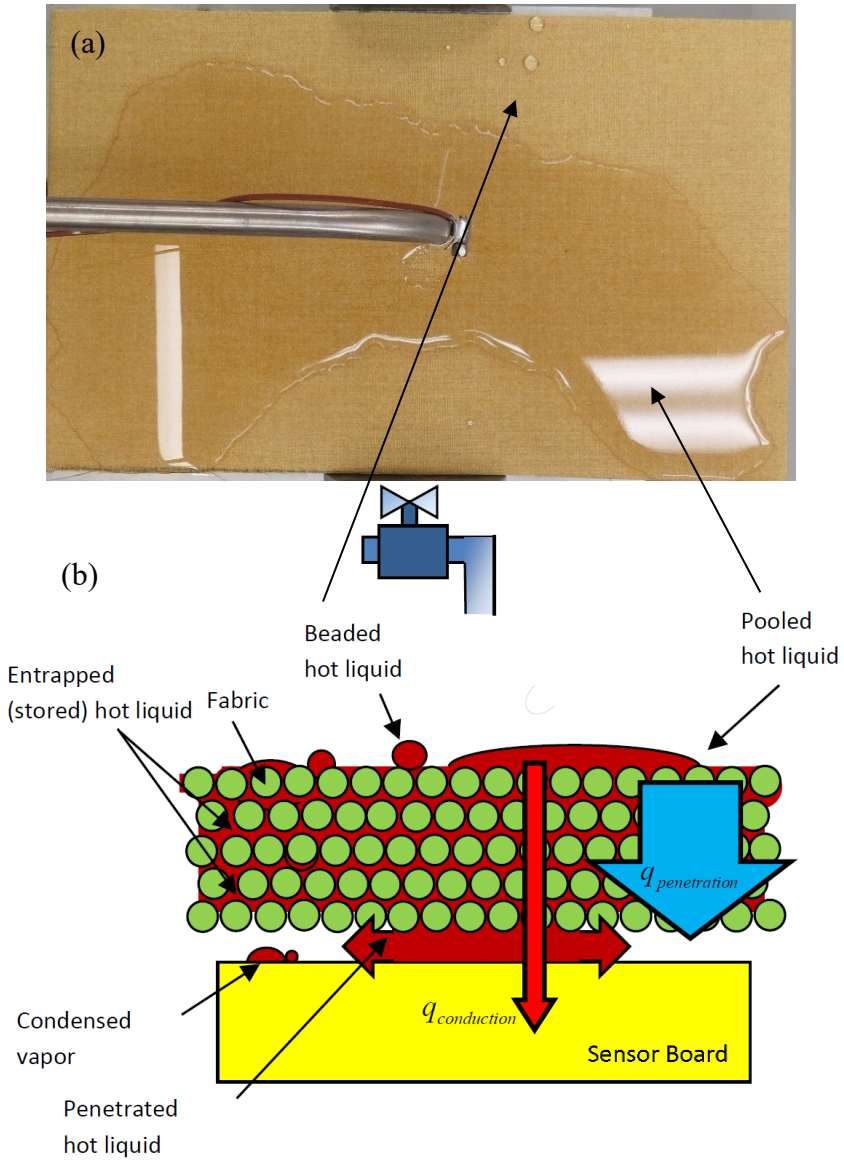

Figure 4.6. (a) Fabric SS-1(Kevlar®/PBI with hydrophobic finish)- photograph taken 60 s after the termination of the exposure to hot water in horizontal test, (b) schematic illustration of fabric exposed to hot liquid in horizontal orientation during cooling period.

Figure 4.7. Fabric SS-3 with hydrophobic finish exposed to hot water at 90°C during cooling period – photographs taken (a) 10 s, (b) 30 s and (c) 60 s after the termination of the exposure in horizontal tests.

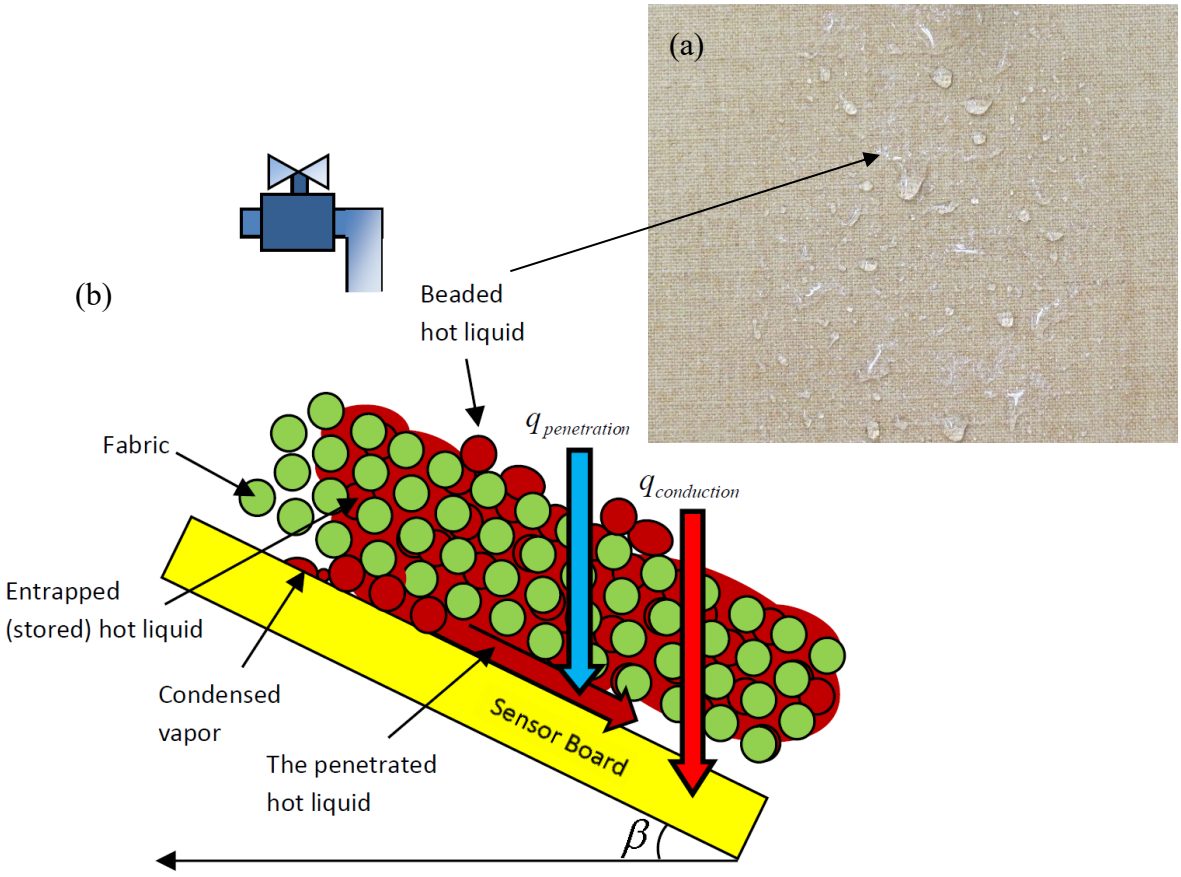

Figure 4.8. (a) Fabric SS-1(Kevlar®/PBI with hydrophobic finish)- photograph taken 60 s after the termination of the exposure to hot water in 45 degree position test, (b) schematic illustration of fabric exposed to hot liquid in 45 degree orientation during cooling period.

As such, the presence of hot liquid on the surface and within the fabric may enhance the overall heat transfer to the skin during both the exposure and cooling periods. In conduction heat transfer, the thickness and mass may affect the rate of heat conduction through the fabric system. In addition, surface finishing of the fabric may affect the effective thermal conductivity of the fabric system. Effective thermal conductivity was studied by Torvi (1997) and others. In the fabric structure, the effective thermal conductivity of the fabric system is influenced by a number of features: fabric packing factor (a higher factor meaning fewer channels and less space between fibers), the thermal conductivity of the air volume fraction in the fabric (k_{air}), the thermal conductivity of the fibrous component (k_{fiber}), and radiation thermal conductivity (k_{rad}). However, in fabrics with poor surface finishing, the space between the fibers may be filled with interfacial hot liquid which affects the thermal conductivity of the fabric system. As such, the thermal conductivity of the trapped hot liquid within the fibrous structure (k_{liquid}) can affect the effective thermal conductivity of the fabric system. Details on the effective thermal conductivity of the fabric systems can be found in Appendix D.

In convection, heat transfer depends on physical properties of the fluid such as viscosity, density, thermal conductivity and specific heat (Incropera & DeWitt, 2007). The flow geometry of the fluid, which can be affected by the shape of the fabric surface and the friction between the surface of the fabric and the fluid, can influence convection heat transfer. The hot liquid flow on the surface of the fabric may also influence convection heat transfer. This phenomenon is influenced by the density of the hot liquid, the mean hot liquid velocity on the surface of the fabric, the viscosity of the fluid and the flow pattern on the fabric.

The convection heat transfer may also be enhanced by flow of hot liquid through the fabric structure ($q_{penetration}$). Hot liquid flows through the air spaces within the fabric depending on the yarn or fabric structure (Pause, 1996). The convection heat transfer due to penetration refers to the moisture transport in capillaries of the fabric structure. The impinging hot liquid penetrates through the fabric pores and the spaces between the fibers and yarns in fabric structure. The characteristics of these spaces may affect hot liquid penetration. The jet of hot liquid forces the moisture to be embedded within the fabric structure. The flow of hot liquid may be sufficient to transfer some of the moisture all the way to the other side of the fabric and cause hot liquid mass transfer.

According to data illustrated in Appendix C, Tables C.1 to C.8, it could be inferred that the predicted thermal performance of the fabric system exposed to hot liquid is mainly affected by exposure orientation, non-dimensional displacement of the sensors with respect to the impingement point and the physical properties of the fabric system. In the subsequent section, the effects of the mentioned parameters on the predicted thermal performance of the fabric systems are investigated. In addition, a detailed statistical analysis is included at the end of this chapter to quantify the effects of the parameters on the predicted thermal performance of the fabric systems.

Effect of fabric orientation on thermal performance

In the horizontal position, water stays on the surface of the fabric until it is pushed by the flow of the liquid from the liquid–fabric stagnation region to the sides of the fabric. In this orientation, the gravitational forces help the liquid to stay on and/or penetrate through the fabric structure more than in the inclined orientation. This allows water to stay on and/or penetrate farther and faster into the fabric. On the other hand, when the fabric is at an angle of 45 degrees, water moves on the inclined surface of the fabric from the stagnation region to the bottom of the sensor board and the drops of hot liquid drip off more from the fabric in comparison to horizontal orientation. Therefore, water has less chance to stay on, penetrate or transfer to the back side of the fabric relative to the horizontal orientation. This phenomenon increases the transmitted energy in the horizontal orientation, resulting in shorter burn times than for the 45-degree orientation. As shown in Figure 4.9, the predicted second degree burn time for the fabric systems exposed to hot water at 45-degree orientation, ranges from 2 to 155 s. Data in Figure 4.10 shows that the values of the predicted second degree burn time are relatively lower in the horizontal orientation, ranging between one second and 139 s. The amount of water on the surface of fabric, within the fabric and transferred from the fabric in horizontal and 45-degree orientation were determined and will be discussed later in Chapter 6.

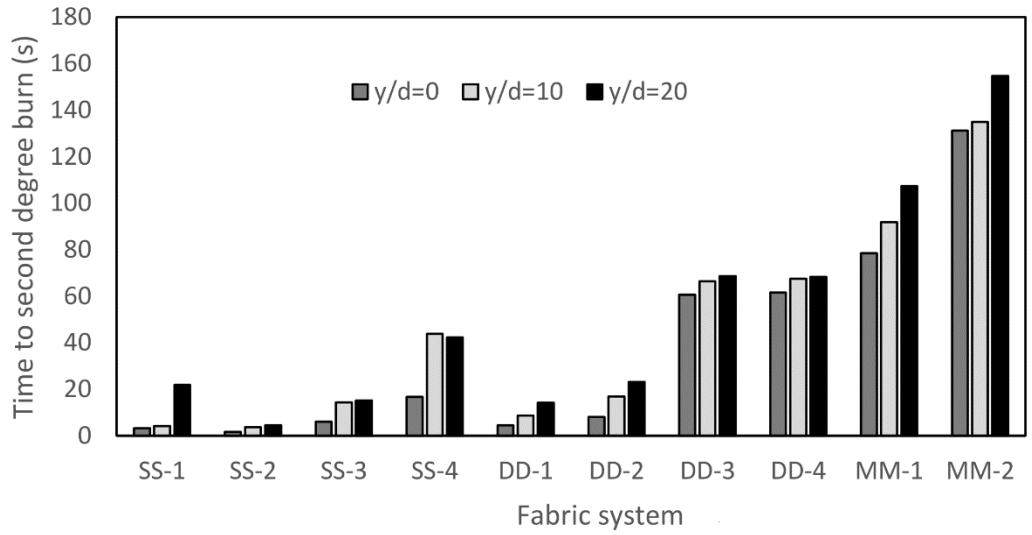

Figure 4.9. Time to second degree burn for fabric systems exposed to hot water in 45-degree orientation for the three sensors. y/d is the non-dimensional displacement of the sensors with respect to the impingement point.

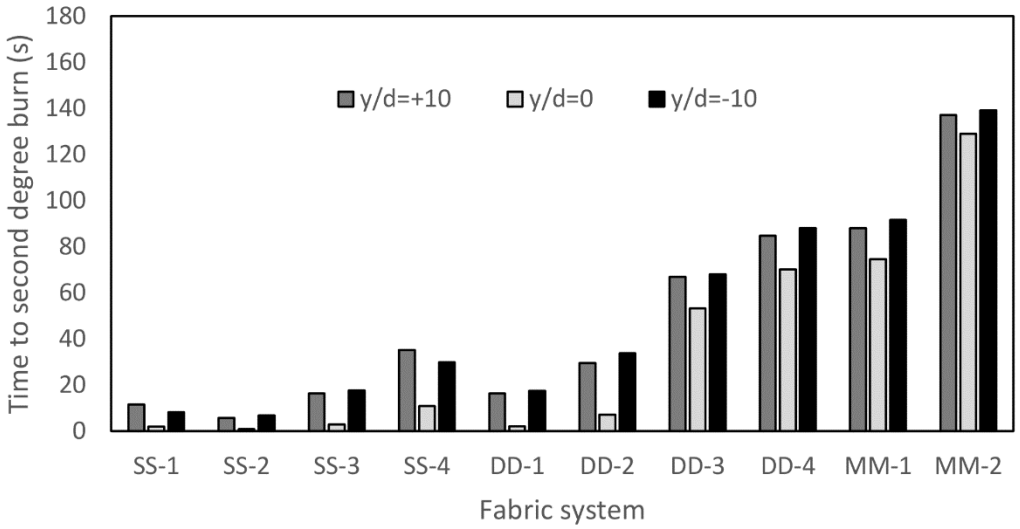

Figure 4.10. Time to second degree burn for fabric systems exposed to hot water in horizontal orientation for the three sensors. y/d is the non-dimensional displacement of the sensors with respect to the impingement point.

Table 4.2 shows that the values of the stored energy coefficient are significantly higher in the horizontal configuration. This confirms that there is a significant amount of thermal energy which is stored in the system due to the effect

of the angle of orientation. It was observed that almost 50 g of water stayed on the surface of the Kevlar®/PBI with water resistant finishing after the termination of exposure in horizontal orientation (Figure 4.6 (a)). Information about the amount of water on the fabrics with surface finishing will be presented in Chapter 7. While in the 45-degree orientation some drops of water in the forms of small beads remained on the fabric after the termination of exposure (Figure 4.8 (b)). In addition, by weighing the fabric after the exposure it was realized that the fabric in horizontal orientation accumulates almost five times more hot water in comparison to 45-degree orientation. The trapped hot water in the fabric system increases the accumulation of thermal energy within the fabric structure in the horizontal configuration.

The effect of stored thermal energy can also be observed in the values of the third degree burn. According to Table 4.2, third degree burn occurred after the termination of hot water exposure. It can also be observed that the occurrence of third degree burn is relatively lower in the horizontal configuration. This confirms that the orientation can significantly affect the thermal performance of fabric systems. Also, fabric ranking does not change regardless of the test orientation.

Table 4.2. Thermal performance of single layer fabric system at the stagnation region (direct exposure hot water at 85°C) in horizontal and 45-degree orientation.

Fabric	Exposure time (s)	Horizontal			45 Degree		
		t_{2nd} (s) (SD)	t_{3rd} (s) (SD)	Ψ (SD)	t_{2nd} (s) (SD)	t_{3rd} (s) (SD)	Ψ (SD)
SS-1	3	2.0 (0.3)	15.9 (0.3)	0.54 (0.06)	3.2 (0.2)	18.5 (1.1)	0.08 (0.02)
SS-2	2	0.8 (0.0)	14.7 (0.2)	0.60	1.6 (0.2)	16.3 (1.2)	0.25 (0.02)
SS-3	7	2.9 (0.8)	18.3 (1.3)	0.56 (0.03)	6.0 (0.6)	22.2 (0.7)	0.09 (0.00)
SS-4	16	10.9 (0.4)	42.6 (0.6)	0.41 (0.03)	16.6 (1.1)	52.4 (1.8)	0.02 (0.00)

The effect of surface properties and fabric finishes on the transmitted and the discharged thermal energy is very significant when a single layer fabric system is exposed to hot water in horizontal orientations. According to Table 4.2, Fabric SS-2, Nomex®IIIA with no finish, has the lowest time to second and third degree burns in the horizontal orientation in single layer fabric system. In addition, the

stored energy coefficient indicates that Fabric SS-2 stores 60% (ψ=0.6) of the total energy in its structure in the horizontal orientation which is the highest value in both configurations.

Fabric SS-2 wets immediately when it is impinged by hot liquid (Figure 4.11 (b)). No beads or pooled water were observed during the cooling period. However, hot liquid penetrated through and/or was entrapped within the fabric system and less ran off the fabric in comparison to the 45-degree configuration. This explains why the time to second degree burn is less than one second in horizontal orientation. In addition, the entirely wet SS-2 fabric discharged a large amount of thermal energy during the cooling period which is more than two times the discharged energy in 45-degree orientation.

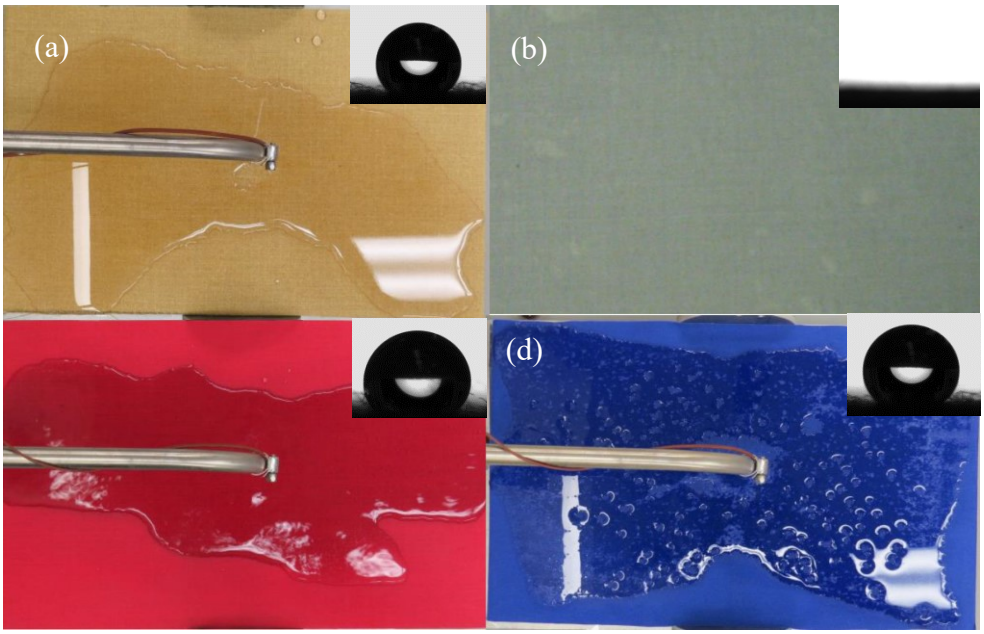

Figure 4.11. Single layer fabrics and the corresponding hot water drop shapes ((a) SS-1, (b) SS-2, (c) SS-3 and (d) SS-4 exposed to hot water at 85°C (photographs taken 10 s after the termination of the exposure in horizontal tests).

In the stagnation region, the finished fabrics SS-1, SS-3 and SS-4 also stored 6.7, 6.2 and 20 times more thermal energy, respectively in the horizontal configuration than in the 45-degree configuration (Table 4.2). The higher values of stored energy coefficient confirm that in addition to heat and mass transfer in finished single layer fabrics, the pooling hot water effects play important roles in accumulation of stored thermal energy in the fabric. In the 45-degree orientation,

no pooling effect was observed on the fabric systems after the termination of hot water exposure. In 45-degree orientation, the beaded hot water was formed at the surface of the fabrics. In the horizontal orientation, hot water accumulated at the surface of fabric in the form of pools, which results in larger bodies of water on the surface than in the case of beading (Figures 4.11 (a), (c) and (d)).

Accumulation of stored energy is also significant in the adjacent zones located at $y/d = \pm 10$, in the horizontal orientation. By comparing the values of stored energy coefficient in both configurations for single layer fabrics, it is realized that the finished fabrics SS-1, SS-2, SS-3 and SS-4 accumulate 3.8, 2, 6.1 and 4 times more thermal energy in the horizontal configuration than in the 45-degree orientation (Figure 4.12). The values of the stored energy coefficient for horizontal tests shown in Figure 4.12 are based on the average of the two sensors that are adjacent to the stagnation point at $y/d = \pm 10$. These results confirm that more thermal energy was stored in the fabric system at $y/d = \pm 10$ than $y/d = 0$. The accumulation of water on the surface of the fabrics and water in the structure of the fabrics in the horizontal orientation in the adjacent zones located at $y/d = \pm 10$ causes the significant discharge of thermal energy.

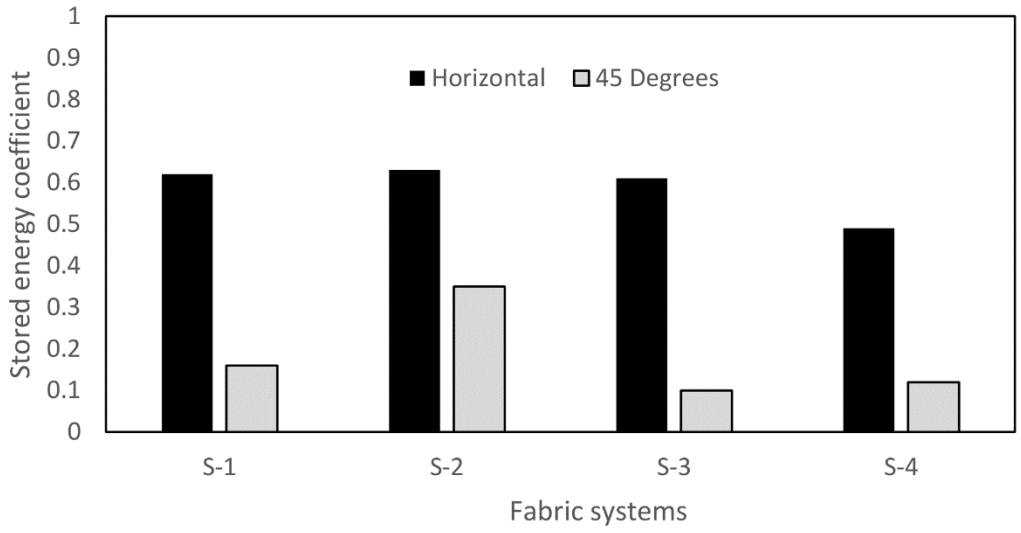

Figure 4.12. Stored energy coefficient at $y/d = \pm 10$ in the horizontal and y=+10 in the 45-degree orientations. y/d is the non-dimensional displacement of the sensors with respect to the impingement point.

Fabric properties and their effects on thermal protection

Table 4.3 shows the average of second degree burn time and stored energy coefficient for the three sensors in the 45-degree orientation for single layer fabrics with a water resistant finish (SS-1, SS-3 and SS-4) exposed to distilled water. According to Table 4.3, fabric SS-1 has the lowest predicted time to second degree burn among single layer fabrics at the stagnation region. Fabric SS-1 has 10 times higher air permeability than Fabric SS-3 (Table 4.3). This suggests that mass transfer occurs through the porous fibrous structure and contributes significantly to skin burn injury. Fabric SS-1 has relatively larger interstices in comparison to SS-3 which let hot liquid penetration happen at a faster rate. For fabrics with similar densities, such as fabrics SS-1 and SS-3, a larger value of air permeability indicates a more porous structure. Therefore, as fabric system SS-1 has a larger value of air permeability than fabric system SS-3, fabric system SS-1 should have a more porous structure than SS-3 and it would be expected that more liquid should be transferred through its structure. Therefore, fabric system SS-3 is expected to provide better protection than fabric system SS-1 at the stagnation point (y/d=0). Caution needs to be exercised in drawing conclusion about the results in this section. The test results are based on a limited number of experiments on specimens from a limited number of fabrics and hence may not be representative of other fabric systems.

The impermeable fabric system SS-4 is able to resist mass transfer (hot liquid penetration) through the use of the encapsulation process into its fabric structure. This resistance to mass transfer prevents the liquid from penetrating through the fabric and directly contacting the skin. Therefore, fabric system SS-4 provides much better protection than permeable single-layer fabrics with the water resistant finish considered in this study (Table 4.3).

Table 4.3. Predicted second degree burn, stored energy coefficient and stored energy index for three sensors in 45-degree orientation for distilled water. y/d is the non-dimensional displacement of the sensors with respect to the impingement point.

Fabric	Air Permeability ($cm^3/cm^2/s$)	Sensor	Distilled Water	
			t_{2nd} (s) (SD)	Ψ (SD)
SS-1	17.1	Upper (y/d=0)	3.2 (0.2)	0.08 (0.02)
		Middle (y/d=10)	4.1 (0.2)	0.21 (0.04)
		Lower (y/d=20)	15.1 (3.5)	0.27 (0.02)
SS-3	1.65	Upper (y/d=0)	6.0 (0.2)	0.09 (0.00)
		Middle (y/d=10)	14.4 (2.1)	0.10 (0.03)
		Lower (y/d=20)	21.8 (0.4)	0.17 (0.02)
SS-4	0	Upper (y/d=0)	16.6 (1.1)	0.02 (0.00)
		Middle (y/d=10)	43.8 (1.9)	0.12 (0.02)
		Lower (y/d=20)	42.2 (1.0)	0.11 (0.03)

Comparing the predicted time to second degree burn for the permeable single layer fabric systems SS-1 and SS-3, and the impermeable fabric system SS-4, it is inferred that as the distance increases from the stagnation point (y/d=10 and y/d=20), the time to second degree burn significantly increases in impermeable fabric system SS-4. The penetrated hot liquid within the structure of the permeable fabrics during the exposure causes accumulation of thermal energy within the structure of fabric system. This phenomenon increases the initial exposure to the heat flux sensor and decreases the predicted burn time.

In addition, the penetrated hot liquid remains in the system and causes additional thermal energy discharge during the cooling period. The stored energy coefficient shown in Table 4.3 shows that 8 to 28% of the thermal energy was discharged during the cooling period in permeable fabrics SS-1 and SS-3, while, less thermal energy was discharged to the sensors in the impermeable fabric system SS-4 (2 to 12%).

Figure 4.13 and 4.14 show the heat flux histories of Fabrics SS-1, SS-3 and SS-4 at y/d=0 and y/d=20 respectively. The figures confirm that minimizing mass transfer by decreasing the permeability of the fabrics with a water resistant finish can decrease the absorbed energy to the sensor during the exposure and cooling period of the fabric. In Figure 4.14, the heat flux curves for permeable fabrics SS-1 and SS-3 rise between 5 to 10 kW/m^2 during the first 17 and 32 s respectively after the onset the exposure to hot distilled water. The rise in the heat flux curve can be due to the heat transfer caused by the flow of liquid on the fabrics. These curves remain at relatively constant values until they rise significantly. These peaks demonstrate that it takes almost 17 s from the beginning of the exposure for fabric systems SS-1 and SS-3 to allow water to penetrate through their structures at y/d=20.

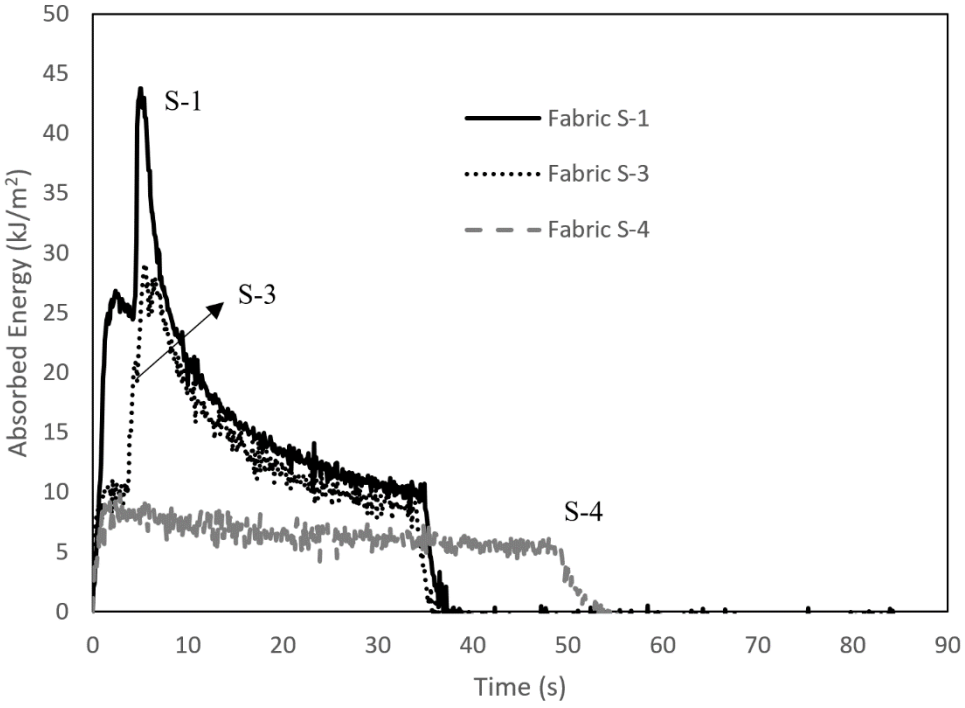

Figure 4.13. Heat flux history for fabric systems SS-1, SS-3 and S-4 at stagnation point (y/d=0) exposed to distilled water.

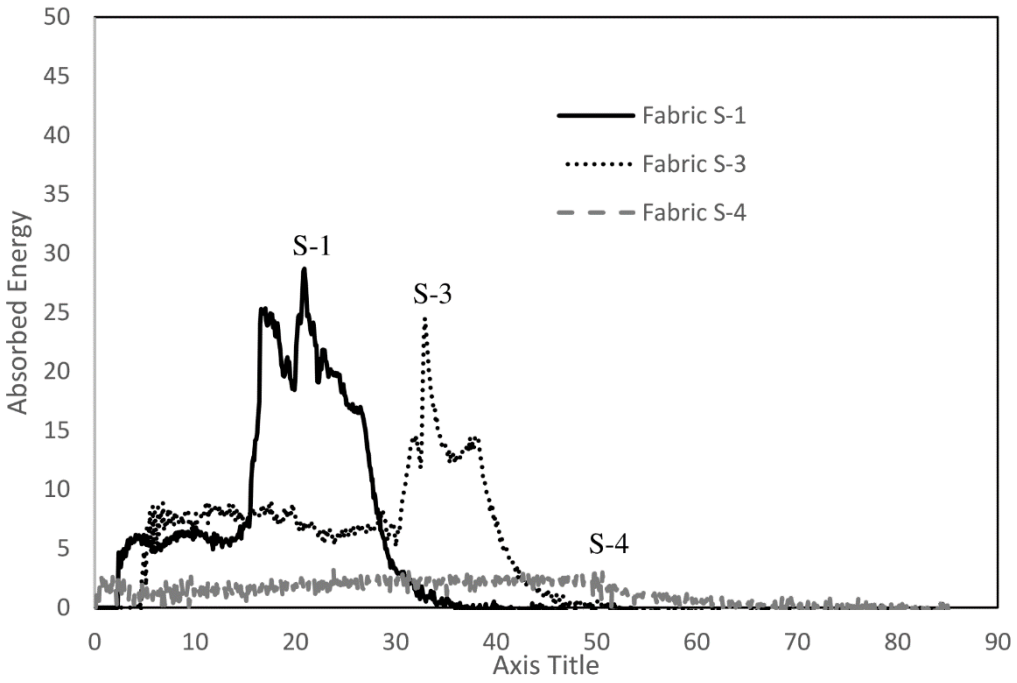

Figure 4.14. Heat flux history for fabric systems SS-1, SS-3 and SS-4 at lower sensor (y/d=20) exposed to distilled water.

Figure 4.15 is a schematic illustration of an impermeable single layer fabric system. The figure helps the understanding of the effect of fabric permeability in hot liquid splash phenomenon. Earlier in this chapter, in Figures 4.8 and 4.9, it was shown that simultaneous hot liquid penetration and heat conduction occurs in permeable fabric systems. However, the impermeable structure of the fabric system illustrated in Figure 4.15 shows that the impermeable fabric structure minimizes hot liquid penetration which causes no penetration through the structure of this fabric. This was confirmed by weighing fabric system SS-4 after the exposure to distilled water which showed that there is less that a gram of water stored in the fabric. More information about the amount of stored water in single layer fabric systems will be shown in Chapter 7. It was also observed that no liquid was transferred to the back side of the fabric.

Therefore, improving the thermal performance of the fabric system with water resistant surface finishing exposed to hot liquids can be obtained by reducing the water penetration property of the fabric by reducing its air permeability. It can be inferred that, in fabrics with water resistant surface finishing, air permeability is a dominant indicator of protection performance against hot liquids. Resistance to

mass transfer is shown to be the key factor for reducing the amount of transmitted and discharged heat to the skin.

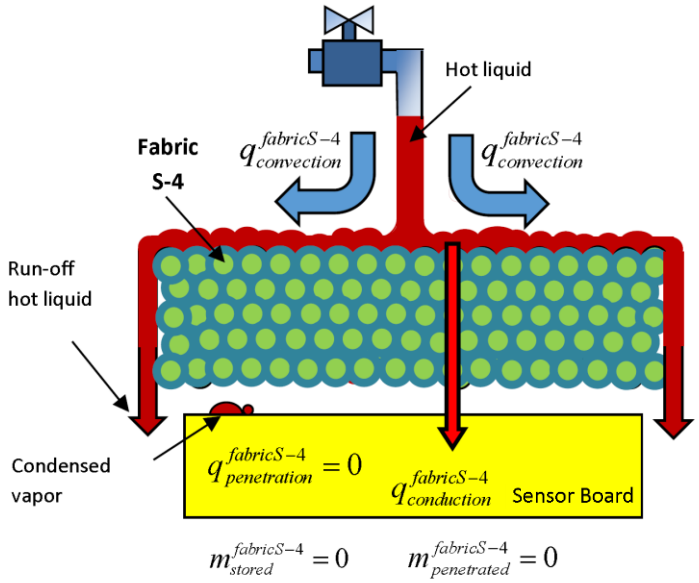

Figure 4.15. Heat and mass transfer through fibrous structure of impermeable single layer fabric.

Surface energy of the fabrics is another factor that affects the thermal performance of the protective clothing upon exposure to hot liquids. Wetting is the main process involved in hot liquid splash, and the contact angle of liquid to fabric is a direct characterization of the fabric wettability. The measured contact angle between the sessile liquid drops and the single layer fabric system is shown in Table 4.4

Table 4.4. The measured contact angle between the sessile liquid drops and the fabrics' surface (the measured ranges are shown with ± in this table).

Fabrics	Contact Angle θ (Degree)		
	Water	Drilling Mud	Canola Oil
SS-1	127± 1.48	105.2± 1.54	91.7± 1.12
SS-2	108± 1.68	0	0
SS-3	130± 1.35	109± 0.87	97± 0.96
SS-4	137± 0.61	107.8± 0.75	95.25± 1.01

A liquid that does not wet the fibers cannot penetrate into the fabric. The flow of liquid through textiles is caused by fiber-liquid molecular attraction at the surface of the fabric, which is mainly determined by the surface energy and the effective capillary pore distribution and pathways (Li and Zhu, 2003). The finished fabric system SS-1 has a higher air permeability and is thinner than the unfinished fabric system SS-2. However, fabric system SS-1 provides better protection than fabric system SS-2 (Table 4.3). The longer second-degree burn time for fabric system SS-1 demonstrates the effect of lower surface energy caused by finishing process.

The contact angle (θ) between the drop of water and the surface of fabric system SS-1 is greater than the contact angle between the water drop and the surface of fabric system SS-2 (Table 4.4). However, for fabric system SS-2, the drop penetrated into the fabric within 25 s (Figure 4.16). It was also observed that drilling fluid and canola oil penetrated into fabric system SS-2 quicker than hot water. According to Table 4.4, a comparison of the contact angles of the finished fabric system SS-1 and Fabric SS-2 for water, drilling mud and for canola oil demonstrate the importance of surface finishing. A lower surface energy enhances a fabric's resistance to liquid penetration. This property results in a reduction in the amount of hot water penetration by more than 150 times and better thermal protection against hot liquid splashes. The comparison of the contact angles between the drops of liquids on single layer fabrics with water resistant surface finishing (Table 4.4) shows that the contact angle values do not vary significantly and surface finishing plays similar roles in these fabrics. Figure 4.16 shows the sessile drops of hot water on fabric system SS-2, which illustrates the wetting phenomenon. This phenomenon was only observed in fabric SS-2.

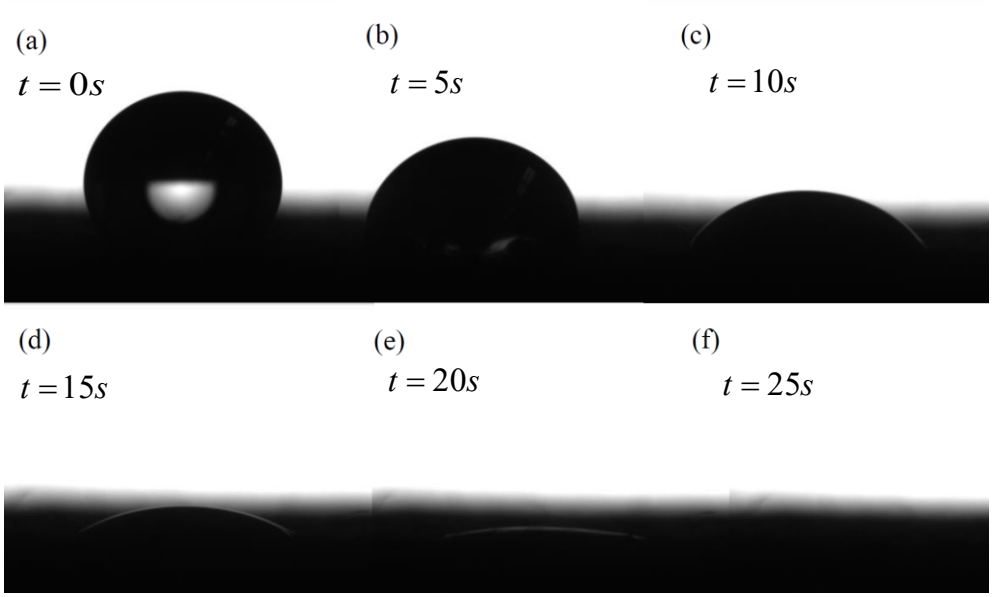

Figure 4.16. The sessile drops of hot water on fabric system SS-2 (The photographs were taken every 5 s over the first 25 second after the drop was set on the fabric).

Surface finishing also has a significant effect on the accumulation of thermal energy in the fabric system. The values of the stored energy coefficient for fabric system SS-2 exposed to distilled water are 0.25, 0.35 and 0.40 at y/d=0, 10 and 20 respectively. The values show that Fabric SS-2 stores the highest amount of thermal energy during the cooling period among the single layer fabric systems. The hydrophobic surface of fabrics SS-1, SS-3 and SS-4 repels most hot water off the surface of the fabric, while fabric system SS-2 cannot resist water penetration and wets entirely. During the hot water exposure, fabric system SS-2 will be saturated with hot water. The penetrated hot water is entrapped within the structure of fabric system SS-2, which has no water resistant finish, and results in a significant amount of stored energy.

The same phenomenon was observed in the exposure of single layer fabrics to drilling fluid and canola oil. Figure 4.17 shows the stored energy coefficient in Fabrics SS-1 and SS-2 for the three studied liquids. The averages of the stored energy coefficient (ψ) in fabric system SS-1exposed to drilling fluid, hot water and canola oil are 0.11, 0.17 and 0.29 respectively. The stored energy coefficient is larger for fabric system SS-2 (0.15, 0.33 and 0.44, respectively) (Figure 4.17). Therefore, reducing the penetration of hot liquid by decreasing the surface energy

of the fabric with a water resistant surface finish enhances the thermal performance of single layer fabrics. It is also noted that there is more differentiation between the results for distilled water than drilling fluid.

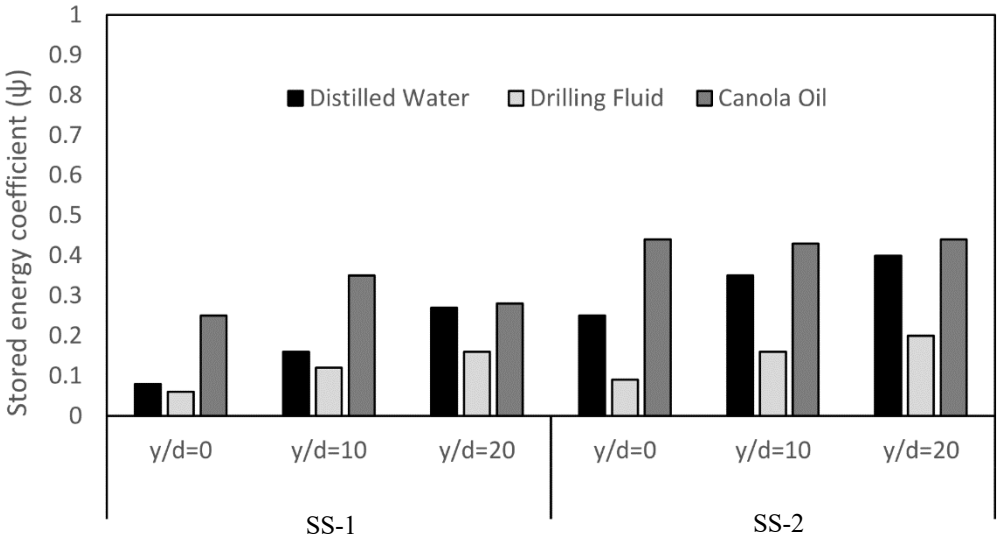

Figure 4.17. Values of stored energy coefficient (ψ) in fabric systems SS-1 and SS-2 exposed to hot distilled water, drilling fluid and canola oil. y/d is the non-dimensional displacement of the sensors with respect to the impingement point.

Effect of the presence of moisture barrier on thermal protection

In order to study the thermal protection offered by different-layered fabric systems and the impact of their construction, different fabric configurations were fabricated. Double-layer fabric systems (DD-1, DD-2, DD-3 and DD-4) and multilayer fabric systems (MM-1 and MM-2) were assembled.

Fabric system DD-1 is constructed from a Kevlar®/PBI shell fabric (shell fabric AA) and a thin thermal liner (thermal liner AA). Fabric system DD-2 employs the same shell and a thicker thermal liner (thermal liner BB). As such fabric system DD-1 and DD-2 are constructed from the same fiber contents. The permeable structure of these two fabrics cannot completely resist mass transfer and will let hot liquid penetrate through their porous structures. Table 4.5 shows the construction, physical properties and the thermal performance of DD-1, DD-2, MM-1 and MM-2. Fabric system MM-1 is similar to fabric system DD-1, but fabric system MM-1 has an additional moisture barrier between the shell fabric AA and the thermal liner AA. The time to second degree burn for fabric MM-1 is

significantly higher than DD-1. The moisture barriers block the hot liquids' penetration from the outer surface through the fibrous structure of the fabric system. As such, the transmitted heat is minimized and would cause less severe burn injuries.

Similar phenomenon can be observed in fabric systems MM-2 and DD-2. These fabrics are constructed from the shell fabric AA and the thermal liner BB, but fabric system MM-2 has an additional moisture barrier between shell fabric AA and the thermal liner BB. The data in Table 4.5 can confirm that the presence of moisture barrier in fabric MM-2 also has a noticeable impact on its thermal performance. This shows that the presence of the moisture barrier restricts water penetration through the fabric and reduces the thermal energy discharge to the skin simulant sensor.

Table 4.5. Construction, physical properties and the thermal performance of DD-1, MM-1, DD-2 and MM-2.

Assembly Code (Assembly Description)	Density (g/cm^3)	Mass (g/m^2)	Thickness (mm)	Air permeability ($cm^3/cm^2/s$)	Water	
					2^{nd} Degree Burn Time (Horizontal Exposure) (s) (SD)	2^{nd} Degree Burn Time (Inclined Exposure) (s) (SD)
DD-1 (Fabric AA+ Thermal liner AA)	0.248	382.1	1.54	13.9	2.1 (0.3)	4.4 (0.4)
MM-1 (Fabric AA+ Moisture BarrierAA+ Thermal liner AA)	0.255	567.9	2.22	0	74.5 (1.0)	78.5 (3.2)
DD-2 (Fabric AA+ Thermal liner BB)	0.135	544.2	4.03	12.5	7.1 (1.0)	8.0 (0.5)
MM-2 (Fabric AA+ **Moisture BarrierAA**+ Thermal liner BB)	0.152	730.0	4.78	0	128.9 (10.4)	131.1 (7.2)

Effect of position of moisture barrier on thermal protection

In order to investigate the effect of resisting mass transfer in the outermost layer in a double-layer fabric system on the thermal performance of the fabric system, a switched-layer fabric system was employed. In the switched-layer fabric system, moisture barrier AA was positioned as a shell fabric in fabric system, DD-4 (Figure 4.18). Although the fabric system DD-4's configuration is not practical, it helps in understanding the effect of minimizing mass transfer in hot liquid splashes. The configurations of the switched-layer fabrics are presented in Table 4.6. Fabric

systems DD-3 and DD-4, have the same fabric density, mass, thickness, and air permeability, but different configurations (Table 4.6). According to the data presented in Table 4.6, the fabric system DD-4 provides better thermal protection than fabric system DD-3.

Table 4.6. Construction, physical properties and the performance of the switched-layer fabric systems.

Assembly Code	**Assembly Description**	Density (g/cm^3)	Mass (g/m^2)	Thickness (mm)	Air permeability ($cm^3/cm^2/s$)	Time to 2nd degree burn (s) (SD)	
						Horizontal Exposure	45-degree Exposure
DD-3	Fabric AA+ Moisture Barrier	0.257	397.3	1.54	0	53.2 (9.2)	60.6 (1.7)
DD-4	Moisture Barrier+ Fabric AA					70.1 (1.6)	61.5 (1.2)

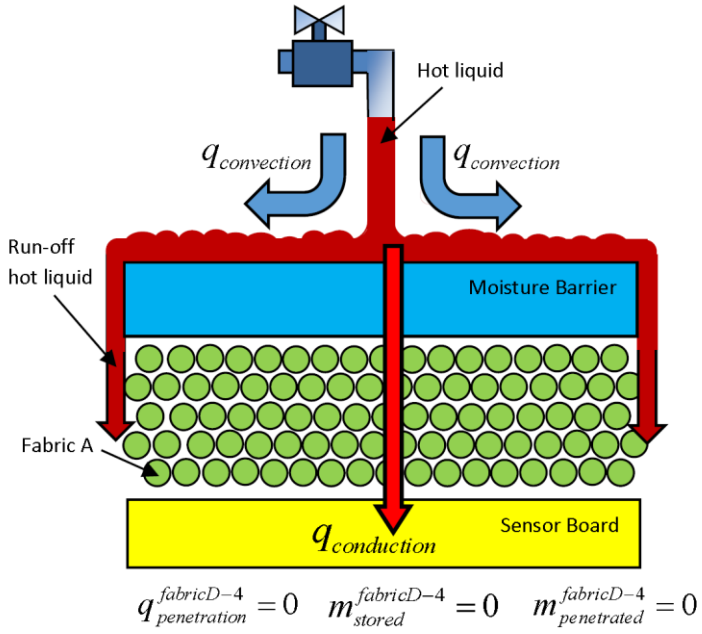

Figure 4.18. Schematic diagram of the moisture barrier and the underlying shell fabric AA (fabric system DD-4) upon exposure to hot liquid.

The position of the moisture barrier affects the thermal protection of these fabric systems against hot liquids because it minimizes mass transfer. When the moisture barrier is positioned at the surface of the fabric system (DD-4), in direct contact with the impinging hot liquid, the mass transfer to the underlying layers is very

significantly reduced and all the heat transferred is by the mode of dry heat conduction (Figure 4.18).

When the moisture barrier is placed underneath the shell fabric (fabric system DD-3), almost two times more hot water was stored in the fabric after the termination of exposure in comparison to fabric system DD-4. This was realized by weighing the fabrics after the termination of exposure. The larger amount of hot water caused a larger amount of thermal energy to be absorbed as the result of the mass flow into the assemblage, contributing to a faster skin burn injury (Table 4.6) and a larger stored energy coefficient (Table 4.7). Table 4.7 shows the stored energy coefficient for fabrics DD-3 and DD-4. When the moisture barrier is placed on top of the shell fabric A, the penetrated and the entrapped hot liquid is blocked from entering into the fabric structure. The stored energy in fabric system DD-4 is as the result of conduction heat transfer ($q_{conduction}^{stored}$), caused by the accumulation of thermal energy in its fibrous material and the pooled hot water at the surface of the fabric. Measurements of the penetrated and the entrapped hot water in double layer fabric system will be shown in Chapter 7.

Table 4.7. Construction, physical properties and the stored thermal energy coefficient of the switched-layer fabric systems.

Assembly Code	**Assembly Description**	Density (g/cm^3)	Mass (g/m^2)	Thickness (mm)	Air permeability ($cm^3/cm^2/s$)	Stored energy Coefficient (ψ) (SD)	
						Horizontal Exposure	45-degree Exposure
DD-3	Fabric AA+ Moisture Barrier	0.257	397.3	1.54	0	0.34 (0.01)	0.06 (0.01)
DD-4	Moisture Barrier+ Fabric AA					0.24 (0.03)	0.04 (0.01)

Effect of thickness of the fabric system on thermal protection

The permeable fabric systems DD-1 and DD-2 have the same fiber content and surface properties but fabric system DD-2 is a thicker fabric due to employment of a thicker thermal liner (thermal liner BB) in its structure. The impermeable fabric systems MM-1 and MM-2 also have the same fiber content and surface properties but fabric system MM-2 is a thicker fabric due to employment of a thicker thermal liner (thermal liner BB) in its structure. Figures 4.9 and 4.10 show the thermal performance of DD-1, DD-2, MM-1 and MM-2 when the fabrics are horizontal and

at an angle of 45 degrees. Increasing the thickness of the fabric system increases the predicted times to second and third degree burn in these fabrics.

However, increasing the fabric thickness increases the stored thermal energy discharge to the sensors at y/d=0, y/d=10 and y/d=20. According to Figure 4.19, the values of stored energy coefficient at the stagnation point (y/d=0) and the distances further from the stagnation point at y/d=10 and y/d=20 are increased.

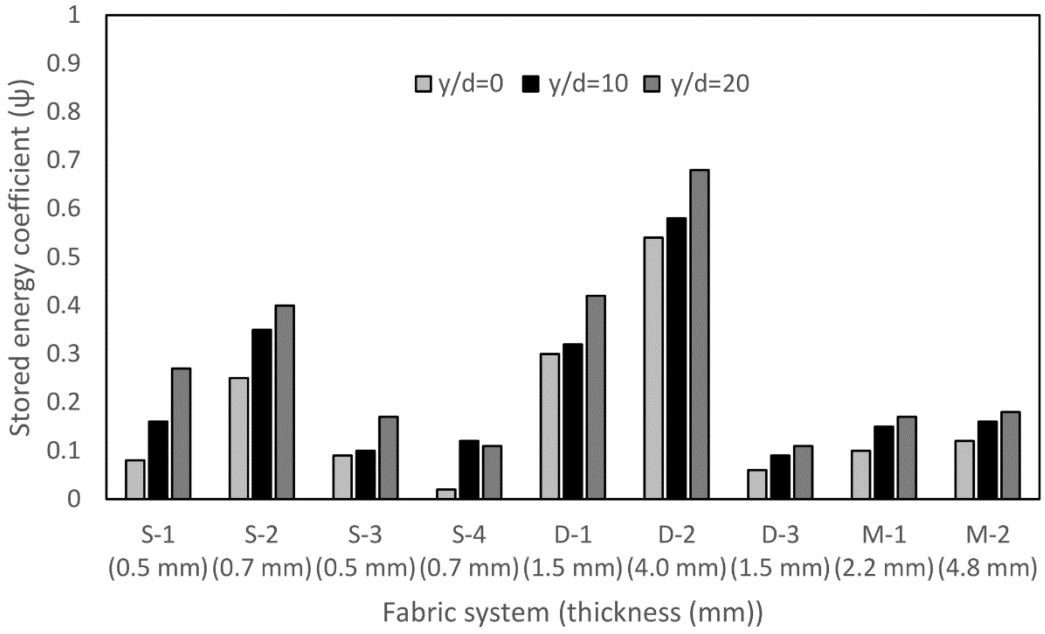

Figure 4.19. Stored energy coefficient (ψ) at y/d =0, y/d =10 and y/d =20 in 45-degree orientations. y/d is the non-dimensional displacement of the sensors with respect to the impingement point.

Table 4.7 shows multilayer fabric systems that consist of shell fabric AA, a moisture barrier AA, and a thermal liner with different thicknesses. These sets of fabrics use shell fabric AA in systems with different thicknesses, mass, densities, but the same air permeability. The penetrating water was transferred through the permeable structure of shell fabric AA in fabric systems MM-1 and MM-2. Further penetration was blocked by the moisture barrier (Figure 4.20) and the water was stored in shell fabric AA and on top of the moisture barrier in fabric systems MM-1 and MM-2. By weighing the fabrics after the termination of exposures in horizontal orientation, it was realized that the amount of stored hot water in fabric

systems MM-1 and MM-2 were the same (almost 9 g). As such, it can be inferred that the amount of thermal energy caused by hot liquid penetration ($q_{penetration}$) is the same for the two fabrics. Measurements of the penetrated and the entrapped hot water in multilayer fabric system will be shown in Chapter 7.

It can also be inferred that since there is limited hot water penetration to the thermal liners underneath the moisture barriers in the structure of fabric systems MM-1 and MM-2, the heat transferred is by sensible heat conduction. As such, the thicker thermal liner can provide a better thermal performance for the fabric systems. As the thickness of thermal liners increases, the density of fiber content in fabric system MM-2 decreases by almost 13%. Less fiber content in the thermal liner BB means more trapped air in fabric system MM-2 than MM-1. Since air is a better insulator than fibers and has a lower thermal conductivity relative to fibers, the effective thermal conductivity of fabric system MM-2 decreases which results in the improvement of the thermal performance of fabric system MM-2 (Figure 4.9 (page 85) and Figure 4.10 (page 85)).

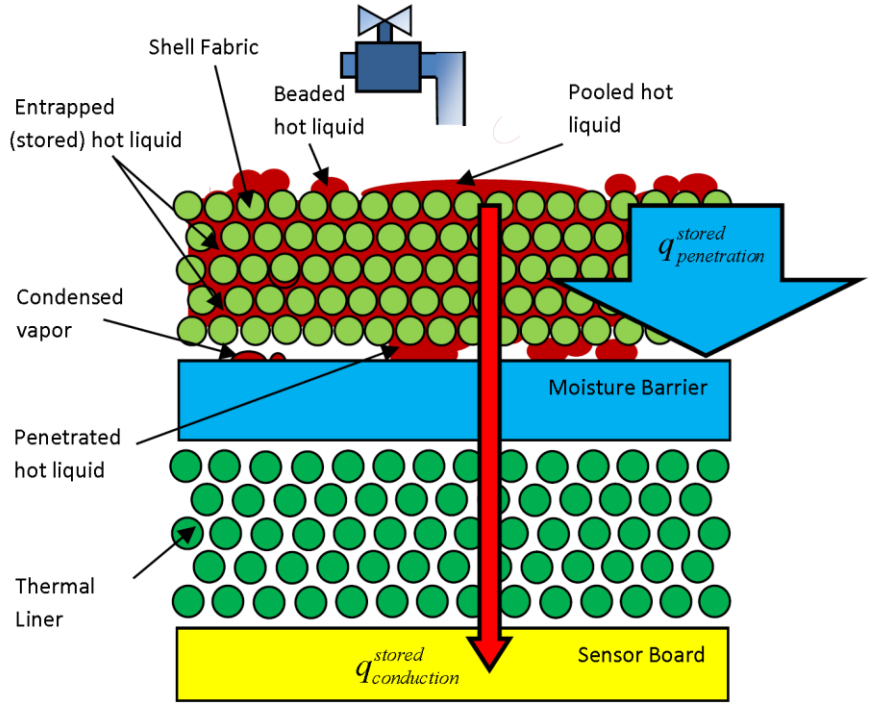

Figure 4.20. The schematic structure of the multilayer fabric system.

By comparing the stored energy values in impermeable multilayer fabric systems, MM-1 and MM-2, it is realized that increasing the thickness of the fabric

in an impermeable multilayer fabric system does not significantly affect the stored energy accumulation in the fabric. Therefore, for the tested fabrics, increasing thickness in the impermeable fabric system improves thermal performance of the fabric system.

It is interesting that the stored energy coefficient is not maximum in the thickest fabric system, MM-2 (thickness=4.8 mm). According to Figure 4.19 the value of the stored energy coefficient is maximum in the thick permeable structure of fabric systems DD-2 (thickness=4.0 mm). The average of the stored energy coefficient of the three sensors in fabric systems MM-2 and DD-2 in 45-degree orientation are 0.14 and 0.60 (Tables C.2 and C.3, Appendix C). Although the thicknesses of fabric DD-2 and MM-2 are relatively close, fabric DD-2 discharges almost 4 time more thermal energy to the sensors in comparison to fabric MM-1. Fabric systems MM-1 and DD-2 have thermal liner BB in their structures. It is realized that the trapped air in the thermal liner may improve or lower the thermal performance of the fabric system during the cooling period depending on how the fabric system is assembled:

- If the thermal liner is assembled underneath an impermeable fabric in fabric system (fabric system MM-2), the hot liquid cannot penetrate within the structure of the thermal liner. As such, the trapped air in thermal liner BB provides thermal insulation and decreases the discharge of thermal energy to a sensor when fabric system MM-2 is exposed to hot liquids (see Table 4.5).

- If the thermal liner is assembled underneath a permeable fabric in the fabric system (fabric system DD-2), the hot liquid can penetrate and be entrapped within the structure of the thermal liner. The accumulation of thermal energy in the fabric system due to entrapment of hot liquid within the structure of thermal liner BB can reduce the level of protection expected from fabric system DD-2 when exposed to hot liquid.

Therefore, thick and low density thermal liners may improve thermal performance of the fabric systems exposed to hot liquid if the thermal liner is assembled underneath an impermeable fabric in the fabric system. As such, it is necessary to take into account the effects of interactions of fabric properties such

as permeability and fabric density on thermal performance of fabric system exposed to hot liquid.

Statistical analysis

In order to further quantify the correlations between the experimental parameters, the fabric properties and the predicted performance of the fabric systems, a detailed statistical analysis is performed and a model to predict the thermal performance of the fabric systems upon exposure to hot water in 45-degree and horizontal orientation is developed. The dependent and the independent variables are shown in Table 4.8.

Table 4.8. Dependent and the independent variables in characterization of the thermal performance of the fabrics exposed to hot water in 45-degree and horizontal orientations.

		Variables	Abbreviations
Dependent Variables		2^{nd} degree burn	t_{2nd}
		Stored energy coefficient	ψ
Independent Variables	Fabric Properties	Contact angle	θ
		Fabric density	ρ_f
		Mass	m
		Thickness	x
		Air permeability	p
		Rct	R
	Experimental Variables	Non-dimensional displacement of the sensors with respect to the impingement point	y/d
		Angle of orientation	β

To eliminate the insignificant independent variables from the model, stepwise multiple linear regression is implemented and t-test is performed to measure variables significance. In this study, any P-values less than 0.05 is deemed to be insignificant (Greene, 2012). This means, if the obtained P-value for any fabric property does not span 95% of the confidence interval, the property is inferred to be statistically significant and to affect the thermal property of the fabric systems. Using StatCrunch® software (Pearson Education, London), the results from correlation and the stepwise multiple linear regression between the dependent and independent variables are shown in Tables 4.9 and 4.10.

Table 4.9. The correlation between the fabric and the hot water properties and the thermal performance of the fabrics, TPP_{eff}^{DW}, (second degree burn and the stored energy coefficient, ψ).

	TPP_{eff}^{DW}	
	Time to 2nd Degree Burn	Stored Energy Coefficient (ψ)
Air Permeability (p)	-0.71	0.50
Rct (R)	0.58	0.06
Thickness (x)	0.62	0.02
Angle of Orientation (β)	-0.08	0.69
Contact Angle (θ)	0.44	-0.22
Mass (m)	0.75	-0.16
Fabric Density (ρ_f)	-0.42	-0.11
y/d	0.15	-0.02

Table 4.10. Multiple linear regression for thermal properties of the fabric systems upon exposure to hot distilled water.

Variable	Distilled Water			
	2nd degree burn (t^{2nd})		Stored energy coefficient (ψ)	
	Tstat	P-value	Tstat	P-value
Intercept	1.6806	0.0996	2.0272	0.0482
Air Permeability (p)	-5.7849	<0.0001	8.6007	<0.0001
y/d	4.5493	<0.0001	2.7095	0.0093
Fabric Density (ρ_f)×Air permeability (p)	5.0576	<0.0001	-5.5981	<0.0001
Fabric Density (ρ_f)× Mass (m)	2.0831	0.0428	-------	-------
Rct (R)	2.9524	0.0050	-------	-------
Fabric density (ρ_f)	-2.4195	0.0196	-------	-------
Mass (m)	-2.0371	0.0474	-------	-------
Angle of Orientation (β)	-------	-------	12.5881	<0.0001
Contact Angle (θ)	-------	-------	-2.9674	0.0047

The "----" means that the variables were eliminated from the model.

According to Table 4.9, it is evident that air permeability is highly negatively correlated with the second-degree burn time and positively correlated with the store energy coefficient. This means the more permeable fabrics show less thermal protection and more stored thermal energy in the fabric system. Considering the effect of air permeability on both second degree burn time and the stored thermal energy in the fabric system, it is inferred that decreasing the air permeability improves the effective thermal performance of the fabric system upon

hot water splash. However, caution needs to be exercised in drawing conclusion about the results in this section. The test results are based on a limited number of experiments on specimens from a limited number of fabrics and hence may not be representative of other fabric systems and conditions.

According to Table 4.10, the P-values for the fabrics' mass, density, thermal resistance, air permeability, contact angle, angle of orientation and non-dimensional displacement of the sensors with respect to the impingement point are less than 0.05. The P-values obtained for these properties indicate that they strongly affect the thermal performance of the fabrics against hot water exposure ($P < 0.05$). In addition, the P-values for the fabrics exposed to hot water show that the interaction of fabric density and air permeability ($P < 0.0001$) is also significant factors in the thermal protective performance of the fabrics in hot water exposures as it was discussed earlier in Chapter 4, page 102.

According to the P-values in Table 4.10, non-dimensional displacement of the sensors with respect to the impingement point has also a significant effect on the effective thermal performance of the fabric system upon exposure to hot water. The P-values of non-dimensional displacement of the sensors with respect to the impingement point for second degree burn time and the stored energy coefficients are <0.0001and <0.0093 respectively. At the stagnation points, second degree burns occur faster and a lower amount of energy is stored in the fabric system. However, as the distance from the stagnation point increases, second degree burn occurs at a longer time and more energy will be stored in the fabric system. As such, for the areas where the fabric system is exposed indirectly due to the flow of the hot water, much attention needs to be paid to the accumulation of the stored energy and its discharge to the skin.

Multiple regression models were also developed (Equations 4.7 and 4.8) between the dependent and the independent variables shown in Tables 4.9. Equations 4.7 and 4.8 are multiple regression models to predict the second degree burn time (t_{2nd}^{DW}) and the stored energy coefficient of the fabric systems (ψ^{DW}) when exposed to hot distilled water in horizontal and 45-degree orientations. Analysis of variance was employed to verify the validity of the models. The P-values of the model were <0.0001. Therefore, at the 0.05 level of significance, the models are valid and each of Equations 4.7 and 4.8 has significant predictive power. The

coefficient of determination (R^2) values of Equations 4.7 and 4.8 are 0.94 and 0.83 respectively, which indicates the credibility of the linear model to predict second-degree burn time and the stored energy coefficient (the symbols are introduced in Table 4.9).

$$TPP_{eff}^{DW}\begin{cases}\psi^{DW} = 0.5081 - 0.0005\theta - 0.0362p - 0.0775\rho_f p \\ -0.0053\beta + 0.0046(^{y}/_{d}) \end{cases} \quad (4.7)$$

$$\begin{cases} t_{2nd}^{DW} = 44.1231 - 0.5493m - 17.6433p - 391.1746\rho_f \\ +39.0597\rho_f p + 1.0712\rho_f m - 2340.7625R + 0.9508\left(^{y}/_{d}\right) \end{cases} \quad (4.8)$$

Caution needs to be exercised in using the results from this study in order to evaluate thermal protective fabrics exposed to hot distilled water, drilling fluid and canola oil. The test results presented in this study are based on tests of specimens from limited quantities and hence may not be representative of other fabric systems. In addition, the results in this study were obtained based on a small number of experiments and fixed experimental variables such as hot liquid temperature, liquid flow and nozzle-to-sensor board separation.

Summary

When exposed to hot liquid splashes, heat and mass transfer to skin are influenced by the physical properties and structure of the fabric system and the nature of the hot liquid. When hot liquid splashes on the surface of the fabric, the hot liquid may run off, stay on, or penetrate through the surface of the fabric. The liquid drops may also penetrate through the fabrics and be stored in the fabric system or directly contact the skin. As a result, the fabric–liquid system transfers heat to the skin during and after exposure and may lower thermal performance of the fabric systems. By analyzing the results of the data collected from this study it can be concluded that the effective thermal performance of the fabric systems exposed to hot liquids corresponds to not only second and third degree burn but also to the amount of thermal energy stored in the system. The range of the stored energy coefficients in this study shows that a significant amount of stored energy during exposure can be discharged to the skin after the termination of the thermal exposure and can contribute to burn injuries. Therefore, it is necessary to determine and predict the thermal response of protective fabric systems upon exposure to hot liquid splash by taking into account the transmitted and thermal stored energy

developed in the fabric system during the exposure and cooling periods of the fabric. For this purpose, the stored energy coefficient (ψ) is introduced and its relationship to the physical properties of the fabrics were investigated.

The range of the predicted second degree burn time for the selected fabric systems was from several seconds to almost 160 s and the fabric systems accumulated up to 68% of the total energy in their structures. The range of the predicted performance was mainly determined by the fabrics' physical properties.

Among the physical properties, air permeability is a dominant factor in the effective protection against hot liquid since resistance to mass transfer is shown to be the key factor for reducing the amount of transmitted and discharged thermal energy to the skin. Fabric surface energy is another important factor in the effective performance of fabrics against hot liquid splash. By blocking or reducing the hot liquid's penetration from the outer surface through the fibrous structure, the transmitted and the discharged energy is minimized, which causes less burn injury and a lower amount of stored thermal energy. Additionally, the introduction of an impermeable membrane into the fabric system proved to be a critical factor that minimizes heat and mass transfer and stored thermal energy in double and multilayer fabrics by keeping hot liquid flow further from the skin. However, garments with impermeable membranes are likely to increase the physiological stress of the wearer (Wen, Petersen, McQueen, & Batcheller, 2015). The amount of entrapped air in the impermeable fabric structure is a critical determinant of the effective thermal performance of the fabric systems. While the impermeable structure of the fabric system resists mass transfer, the entrapped air in the fabric system provides thermal insulation and decreases the transmission and the discharge of thermal energy to skin.

This research introduces some interactions of fabric properties such as the combined effect of fabric density and air permeability that significantly affects the performance of fabric system against hot liquid splashes. In conclusion, improving the thermal performance of the fabric system exposed to hot liquid splash means a longer predicted time to second degree and third degree burn, and also reducing the stored energy coefficient. As such, fabric and garment properties that play crucial roles in increasing time to burn and reducing the stored thermal energy should be manipulated in fabric systems in order to increase thermal protection against hot

liquid. This is referred to as “effective thermal protective performance” (ETPP) in this study.

In the next chapter, the effective thermal performance of the fabric systems upon exposure to various hazards will be investigated. The discharge of stored energy to the skin after the termination of the thermal exposure and its contribution to burn injuries will be discussed. It is also intended to show the contributions of the stored energy coefficient in the effective thermal performance of the fabric when exposed to various hazards such as hot water splash, steam and radiation.

CHAPTER 5 EVALUATION OF THERMAL PROTECTIVE CLOTHING PERFORMANCE EXPOSED TO VARIOUS HAZARDS[2]

Introduction

Firefighters and industrial workers may sustain burn injuries caused by the exposure of the individuals to various thermal hazards such as flash fires, radiant heat, hot liquid splashes, impingement of hot gases and steam, hot surface contact, or any combination thereof. Thermal protective clothing ensembles slow down the rate of heat transfer to the skin. However, while working in a thermal environment, the clothing is heated and may store thermal energy which can be discharged to the skin later and contribute to burn injuries (G. Song, Cao, et al., 2011). The discharge of stored energy may occur without any changes to the air spaces between the fabric and skin or along with compression of the garment against the skin.

The overall goal of this chapter is to gain a fundamental understanding of the heat and mass transfer mechanisms associated with protective clothing systems when exposed to various thermal hazards, and during the cooling period immediately afterwards. This goal relates to the understanding of the thermal response of fabrics and amount of thermal energy discharged to the skin during the cooling phase. As such, it is intended to investigate the stored thermal energy developed in the fabric system subjected to various thermal hazards such as hot

[2] This chapter is an original work by the author. Some portions of this chapter have been presented at the following conferences (the author was responsible for the data collection, analysis as well as manuscript composition. G. Song and M. Ackerman were the supervisory authors and provided critical review of the manuscripts):

- Gholamreza, F., Song, G., & Ackerman, M. (2012). *Analyzing the discharged energy and its contribution to thermal performance of protective clothing upon hot liquid splash.* Paper presented at the Fiber Society Conference, Spring, St. Gallen, Switzerland.
- Gholamreza, F., Song, G., & Ackerman, M. (2012). *Thermal protective performance of protective clothing upon steam and hot liquid splash.* Paper presented at the Fiber Society Conference, Fall Boston, MA.
- Gholamreza, F., Song, G., & Ackerman, M. (2013). *Stored energy and thermal protective performance of protective clothing upon steam and hot liquid.* Paper presented at the 13th Autex World Textile Conference, Dresden, Germany.
- Gholamreza, F., Song, G., & Ackerman, M. (2014). *Thermal stored energy and protective performance upon various hazards.* Paper presented at the Fiber Society Conference, Spring, Liberec, Czech Republic.
- Gholamreza, F., Song, G., & Ackerman, M. (2014). *Thermal stored energy and protective performance of protective clothing upon radiant heat.* Paper presented at the 14th Autex World Textile Conference, Bursa, Turkey.

water splashes, steam and radiant heat exposures, along with their contributions to burn injuries.

As existing methods in standard tests consider stored energy when making burn predictions rely on iterations that require multiple tests, a number of investigators have proposed new methods to consider stored energy in these tests (e.g., (He, & Li, 2016a, 2016b; He, Wang, & Li, 2015)). Therefore, an additional goal of the study in this chapter relates to the development of a model that considers stored energy when predicting the minimum exposure time to cause a second degree burn. Using the stored energy model in conjunction with an appropriate skin heat transfer model and Henriques burn model enables the calculation of temperatures within the skin and the prediction of burn injury by taking into account the discharge of the thermal energy during the cooling period. Possible modifications to existing bench top test methods and equipment will also be investigated in order to better predict the thermal protection provided by thermal protective clothing systems considering the stored energy effects.

Experimental procedure

The fabric systems were evaluated by exposure to radiant heat, steam and hot water. The equipment employed in this chapter was explained in Chapter 3. Hot water at 85°C flows onto the fabric system mounted on the sensor board in a horizontal orientation at a flow rate of 67 mL/s. The specimens were cut to 404 mm by 253 mm and were conditioned at 20 ± 2°C with 65 ± 5% relative humidity for at least 24 hours prior to the testing. The analysis of the middle sensor (Figure 3.2) is used for the evaluation of the thermal performance of the fabric system exposed to hot water in this chapter.

The fabric systems were exposed to steam at 150°C. The test specimens for a given fabric system were cut to 200 mm by 200 mm and were conditioned at 20 ± 2°C with 65% relative humidity for at least 24 hours prior to the testing. Each specimen was placed on a Teflon-plated sample holder which was equipped with a skin stimulant sensor. The generated steam impinged upon the fabric specimen at a pressure of 200 kPa. In this study, it was intended to expose the fabric and let it cool by natural convection. As such, an open jet spacing with a nozzle-to-sensor spacing of 5 cm was used to expose the fabric systems to steam. The nozzle-to-sensor spacing was the maximum spacing possible in this apparatus in

order to provide enough space for the compression of the specimen during the cooling period.

For radiant heat exposures, specimens were cut to 15 cm by 15 cm and mounted on the sensor board horizontally below the heated coil. The heat flux (50 kW/m^2) was measured using a Schmidt-Boelter heat flux gauge. A transverse shutter was used to protect the specimen from the heat source before the test and during the cooling period (Figure 3.8).

For the first phase of experiments, the TPP approach was employed. According to this approach, the fabric specimen was exposed to each of the thermal hazards until the second degree burn time was predicted employing the burn evaluation criteria (TPP approach). Once the burn time was predicted, the exposure was terminated in order to minimize the exposure effect on the total absorbed energy. Data acquisition systems continued to record the discharged energy in the system after the exposure ended. Data was acquired until the discharged thermal energy transfer between the sensor and the back of the fabric was minimized and the fabric system was cooled.

Two procedures were employed to evaluate the discharged energy during the cooling period of the fabric system, compressive discharge and ordinary discharge.

Compressive discharge

After the exposure was terminated employing the TPP approach, the fabric was compressed against the sensor and the measured heat flux as a function of time was obtained (Figure 5.1). This procedure was implemented in order to measure the amount of discharged energy due to compression.

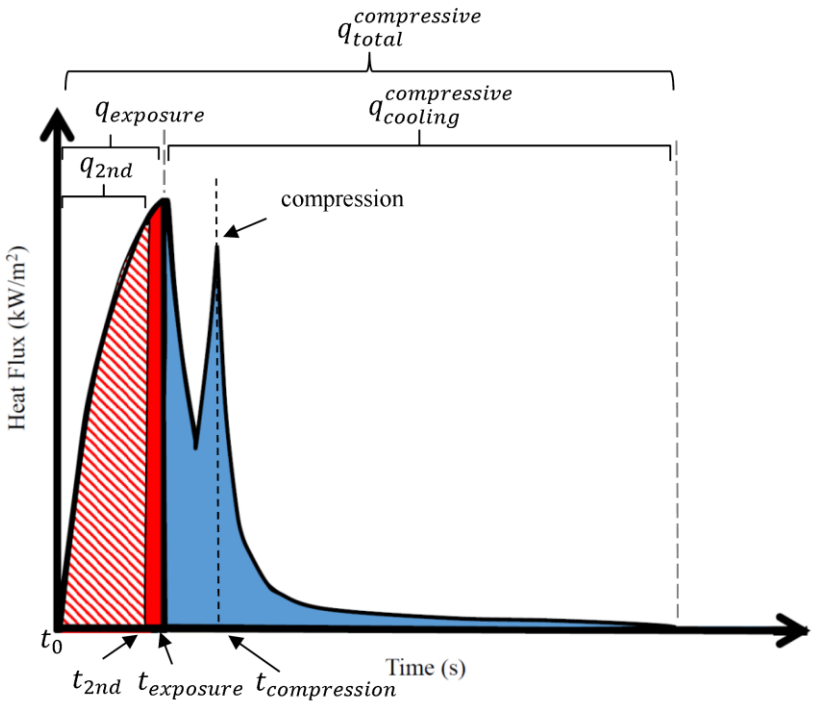

Figure 5.1. Schematic illustration of compressive discharge employing the TPP approach.

Based on the heat flux history for each specimen, the energies such as the energy required to generate the second degree burn (q_{2nd}), the compressive discharge thermal energy to the sensor during the cooling period ($q_{cooling}^{compressive}$) and the total absorbed thermal energy with compressive cooling ($q_{total}^{compressive}$) were determined. In addition, the following parameters are introduced:

Compressive discharge stored energy coefficient (ψ_{CD}): the compressive discharged energy's contribution to total absorbed energy (Equation 5.1).

$$\psi_{CD} = \frac{q_{cooling}^{compressive}}{q_{total}^{compressive}} \tag{5.1}$$

Compressive discharge stored energy index (φ_{CD}): the compressive discharged energy's contribution to the generation of second degree burn injury (Equation 5.2).

$$\varphi_{CD} = \frac{q_{cooling}^{compressive}}{q_{2nd}} \tag{5.2}$$

Ordinary discharge

For ordinary discharge, once the burn time was predicted and the exposure was terminated, the discharge of stored thermal energy was determined without compression. The fabric system was cooled and the data acquisition systems continued to record the ordinary discharged energy (Figure 5.2).

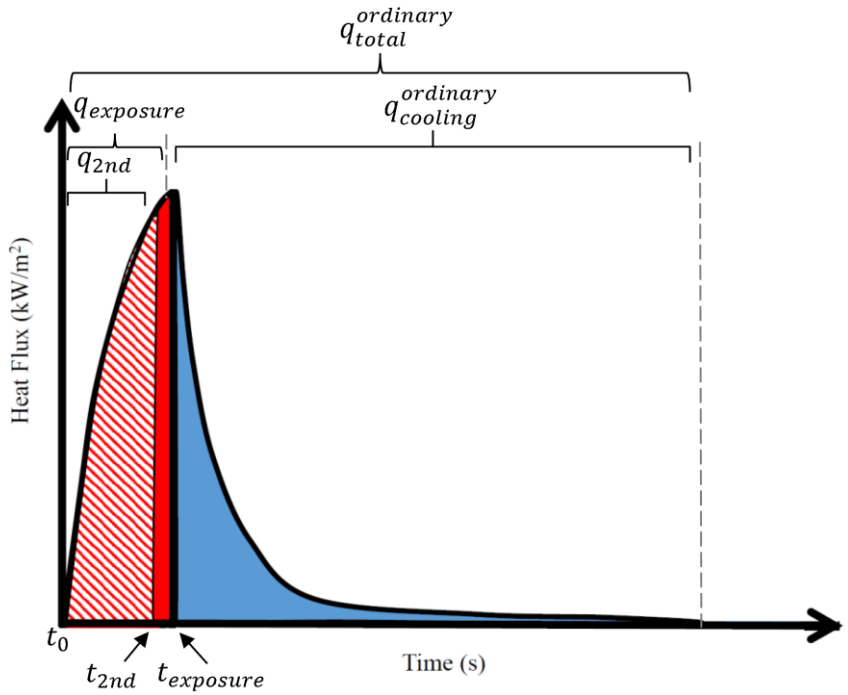

Figure 5.2. Schematic illustration of ordinary discharge employing the TPP approach.

Based on the heat flux history for each specimen, the energies such as the energy required to generate the second degree burn (q_{2nd}), the ordinary discharge thermal energy to the sensor during the cooling period ($q_{total}^{ordinary}$) and the total absorbed thermal energy with ordinary cooling ($q_{total}^{ordinary}$) were determined. In addition, the following parameters are introduced:

Ordinary discharge stored energy coefficient (ψ_{OD}): the ordinary discharged energy's contribution to total absorbed energy (Equation 5.3).

$$\psi_{OD} = \frac{q_{cooling}^{ordinary}}{q_{total}^{ordinary}} \tag{5.3}$$

Ordinary discharge stored energy index (φ_{OD}): the ordinary discharged energy's contribution to the generation of second degree burn injury (Equation 5.4).

$$\varphi_{OD} = \frac{q_{cooling}^{ordinary}}{q_{2nd}} \tag{5.4}$$

Minimum exposure time approach

The minimum exposure time approach (MET approach) is an approach which is used to predict the second degree burn time for a fabric system exposed to a thermal hazard by taking into account the transmitted and stored thermal energy developed in the fabric system during the exposure and the cooling period. Employing this approach, the minimum exposure time to second degree burn is used as the exposure time for a thermal hazard that will provide a second degree burn at the end of the cooling period (i.e. the omega value in Equation 2.2 (page 14) approaches 1.0 at the end of the cooling period). Figures 5.3 and 5.4 illustrate the minimum exposure time to second degree burn in ordinary and compressive situations respectively. For the sake of clarity, the terms "minimum exposure time" and "minimum exposure time to second degree burn" are interchangeably used in the discussions in this thesis.

Stored energy model

In this research, the stored energy model is an equation that takes into account the transmitted and thermal stored energy developed in the fabric system during the exposure and cooling period. The stored energy model determines the minimum exposure time to second degree burn (t_{MET}) for the fabric system using the data obtained for the fabric using the TPP approach.

In order to develop the model, it is assumed the stored energy coefficient is not dependent on the exposure time. It means when a fabric system is exposed to a hazard with exposure time A in one test and exposure time B in another test, the proportion of the discharge energy of the fabric to the total absorbed energy ($\frac{q_{cooling}}{q_{total}}$) for the two tests are the same. Caution needs to be exercised as the assumption may not be valid for all circumstances. For instance, in cases of flame and other high heat flux exposures, thermochemical reactions may occur in fabrics, which could be endothermic or exothermic (Torvi, 1997). These reactions would affect the energy transferred to the skin or test sensor. There could be a case where one exposure time may be sufficient to produce these thermochemical reactions,

while a second, slightly shorter exposure time may not be sufficient to produce these thermochemical reactions.

Applying this assumption, the stored energy coefficient for a fabric system exposed to a thermal hazard using the TPP approach and the MET approach is identical (Equations 5.5 and 5.6).

$$\psi_{TPP} = \psi_{MET} = \psi \tag{5.5}$$

$$\frac{q_{cooling\ (TPP)}}{q_{total\ (TPP)}} = \frac{q_{cooling\ (MET)}}{q_{total\ (MET)}} = \psi \tag{5.6}$$

The total absorbed energy to second degree burn in the TPP approach and the MET approach are $q_{2nd\ (TPP)}$ and $q_{2nd\ (MET)}$, respectively. In the MET approach, it is expected that a second degree burn occurs at the end of the cooling period due to the transmitted and the discharged thermal energy. It is assumed that the energy to produce a second degree burn in TPP approach is equal to the total to the total absorbed energy to second degree in the MET approach (Equation 5.7).

$$q_{2nd\ (TPP)} = q_{total\ (MET)} \tag{5.7}$$

The total absorbed energy is equal to the total transmitted energy during exposure time plus the discharge energy. Therefore, for the MET approach, one has:

$$q_{total\ (MET)} = q_{exposure\ (MET)} + q_{cooling\ (MET)} \tag{5.8}$$

Substituting Equation 5.7 into 5.8, one has:

$$q_{2nd\ (TPP)} = q_{exposure\ (MET)} + q_{cooling\ (MET)} \tag{5.9}$$

By dividing Equation 5.9 by $q_{2nd\ (TPP)}$, Equation 5.10 is obtained.

$$\frac{q_{2nd\ (TPP)}}{q_{2nd\ (TPP)}} = \frac{q_{exposure\ (MET)}}{q_{2nd\ (TPP)}} + \frac{q_{cooling\ (MET)}}{q_{2nd\ (TPP)}} \tag{5.10}$$

Employing Equation 5.6 and 5.7, Equation 5.11, 5.12 and 5.13 are obtained as follow:

$$1 = \frac{q_{exposure\ (MET)}}{q_{2nd\ (TPP)}} + \frac{q_{cooling\ (MET)}}{q_{total\ (MET)}} \tag{5.11}$$

$$1 = \frac{q_{exposure\ (MET)}}{q_{2nd\ (TPP)}} + \psi \qquad (\psi = \text{constant}) \tag{5.12}$$

$$q_{2nd\ (TPP)}(1 - \psi) = q_{exposure\ (MET)} \tag{5.13}$$

The time corresponding to the energy at the minimum exposure time to second degree burn ($q_{exposure\ (MET)}$) is assumed to be the minimum exposure time required to generate a second degree burn (t_{MET}).

$$q_{exposure\ (MET)} = \int_{t_0=0}^{t_{MET}} q''\, dt \tag{5.14}$$

By substitution of Equation 5.13 in 5.14, the stored energy equation is obtained:

$$q_{2nd\ (TPP)}(1 - \psi) = \int_{t_0=0}^{t_{MET}} q''\, dt \tag{5.15}$$

In this equation, $q_{2nd\ (TPP)}$ is the thermal absorbed energy required to produce a second degree burn obtained by the TPP approach (continuous heating), ψ is the stored energy coefficient, q'' is heat flux and t_{MET} is the minimum exposure time to second degree burn.

The stored energy index can also be used for the determination of the minimum exposure time in the stored energy equation. The relation between the stored energy index and the stored energy coefficient can be obtained as follows. In the TPP approach, the exposure time is terminated once the second degree burn is predicted. Therefore, it can be said that the total energy absorbed by the sensor during exposure is equal to the total energy absorbed by the sensor at the time at which second degree burn time occurs (Equation 5.16).

$$q_{exposure} = q_{2nd} \tag{5.16}$$

Therefore, the total thermal energy absorbed by the sensor during the exposure and post-exposure is

$$q_{total} = q_{2nd} + q_{cooling} \tag{5.17}$$

According to the stored energy coefficient, one has

$$\psi = \frac{q_{cooling}}{q_{total}} \tag{5.18}$$

By Substitution of Equation 5.17 in 5.18:

$$\psi = \frac{q_{cooling}}{q_{cooling+}q_{2nd}} \tag{5.19}$$

$$\frac{1}{\psi} = \frac{q_{cooling} + q_{2nd}}{q_{cooling}} \tag{5.20}$$

$$\frac{1}{\psi} = 1 + \frac{q_{2nd}}{q_{cooling}} \tag{5.21}$$

The stored energy index is the discharged energy's contribution in the generation of second degree burn injury (Equation 5.21). Comparing Equations 5.21 and 5.22:

$$\varphi = \frac{q_{cooling}}{q_{2nd}} \tag{5.22}$$

$$\frac{1}{\psi} = 1 + \frac{q_{2nd}}{q_{cooling}} \tag{5.23}$$

$$\frac{1}{\psi} = 1 + \frac{1}{\varphi} \tag{5.24}$$

Therefore, the stored energy coefficient and the stored energy index have the following relations:

$$\varphi = \frac{\psi}{1-\psi} \tag{5.25}$$

$$\psi = \frac{\varphi}{1+\varphi} \tag{5.26}$$

These equations are valid if the exposure time is terminated once the second degree burn is obtained. The relation between the stored energy coefficient and the stored energy index can also be confirmed by the data in Tables C.1 to C.8 in Appendix C and Tables 5.1, 5.2 and 5.3 later in this chapter.

As such, the minimum exposure time to second degree burn can also be obtained by employing the following equation where $q_{2nd\,(TPP)}$ is the thermal absorbed energy to second degree burn obtained by the TPP approach, φ is the stored energy index, q'' is heat flux and t_{MET} is the minimum exposure time.

$$q_{2nd\,(TPP)}\left(\frac{1}{1+\varphi}\right) = \int_{t_0=0}^{t_{MET}} \dot{q}\ dt \tag{5.27}$$

It is necessary to note that the abovementioned equations are valid when a second degree burn is predicted by the TPP approach. When a second degree burn is not predicted ($q_{2nd\,(TPP)} = 0$), one of the following two cases may happen:

- there is no burn prediction ($q_{2nd\,(TPP)} = 0$), and there is no stored thermal energy during the cooling period in the fabric system ($\psi = 0$). This means that no energy is received from the fabric to the heat flux sensor during the cooling period. Under this circumstance, the fabric system can be called as an "an efficient fabric system" for the specific testing condition.

- there is no burn prediction ($q_{2nd\,(TPP)} = 0$), and there is some stored thermal energy during the cooling period in the fabric system ($\psi > 0$). Under this circumstance, the stored thermal energy in the fabric system is not enough to cause a second degree burn during the cooling period. However, the fabric system can be called as a "potential fabric system" for the specific testing condition. The stored thermal energy in the system is important for the cases when the fabric system is reheated by a secondary thermal exposure before the fabric system is cooled.

The minimum exposure time is dependent on the type of thermal energy discharge. Based on the ordinary discharge or the compressive discharge, the minimum exposure time may be different for the same fabric system.

Ordinary Discharge Minimum Exposure Time

By the substitution of the ordinary discharge stored energy coefficient (ψ_{OD}) in Equation 5.15 or the ordinary discharge stored energy index (φ_{OD}) in Equation 5.27, the ordinary discharge minimum exposure time (t_{MET}^{OD}) is predicted. The ordinary discharge minimum exposure time is the exposure time which causes a second degree burn during the cooling period due to an ordinary discharge. In Figure 5.3, the exposure time is the ordinary discharge minimum exposure time (t_{MET}^{OD}). According to the proposed MET method, t_{MET}^{OD} can be referred to as the second degree burn threshold when an ordinary discharge condition is applied. This means that for values of less than t_{MET}^{OD} (s) in Figure 5.3, there is no second degree burn prediction when an ordinary discharge condition is applied. According to the proposed method, it is also assumed that a second degree burn occurs at the end of the cooling period due to the transmitted and discharge thermal energy.

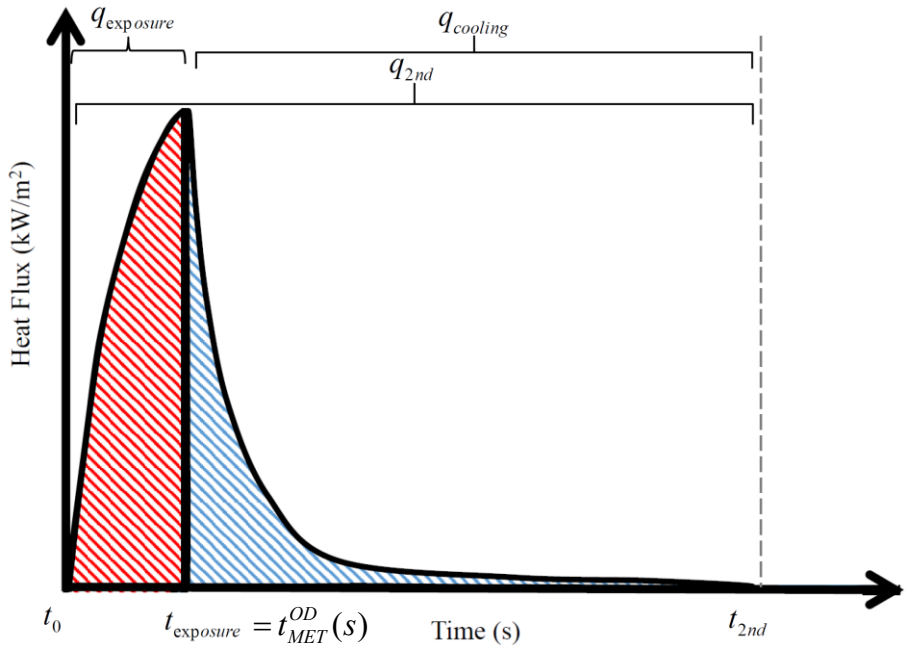

Figure 5.3. Stored energy approach when an ordinary discharge condition is applied and the ordinary discharge minimum exposure time, t_{MET}^{OD} (s).

Compressive discharge minimum exposure time

In addition, by the substitution of the compressive discharge stored energy coefficient (ψ_{CD}) in Equation 5.15 or compressive discharge stored energy index (φ_{CD}) in Equation 5.27, the compressive discharge minimum exposure time (t_{MET}^{CD}) can be predicted. The compressive discharge minimum exposure time is the exposure time which causes a second degree burn during the cooling period due to a compressive discharge.

In Figure 5.4, the exposure time is the compressive discharge minimum exposure time (t_{MET}^{CD}). According to the proposed MET method, t_{MET}^{CD} can also be referred as the second degree burn threshold in the compressive situation. This means that for the values less than t_{MET}^{CD} (s), there is no second degree burn prediction when a compressive discharge condition is applied.

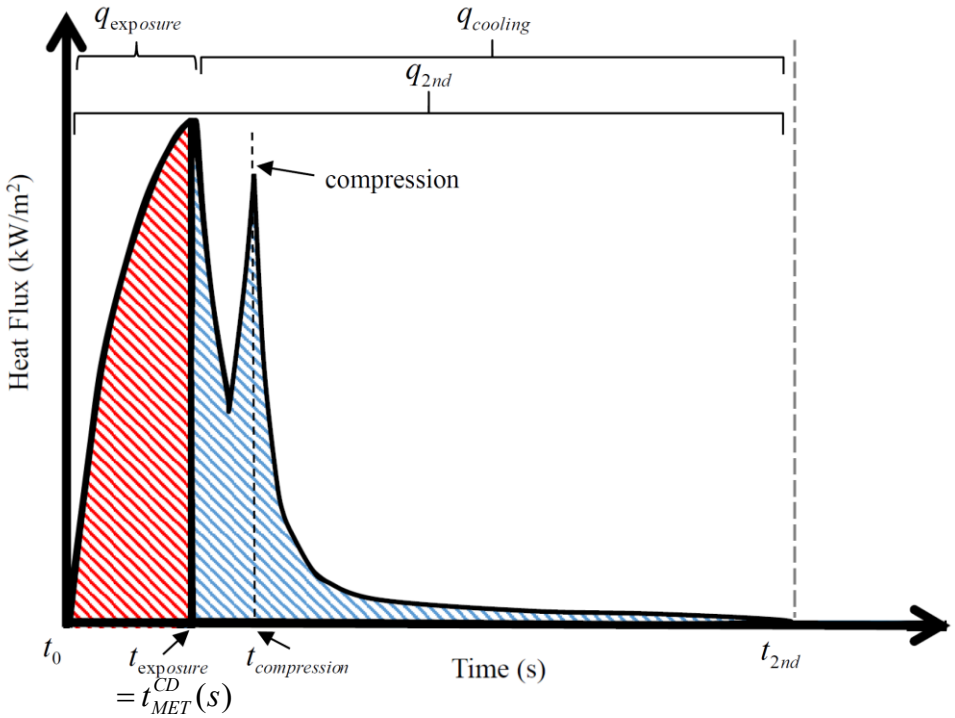

Figure 5.4. Stored energy approach when a compressive discharge condition is applied and the ordinary discharge minimum exposure time, t_{MET}^{CD} (s).

Determination of the minimum exposure time using the stored energy model

In this chapter, the testing conditions were set to provide a range of thermal exposures in order to compare the results obtained from different hazards for each fabric system. Once burns were predicted, the exposure was terminated. The data acquisition systems continued to record the discharged energy in the system after the exposure ended until the fabric was cooled. For the compression tests, once the exposure was terminated, the fabric-sensor assembly was compressed upon the skin simulant using the compressors shown in Figure 3.9.

Employing the stored energy model in conjunction with an appropriate sensor model, skin model and Henriques burn model enables the calculation of temperatures within the skin and the prediction of burn injury exposed to various boundary conditions on the skin considering the stored energy effect. These procedures result in the development of the burn evaluation model shown in Figure 5.5.

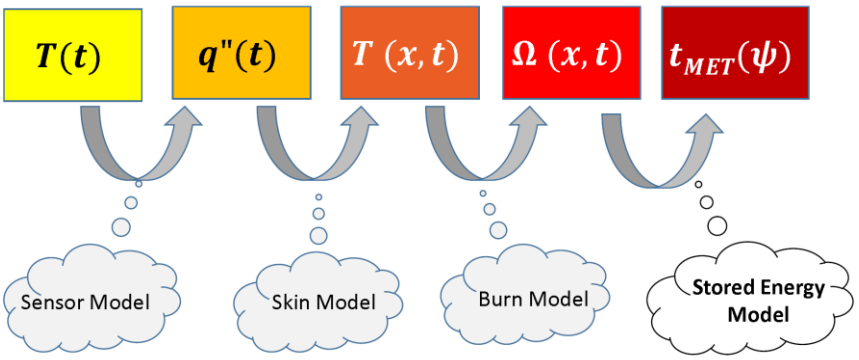

Figure 5.5. The proposed burn evaluation model.

In order to predict the minimum exposure time to second degree burn, the proposed burn evaluation model was implemented. Employing the TPP approach, the specimen was exposed to the hazards until the second degree burn occurred. The data acquisition system continued recording the discharged energy in the system for 60 s after the exposure ended. Based on the discharged, transmitted energy and total energy, the predicted total absorbed energy to second degree burn time ($q_{2nd\,(TPP)}$), stored energy coefficient and stored energy index were determined. Using the stored energy model (Equations 5.15 or 5.27), the minimum exposure time to cause a second degree burn was predicted. These steps were used for both ordinary and compressive discharges.

Results and discussion

The predicted minimum exposure time that causes a second degree burn and the predicted second degree burn times obtained for the different fabric systems exposed to distilled water, steam and radiant heat in ordinary and the compressive situations are shown in Tables 5.1 to 5.3. The values in these tables are the average values of three specimens tested for each fabric.

Table 5.1. Predicted thermal performance of the fabric system exposed to distilled water employing TPP approach.

Fabric system and assembly description		Distilled Water							
				Ordinary Discharge			Compressive Discharge		
		Exposure Time (s)	$t_{2nd\ (s)}$ (SD)	Ψ_{OD} (SD)	φ_{OD} (SD)	$t^{OD}_{MET\ (s)}$ (SD)	Ψ_{CD} (SD)	φ_{OD} (SD)	$t^{CD}_{MET\ (s)}$ (SD)
SS-1	Fabric AA	3.0	3.0 (0.3)	0.44 (0.04)	0.79 (0.13)	1.7 (0.1)	0.37 (0.02)	0.55 (0.03)	1.9 (0.3)
SS-4	Fabric DD	15.0	13.9 (1.2)	0.16 (0.01)	0.20 (0.02)	12.5 (0.7)	0.16 (0.04)	0.19 (0.05)	10.4 (1.9)
DD-1	Fabric AA+ Thermal liner AA	8.0	7.5 (0.4)	0.29 (0.00)	0.42 (0.00)	5.5 (0.4)	0.29 (0.08)	0.42 (0.17)	5.4 (0.5)
DD-2	Fabric AA+ Thermal liner BB	14.0	13.2 (0.5)	0.64 (0.07)	1.88 (0.58)	7.0 (0.9)	0.67 (0.05)	2.11 (0.46)	7.3 (0.5)
DD-3	Fabric AA+ Moisture barrier AA	17.0	17.8 (0.8)	0.30 (0.04)	0.40 (0.09)	12.3 (0.9)	0.20 (0.05)	0.25 (0.09)	14.7 (0.6)
DD-4	Moisture barrier AA+ Fabric AA	22.0	21.9 (1.0)	0.25 (0.03)	0.33 (0.6)	15.4 (0.1)	0.19 (0.03)	0.24 (0.09)	17.3 (1.3)
MM-1	Fabric AA+ Moisture barrier AA+ Thermal liner AA	35.0	33.6 (0.8)	0.18 (0.01)	0.21 (0.01)	28.1 (1.9)	0.15 (0.01)	0.18 (0.01)	28.5 (0.6)
MM-2	Fabric AA+ Moisture barrier AA+ Thermal liner BB	55.0	53.7 (1.1)	0.18 (0.01)	0.21 (0.02)	42.1 (1.5)	0.10 (0.01)	0.11 (0.01)	51.4 (2.4)

Table 5.2. Predicted thermal performance of the fabric system exposed to steam employing TPP approach.

Fabric system and assembly description		Steam							
				Ordinary Discharge			Compressive Discharge		
		Exposure Time (s)	$t_{2nd\ (s)}$ (SD)	Ψ_{OD} (SD)	φ_{OD} (SD)	$t^{OD}_{MET\ (s)}$ (SD)	Ψ_{CD} (SD)	φ_{OD} (SD)	$t^{CD}_{MET\ (s)}$ (SD)
SS-1	Fabric AA	1.0	0.5 (0.2)	0.72 (0.06)	2.81 (0.03)	0.4 (0.2)	0.79 (0.03)	3.87 (1.01)	0.3 (0.2)
SS-4	Fabric DD	3.0	2.0 (0.2)	0.66 (0.05)	1.96 (0.33)	0.9 (0.0)	0.63 (0.05)	1.74 (0.37)	0.8 (0.0)
DD-1	Fabric AA+ Thermal liner AA	1.0	0.5 (0.1)	0.79 (0.02)	4.08 (0.44)	0.4 (0.1)	0.79 (0.00)	3.92 (0.07)	0.3 (0.1)
DD-2	Fabric AA+ Thermal liner BB	1.0	0.7 (0.1)	0.88 (0.01)	8.25 (0.01)	0.4 (0.1)	0.83 (0.02)	4.90 (0.09)	0.3 (0.0)
DD-3	Fabric AA+ Moisture barrier AA	10.0	9.3 (0.9)	0.43 (0.04)	0.74 (0.09)	5.5 (0.9)	0.40 (0.01)	0.71 (0.00)	5.2 (0.1)
DD-4	Moisture barrier AA+ Fabric AA	11.0	10.4 (0.7)	0.40 (0.08)	0.66 (0.04)	7.0 (1.2)	0.38 (0.03)	0.60 (0.09)	7.2 (0.9)
MM-1	Fabric AA+ Moisture barrier AA+ Thermal liner AA	30.0	No Burn	0.41 (0.07)	---	---	0.38 (0.04)	---	---
MM-2	Fabric AA+ Moisture barrier AA+ Thermal liner BB	30.0	No Burn	0	---	---	0	---	---

Table 5.3. Predicted thermal performance of the fabric system exposed to radiant heat employing TPP approach.

Fabric system and assembly description		Radiant Heat							
				Ordinary Discharge			Compressive Discharge		
		Exposure Time (s)	$t_{2nd\ (s)}$ (SD)	Ψ_{OD} (SD)	φ_{OD} (SD)	$t_{MET\ (s)}^{OD}$ (SD)	Ψ_{CD} (SD)	φ_{OD} (SD)	$t_{MET\ (s)}^{CD}$ (SD)
SS-1	Fabric AA	6.0	5.7 (0.3)	0.63 (0.05)	1.63 (0.01)	2.9 (0.3)	0.74 (0.04)	2.60 (0.01)	2.7 (0.1)
SS-4	Fabric DD	10.0	7.8 (0.4)	0.74 (0.01)	2.84 (0.04)	3.8 (1.1)	0.74 (0.04)	2.73 (0.03)	3.9 (0.5)
DD-1	Fabric AA+ Thermal liner AA	15.0	12.1 (0.9)	0.75 (0.03)	2.96 (0.05)	4.3 (0.1)	0.77 (0.05)	3.41 (0.11)	4.0 (0.3)
DD-2	Fabric AA+ Thermal liner BB	28.0	24.6 (1.0)	0.79 (0.04)	4.12 (0.10)	9.7 (0.8)	0.81 (0.04)	4.28 (0.11)	5.8 (0.9)
DD-3	Fabric AA+ Moisture barrier AA	13.0	11.1 (0.9)	0.74 (0.01)	2.79 (0.09)	5.4 (0.3)	0.77 (0.02)	3.30 (0.08)	4.9 (0.2)
DD-4	Moisture barrier AA+ Fabric AA	---	---	---	---	---	---	---	---
MM-1	Fabric AA+ Moisture barrier AA+ Thermal liner AA	20.0	18.5 (0.2)	0.78 (0.02)	3.63 (0.01	8.3 (0.4)	0.82 (0.03)	4.60 (0.09)	5.1 (0.3)
MM-2	Fabric AA+ Moisture barrier AA+ Thermal liner BB	30.0	25.1 (0.1)	0.86 (0.05)	6.80 (0.02)	9.6 (0.7)	0.91 (0.04)	10.01 (0.02)	6.9 (1.1)

The stored energy model validation

In this step, the calculated minimum exposure times obtained from the stored energy model were compared to the minimum exposure times obtained from the iterative tests used in ASTM F 2731-10. A series of iterative tests were conducted to validate the proposed stored energy model for the tested fabric system upon exposure to the hazards.

Determination of the minimum exposure time using the iterative approach

In order to determine the minimum exposure time using the iterative approach, the specimen is exposed to the heat source long enough so that the second degree burn time is predicted. The exposure time is assigned as $t_{\max}$. Then, the data acquisition continues to record the sensor data until the thermal stored energy in the fabric system is released. The length of time for the data acquisition may be different due to the nature and magnitude of hazard or based on the thermal properties of the fabric. For the second test, the time will be maximum time ($t_{\max}$) divided by two ($t_{trial} = t_{\max} / 2$). If the second degree burn time is not predicted, the new trial time will be half way between the just completed trial time and the maximum time. If the second degree burn was predicted, the new trial time will be half way between the just completed trial time and the lower time (when burn was not predicted). For the first time through, the lower previous exposure time will be zero. (ASTM, 2008b). The method of halving will be continued until the difference between the current trial time and the previous trial time will be less than 1 s.

Using the iterative approach, the compressive discharge minimum exposure time and the ordinary discharge minimum exposure time for the fabrics systems exposed to distilled water, steam and radiant heat were obtained and are shown in Tables 5.4, 5,5 and 5.6. The minimum exposure time for fabric systems SS-1, SS-4, DD-1 and DD-2 are not obtained since these values were less that a second.

Table 5.4. The ordinary discharge minimum exposure time and the compressive discharge minimum exposure time for the fabrics systems exposed to distilled water.

Distilled Water					
Fabric system	Assembly Description	Minimum Exposure Time (s) (SD)			
		Ordinary Discharge (t_{MET}^{OD})		Compressive Discharge (t_{MET}^{CD})	
		Predicted	Iterative	Predicted	Iterative
SS-1	Fabric AA	1.7 (0.1)	2.3 (0.6)	1.9 (0.3)	2.3 (0.6)
SS-4	Fabric DD	12.5 (0.7)	10.3 (0.6)	10.4 (1.9)	11.7 (0.6)
DD-1	Fabric AA+ Thermal liner AA	5.5 (0.4)	6.3 (0.6)	5.4 (0.5)	6.0 (1.0)
DD-2	Fabric AA+ Thermal liner BB	7.0 (0.9)	7.3 (0.6)	7.3 (0.5)	8.0 (0.0)
DD-3	Fabric AA+ Moisture barrier AA	12.3 (0.9)	10.7 (0.6)	14.7 (0.6)	16.0 (1.0)
DD-4	Moisture barrier AA+ Fabric AA	15.4 (0.1)	16.7 (0.6)	17.3 (1.3)	17.7 (0.6)
MM-1	Fabric AA+ Moisture barrier AA+ Thermal liner AA	28.1 (1.9)	27.3 (0.6)	28.5 (0.6)	28.0 (0.0)
MM-2	Fabric AA+ Moisture barrier AA+ Thermal liner BB	42.1 (1.5)	44.7 (0.6)	51.4 (2.4)	52.3 (0.6)

Table 5.5. The ordinary discharge minimum exposure time and the compressive discharge minimum exposure time for the fabrics systems exposed to steam.

Steam					
Fabric system	Assembly Description	Minimum Exposure Time (s) (SD)			
		Ordinary Discharge (t_{MET}^{OD})		Compressive Discharge (t_{MET}^{CD})	
		Predicted	Iterative	Predicted	Iterative
SS-1	Fabric AA	0.4 (0.2)	---	0.3 (0.2)	---
SS-4	Fabric DD	0.9 (0.0)	1.3 (0.6)	1.3 (0.0)	1.7 (0.6)
DD-1	Fabric AA+ Thermal liner AA	0.4 (0.1)	---	0.3 (0.1)	---
DD-2	Fabric AA+ Thermal liner BB	0.4 (0.1)	---	0.3 (0.0)	---
DD-3	Fabric AA+ Moisture barrier AA	5.5 (0.9)	7 (1.0)	5.2 (0.1)	7.3 (0.6)
DD-4	Moisture barrier AA+ Fabric AA	7.0 (1.2)	7.7 (0.6)	7.2 (0.9)	8.3 (0.6)
MM-1	Fabric AA+ Moisture barrier AA+ Thermal liner AA	No Burn	No Burn	No Burn	No Burn
MM-2	Fabric AA+ Moisture barrier AA+ Thermal liner BB	No Burn	No Burn	No Burn	No Burn

The "---" means the iterative test was not performed.

Table 5.6. The ordinary discharge minimum exposure time and the compressive discharge minimum exposure time for the fabrics systems exposed to radiant heat.

Radiant Heat					
Fabric system	Assembly Description	Minimum Exposure Time (s) (SD)			
		Ordinary Discharge (t_{MET}^{OD})		Compressive Discharge (t_{MET}^{CD})	
		Predicted	Iterative	Predicted	Iterative
SS-1	Fabric AA	2.9 (0.3)	4.3 (0.6)	2.7 (0.1)	2.0 (1.0)
SS-4	Fabric DD	3.8 (1.1)	5.7 (0.6)	3.9 (0.5)	5.0 (1.0)
DD-1	Fabric AA+ Thermal liner AA	4.3 (0.1)	4.7 (0.6)	4.0 (0.3)	4.7 (0.6)
DD-2	Fabric AA+ Thermal Liner B	9.7 (0.8)	11.0 (1.0)	5.8 (0.9)	7.3 (0.6)
DD-3	Fabric AA+ Moisture barrier AA	5.4 (0.3)	6.3 (0.6)	4.9 (0.2)	6 (1.0)
DD-4	Moisture barrier AA+ Fabric AA	---	---	---	---
MM-1	Fabric AA+ Moisture barrier AA+ Thermal liner AA	8.3 (0.4)	9.0 (0.0)	5.1 (0.3)	6 (1.0)
MM-2	Fabric AA+ Moisture barrier AA+ Thermal Liner B	9.6 (0.7)	10.7(0.6)	6.9 (1.1)	7.3 (0.6)

The "---" means not test was done for fabric system DD-4.

In this research, 108 iterative experiments were conducted to validate the stored energy model. Figure 5.6 shows the predicted values of minimum exposure time with the stored energy model and the minimum exposure time obtained by the iterative method. According to the plotted data in Figure 5.6, it can be inferred that the stored energy model can predict the minimum exposure time close to the minimum exposure time obtained from the iterative tests (R^2=0.99). The stored energy model is able to predict the minimum exposure time within 10% of accuracy. 89% of the predicted minimum exposure times to produce a second degree burn using the stored energy model are less than the predicted METs by the iterative test. This show that in majority of the tests, the model under-predicts the values of MET. In the vast majority of cases, the predictions are within 10% of the experimental values.

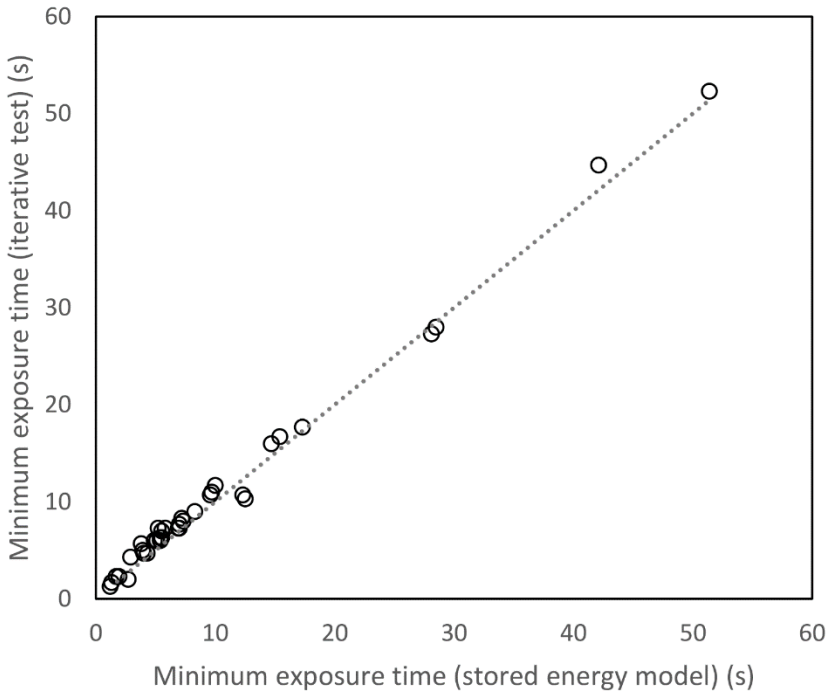

Figure 5.6. Minimum exposure time (s): iterative vs. stored energy model.

Caution needs to be exercised in applying the stored energy model to all situations as small numbers and types of exposures were being investigated in this thesis. In future works, it is recommended to investigate a wider range of exposures in order to better evaluate the predictive model.

Analysis of the thermal performance of the fabric systems exposed to various hazards

In the analysis of the performance of the fabric exposed to hot liquid in Chapter 3, the effects of fabric properties on the second degree burn time and the stored energy coefficient were investigated. Also, the effective thermal performance was proposed in order to evaluate the fabric performance by taking into account the stored thermal energy developed in the fabric system during the exposure and cooling periods of the fabric.

In this chapter, by introducing the ordinary discharge and the compressive discharge minimum exposure time and incorporating the stored energy effect into the minimum exposure time to second degree burn, the effective thermal protective

performance (ETPP) is further developed. It is comprised of two parts: the predicted time to second degree burn by continuous heating (TPP approach), and the predicted minimum exposure time to second degree burn employing the stored energy model. As such, in this part, the effects of fabric properties on the ordinary discharge minimum exposure time and the compressive discharge minimum exposure time will be investigated.

According to Tables 5.4, 5.5 and 5.6, the range of the ordinary discharge stored energy coefficient (ψ_{OD}) in hot water splash (0.16 to 0.64), steam (0 to 0.88) and radiant heat (0.63 to 0.86) confirms that there may be considerable amount of stored thermal energy in fabrics after the exposures end in ordinary cooling of the garment. In addition, the range of the compressive discharge stored energy coefficient (ψ_{CD}) in hot water splash (0.10 to 0.67), steam (0 to 0.83) and radiant heat (0.74 to 0.91) also confirms that there may be considerable amount of stored thermal energy in fabrics after exposures end in compressive cooling of the garment. The difference between the ranges of the stored energy coefficient in compressive and the ordinary discharge indicates that the type of discharge affects thermal performance of the fabric systems.

By comparison of the second degree burn and minimum exposure times, it is confirmed that the discharge of the stored energy lowers the protective performance expected from fabric systems. Figure 5.7 shows the heat flux history for fabric system SS-4 exposed to hot water with ordinary discharge. The burn time predicted for this fabric using the TPP approach is 15.8 s. However, this burn value is obtained through a continuous exposure time until burn injury is predicted, which excludes the contribution of stored energy during cooling period. Taking into account the discharge of thermal energy during the ordinary cooling period, the exposure time required to cause a second degree burn for fabric system SS-4 is 11.0 s (Figure 5.7). Therefore, the ordinary discharge minimum exposure time predicted for fabric system SS-4 is 11.0 s. This means that if the fabric is exposed for 11 s, the burn is predicted to occur during the cooling period of the fabric (t_{2nd}=24 s). For the values less than 11.0 s, no second degree burn was predicted for fabric system SS-4 exposed to 85°C in horizontal orientation (Flow rate: 67 mL/s and 6 cm of nozzle-to-plate spacing).

Figure 5.7 also shows the two last trials of the iterative methods. The burn evaluation criteria predict first degree burn for fabric system SS-4 exposed to hot water for 10.0 s, while 11.0 s exposure causes the prediction of a 2nd degree burn during the cooling period. As such, 11.0 s is reported as the ordinary discharge minimum exposure time for fabric system SS-4 and the approach is named as minimum exposure time approach with ordinary discharge (METO).

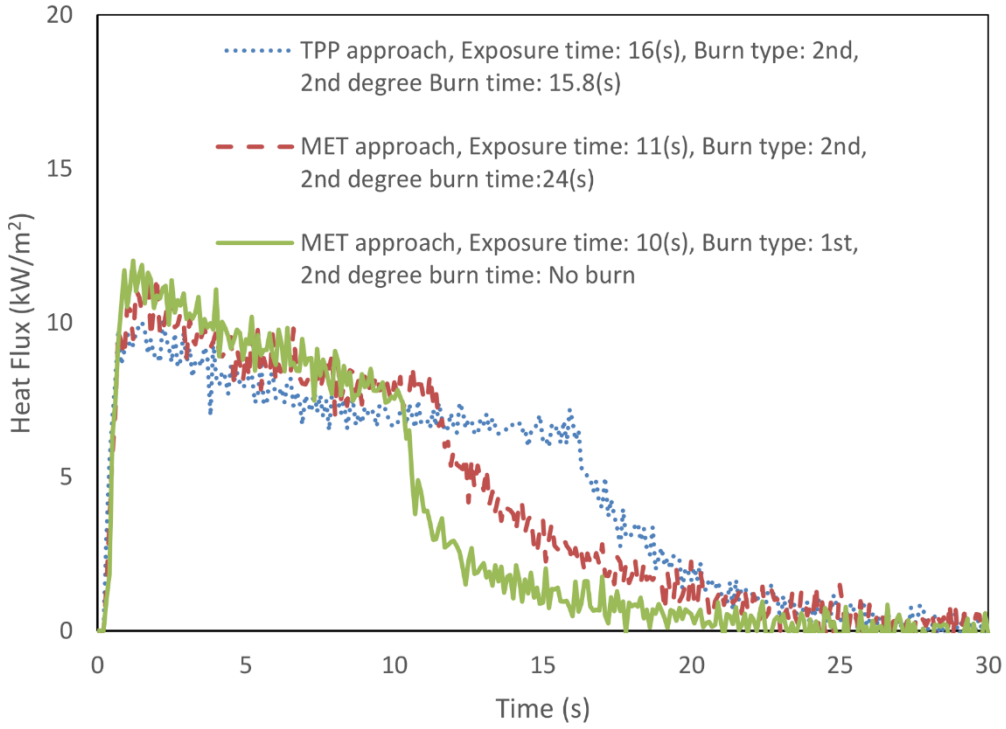

Figure 5.7. Heat flux history of fabric system SS-4 exposed to hot water with ordinary discharge.

Figure 5.8 shows the heat flux history for fabric system SS-4 exposed to hot water with compressive discharge. The first trial is the TPP approach which shows that the 2nd degree burn time prediction for continuous heating of fabric system S-4 is 12 s. However, when the fabric is exposed to 11 s of hot water, there is no prediction of second degree burn and the omega value (Ω) (Equation 2.2, page 14) approaches to 0.77. For the next step, 12 s exposure time is chosen which causes 2nd degeree burn during the compressive discharge of the stored energy to the sensor. In order to follow the iterative precedure explained earlier in the chapter, 11.5 s is also chosen as exposure time. This exposure time causes no second degree burn and predicts an omega values of almost 0.90 for fabric system SS-4. As such,

12 s is reported as the ordinary discharge minimum exposure time for fabric system SS-4 and the approach is named as minimum exposure time approach with compressive discharge (METC).

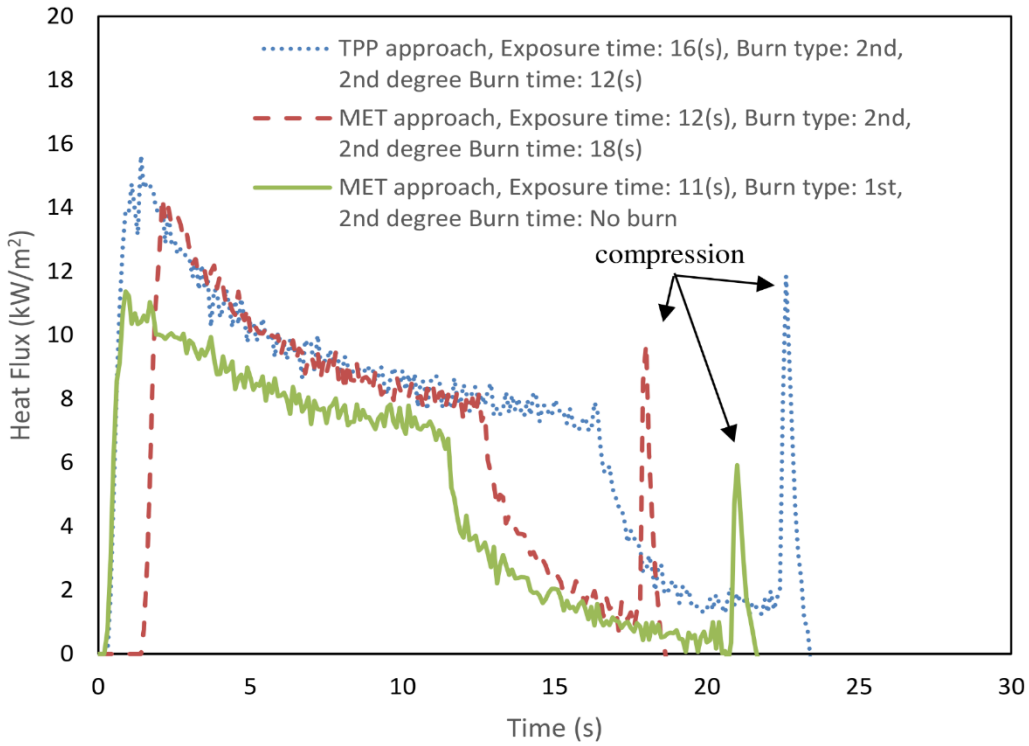

Figure 5.8. Heat flux history of fabric system SS-4 exposed to hot water with compressive discharge.

The contribution of stored energy in the thermal performance of the fabric is also significant in exposures to other hazards such as steam and radiant heat and can affect the thermal performance of the fabric systems. Figure 5.9 shows the heat flux history of fabric system SS-4 exposed to steam. The ordinary and compressive discharge conditions were applied after the termination of the exposure. It is observed that there is a considerable amount of stored energy in the fabric system after the exposure ends. Employing the TPP approach, the predicted second degree burn time for this fabric is almost 3 s. This method excludes the discharge energy's contribution for prediction of the second degree burn. However, in the MET approach, 1 s exposure of fabric system SS-4 to steam can cause the prediction of a second degree burn when ordinary condition was applied (t_{MET}^{OD}= 1 s). In addition, 1.7 s exposure of fabric system SS-4 to steam can cause the prediction of a second degree burn when compressive condition was applied (t_{MET}^{CD}= 1.7 s).

In the minimum exposure time approach (MET approach) in hot water exposure, the minimum exposure time with compressive discharge (t_{MET}^{CD}) is predicted to be slightly higher than the minimum exposure time for ordinary discharge (t_{MET}^{OD}) since the absorbed energy by the skin simulant sensor is greater in ordinary discharge than compressive discharge. The compression of the face of the heated fabric systems to the compressor may cause more heat loss from the fabric than the ordinary discharge where the face of the fabric loses heat via natural convection.

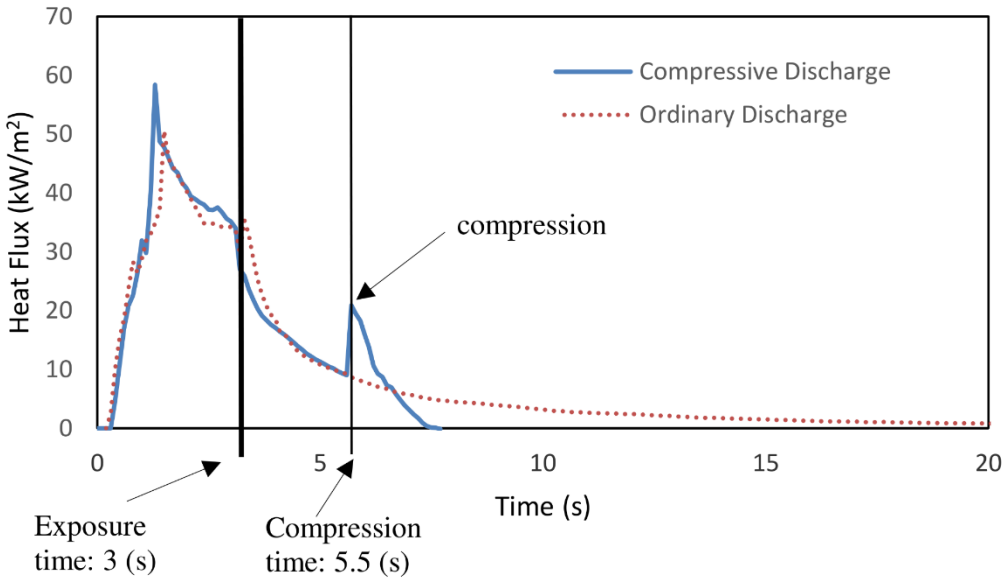

Figure 5.9. Heat flux history of fabric system SS-4 exposed to steam with ordinary and compressive discharge.

Figure 5.10 illustrates the heat flux history of fabric system SS-4 exposed to radiant heat with ordinary and compressive discharge. According to the figure, it is confirmed that there is a significant amount of stored energy in the fabric system after the 3s exposure ends. The values of the stored energy coefficient in Table 5.3 (page 124) shows that 74% of the total energy during the entire test is discharged to the skin simulant sensor during the cooling period of fabric system SS-4.

The predicted second degree burn time for fabric system SS-4 is almost 8 s using a TPP approach. Taking into account the stored energy accumulation, the exposure time that causes the prediction of a second degree burn is 5.0 s (compressive discharge) and 5.7 s (ordinary discharge). This confirms that the stored energy discharge phenomenon can reduce the thermal performance of the

fabric systems upon exposure to radiant heat (50 kW/m^2). Compression of the heated fabric to skin simulant caused a larger amount of thermal energy discharge in comparison to ordinary discharge (Figure 5.10). As such, shorter minimum exposure time is predicted when compression discharge condition is applied. In addition, any air spaces are smaller in compressive discharge and there is a closer contact of the heated fabric to the sensor.

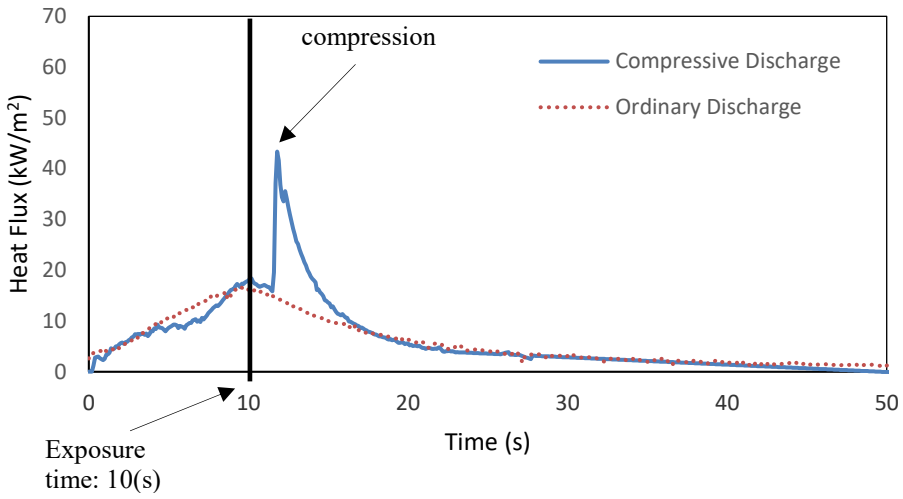

Figure 5.10. Heat flux history of fabric system SS-4 exposed to radiant heat with ordinary and compressive discharge.

Figures 5.11 and 5.12 illustrate fabric system SS-4 heat flux curves for exposures to hot water, steam and radiant heat with ordinary discharge and compressive discharge respectively. In addition, Figures 5.13 and 5.14 depict fabric system MM-2 heat flux curves exposed to the hazards when ordinary and compressive conditions were applied, respectively. These figures show the discharge of the stored energy. In ordinary discharge, once the exposure is terminated, the heated fabric discharges thermal energy to skin simmlant until the fabric system is cooled (Figures 5.11). In compressive discharge, once the thermal hazard exposure is stopped, the fabric system loses thermal energy until it is compressed (Figures 5.11). The compression of the fabric causes a sudden discharge of thermal energy to the sensor and shapes a peak in the heat flux curve.

The occurrence of the peak in heat flux curve is due to the enhancement of the conductive heat transfer by compression. According to Table 3.5, applying compression with the pressure of almost 13.8±0.7 (kPa), reduces the thickness and

increase the density of the fabric system. Equation 5.28, shows Fourier's law of heat conduction, which can be written for finite dimensions and constant properties as

$$q'' = -\mathrm{k}\frac{\Delta \mathrm{T}}{\Delta \mathrm{x}} \tag{5.28}$$

where:

q''= heat flux, W/m^2

k= thermal conductivity, W/m°C

ΔT= temperature difference, °C

Δx= thickness, m.

According to the equation, conduction heat transfer is invesly proportional to thickness of the material. As such, the decrease in the thickness of the fabric system in the compressive situation enhances conduction heat transfer. Also the increase in the density of the fabric after the compression shows that the applied compression reduces the volume of the trapped air within the fabric structure and increases the effective thermal conductivity of the fabric system. After the peak in the heat flux curve, the fabric system loses thermal energy at a faster rate in comparison to the ordinary discharge due to the fact that most of thermal energy is discharged by compression (Figures 5.13 and 5.14).

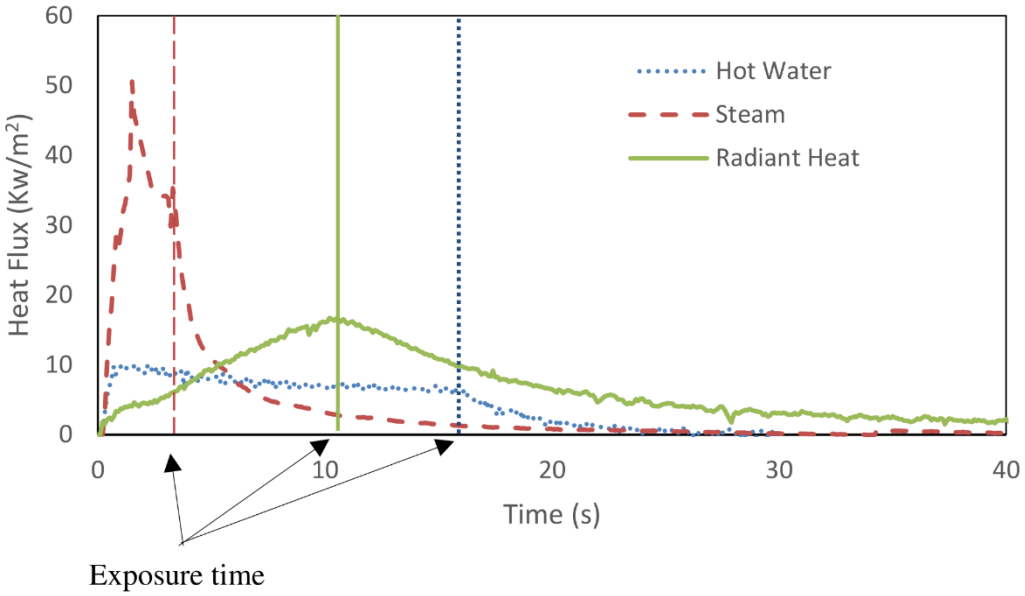

Figure 5.11. Fabric system SS-4 heat flux curves exposed to hot water, steam and radiant heat with ordinary discharge.

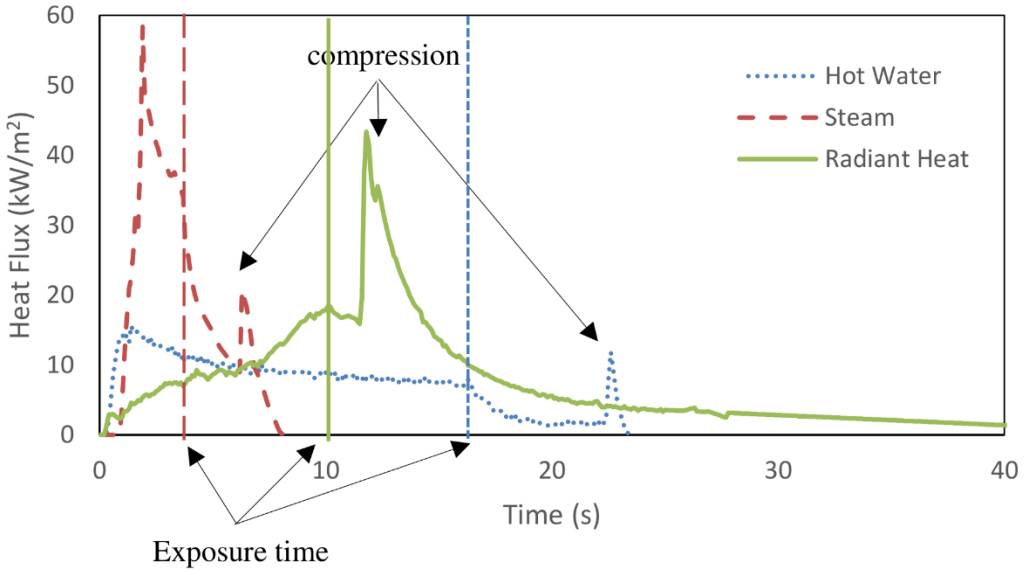

Figure 5.12. Fabric system SS-4 heat flux curves exposed to hot water, steam and radiant heat with compressive discharge.

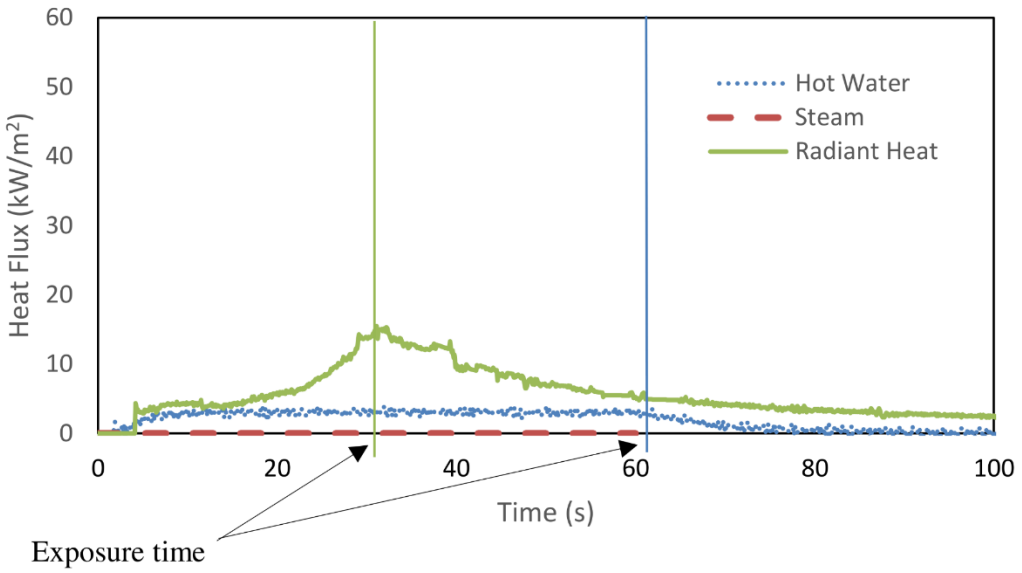

Figure 5.13. Fabric system MM-2 heat flux curves exposed to hot water, steam and radiant with ordinary discharge.

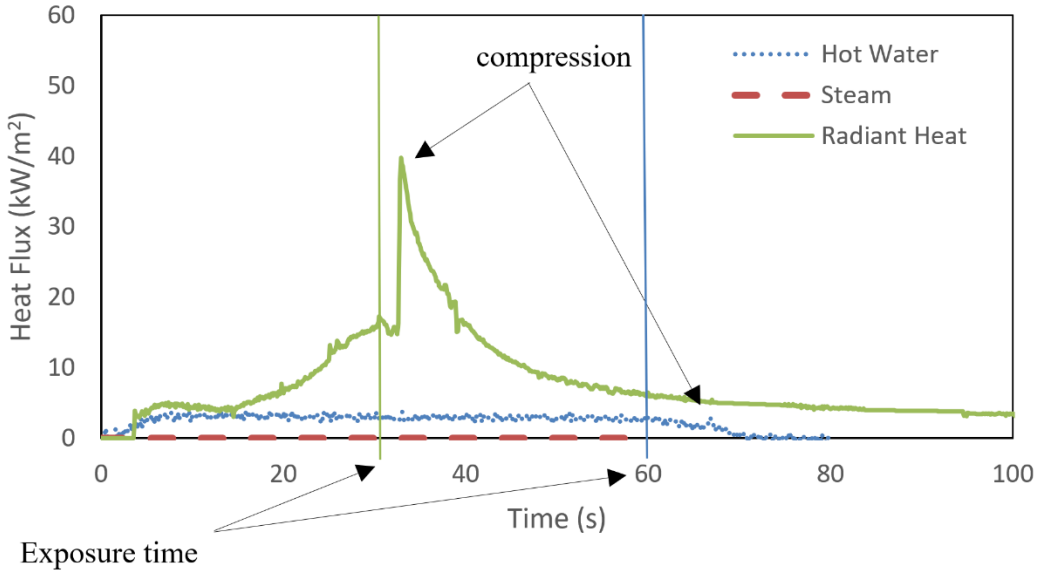

Figure 5.14. Fabric system MM-2 heat flux curves exposed to hot water, steam and radiant heat with compressive discharge.

Among the fabric systems, Fabric system MM-2 (shell fabric AA+ moisture barrier AA+ thermal liner B) has the best thermal performance, based on the second degree burn time obtained when exposed to the hazards by the TPP approach and the minimum exposure time obtained by the MET approach. No burn is predicted

for the impermeable thick structure of fabric system MM-2 when exposed to steam in compressive and ordinary discharge (Table 5.2, page, 123). Also, the data in Table 5.1 shows that this fabric system is predicted to provide the best performance when exposed to hot water. The impermeable structure of fabric system MM-2 resists mass transfer within its structure upon steam and hot water exposure due to presence of the moisture barrier in the assembly. The thick and low density thermal liner provides thermal insulation caused by the entrapped air within its structure. The effect of density on thermal performance of fabric system was discussed in Chapter 4.

According to Table 5.3, the second degree burn time for fabric system MM-2 indicates that this fabric provides the best thermal performance among the fabric systems exposed to radiant heat exposure due to its thickness. However, the high value of the stored energy coefficients in fabric system MM-2 (Ψ_{CD} =0.91 and Ψ_{OD} =0.86) suggests that the fabric has a large amount of stored thermal energy in its structure. Although fabric system MM-2 stores a large amount of stored energy, this fabric still has the highest values of the compressive and ordinary discharge minimum exposure times among the tested fabrics to radiant heat (t_{MET}^{OD} =9.6 s and t_{MET}^{CD} =6.9 s). Therefore, fabric system MM-2 has the best thermal performance when exposed to radiant heat.

Upon exposure to hot water, steam and radiant heat, it can be inferred that the fabric system MM-2 has a superior performance when exposed to these hazards, taking into account the transmitted and thermal stored energy developed in the fabric system during the exposure and cooling periods of the fabric.

Steam and hot water exposure

According to the data in Tables 5.1 and 5.2 (page 122 and 123), it is observed that the impermeable fabric systems is predicted to show better thermal performance upon exposure of the discharge thermal energy to hot water and steam. In single layer fabric system, the minimum exposure time for the permeable fabric system SS-1 is 1.7 s for hot water and almost half a second for steam exposure. The minimum exposure time for the impermeable structure of fabric system SS-4 is 12.5 s and 1.2 to 1.3 s upon exposure to hot water and steam exposure, respectively.

Figure 5.15 show a proposed schematic illustration of fabric system SS-1 during exposure to hot water and steam. When a fabric system is exposed to hot water and steam, it transfers heat through its structure via external convection, conduction. The net heat fluxes due to radiation exchanges between the nozzle, fabric and ambient was determined to be negligible in hot water and steam exposure in this study.

In the presence of hot liquid splash and steam, the permeable fabric systems may permit movement of hot water and steam through the fabric structure. In addition, due to the pressure and temperature drop in steam, it may condense and form hot water drops on the surface of and within the fabric during exposure. Exposure of fabric system SS-1 to hot water and steam jet causes external convection at the surface of the fabric ($q_{convection}$). The external convection delivers convective thermal energy to the fabric system, causes thermal energy accumulation in the fibrous part of the fabric and enhances conductive heat transfer to the skin ($q_{conduction}$). In a steam exposure, the fabric is exposed to a significant amount of thermal energy caused by steam condensation. The latent heat of condensation released from the steam enhances the overall heat transfer to the fabric and skin. In addition, the hot water and steam impingement on fabric system SS-1 causes hot liquid and steam penetration through the fabric structure during exposure and delivers heat to the skin ($q_{penetration}$). The pressure of the steam jet on the fabric system during exposure can also decrease the thickness of the fabric system and enhances heat transfer to the skin. Furthermore, the hot water and steam penetration cause the entrapment of hot water and condensed steam in the structure of the fabric and on the fabric-skin interface during the exposure and the cooling period of the fabric and deliver additional discharge to the skin. The entrapped hot water and condensed steam can increase the effective thermal conductivity of the fabric system and enhance conduction heat transfer to the skin. However, in single layer fabric and permeable double layer fabric systems (D-1 and D-2), it was hard to differentiate the effects of fabric properties in steam exposure because the burn times were so short (less than a second).

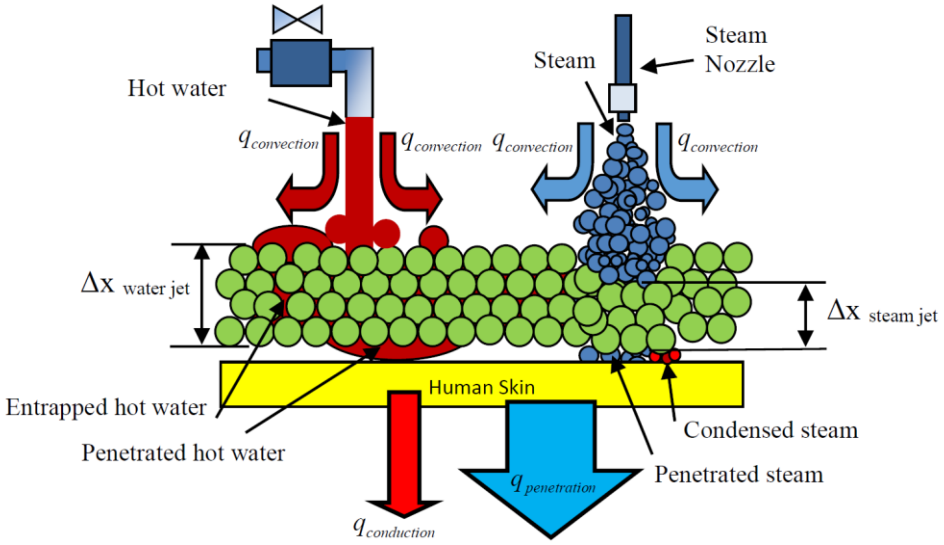

Figure 5.15. Schematic illustration of fabric system SS-1 during exposure to hot water and steam.

The short second degree burn time with continuous heating (TPP approach) for fabric system SS-1 to hot water and steam confirms that the permeable fabric provides little protection upon exposure to these hazards (Tables 5.1 and 5.2). However, in impermeable fabric system SS-4, the values of second degree burn time for the TPP approach increase significantly in steam (3 times higher) and hot water exposure (5 times higher) in comparison to permeable fabric SS-1.

The impermeable fabric system SS-4 is able to resist hot water and steam penetration through the use of the encapsulation process into its structure ($q_{penetration}$ =0). Resisting mass transfer stops hot water and steam from penetrating through the fabric and directly contacting the skin. Therefore, fabric SS-4 shows much better protection in comparison to fabric system SS-1.

This suggests that the encapsulation process has filled the pores in the fabric's fibrous structure and has minimized the hot water and steam penetration through the fabric, and in turn has provided greater resistance to heat and mass transfer. Therefore, in general, air permeability is a dominant indicator of protection performance against hot water and steam, since resistance to mass transfer is shown to be the key factor for reducing the amount of transmitted heat to the skin.

A comparison of the minimum exposure time to second degree burn also confirms that air permeability is also a dominant indicator of protection against hot water and steam, taking into account the stored thermal energy developed in the fabric system during the exposure and cooling periods.

It is also to be noted that during steam exposure, the heat transfer to the skin is enhanced due to impingement of the steam jet which decreases the thickness of the fabric and enhances conductive heat transfer (Figure 5.15). In addition, the latent heat of condensation released from the condensed steam also delivers a significant amount of thermal energy to the fabric and skin. Therefore, the second degree burn and minimum exposure times are noticeably lower than hot water exposure for single layer fabrics (SS-1 and SS-4) and permeable fabric structures (SS-1, DD-1 and DD-2).

Figure 5.16 illustrates the heat flux history of the compressive discharge of thermal energy in the fabric systems exposed to hot water. The pattern of stored energy discharge proves that compression reduces the thickness of the fabric system and enhances the conductive heat transfer to the skin. According to Figure 5.16, it can also indicate that the amount of compressive thermal energy discharged is relatively higher in permeable fabric structures specifically when the fabric is thicker. Fabric system DD-2 is the thickest permeable fabric system which stored a large amount of hot water in its structure during the cooling period of the garment. Compression is able to push the entrapped hot water more into the fabric toward the skin. This phenomenon is named “the wringing effect” because the discharge of the stored liquid in a permeable fabric is due to compression.

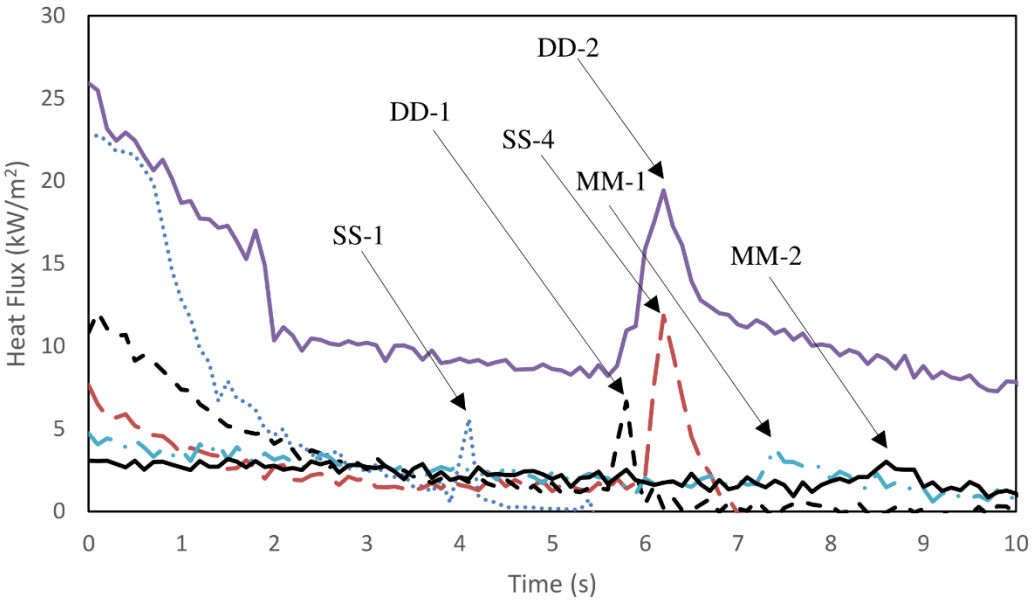

Figure 5.16. The heat flux history of the compressive discharge of the thermal energy in the fabric system exposed to hot water.

Conversely, the impermeable fabric structures exposed to hot water and steam had relatively lower values of the stored energy coefficient and higher values of minimum exposure time. The ordinary discharge minimum exposure time to second degree burn is 12.5 s in impermeable fabric system SS-4, while this value was 1.7 s in permeable fabric system SS-1.

In contrast to the thick permeable fabrics, the impermeable thick structures show superior performance when the stored energy was discharged after hot water and steam exposure. According to the data in Tables 5.1 and 5.2 (page 122 and 123), fabric systems MM-1 and MM-2 stored the minimum amount of stored energy in their structure when they were exposed to steam and hot water. This showed that the moisture barrier in the fabric system resisted mass transfer and the thermal liner provided thermal insulation. Also, these fabrics had the highest values of minimum exposure time to second degree burn in hot water exposure. Figure 5.16 confirms that the discharge of the stored energy in fabric systems MM-1 and MM-2 was insignificant.

The porous nonwoven structures of the thermal liners A and B in the fabric systems enhanced performance of the fabric system when they are used underneath a moisture barrier as in fabric systems MM-1 and MM-2. Both these fabric systems

trapped air in the structure of the thermal liner. This improves the effective thermal performance of the fabric systems due to its improved thermal insulation. As a result, for fabric systems MM-1 and MM-2, no burn prediction was observed in the steam exposure and the highest minimum exposure time to second degree burn was obtained for hot water splash (Table 5.1). This indicates that a proper engineering of a fabric system is to limit the mass transfer and increase thermal insulation to ensure a better thermal performance. Therefore, the interaction between the permeability of the fabric and fabric's thickness is shown to be a critical factor that minimizes the transmitted and the stored thermal energy discharge to the skin upon exposure to hot liquid and steam.

According to Tables 5.1 and 5.2, it was observed that the position of moisture barrier affected the minimum exposure time to second degree burn and the effective thermal protection of these fabric systems against hot water and steam because it minimized mass transfer. Although positioning a moisture barrier at the surface of the fabric system is not a practical setting, it provided a fabric system with the same mass, thickness, density, air permeability and thermal resistance as fabric system DD-3. The only advantage of the impractical assembly of fabric system DD-4, with moisture barrier AA outside the shell fabric, was that it could resist mass transfer farther to the skin than in fabric system DD-3.

When the moisture barrier was positioned at the surface of the fabric system (DD-4), in direct contact with the impinging hot water and steam, the mass transfer to the underlying layers was eliminated and all the heat transferred was by the mode of heat conduction. On the contrary, when the moisture barrier was placed in the underlying layer of the fabric system (DD-3), relatively more energy could be stored in the fabric system in comparison to fabric system DD-4. Mass flow into the assemblage contributed to a lower value of second degree burn and minimum exposure time.

According to Table 5.2, there was no burn prediction for fabric system MM-1 exposed to steam. However, the stored energy coefficients show that under ordinary (ψ^{OD}=0.41) and compressive discharge (ψ^{CD}=0.38), 41% and 38% of the total thermal energy in fabric system MM-1 was discharged to the sensor, respectively. The stored energy in fabric system MM-1 did not contribute to the occurrence of the second degree burn. However, fabric system MM-1 could be called a "potential fabric system" under the thermal conditions that were used. The

stored thermal energy in the system was important for the cases when the fabric system is reheated by a secondary thermal exposure before fabric system was cooled.

On the other hand, fabric system MM-2 protected the skin from second degree burn and also did not accumulate stored thermal energy in its structure (($\psi = 0$). As such, fabric system MM-2 could be called as an "efficient fabric system" under the thermal conditions tested.

The stored energy coefficients for ordinary (ψ^{OD}=0.41) and compressive discharge (ψ^{CD}=0.38), in fabric system MM-1 confirm that there is a significant amount of thermal energy in the fabric system during the cooling period. However, the magnitude of the discharge energy is small and cannot cause the prediction of a second degree burn during the cooling period. As such, the comparison of the stored energy coefficient between the fabric may not be sufficient to evaluate the effects of stored energy on thermal performance of the fabric system and the magnitude of the discharged energy also needs to be considered. Therefore, in the following Chapter, stored thermal energy rating (STE rating) will be introduced and used as a predictive parameter in order to evaluate thermal performance of the fabric system. More details on stored thermal energy rating can be found in Chapter 6.

Radiant heat exposure

In radiant heat exposure, almost all of the fabric systems stored a high amount of thermal energy within their structures. The range of the stored energy coefficient was significantly higher in radiant heat exposure in comparison to hot water and steam exposure.

By comparing the second degree burn and minimum exposure times after radiant heat exposure, it appeared that the discharge of the stored thermal energy diminished the thermal performance of the fabric systems when exposed to high levels of thermal radiation. The fabric systems in this study are predicted to provide a minimum exposure time from approximately 3 to 10 s for primarily radiant exposures of 50 kW/m^2. The range of stored energy coefficients (SEC) obtained after radiant heat exposure is between 0.63 to 0.86 in ordinary discharge and 0.74 to 0.91 in compressive discharge. These ranges confirm that there is a considerable amount of stored thermal energy in fabrics after exposure ends.

In radiant heat exposure, the incident thermal energy exposed to fabric system may be transmitted, and/or reflected and/or absorbed. In this study, Kevlar®/PBI and Nomex® are mainly used in the fabric systems. These fabrics are assumed to have high emissivity (~0.88-0.91) (Torvi, 1997). It is assumed that the emissivity of the coated shell fabrics in this study is similar to these values. Under this assumption, very little radiation is reflected and almost all of the radiant heat energy is absorbed by the fabric system or transmitted toward the underlying fabrics or skin. Therefore, the absorptivity of the fabric can be one of the key factors that influences the transmitted and the discharged thermal energy upon radiant heat exposure in all of the fabric systems.

Fabric thickness was also a contributing factor in transmitted and discharged thermal energy and influenced the effective thermal performance that the fabric systems provided upon radiant heat exposure of 50 kW/m^2.

The increase in the thickness of fabric system improved the effective thermal performance of the fabric system exposed to radiant heat. This means that time to second degree burn and minimum exposure time to second degree burn were significantly increased by an increase in the thickness of the fabric system. For fabric system SS-1 (shell fabric AA), the thinnest fabric system with the thickness of 0.51 mm, the second degree burn time was 5.7 s. While the second degree burn time was 25.1 s for the thickest fabric system, MM-2 with the thickness of 4.78 mm (shell fabric AA+ moisture barrier+ thermal liner B). Also, the minimum exposure time to second degree burn for fabric system SS-1 were 2.9 (ordinary discharge) and 2.7 s (compressive discharge) for fabric system SS-1. While the minimum exposure time to second degree burn for fabric MM-2 were 9.6 s (ordinary discharge) and 6.9 s (compressive discharge). The relatively higher values of the second degree burn and minimum exposure time to second degree burn for fabric system MM-2 showed that increasing thickness lowered the heat transfer to the skin during and after the exposure of the fabric system to 50 kW/m^2 radiant heat.

Modifications to the existing test methods

In Chapter 4 and earlier in Chapter 5, analyses of the absorbed energy by the sensors during the cooling phase and the stored energy coefficient showed that stored thermal energy contributes significantly to the occurrence of the second degree burns when a fabric system is exposed to hot liquids, steam and radiant heat.

However, the current standard test methods used for a thermal performance evaluation, such as NFPA 1971 and 2112, exclude the contribution of stored energy in their test method and performance requirements (NFPA, 2012, 2013). In addition, the current standard test method for measuring the transmitted and discharged energy to the skin (ASTM F 2731-10, Standard Test Method for Measuring the Transmitted and Stored Energy of Firefighter Protective Clothing System) is limited to low levels of convective radiant thermal exposures. Also, the test method employs the iterative method as a burn evaluation approach.

Thermal protective performance (TPP) rating

The TPP rating is the energy that is required to be transmitted to the skin until a second degree burn is predicted. The TPP rating has been used to evaluate thermal performance of fabric. The "TPP rating (J/cm^2)" is determined according to Equation 5.29 where q'' is the exposure heat flux (kW/m^2) and t_{2nd} (s) is the time to second degree burn obtained from the TPP approach (NFPA, 2012). As it is indicated earlier in this study, the TPP approach burn time refers to the second degree burn time obtains from continuous heating of the specimen. Therefore, the TPP rating excludes the contribution of stored energy during cooling period in order to evaluate thermal performance of fabric. In Equation 5.29, q'' is divided by 10 in order to convert kW/m^2 to J/s/cm^2.

$$TPP_{Rating} = \frac{q''}{10} t_{2nd} \tag{5.29}$$

Effective thermal protective performance (ETPP) rating

It is necessary to obtain a rating system in order to evaluate thermal performance of the protective fabric systems upon thermal hazards by taking into account the transmitted and thermal stored energy developed in the fabric system during the exposure and cooling periods of the fabric. As such, the energies related to the cooling period are necessary to be included in performance rating of the fabric. Therefore, the following performance rating can be proposed considering the stored thermal energy in the system that may be discharged in an ordinary or a compressive situation:

- ETPP ordinary discharge rating, J/cm^2 ($ETPP^{OD}_{Rating}$) is the total energy of exposure and the ordinary discharge thermal energy (Equation 5.30). In the

following equation $q"$ is the exposure heat flux (kW/m^2) and t_{MET}^{OD} is the ordinary discharge minimum exposure time.

$$ETPP_{Rating}^{OD} = \frac{q"}{10} t_{MET}^{OD} \quad (5.30)$$

- ETPP compressive discharge rating, J/cm^2 ($ETPP_{Rating}^{CD}$) is the total energy of exposure and the compressive discharge thermal energy (Equation 5.31). In the following equation $q"$ is the exposure heat flux (kW/m^2) and t_{MET}^{CD} is the ordinary discharge minimum exposure time.

$$ETPP_{Rating}^{CD} = \frac{q"}{10} t_{MET}^{CD} \quad (5.31)$$

In NFPA 2112, the fabric system with higher HTP value shows that the material has expected to have a better thermal performance when exposed to a flash fire (NFPA, 2012). In the proposed ETPP ordinary and compressive rating, a fabric system with higher ETPP value can be referred to as a material which has a relatively better predicted performance when exposed to a thermal hazard. However, the value of TPP rating or HTP rating obtained from continuous heating of the specimen predicts a higher value for the evaluation of the same fabric. This value does not seem to provide a realistic system with which to rate the thermal protective evaluation of the fabric systems. Therefore, $ETPP_{Rating}^{OD}$ and $ETPP_{Rating}^{CD}$ need to be considered in order to improve the thermal protective evaluation rating of the current standard and provides a more efficient system with which to rate the thermal protective performance of the fabric systems. In Equations 5.30 and 5.31, the exposure heat flux, $q"$ is divided by 10 in order to convert kW/m^2 to J/s/cm^2.

Summary

It is important to understand the amount of the stored thermal energy that is transferred to the skin. This research was able to identify the key factors related to thermal stored energy and its contribution to skin burn injuries in wider ranges of heat exposures and hazards. The findings from this study contribute to the improvement of the current protective clothing standards. The findings relate to a means to improve the thermal protective performance rating of the current standard and provide a more efficient system with which to rate the thermal protective performance of the fabric systems. Also, a new approach has been introduced in

order to suggest only one test for the prediction of the minimum exposure time to second degree burn specified in the existing standards. Additionally, findings of this research result in the development and redesign of the existing bench top tests and equip them with an additional compressor which would enable the rating of the thermal performance of protective clothing while taking into account the stored energy discharge in each test.

The test results presented in this study are based on a limited number of experiments on the tests of specimens from limited quantities and hence may not be representative of other fabric systems. In addition, the specimens were tested under very specific ranges of exposures. Caution needs to be exercised in applying the finding from this work for wider ranges of exposures, thermal hazards and fabric systems. In future works, it is recommended to investigate a wider range of exposures on different types of fabric systems.

Some of the findings that have already been obtained are summarized as follows.

- As in exposures to convective and radiant sources, stored energy in fabrics after exposures to hot liquid and steam could contribute significantly to burn injuries. In the case of hot liquid and steam, minimizing mass transfer could significantly improve the predicted performance of fabric systems.

- In hot liquid and steam exposures, there is a significant amount of stored thermal energy in permeable fabrics, specifically when the thickness of the fabric system is increased.

- An increase in fabric thickness can improve the thermal performance of impermeable fabric systems after exposure to hot water splash and steam.

- The compression of the fabric during the cooling period causes a sudden discharge of thermal energy to the sensor and shapes a peak in the heat flux curve. This phenomenon may lower the predicted performance of the fabric system.

- In radiant heat exposure experiments, the absorptivity of the fabric can be one of the key factors that influences the transmitted and the discharged thermal energy upon radiant heat exposure in all of the fabric systems.

- In this study, the effective thermal performance of the fabric systems was evaluated using various thermal exposures such as hot water, steam and radiant heat. It is also recommended that additional exposures such as flame, ISO 9151 (ISO, 2016) and hot surface contact, F 1060-05 (ASTM, 2016) can be combined with the results obtained from this study in order to see if the proposed stored energy and burn evaluation model are able to predict the minimum exposure time close to the minimum exposure time obtained from the iterative tests.

CHAPTER 6 LABORATORY EVALUATION OF EFFECTIVE THERMAL PERFORMANCE OF PROTECTIVE CLOTHING EXPOSED TO HOT WATER USING INSTRUMENTED SPRAY MANNEQUIN[3]

Introduction

In previous chapters, the thermal response of protective fabric systems exposed to hot liquid, steam and radiant heat was evaluated by taking into account the transmitted and stored thermal energy developed in the fabric system during the exposure and cooling periods of the fabric. In addition, the thermal performance of the protective fabrics has been analyzed for the abovementioned hazards using bench-scale test results. The analysis of the data confirmed that the fabric systems accumulate thermal energy, which can be discharged to the skin after the termination of the thermal exposure, reducing the performance of the thermal protective fabric systems. As such, an effective thermal performance of protective fabric systems was proposed which comprised of two parts: the prediction of the time to second degree burn by continuous heating (TPP approach) plus the prediction of the minimum exposure time using the stored energy model. Moreover, an effective thermal protective performance rating of the fabric system was

[3] This chapter is an original work by the author. Y. Lu was responsible for the spray mannequin data collection and air gap measurements. Some portions of this chapter have been presented at the following conferences:

- Gholamreza, F., Song, G., & Lu, Y. (2015). *Analyzing the discharged energy and its contribution to thermal performance of protective clothing upon hot water exposure using instrumented spray manikin.* Paper presented at the Fiber Society Conference, Spring, Shanghai, China. The author was responsible for the analysis as well as manuscript composition. G. Song was the supervisory author and provided critical review of the manuscript. Y. Lu was responsible for the data collection.
- Gholamreza, F., Torvi, D., Kerr, N., Ackerman, M. & Song, G. (2016). *A new protocol to characterize thermal protective performance of garments using instrumented flash fire and spray mannequin*. Paper presented at the 7th European Conference on Protective Clothing and Nokobetef 12. Innovative Protective Clothing in a Changing World: Protective, Comfortable, Intelligent, Integrated, Ecological and Economical, Izmir, Turkey. The author was responsible for the analysis as well as manuscript composition. D. Torvi and N. Kerr were the supervisory authors and provided critical review of the manuscript. M. Ackerman assisted with the data collection and test method. G. Song was involved with concept formation.
- Gholamreza, F., Torvi, D., Dale, D., Kerr, N., & Ackerman, M. (2017). *Laboratory evaluation of thermal protective clothing using instrumented flash fire and spray mannequin*. Paper presented at the 17th Autex World Textile Conference, Corfu, Greece. The author was responsible for the analysis as well as manuscript composition. D. Torvi and N. Kerr were the supervisory authors and provided critical review of the manuscript. M. Ackerman assisted with the data collection and test method. D. Dale also assisted with the test method.

proposed in order to include the energies related to the cooling period in performance rating of the fabric.

In Chapters 4 and 5, studies of the transmitted and stored thermal energy focused on the thermal performance of the fabric systems after exposure to steam, hot liquids and radiant heat on bench-scale tests with no air gap between the fabric and the sensors. The presence of air gap between the fabrics and the skin is an important factor that affects the performance of protective clothing. In a study by Kim et al. (2002), it was reported that severity of burn injuries increased as the size of the air gap decreased in thermal protective clothing.

In this chapter, the contribution of the stored energy to the thermal performance of the garments is investigated. In addition, the parameters that were discussed in small scale testing will be used to investigate stored energy in full-scale tests. As such, the predictive parameters such as total discharged energy (TDE), total stored energy coefficient (SEC), and stored thermal energy rating are introduced. Also, the effects of the fabric properties and garment design on the proposed predictive parameters are analyzed.

Experimental procedure

Three replicates of each garment were tested. The details on the garment system (pages 50 to 52) and the instrumented mannequin (pages 65 and 66) were provided in Chapter 3. The garments were first conditioned at 20±2°C with 65±5% relative humidity for at least 24 hours prior to the testing. Based on the data obtained from each heat flux sensor, the following predictive parameters are obtained:

- *The predicted mannequin area of second degree burn (%)*: is the sum of the weighted areas corresponding to the heat flux sensors that predict a second-degree burn.

- *The predicted mannequin area of third degree burn (%)*: is the sum of the weighted areas corresponding to the heat flux sensors that predict a third-degree burn.

- *The predicted total mannequin area of burn injury (%)* is the sum of the predicted mannequin area of second and third degree burn.

- *Total absorbed energy (TAE)* is the total energy received by all heat flux sensors as the average of the weighted total energy transferred to each heat flux sensor over the data sampling period (kJ/m^2). In Equation 6.1, $q_{total\,(i)}$ is the total energy transferred to the ith sensor throughout the test, and A_i is the weighted surface area of the ith sensor.

$$TAE = \frac{\sum_{i=1}^{110} q_{total\,(i)} \times A_i}{\sum_{i=1}^{110} A_i} \tag{6.1}$$

In addition, considering the data obtained from each heat flux sensor, the following predictive parameters are proposed.

Total discharged energy (TDE)

Total discharged energy (TDE), is the total energy received by all heat flux sensors during the cooling period. Total discharged energy is determined by using Equation 6.2 which is the average of the weighted energy transferred to each sensor after the termination of exposure (kJ/m^2). In this equation $q_{cooling\,(i)}$ is the discharged energy to the ith sensor during cooling period and A_i is the weighted surface area of the ith sensor.

$$TDE = \frac{\sum_{i=1}^{110} q_{cooling\,(i)} \times A_i}{\sum_{i=1}^{110} A_i} \tag{6.2}$$

Total stored energy coefficient (SEC)

The total stored energy coefficient (SEC) is the total discharged energy's contribution to the total absorbed energy measured by all the sensors in the mannequin. The total stored energy coefficient is determined by using Equation 6.3 which is the average of the weighted stored energy coefficient for each sensor in the mannequin. In Equation 6.3, ψ_i and A_i are the ith sensor stored energy coefficient and weighted surface area (i) respectively.

$$SEC = \frac{\sum_{i=1}^{110} \psi_{(i)} \times A_i}{\sum_{i=1}^{110} A_i} \tag{6.3}$$

Stored thermal energy rating

The STE rating (kJ/m^2) is a criterion to evaluate the garment system based on its ability to store thermal energy. The stored energy rating is determined by considering the amount of the stored thermal energy discharged to the skin during

the entire test until the garment is cooled down (TDE) and the potential of the garment to store thermal energy (SEC). The STE rating is the average of the weighted energy transferred to each sensor after the termination of exposure which considers the proportion of the stored energy to the total absorbed energy by the same sensor.

In the analyses of the total absorbed energy by the sensors in the spray manikin test for each test it was observed that some sensors absorbed similar amounts of discharged thermal energy during the cooling periods. However, the amount of the discharged energy was caused by different amounts of transmitted energy during the exposure. For instance, in garment G-6 (88% cotton/ 12% HT nylon with polymer finishing), the sensor underneath an unflapped side pocket (the front center of the left upper thigh (sensor 102, Figure 3.9, page 66)) and the sensor underneath the outer part of the right low leg (sensor 63, Figure 3.9, page 66), absorbed almost 100 kJ/m^2 thermal energy during the cooling period. However, the transmitted energy during the exposure to sensors 102 and 63 were 23 kJ/m^2 and 95 kJ/m^2, respectively. By considering the discharged energy only, it is difficult to differentiate the effect of the stored energy. Taking to account the values of stored energy ratings for the two sensors, it can be inferred that the garment has the ability to store more thermal energy on the front center of the left upper thigh (79.0 kJ/m^2) as compared to the outer part of the right low leg (48.4 kJ/m^2). The accumulated volume of hot water in the left pocket of garment G-6 caused a significant amount of discharged thermal energy to the sensor on front center of the left upper thigh.

As such, the stored energy rating is introduced in order to differentiate the ability of the garment to store thermal energy. The stored energy rating comprises two features: (1) the magnitude of stored energy and (2) the portion of the stored energy in the total absorbed energy during the test. The stored energy rating is determined from the average of the weighted discharged energy to the ith sensor during cooling period ($q_{cooling\ (i)}$) multiplied by the stored energy coefficient of the ith sensor (ψ_i) according to Equation 6.4.

$$STE_{Rating} = \frac{\sum_{i=1}^{110}(q_{cooling(i)} \times \psi_{(i)} \times A_i)}{\sum_{i=1}^{110} A_i} \qquad (6.4)$$

The other advantage of stored energy rating is to rate the ability of fabric systems or the garments to store thermal energy when the second degree burn is not

predicted in a test. For instance, in a test where a second degree burn is not predicted and the stored energy coefficient is 0.5, half of the absorbed energy is discharged to the sensor during the cooling period, while the magnitude of the thermal energy is not sufficient to produce a second degree burn. As such, the magnitude of the discharge energy needs to be considered for rating of a fabric.

Results and discussion

In Table 6.1, test results include the percentage of the area of predicted second and third degree burn, total absorbed energy (TAE), total discharged energy (TDE), total stored energy coefficient (SEC) and stored thermal energy rating ($STE\ rating$). The abovementioned predictive parameters are obtained by the average of a minimum of three tests for each garment exposed to 85°C hot water for 10 s and 60 seconds of cooling period.

Table 6.1. Performance of garments exposed to hot water at 85°C.

Garment code	Fiber Content	Second Degree Burn (%) (SD)	Third Degree Burn (%) (SD)	TAE (kJ/m^2) (SD)	SEC (SD)	TDE (kJ/m^2) (SD)	STE Rating (kJ/m^2) (SD)
Nude mannequin	No Garment	71.9 (7.5)	4.2 (8.0)	188.6 (11.4)	0.11 (0.003)	18.8 (2.4)	2.3 (0.4)
G-1	100% Nomex® IIIA	48.1 (4.5)	8.2 (4.3)	171.4 (6.8)	0.44 (0.013)	67.4 (1.6)	26.4 (1.1)
G-2	100% Nomex® IIIA	20.9 (1.0)	6.6 (1.8)	81.5 (1.2)	0.55 (0.021)	58.5 (3.5)	31.8 (1.0)
G-3	88% Cotton and 12% Nylon	49.5 (1.8)	2.7 (2.3)	158.8 (3.3)	0.46 (0.029)	65.0 (5.2)	26.9 (3.9)
G-4	88% Cotton and 12% Nylon	47.8 (1.9)	1.8 (2.4)	151.4 (7.6)	0.47 (0.018)	64.5 (5.2)	27.7 (2.0)
G-5	88% Cotton and 12% Nylon with polymer finishing	8.9 (2.0)	0.0 (0.0)	53.3 (4.3)	0.66 (0.019)	31.6 (1.6)	19.5 (0.5)
G-6	88% Cotton and 12% HT Nylon with polymer finishing	6.3 (1.9)	0.0 (0.0)	49.4 (2.5)	0.67 (0.015)	28.7 (0.6)	17.4 (0.7)
G-7	88% Cotton and 12% Nylon	40.4 (2.2)	0.7 (0.6)	131.3 (6.5)	0.54 (0.006)	68.2 (3.3)	35.3 (1.4)
G-8	88% Cotton and 12% Nylon	37.8 (2.4)	1.2 (1.0)	132.0 (3.9)	0.56 (0.027)	68.7 (3.1)	35.4 (2.5)
G-9	88% Cotton and 12% Nylon	34.8 (0.9)	0.6 (0.6)	127.6 (6.6)	0.57 (0.007)	69.9 (2.8)	35.6 (1.5)
G-10	100% Cotton	16.7 (5.5)	No burn	90.8 (4.6)	0.67 (0.024)	56.6 (2.8)	35.3 (2.5)
G-11	FR Cotton/quilted lining Arcxel™	No burn	No burn	18.7 (0.5)	0.79 (0.011)	12.8 (0.2)	8.9 (0.2)
G-12	Polyvinyl chloridecoated Cotton	0.2 (0.3)	No burn	22.1 (2.0)	0.69 (0.018)	13.5 (0.8)	8.3 (0.4)
G-13	Polyurethane-coated Nomex®IIIA knit	No burn	No burn	16.7 (1.5)	0.69 (0.017)	10.1 (1.1)	6.1 (0.7)

TAE is the total energy received by all sensors throughout the test; SEC is the total stored energy coefficient; TDE is the total energy received by all heat flux sensors during cooling period; STE rating is the total energy received by all sensors during cooling period considering the proportion of the discharge energy to the total absorbed energy.

According to Table 6.1, the total burn injury predicted in the nude test was 71.9 %. The total heat absorbed during the test and the total discharged energy were 188.6 and 18.8 kJ/m^2 respectively. Therefore, 11% (SEC= 0.11) of the total heat absorbed by the entire mannequin was discharged during the cooling period. The heat transfer during the cooling period was due to discharge of the thermal energy from water vapor and/or steam and/or condensed steam in the chamber and on the mannequin surface.

The stored thermal energy rating (STE) value demonstrates that the entire nude mannequin was exposed to an average value of 2.3 kJ/m^2 thermal energy during the cooling period. The stored energy rating for the nude test was the lowest value among the garments system shown in Table 6.1. The comparison of the stored energy ratings for the nude and clothed mannequin reveals that the stored thermal energy in the exposed garment can be a potential hazard for its wearer during the cooling period of the garment (Figure 6.1). Comparison of the stored energy ratings for the nude test and the garments tests suggest that the mannequin with no garment after the termination of hot water exposure can minimize the stored energy discharge to the skin. Although it is not a practical solution, this means that if the single layer garment is taken off appropriately after the termination of hot liquid exposure, the effect of stored energy discharge can be minimized. The appropriate procedure refers to a method that ideally does not cause compression of the garment to the skin during doffing. The data presented in Chapter 4 confirms that compression of the fabric to the skin during the cooling period can cause a sudden discharge of the thermal energy to the skin and reduce the effective thermal performance of the fabric.

Figure 6.1 shows the local stored thermal energy rating distributions of the mannequin for garments G-9, G-13 and the nude test. These two garments were chosen since G-9 has the highest (35.6 kJ/m^2) and G-13 has the lowest (6.1 kJ/m^2) stored thermal energy among the garments. Figure 6.1 illustrates the stored thermal energy rating distributions within the mannequin for garments G-9, G-13 and the nude test.

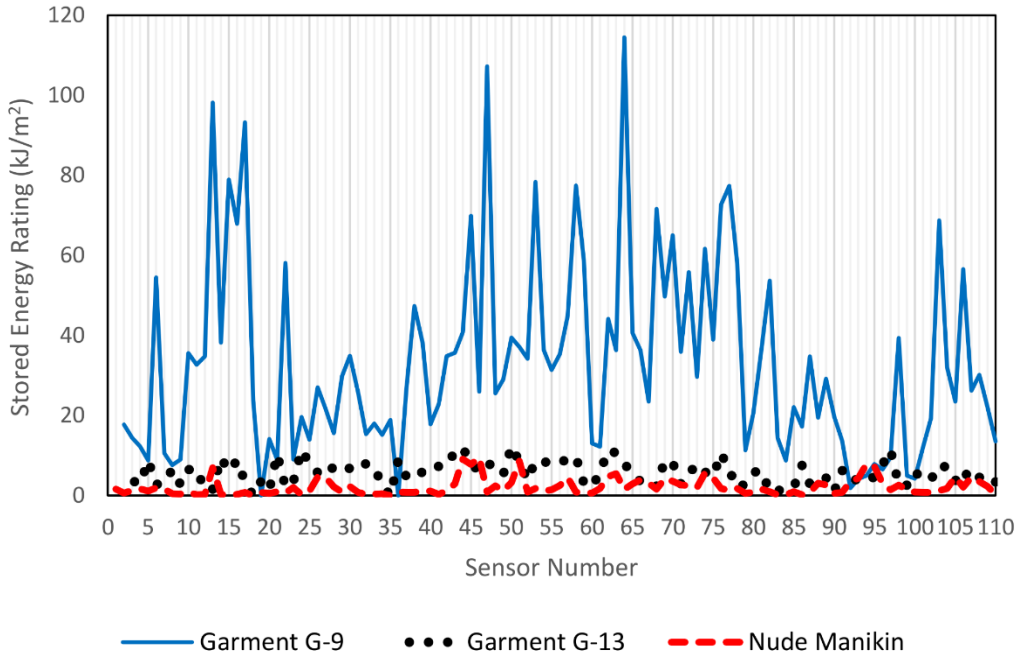

Figure 6.1. The local stored thermal energy rating distributions within the mannequin for garments G-9 (single layer, 88% cotton and 12% nylon), G-13 (bib pant and a jacket, polyurethane-coated Nomex®IIIA knit) and nude test.

Effect of fabric properties on stored thermal energy

Some of the fabric properties were discussed in terms of their effects on the results of small scale fabric tests. In this chapter, the fabric properties are discussed in terms of their effects on results of full scale garment tests. The flow of liquid through the fabric is affected by pore size and capillary pore distribution (see Chapter 4, page 94). Air permeability is the rate of air flow passing through a known area which can be an indicator of how well liquid can flow through the fabric structure. In this study, polymer finishing was used to fill the pores in the fabric's fibrous structure and minimized liquid penetration through the fabric. The impermeable structure of some garments in this study results from a water resistant polymer finish.

According to Table 6.1, the impermeable single layer garments (garments G-5 and G-6, 88% cotton and 12% HT nylon with polymer finishing) had relatively lower stored energy ratings (19.5 and 17.4 kJ/m^2, respectively) in comparison to permeable single layer garments (garments G-1 to G-4 and G-7 to G-9). Additionally, the values for the areas of the total second and third degree burn for

garments G-5 and G-6 (8.9 and 6.3 % respectively) suggest that these two impermeable garments showed superior performance among the single layer garments exposed to hot water exposure. This confirms that air permeability is a dominant factor in protective performance against hot water exposure during the exposure and the cooling period of the garment.

Garments G-5 and G-6 are made of fabrics with polymer finishes. The fabrics in these two garments are treated using an encapsulation process which has filled the pores in the yarns and fabric structure and minimizes the hot liquid penetration. Therefore, resistance to hot liquid penetration by garments is shown to be a key factor for reducing the amount of transmitted and the discharged energy to the skin.

A comparison of garments G-4 and G-5 also demonstrates the importance of surface finishing in garments exposed to hot water spray. Garments G-4 and G-5 are made of 88% cotton and 12% nylon with a fire retardant finish but garment G-5 is also treated using an encapsulation finish. As such, garment G-5 provided greater resistance than G-4 to heat and mass transfer to the skin during the exposure and the cooling period. The data presented in Table 6.1 shows that the total second and third degree burn is reduced from 49.6% in garment G-4 to 8.9% in garment G-5. In addition, the stored energy rating decreased significantly from 27.7 kJ/m^2 in garment G-4 to 19.5 kJ/m^2 in garment G-5. Although polymer finishing improved the surface property and enhanced the overall performance of garment G-5, the values of stored energy rating showed that there was still a noticeable amount of stored thermal energy in the garment during the cooling period. This can be inferred by the comparison of the stored energy rating in garment G-5 (19.5 kJ/m^2) with the stored energy rating in double layer garment G-11 (8.9 kJ/m^2) and impermeable garments G-12 (8.3 kJ/m^2) and G-13 (6.1 kJ/m^2) which consist of bib-pants and a separate jacket.

Figure 6.2 shows the stored energy ratings for impermeable garment G-6 and permeable garment G-2 exposed to hot water. The impermeable garment G-6 had a relatively lower local stored energy rating value. This confirms the role of polymer finishing and the encapsulation process that caused the fabric to be resistant to water penetration. In addition, the permeable garment G-2 showed higher local values for stored energy ratings. The higher values of the stored energy

rating suggest that permeable garment G-2 stored more thermal energy within its structure in comparison to the impermeable fabric in garment G-6.

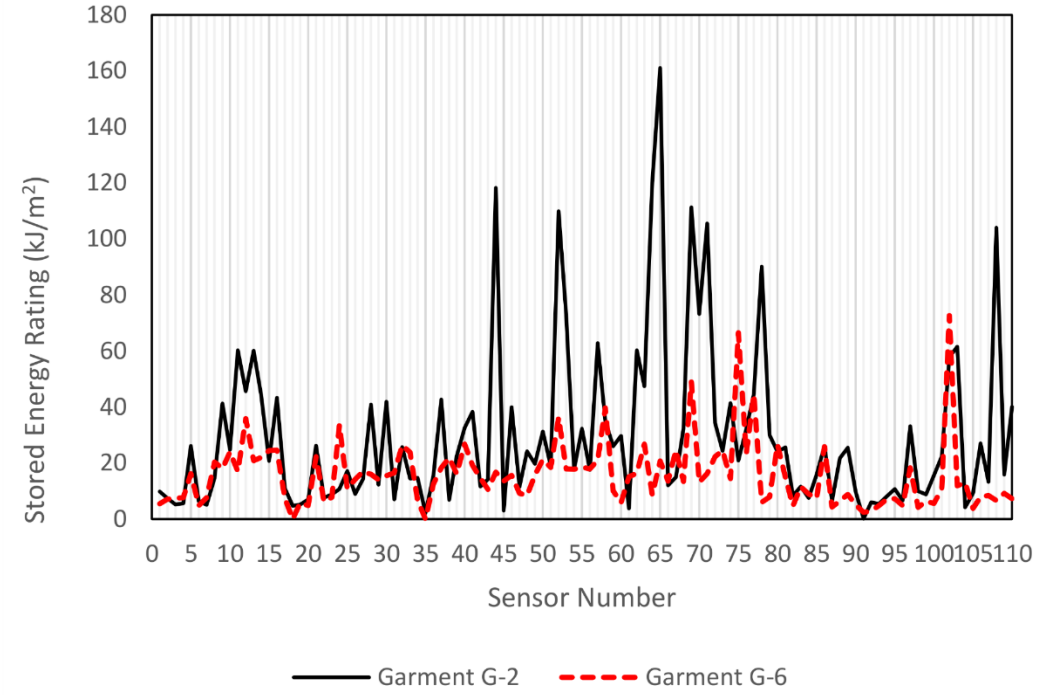

Figure 6.2. The local stored thermal energy rating values of sensors within the mannequin for garments G-2 and G-6.

In the impermeable garment fabrics, when hot water splashes on the s`urface of the garment, it spreads on the garment and flows toward the lower parts of the garment. The hot liquid may also run off or stay on the surface of the garment. No penetration occurred through the impermeable garments (non-penetration). In permeable garments, hot water may also penetrate through the garment structure. The penetrated hot water may be stored within the garment structure (partial penetration). Hot liquid may also penetrate to the underside of the fabric and in the air gaps and contact the skin (total penetration). In total penetration, the penetrated hot water may stay within the air gaps between the garment and the skin or it may flow within the air gaps through the bottom regions. Non-penetration, partial and total penetration will be explained later in the chapter.

By looking at the local stored energy ratings in Figure 6.2, it is evident that the sensors in the lower regions accumulate more discharged energy during the cooling period than the rest of the regions on the mannequin. Sensors 65, 64, 52,

44, 69, 71 and 108 which respectively represent the area around right calf, right shin, left mid-thigh (front), left lower leg (outer), right lower thigh (front outer), right mid thigh (front) and right mid leg (back) received a significant amount of thermal energy in the mannequin during the cooling period. In addition, areas around the lower body such as right lower leg, inner area (sensor 62), left upper thigh, rear (sensor 57) left mid-thigh, outer area (sensor 53), left mid thigh, front (sensor 52), right lower thigh, rear (sensor 70) upper thigh, front-center (sensor 102), right lower leg, front (sensor 103) left calf (sensor 46), right upper thigh, front inner (sensor 74) also received a considerable amount of stored thermal energy. This confirms that the flow of hot water on the surface from the upper regions of the garment through the lower regions causes the accumulation thermal energy in lower regions.

Figure 6.3. shows the clothed mannequin (Garment G-6) and the position of the water spray jets relative to the mannequin. The dashed arrows indicate approximately what parts of the upper body can be impinged by the water jets.

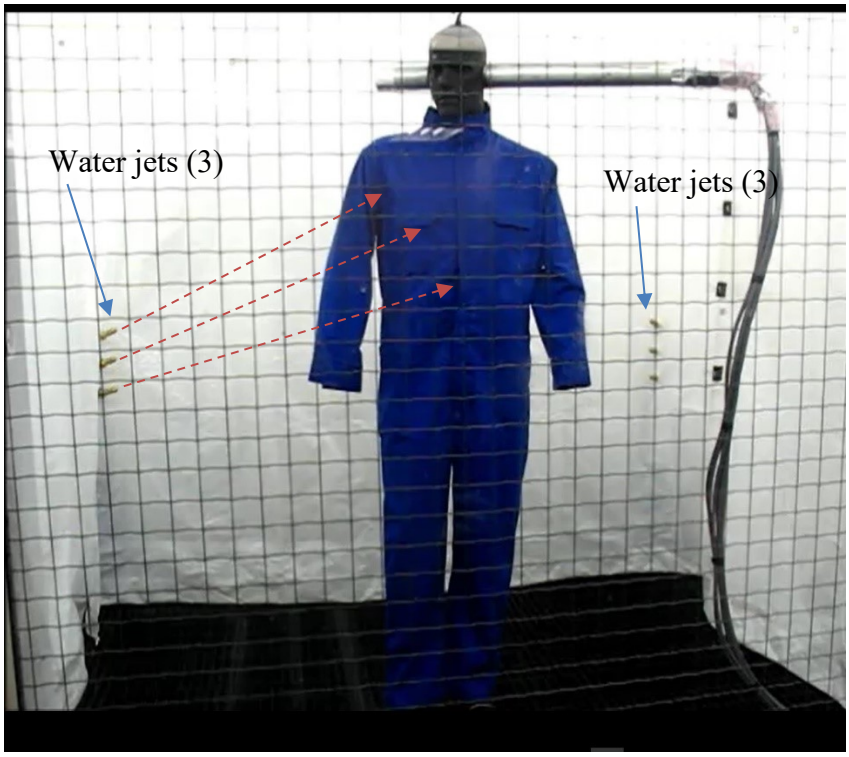

Figure 6.3. Clothed mannequin (Garment G-6) and position of hot water jets relative to the mannequin.

Figure 6.4 depicts the local stored thermal energy rating values within the mannequin for permeable single layer garments (G-1to G-4 and G-7 to G-10) and impermeable single layer garment G-6. According to Figure 6.4, the local stored energy ratings of the sensors underneath the impingement areas show that a considerable amount of stored thermal energy is discharged to the sensors in the impingement regions. These regions were the abdomen, lower left (sensor 11) abdomen, upper center (sensor 12), abdomen, upper left (sensor 13), abdomen, lower center (sensor 9) chest, lower left (sensor 16), side of trunk, lower left (sensor 28), lower back, lower left (sensor 30), lower back, lower right (sensor 37), side of trunk, lower right (sensor 41), right buttock, side (sensor 78), right buttock (sensor 77) and left buttock (sensor 58). However, the local stored energy ratings at the impingement regions are relatively lower than the local stored energy ratings of the lower body regions where the thermal energy was stored due to the flow of hot water.

The distributions of the permeable garments' thermal energy rating values are indicated with solid lines. Figure 6.4 also shows the local stored thermal energy rating for the impermeable garment G-6 (the squares). Among single layer garment systems, the impermeable garment structure showed a superior performance during the cooling period. In Figure 6.4 the impingement regions are indicated. According to the figure, it is evident that the sensors on the right and left leg had significantly higher values of stored energy. This is due to the fact that hot water flowed toward the lower regions of the mannequin after the hot water jets hit the garments. This phenomenon was explained earlier for garment G-2. According to Figure 6.4, the stored energy rating distribution for each single layer permeable garment system follows closely the same pattern in the impingement regions and the regions affected by hot liquid flow.

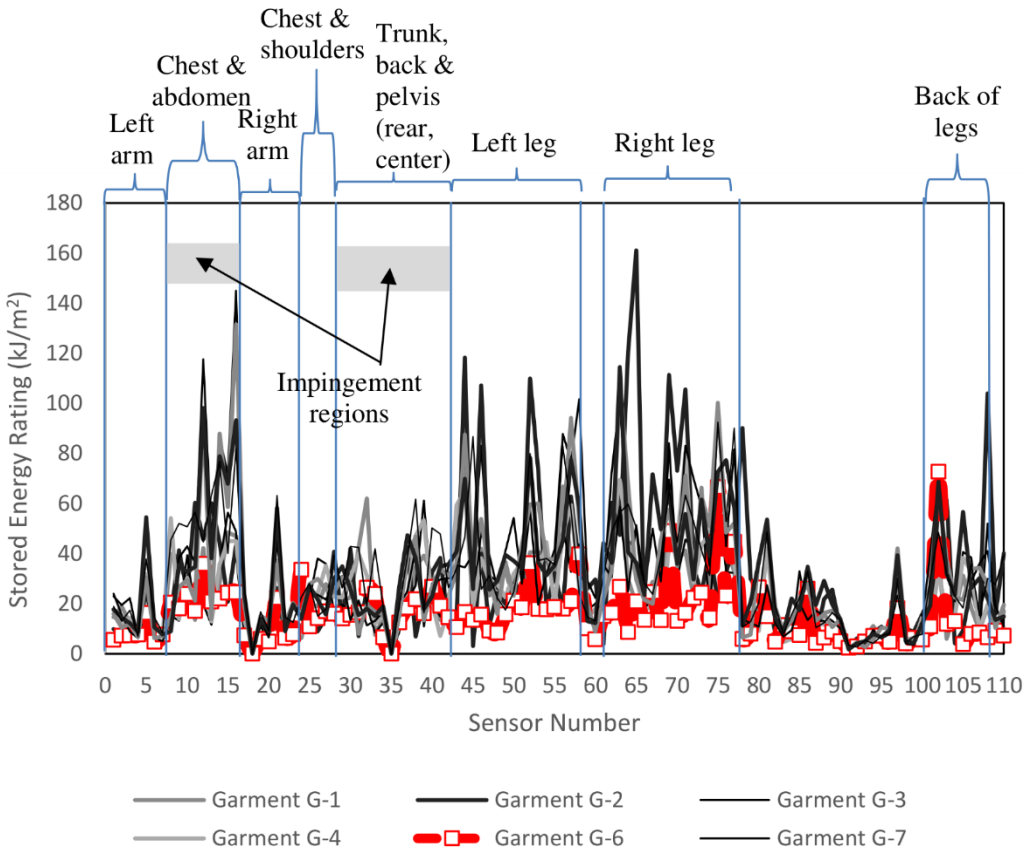

Figure 6.4. The local stored thermal energy rating distributions within the mannequin for the impermeable garment G-6 and permeable single layer garments (G-1to G-4 and G-7 to G-10).

Single layer garments G-7, G-8 and G-9 had the same fiber content and fabric structure but different sizes (Sizes 40, 42 and 44, respectively). This variation in size and fit on the mannequin provided different air gap sizes among the garments. As such, the average air gap size for garments G-7, G-8 and G-9 were 25.5, 28 and 31 mm. The determination of the air gap sizes was discussed in Chapter 3. According to Table 6.1, by increasing the air gap size, the total second and third degree burn decreased from 41.2% to 35.4%. However, the values of the stored energy rating and the stored energy discharge did not change significantly as the air gap size increased. The effect of an increase in the air gap size on burn injuries was significant in garment G-10. This garment has the largest air gap size among the single layer garments. This garment maintained its shape relatively well during hot water exposure except in the impingement regions (Lu, Song, & Li, 2013). This resulted in a lower transmission of thermal energy during the exposure and lower

values of second and third degree burn (16.7%). The stored energy rating values for G-10 (35.3 kJ/m^2) suggest that this garment was capable of discharging a significant amount of thermal energy to the mannequin in spite of its large air gap size.

The double-layer garment G-11 consists of a single layer garment of G-10 fabric as its outer layer and a thermal liner. The double layer garment structure of G-11 had a relatively thick structure (1.9 mm) and a large air gap size (38.5 mm). The combination of these two properties may have influenced the temperatures across the gap and decreased the heat transfer to the mannequin. The presence of thermal liner could decrease the effective thermal conductivity of the fabric system due to the air volume fraction in its structure (k_{air}). In addition, an increase in the thickness of the garment could decrease the conductive heat transfer. Therefore, no burn injury was predicted and there was a relatively low amount of discharged energy to the mannequin. The large air gap size may also have influenced the temperatures across the gap during the exposure and the cooling period. Caution should be exercised as convection heat transfer may occur for large air spaces (Torvi, Dale, & Faulkner, 1999).

The air gap between the fabric and the skin can lower the effective thermal performance of the garment system if the penetrated liquid within the fabric structure is transferred to the air gap. The air gap in garments with permeable structures may be filled with hot water and enhance the effective thermal conductivity of the system. Therefore, based on the fabric property and the intensity of thermal exposure, three types of penetration may occur: non-penetration, partial penetration and total penetration (Figure 6.5 (a), (b) and (c).

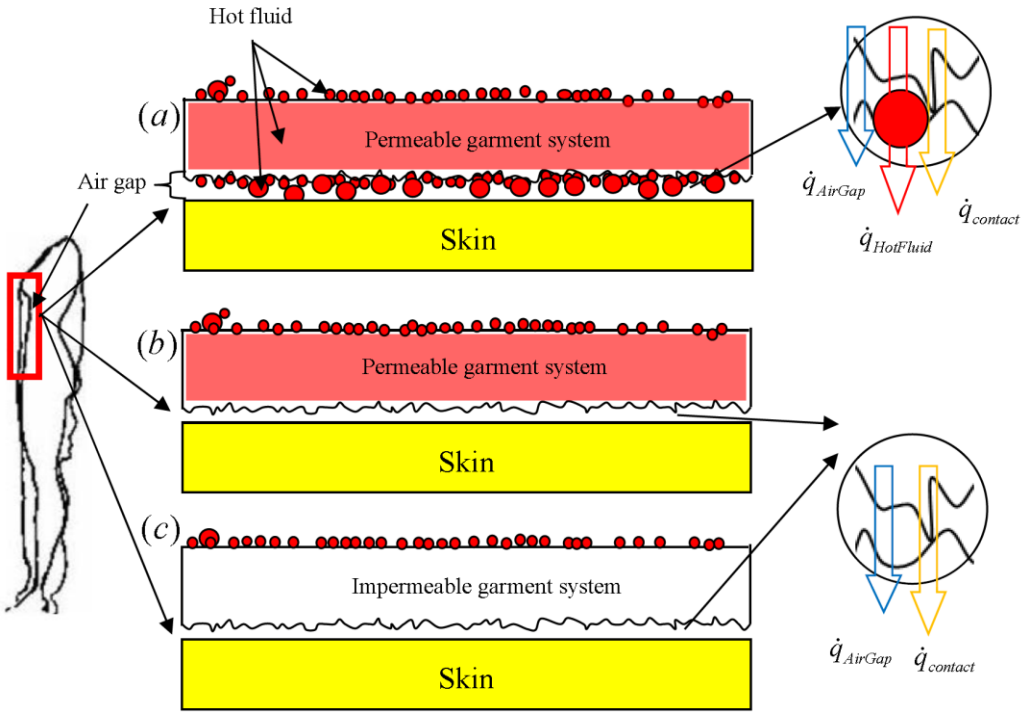

Figure 6.5. Schematic illustration of (a) total penetration, (b) partial penetration and (c) non-penetration in garment system.

Penetration does not occur when the garment has an impermeable or a semi permeable garment structure (Figure 6.5 (c)). In a "non-penetration" garment type, the hot liquid does not go through the fabric structure and the air gap. However, water vapor may penetrate and condense on the mannequin. This type of penetration was observed in impermeable single layer garments G-5 and G-6.

Partial penetration occurs when the garment system is slightly permeable or the garment system is permeable but the fabric characteristics, exposure time and intensity of the exposure cause the hot liquid to penetrate and be entrapped within the fabric structure. In partial penetration, the hot water does not enter into the air gap between the fabric and the skin (Figure 6.5 (b)). In total penetration, hot fluid penetrates through the fabric system and through the air gap and touches the skin (Figure 6.5 (a)). Once total penetration of the garment system occurs, the interfacial hot water, which has a higher thermal conductivity than fibers and air, penetrates through the air gap. Therefore, once a permeable garment system is exposed to hot liquid, the air gaps may be filled with an interfacial hot liquid, and increase the

effective thermal conductivity of the system. Total penetration leads to more thermal energy being transferred to the skin.

In this study, partial penetration occurred during the ten-second exposure of garment G-11 to hot water. For longer exposures, total penetration may occur and hot water may fill the large air gap between the garment and skin. In addition, the thick structure of the thermal liner can entrap a significant amount of hot water within its permeable structure in longer exposures. The penetrated and the trapped hot water within the garment structure may have the chance to be compressed to the skin and suddenly discharge the accumulated thermal energy to the skin (compressive discharge). Therefore, the effective thermal performance of garment G-11 exposed to hot water spray (no burn and low stored thermal energy accumulation in the garment) may be misleading and further investigation is needed for this garment.

The effect of garment design significantly affects the effective thermal performance of the garments upon hot water exposure. Figure 6.6 illustrates the double layer garment G-11 and two-part garments (bib-pants and a separate jacket) G-12 and G-13. It is evident that in spite of large thickness (1.91 mm), garment G-11 had high values of stored energy in the impingement zones around the chest and abdomen. This phenomenon can be due to the permeability of the fabric in the structure of the garment. The thick and permeable thermal liner (quilted lining Arcxel^{TM}) employed in the garment structure causes hot water to be entrapped within the garment structure during the exposure. In addition, the pressure of the hot water jet on the impingement region reduced the air gap under the impingement areas and increased the conductive heat transfer to the skin (Figure 6.6). Therefore, the entrapped hot water was closer to the skin which caused a relatively higher discharge of thermal energy during the cooling period in the impingement zones.

In Figure 6.6, it is observed that the areas of the mannequin such as jaw, cheek, forehead, head and neck (sensors 91 to 96) which are not covered by the garment can absorb thermal energy during the cooling period. Similar to the nude test, the heat transfer during the cooling period to the uncovered areas was due to discharge of the thermal energy from water vapor and/or steam and/or condensed steam in the chamber and the uncovered surfaces. However, in Figure 6.6, a comparison of the local stored energy rating values of the uncovered areas in garment G-9 and G-13 with the local stored energy rating values of same areas in

the nude test, shows that the presence of garment in a close proximity to the uncovered jaw, cheek, forehead, head and neck can enhance heat transfer to these areas during the cooling period.

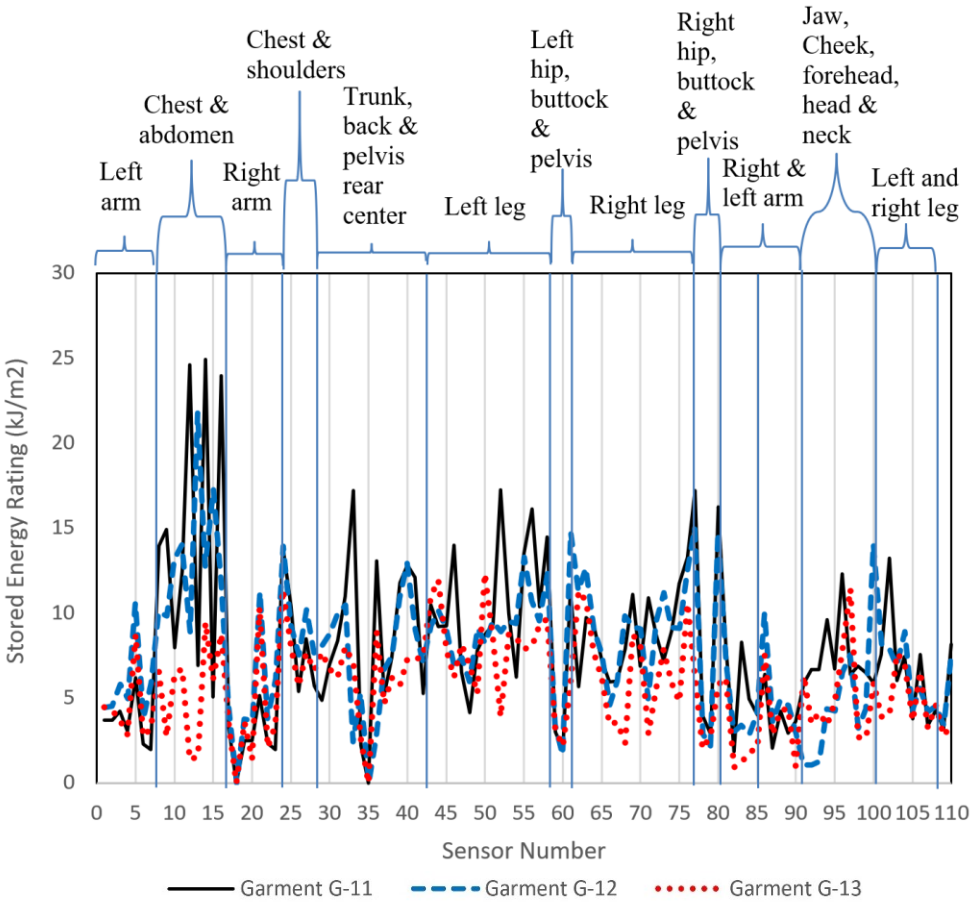

Figure 6.6 The local stored thermal energy rating distributions within the mannequin for garments G-11, G-12 and G-13.

The impermeable garments G-12 and G-13 both consist of bib pants and a separate jacket. There were no second and third degree burn for these two garments. The impermeable structure of the fabrics used in the garments minimized the transmitted and the discharged energy to the sensors. The values of the stored energy rating in these garments were considerably lower than the permeable and impermeable single layer garments. However, the stored energy rating for garment G-12 was higher than for garment G-13, specifically in the impingement zones. The thin layer of fabric used in garment G-12 (0.49 mm) could conduct more heat to the skin in comparison to the thicker garment G-13 (1.19 mm). The conductive heat transfer was greater in garment G-12's overlapped zones than garment G-13's

overlapped zones. The overlapped zone refers to areas where the jacket and the bib pants overlap. In the overlapped zones, garment G-12's overall thickness was approximately 0.98 mm where this value was approximately 2.38 mm for garment G-13.

Garment G-13 provided a superior effective thermal performance. The thick impermeable structure of garment G-13 showed no burn injury for 10 s exposure of the garment to water at 85°C. Also, the fact that G-13 had the lowest value of stored energy rating showed that this garment had the lowest ability to store thermal energy during 60 s of cooling period. The design of the garment is related to its superior performance in hot water exposures. The relatively thick jacket (1.19 mm) overlaps the bib-pants with the same fabric in the torso and pelvis areas. The overlapped fabrics provided an overall thickness of approximately 2.38 mm plus an additional air layer between the jacket and the pants. As such, the areas around the pelvis, buttocks, hips, abdomen, and the lower back had relatively lower values of stored energy rating in garment G-13 (Figure 6.6). It can also be confirmed that, similar to single layer garments, the areas around the legs stored more thermal energy than the rest of garment G-13 (see Figure 6.6).

Caution needs to be exercised in drawing conclusions in this section since the thick and heavy structures of the impermeable garments such as G-12 and G-13 need to be investigated from a comfort perspective. The thick impermeable structure of these fabrics may impede moisture and heat transfer from the skin to the environment and disturb sensorial and thermo-physiological comfort. In addition, the heavy garment systems may restrict individual's mobility and disturb body movement comfort.

Garments G-1, G-3, G-10, G-11 and G-13 were equipped with reflective tape. The tape was attached to the cuff of the sleeves, legs, back and shoulders. The reflective tapes were crisscrossed at the back of the garment in the form of an X shape. Figure 6.7 demonstrates the average stored energy rating for sensors 26, 27, 30 to 40, 109 and 110. These sensors represent right and left shoulders, lower, middle and upper back (Appendix B). The stored energy rating values of the garments with reflective tapes are shown with stripped bars in Figure 6.7. The data shown in Figure 6.7 shows that the crisscross reflective tapes at the back of garments reduced the stored thermal energy accumulation at the back of the garments. This can be confirmed by comparing the data for garments G-1 and G-2,

G-3 and G4 as well as G-12 and G-13. Providing additional thickness for the fabric at the areas where the reflective tape was attached may explain this phenomenon.

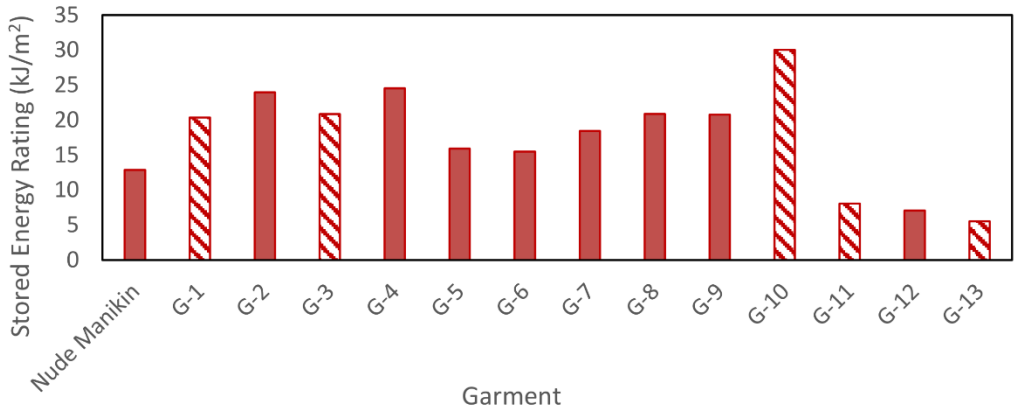

Figure 6.7. The average stored energy rating for sensors 26, 27, 30 to 40, 109 and 110. The sensors represent the area under the crisscrossed reflective tapes.

In this study, different styles of pockets such as chest patch pockets with a flap, rear patch pockets, un-flapped pocket and in-seam pockets were included in the garment system. It is realized that hot liquid flowed into the unflapped pockets and was trapped in these pockets. Figure 6.8 depicts the stored energy rating for garments G-5 and G-6.

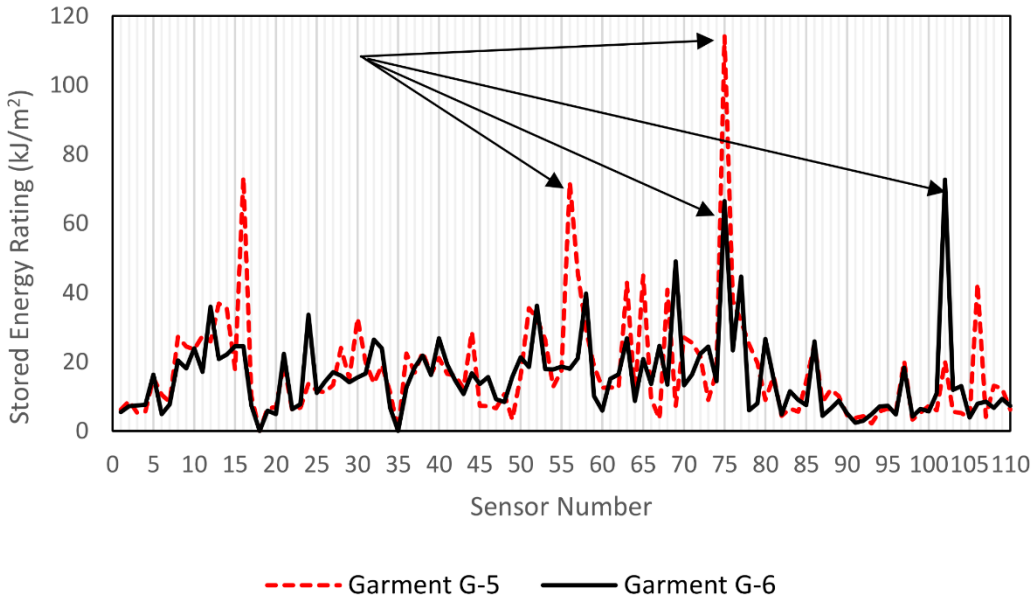

Figure 6.8. The local stored thermal energy rating distributions within the mannequin for impermeable garments G-5 and G-6.

The two garments had unflapped side pockets. The maximum values of the stored energy rating relate to sensors which are located under the unflapped side pockets. These sensors are shown with arrows in Figure 6.8. The accumulated volume of hot water in the pocket caused a significant amount of discharged thermal energy to these sensors.

Summary

This study was carried out to investigate the effects of body geometry and garment design on stored thermal energy developed in the garment and its discharge to the skin in the cooling. The effective thermal performance relates to performance criteria that considered the transmitted and the discharged thermal energy in rating the performance of the fabric systems in exposures to thermal hazards.

The results obtained from this study confirm the results obtained from bench scale tests in Chapters 4 and 5 namely, that mass transfer is a critical factor influencing the transmitted and the discharge energy to the skin. Minimizing hot liquid transfer is an important factor that reduces transmitted and discharged thermal energy transfer to the skin. As such, impermeable garments provide good protection upon exposure to hot water spray. The fabric mass and thickness also influence the amount energy discharged to the skin.

The stored thermal energy (STE) rating (kJ/m^2) is a criterion to evaluate the garment system based on its ability to store thermal energy. The analysis of the local stored thermal energy rating values showed that these values are higher in the lower body regions than the impingement regions. The lower parts of the body are where the thermal energy is discharged to the mannequin due to the flow of hot water on the lower regions of the garments such as the legs. Therefore, from the lower to upper body, the areas on the lower body affected by hot liquid flow receive a significant amount of thermal stored energy. As such, data analysis technique in test methods need to be modified so that they would be able to consider the local stored energy discharge in order to see which parts of the mannequin receive the most thermal energy during the cooling period of the garments.

Loose fitting garments provided better effective thermal protection than the close fitting garments. When the garment maintained its shape relatively well during a hot water exposure, it enhanced the effective thermal performance of the garment. The styles of the garment, such as pocket styles, has a great influence on the performance of the garments. Adding layers also has a positive effect on the reduction of thermal energy discharge to the skin.

The information in Table 6.1 can be helpful to provide a technical basis to fabric and garment design based on the applications of the garment. The data in Table 6.1 are mainly focused on the stored energy phenomenon. The stored energy discharge and the stored energy rating in Table 6.1 reveal how much stored energy is in the garment system. The amounts of stored thermal energy shown in Table 6.1 are obtained from all sensors in the mannequin whether or not the sensor predicted burn injury.

Varying the exposure conditions such as changing the pressure of the impinging hot water jet and changing the duration of exposure may also affect the effective thermal performance of the thermal protective clothing. The intensity of the hot water exposure may increase total penetration in the permeable garment and fill the air gaps between the garment and the skin, particularly in the lower body and in loose-fitting garments. As such, further investigations are needed.

The stored thermal energy analysis in this study was focused on the ordinary discharge of the thermal energy during the cooling period of the garment for the mannequin in static positions. Movement of the body during and after the thermal exposure may cause compression of the heated garment to the individual's skin and can reduce the level of protection expected from the protective garment. Therefore, a new test method should be developed in order to study the effect of the compressive discharge on the effective thermal performance of the garment system. An articulated instrumented mannequin such as Thermo-Leg® can be used in order to simulate individuals' activities and to evaluate the performance of the garment system in dynamic situations (Behnke, Geshury, & Barker, 1992).

CHAPTER 7 EXPERIMENTAL INVESTIGATION OF FABRIC MOISTURE TRANSFER PROPERTIES AND HOT WATER FLOW PATTERN ON A HORIZONTAL AND AN INCLINED FABRIC IMPINGED BY A CIRCULAR WATER JET[4]

Introduction

Evaluations of fabric systems exposed to hot liquid splash were conducted in the inclined and horizontal orientations. Experimental parameters were the nozzle-to-fabric separation, and the flow rate and temperature of hot water. Each of these parameters was kept constant in the evaluations of fabric systems in Chapters 4 and 5.

Different experimental settings were employed to evaluate hot water transport properties of the fabric systems. The flow patterns created by the impingement of a circular jet of water on the surface of horizontal (β=0°) and inclined (β=45°) single layer fabric systems are studied. The effect of water temperature on the contact angle in horizontal single layer fabrics, and the relation between the contact angle and flow pattern were examined. In addition, the effect of experimental variables such as water temperature, water flow rate, orientation of sensor board to the stream of water, and nozzle-to-plate separation on impact penetration of water were investigated. Moreover, the effect of fabric properties on impact penetration of water was explored. The findings from the analyses of the flow patterns and moisture transfer properties will also be used to evaluate the thermal protective fabric systems.

Results and discussion

For evaluations of fabric systems exposed to hot liquid splash in the next two chapters (Chapters 7 and 8), the sensor board with 29 sensors was used which was described in Chapter 3. The test matrix of the experiments is shown in Table 7.1. The orientation of the skin simulant plate (β), hot water flow rate ($\dot{m}$), temperature of the liquid (T_l) and the dimensionless nozzle-to-sensor board separation (z/d) were adjusted to the desired settings. The diameter of the nozzle (d) is 10 mm and the nozzle-to-sensor board separation (z/d) was adjusted to z/d=3

[4] This chapter is an original work by the author. No part of this chapter has been previously published nor presented at conferences.

and z/d=9. The nozzle-to-sensor board separation values were the smallest and the largest possible spacings of the apparatus.

Table 7.1. The experimental settings and variables.

Liquid	Angle of orientation, β (degrees)	Flow rate, $\dot{m}$ (mL/s)	Water temperature, T_l (°C)	Dimensionless nozzle-to-sensor board separation (z/d)
Distilled water	45	40	60	3
				9
			±	3
				9
		80	60	3
				9
			90	3
				9
	0	40	60	3
				9
			90	3
				9
		80	60	3
				9
			90	3
				9

The fabric specimens were cut to 410 mm by 257 mm in order to cover the surface of the sensor board. Each specimen contained a different set of warp and weft yarns. The single layer fabrics were mounted on the sensor board and were taped flat. A Canon digital camera PowerShot SX60 HS (Canon U.S.A., Inc, New York) was mounted on a tripod at a constant distance from the sensor board in order to take images of the water flow patterns on the surface of the fabric. Hot water was heated to a pre-set temperature. The physical properties of water at three temperatures are shown in Table 7.2. The valve was opened and the skin simulant plate was exposed for 60 s.

Infrared images were taken of the surface of the fabric during exposure and after termination of the exposure in order to investigate the temperature profile on the surface of fabrics. The images were taken using a FLIR InfraCAM SD thermal imager (FLIR Systems, Inc., Oregon). The emissivity of the fabric system was set

at 0.9 for all the images as discussed in Chapter 5. The position of the Canon digital camera and FLIR Infrared camera with respect to the hot liquid splash apparatus is illustrated in Figure 7.1 (a) and (b).

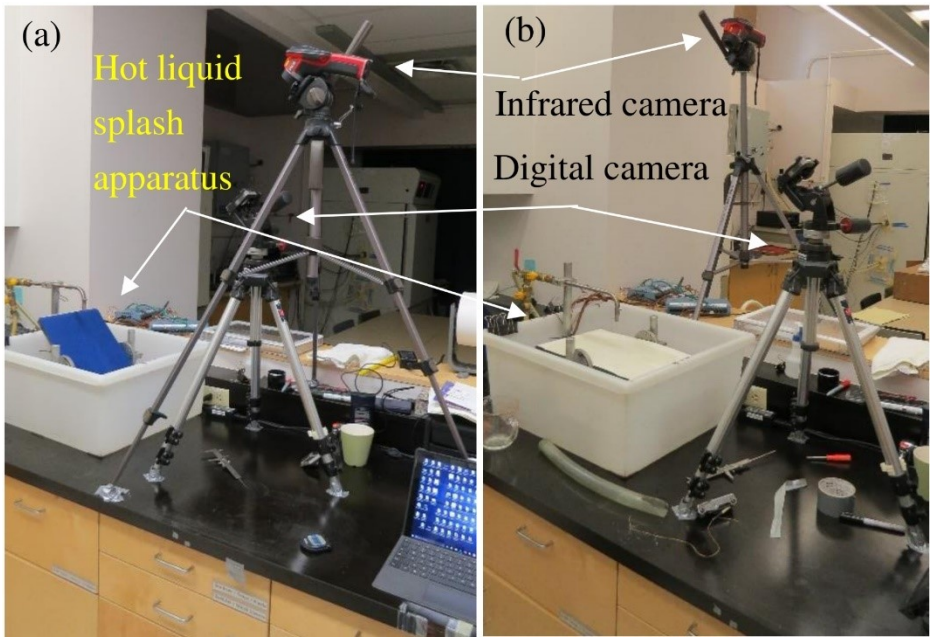

Figure 7.1. The setting of Canon digital and FLIR Infrared camera in (a) 45-degree and (b) horizontal orientation.

Table 7.2. Physical properties of water (Cengel & Ghajar, 2011, p. 854)

Temp (°C)	Density (kg/m^3)	Dynamic Viscosity (kg/m.s)	Surface Tension (N/m)	Specific heat (kJ/kg°C)	Thermal conductivity (W/m°C)
22	998	0.959×10^{-3}	0.073	4.18	0.606
60	983	0.467×10^{-3}	0.061	4.18	0.654
90	965	0.315×10^{-3}	0.061	4.21	0.675

The Reynolds and Weber numbers were determined for the water jet using Equations 2.11 and 2.13 (page 27), and the results are shown in Table 7.3. The volumetric flow rate of hot water was converted to a linear velocity by dividing the flow rate by the area of the nozzle. Therefore, the liquid velocity at the jet outlet was determined from Equation 7.1 where $V$is the volumetric flow of water and d (m) is the nozzle diameter (10 mm). As such, for hot water flow rate with 60 and

80 mL/s, the values of linear velocity were 0.51 and 1.02 m/s respectively and assumed to be the mean velocity.

$$v_{nozzle} = \frac{V}{A} = \frac{4V}{\pi d^2} \tag{7.1}$$

Table 7.3. Weber and Reynolds numbers of the jet at various temperatures.

Temp (°C)	22	60		90	
Flow rate (mL/s)	80	40	80	40	80
Reynolds number, Re_d	10604	10724	21456	15607	31227
Weber number, We_d	142	42	168	41	163

The pressure of the water jet at impingement on the fabric surface (Pa) can be estimated from Equation 7.2 (Çengel, 2005, p. 189)

$$P_{impingment} = \frac{1}{2}\rho\left(v_{impingment}\right)^2 \tag{7.2}$$

where:

ρ = the density of water, kg/m^3

v = the velocity of the water jet at impingement point, m/s.

According to the law of conservation of energy, the amount of kinetic energy at the surface of the fabric is equal to the amount of kinetic energy and potential energy at the nozzle provided that the energy losses due to friction are neglected. As such, the velocity of the water jet at impingement on the fabric surface (m/s) can be estimated from Equation 7.3

$$v_{impingment} = \sqrt{v_{nozzle}^2 + 2gz} \tag{7.3}$$

where

v_{nozzle} = the velocity of water at the nozzle outlet, m/s

z = the nozzle-to-sensor board spacing, m

g = the gravitational acceleration m/s^2.

From Equations 7.1, 7.2 and 7.3, the total pressure at the stagnation point is

$$P_{impingment} = \frac{1}{2}\rho \left[\left(\frac{4V}{\pi d^2}\right)^2 + 2gz\right] \quad (7.4)$$

Therefore, the pressure of the water jet at impingement can be determined by employing Equation 7.4 as shown in Table 7.4.

Table 7.4. The pressure of the water jet at impingement under different experimental settings.

Angle of orientation, β (degrees)	Flow rate, $\dot{m}$ (mL/s)	Water temperature, T_l (°C)	Dimensionless nozzle-to-plate separation (z/d)	Pressure at stagnation region, $P_{stagnation}$ (Pa)
0	40	60	3	417
			9	996
		90	3	409
			9	977
	80	60	3	799
			9	1378
		90	3	785
			9	1353

Determination of contact angle of water drop on horizontal flat single layer fabrics

Contact angles on the surface of the fabric systems were determined by using two approaches. In the first approach, a water droplet at room temperature (20 ± 2°C) was placed on the surface of the fabric system. For the second approach, the droplet was taken from hot water (95± 5°C) and placed on the surface of the fabric. For the fabrics with water resistant finishes (fabric systems S-1 to S-4 and S-6 to S-9), the contact angle was determined by analyzing the drop profile. Once the sessile drop was placed on the surface of the fabric with water resistant finish, it created a bead-shape profile which wet the surface of the fabric at the interface between the drop and the fabric. This phenomenon is defined as partial wetting in this study (Figure 7.2 (a)). For the fabric with no finish (S-5), it was observed that the drop penetrated after it was placed on the surface of the fabric. As such, total wetting occurred and wetting time was measured which will be discussed later in Chapter 7. In this study, the wetting time refers to the time from when the drop hit the surface of the fabric until the drop penetrated completely into the fabric (Figure 7.2 (b)). Table 7.5 shows the contact angles determined for single layer fabric

systems which are the average values of three specimens tested for each fabric. It should be noted that a 5°C tolerance (±5°C) is given for the water drop at 95°C to include the temperature drop that may happen from taking a water drop from boiling water until it is dropped on the fabric for contact angle measurement.

Table 7.5. The measured contact angle between the sessile water drop at 22±2°C and 90±5°C and fabric systems S-1 to S-4 and S-6 to S-9.

Assembly code	Contact angle (degrees) (SD)	
	22±2°C ($\theta_{22°C}$)	95±5°C ($\theta_{90°C}$)
S-1	127 (5.02)	114 (5.20)
S-2	131 (4.10)	121 (5.46)
S-3	141 (4.45)	134 (2.47)
S-4	131 (1.27)	128 (3.84)
S-5	0	0
S-6	133 (1.21)	130 (1.30)
S-7	132 (2.12)	124 (0.92)
S-8	137 (0.49)	129 (1.03)
S-9	107 (6.58)	81 (1.41)

The "0"means that total wetting occurred and no drop formed on the fabric.

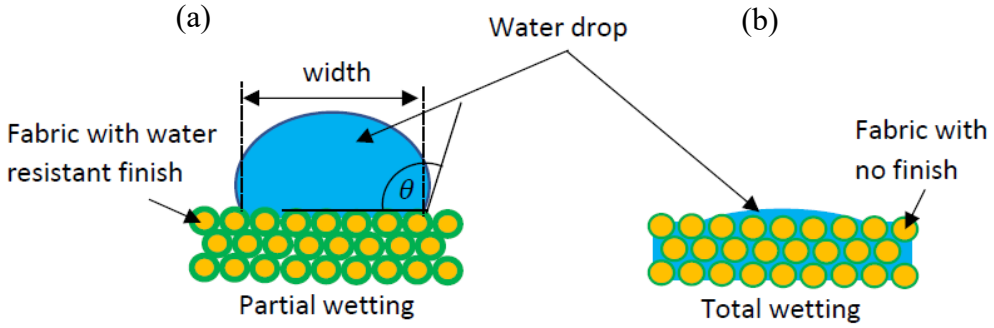

Figure 7.2. Schematic illustration of (a) partial wetting of fabric with water resistance finish (b) total wetting of fabric with no finish.

Hydraulic jump and water flow pattern due to the impingement of a circular jet of hot water on the surface of flat single layer fabrics

It was stated earlier that in the evaluation of a thermal protective fabric system exposed to a circular jet of hot water, the position of hydraulic jump can be important because the heat transfer decreases significantly at the location of the hydraulic jump (Stevens & Webb, 1991). Analysis of the predicted data obtained from the evaluation of the fabric systems in this study was carried out using two approaches. In the first approach, the effects of experimental variables (hot water

flow rate, hot water temperature, nozzle-to-plate separation and orientation of fabric surface) on the position of the hydraulic jump were investigated. In the second approach, the effects of different fabrics on the position, shape, and stability of the hydraulic jump were analyzed.

Investigation of a liquid water jet flowing onto the surface of horizontally oriented fabrics

A circular hydraulic jump was observed during the exposure of horizontal (β=0°) fabric systems listed in Table 3.4 to a hot water jet. In the hot water splash in this study, the water leaving the nozzle hit the fabric and flowed on the surface in a thin layer, and spread radially from the stagnation point (Figure 7.3 (a)). This region is referred to as the supercritical region in this study (Liu & Lienhard, 1993). According to Equations 2.5 and 2.6 (page 24), as the radius of the supercritical region increases, the velocity of the liquid and Froude number decrease and the liquid film gains potential energy. While water spreads and gains potential energy, it decelerates at the onset of the hydraulic jump (Figure 7.3 (b)). In the hydraulic jump zone, the water film rises to a greater depth after a certain distance. The occurrence of the hydraulic jump causes an increase in water depth (subcritical depth) and creates a tranquil flow of the liquid in the subcritical zone (Figure 7.3 (c)). The region downstream of the jump flows on the surface of the flat horizontal fabric until it is runs off the surface (Figure 7.3 (d)).

Figure 7.3 illustrates the occurrence of a hydraulic jump by a vertical circular jet of hot water on a horizontal flat surface of fabric system S-4: (a) the transition of the vertical to horizontal fluid flow at the stagnation region as the water expels radially, (b) onset of the hydraulic jump, and (c) and (d) formation of the supercritical region, hydraulic jump radius and the subcritical region. Figures 7.3 (e) and (f) show infrared images of fabric system S-4 during an exposure to water at 90°C at the onset of the hydraulic jump and the liquid flow 30 s after the start of the exposure. In the infrared images, there are areas beside the fabrics where hot water ran-off the surface of the fabric and accumulated in the drainage basket underneath the skin simulant plate. These areas are indicated with dashed rectangles in Figure 7.3.

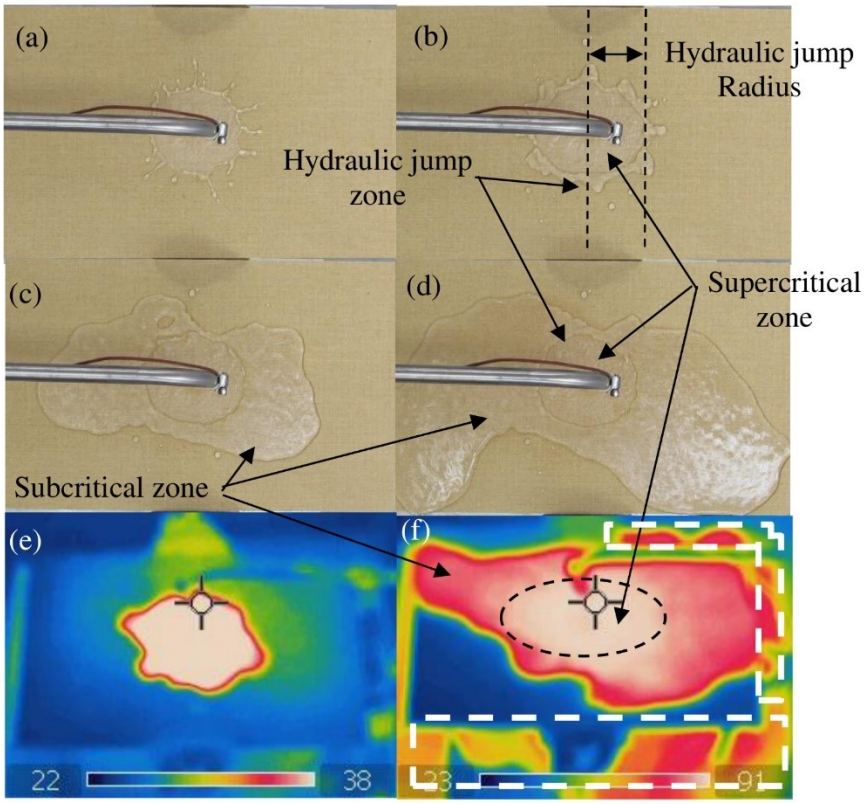

Figure 7.3. Surface impingement of on fabric system S-4 by a 90°C water jet at different stages. The images (a), (b) and (e) were taken less that a second after the onset of exposure. Images (c), (d) and (f) were taken 2, 5 and 30 s after the start of the exposure to water at 90°C (flow rate = 80 mL/s and z/d = 9).

From a heat transfer perspective, the development of the jump causes a significant decrease in the water temperature. Figure 7.3 (e) confirms that the temperature at the onset of the hydraulic jump is relatively lower than the temperature of the supercritical zone which is encompassed by the jump. In addition, it can be inferred from Figure 7.3 (f) that the temperature is approximately uniform in the supercritical zone and it does not change from the stagnation point to the location of hydraulic jump. However, in the hydraulic jump zone, the temperature decreases noticeably and the decrease in temperature continues as the radius of the subcritical zone increases. This phenomenon was observed in all fabric systems (Figure 7.4).

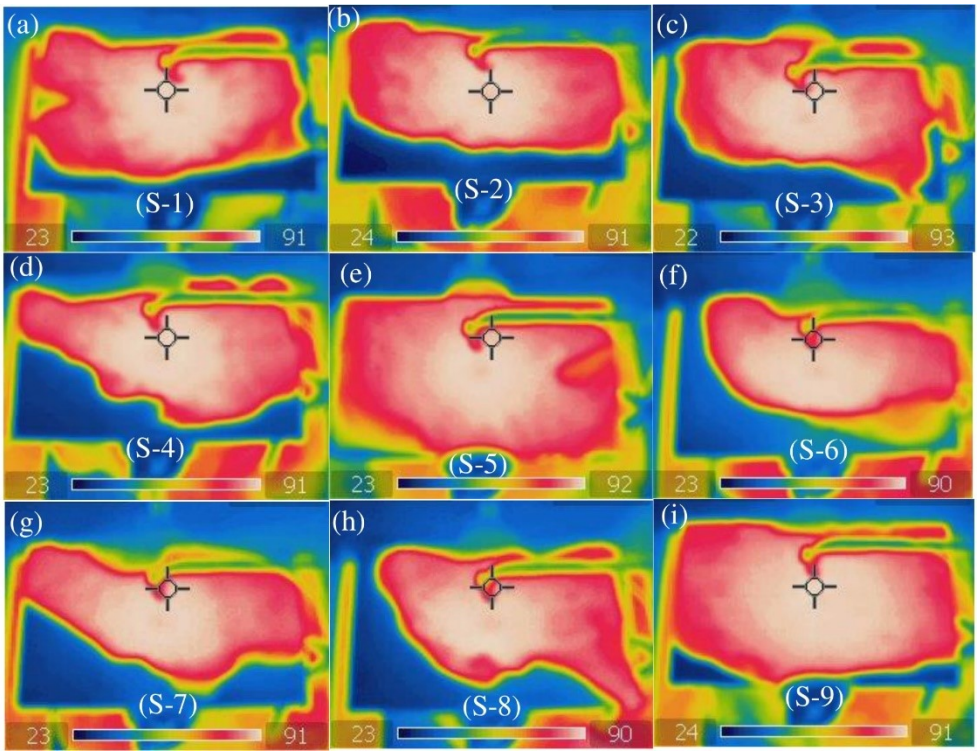

Figure 7.4. Infrared images of single layer fabrics (impingement angle 90 degrees): (a) S-1, (b) S-2, (c) S-3, (d) S-4, (e) S-5, (f) S-6, (g) S-7, (h) S-8 and (i) S-9 exposed to 90°C water with 80 mL/s flow rate and a dimensionless nozzle-to-plate separation (z/d) of 9. The images were taken 30 s after the onset of exposure.

Figure 7.4 (a) to (i) depict infrared images of single layer fabric systems in the horizontal orientation exposed to 90°C water (80 mL/s flow rate, z/d=9). The temperature of water in the supercritical zone was approximately uniform and considerably higher in comparison to the subcritical zone. Therefore, the determination of the position of hydraulic jump or the area of the subcritical zone is a crucial factor in the evaluation of thermal performance of the fabric systems exposed to water. Considering the importance of the area of the supercritical zone (A_{sup}), the values of the area were determined for nude tests (skin simulant plate with no fabric) as well as fabric tests. In nude and fabric tests, the hydraulic jump resembles a circular shape such as a circle or an ellipse with known areas (Figure 7.5). In the fabric tests with partially unstable hydraulic jump shapes such as fabric system S-8, the area is approximated by fitting a circle or ellipse to the jump. Three images of water flow patterns taken approximately 25 to 35 s after the start of the water flow were used for each experimental setting.

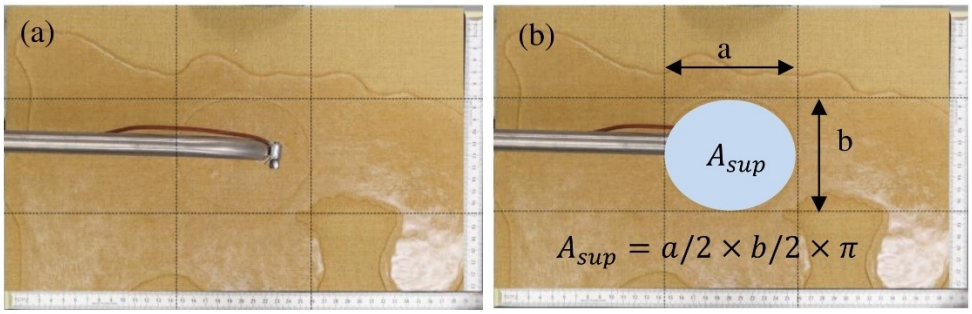

Figure 7.5. (a) Fabric system S-4 (Kevlar®/PBI) exposed to hot 90°C water (flow rate= 80 mL/s and nozzle-to-plate separation, z/d=9); (b) geometrical shape used for the determination of the area of flow pattern on horizontal fabric systems.

The effect of experimental variables on water jet flow on the skin simulant plate (nude test)

Using the experimental setting mentioned in Table 7.1, the horizontally oriented skin simulant plate, was exposed to the hot water jet. For low Reynolds and Weber numbers, it was observed that the hydraulic jump was stable with a single roller (Figure 7.6 (a)). However, the increase in Reynolds and Weber numbers caused the flow of liquid to be more affected by the inertial forces. The increase in inertial forces increased Froude number and the ratio of the subcritical depth to supercritical depth increased according to Equation 2.9 (page 25). By increasing the depth of the subcritical region, the single roller on the jump surface became lower than the height of the subcritical region and gave the hydraulic jump a double roller (Figure 7.6 (b)) or unstable shape (Figure 7.6 (c)).

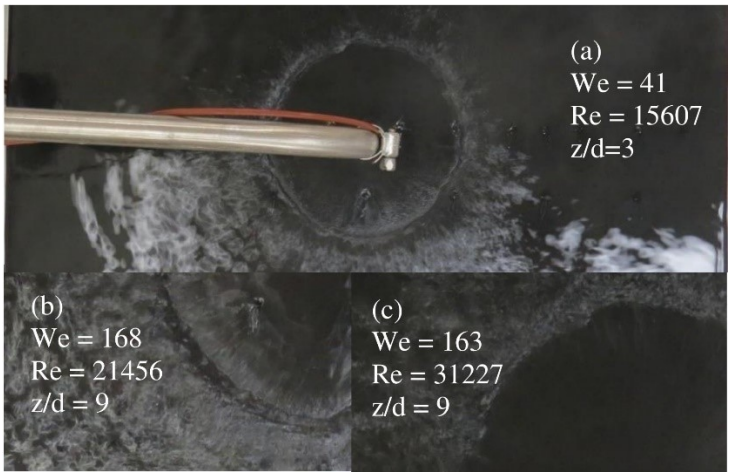

Figure 7.6. Stability and shape of the hydraulic jump in nude horizontal test: (a) a single roller jump, (b) a double roller jump and (c) an unstable jump.

The area of the supercritical region was determined and the results are presented in Table 7.6. The areas were measured based on the photographs taken during the tests. In each photo, a ruler was used to determine the dimensions of the flow. Using StatCrunch software, the results from the correlation coefficient between the supercritical zone area (dependent variable) and the pressure at the stagnation point, as well as the jet's Weber, Reynolds and Froude numbers (independent variables) were obtained and shown in Table 7.7.

Table 7.6. Supercritical zone area on nude skin simulant plate exposed to water jet.

Angle of orientation, β (degrees)	Flow rate, $\dot{m}$ (mL/s)	Liquid temperature, T_l (°C)	Dimensionless nozzle-to-sensor board separation (z/d)	Supercritical zone area, A_{sup}^{nude} (cm^2) (SD)
0	40	60	3	58 (0.87)
			9	63 (0.59)
		90	3	64 (0.38)
			9	93 (0.26)
	80	60	3	223 (1.13)
			9	268 (1.25)
		90	3	218 (2.11)
			9	227 (1.36)

Table 7.7. Correlation coefficients between the area of the supercritical region in nude test (A_{nude}^{sup}) and We_d, Re_d, Fr_d and $P_{impingment}$

	Supercritical region area (A_{sup}^{nude}) (cm^2)
Impingement pressure, $P_{impingment}$, (Pa)	0.65
Jet Weber number, We_d	0.98
Jet Reynolds number, Re_d	0.82
Jet Froude number, Fr_d	0.97

According to the correlation coefficients in Table 7.7, it can be inferred that the area of supercritical region is highly positively correlated with the jet's Weber number, Reynolds number and Froude number. Therefore, the inertial forces, surface tension and viscous forces of the liquid jet strongly affect the area of the supercritical region and the position of hydraulic jump, result that was also obtained by Liu and Lienhard (1993). The impingement pressure of the liquid jet at the

stagnation point is also positively correlated with the area of the supercritical zone. As such, increasing the water temperature, flow rate and nozzle-to-plate separation can increase the area of the supercritical region on the nude skin simulant plate.

The effect of experimental variables on water jet flow on single layer fabrics

Using the experimental settings mentioned in Table 7.1, single layer fabric systems S-4, S-6, S-7 and S-8 that are typical shell fabrics in thermal protective clothing, were exposed to a hot water jet when placed in horizontal orientation. Analysis of the areas of the supercritical region in a nude test (skin simulant plate only) and the fabric tests revealed that the supercritical region was smaller on a clothed skin simulant plate than a bare plate. The range of supercritical region areas on a bare plate was from 58 to 227 cm^2 while this range was 18 to 87 cm^2 for fabric system S-4, 17 to 86 cm^2 for fabric system S-6, 13 to 80 cm^2 for fabric system S-7 and 18 to 54 cm^2 for fabric system S-8 (Table 7.8). The significantly lower range of supercritical area for the fabrics suggested that the hot water splash phenomenon covered a smaller area on fabrics than on a nude plate.

Table 7.8. The area of the supercritical zone on fabric systems S-4, S-6, S-7, S-8 and on a nude skin simulant plate.

Angle of orientation, β (degrees)	Flow rate, $\dot{m}$ (mL/s)	Water temperature, T_l (°C)	Dimensionless nozzle-to-sensor board separation (z/d)	Supercritical zone area, A_{sup} (cm^2) (SD)				
				Nude	S-4	S-6	S-7	S-8
0	40	60	3	58 (0.87)	18 (0.66)	18 (0.40)	13 (0.26)	18 (0.05)
			9	63 (0.59)	22 (0.39)	25 (0.98)	18 (0.15)	22 (0.43)
		90	3	64 (0.38)	20 (0.07)	21 (1.02)	18 (0.21)	25 (0.37)
			9	93 (0.26)	20 (0.56)	24 (0.53)	17 (0.21)	24 (0.61)
	80	60	3	223 (1.13)	60 (0.21)	59 (0.69)	41 (0.40)	41 (0.88)
			9	268 (1.25)	48 (0.66)	54 (0.13)	32 (0.65)	39 (1.51)
		90	3	218 (2.11)	83 (0.90)	75 (0.91)	80 (1.30)	54 (0.97)
			9	227 (1.36)	87 (0.82)	86 (1.54)	51 (0.97)	49 (2.39)

By analysis of the shape of hot water flow patterns on fabric system S-4 (Figures 7.7 (a) and (c)) and fabric system S-8 (Figures 7.7 (b) and (d)), it is evident that the hydraulic jump has a stable shape with a single roller jump for low Reynolds and Weber numbers. However, an increase in the Reynolds and Weber numbers as well as an increase in the impingement pressure at the stagnation region resulted in an unstable appearance of the hydraulic jump (Figure 7.7 (a) and (b)). As such, the finding that the increase in inertial forces increased the instability in fabric hydraulic jumps, was similar to the results reported by Liu and Lienhard on a flat surface (Liu & Lienhard, 1993).

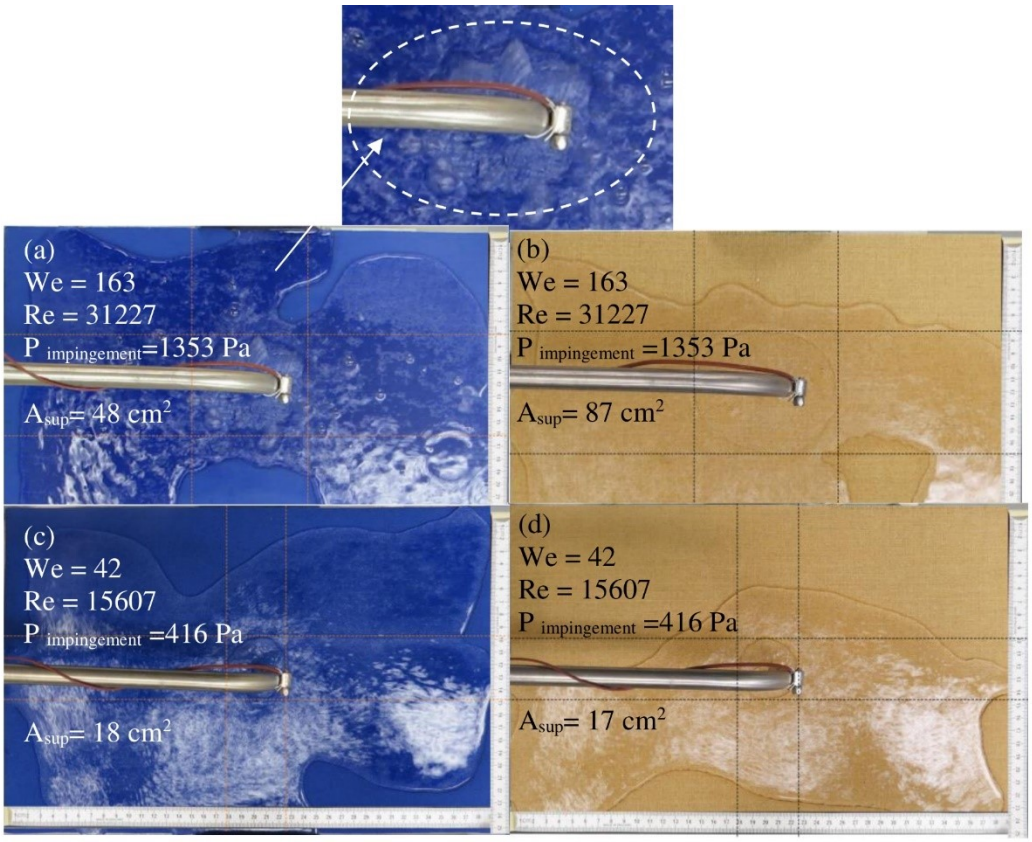

Figure 7.7. Fabric systems S-8 (88% cotton/12% nylon with polymer finishing) and S-4 (Kevlar®/PBI) exposed to hot water jet.

The correlation coefficient between the area of the supercritical region on the fabrics (dependent variable) and the impingement pressure at the stagnation point as well as the jet's Weber, Reynolds and Froude numbers (independent

variables) is shown in Table 7.9. It can be inferred that the inertial, surface tension and viscous forces of the liquid jet strongly affect the area of the supercritical region and the position of hydraulic jump. The impingement pressure is influenced by the nozzle-to-sensor board spacing, and has minimal effect on the area of the supercritical region as compared to the effect of the jet's Weber number, Reynolds number and Froude number. As such, the correlation coefficient between the impingement pressure and the supercritical area is much smaller than the other correlation coefficients.

Table 7.9. The correlation between the area of the supercritical region on fabric (A_{sup}^{fab}) and We_d, Re_d, Fr_d and $P_{impingement}$.

	Supercritical region area (A_{sup}^{fab}) (cm^2)
Impingement pressure, $P_{impingement}$ (Pa)	0.43
Jet Weber number, We_d	0.83
Jet Reynolds number, Re_d	0.89
Jet Froude number, Fr_d	0.84

The effect of physical properties of single layer fabrics on water jet flow

By comparing Figures 7.7 (a) and (b), for which fabric systems S-4 and S-8 were exposed to similar experimental conditions, the instabilities of the hydraulic jump in fabric system S-8 were more apparent than for fabric system S-4 during the exposure. The instability of the hydraulic jump on fabric surface can be attributed to the roughness of the fabric and other fabric properties that can affect the inertial forces at the impingement or hydraulic jump regions

The roughness of the fabric during exposure can be classified into two subgroups in this study: (1) intrinsic and (2) extrinsic roughness. The intrinsic roughness can be referred to the roughness of a fabric due to the physical properties of its fiber, yarn and fabric structure such as weave pattern. The extrinsic roughness can be referred to as unevenness of the surface of the fabric due to external forces such as inertial forces caused by the jet of water at the stagnation region or the supercritical area. The unevenness of the surface of the fabric in the supercritical region due to external forces will be discussed later in Chapter 7.

In hot liquid exposures of fabric systems, the applied pressure in the stagnation region can decrease the thickness of the fabric during exposure and affect

the shape of hydraulic jump. According to the data presented in Table 7.4, the pressure of water at the stagnation region varied from 417 to 1,378 Pa. As such, the thickness of fabric can decrease when higher pressure is applied to the fabric as shown in Chapter 4, Table 3.5. The thickness of the fabric made from 88% cotton/12% nylon with polymer finish (mass= 412.5 g/m^2) decreased by 15% (from 0.67 mm to 0.57 mm) when the pressure increased from 1000 to 13,800 Pa (Chapter 3, Table 3.5). In the thinner fabric (Kevlar®/PBI, mass=211.5 g/m^2), the thickness decreased by 6% from 0.51 to 0.48 mm. Therefore, it appears that for the fabrics used in this study, the compressibility and thickness were inversely proportional to the pressure at the stagnation region.

When the hot water leaving the nozzle hit a fabric system, the thickness of the fabric at the stagnation point decreased. As the water started to spread radially from the stagnation point, the difference between the thickness of fabric at the stagnation (z_{fab}^{stag}) and the wall zone (z_{fab}^{wall}) may have caused eddies in the wall jet close to the stagnation point. This phenomenon decreases the inertial forces of the supercritical region and created an unstable hydraulic jump (Figure 7.8). The increase in the depth of the subcritical region entrained air, traps air bubbles and disturbed the axisymmetric shape of the jump (Figure 7.8 (a)).

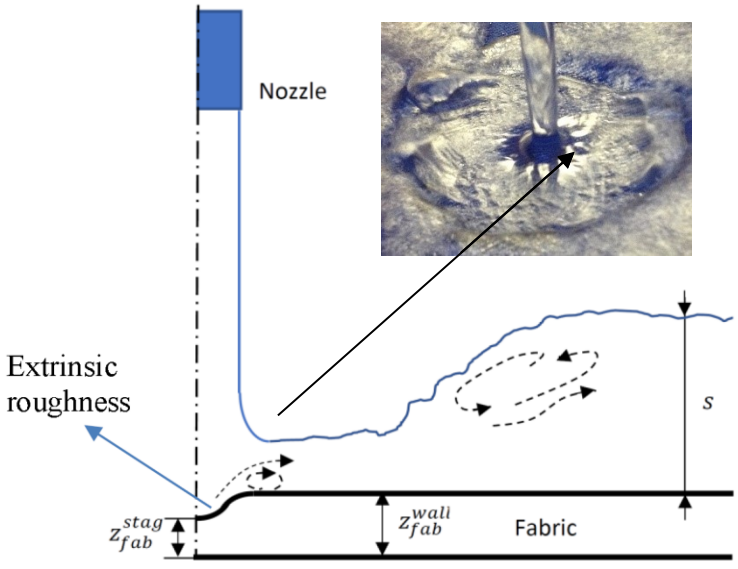

Figure 7.8. Schematic illustration of extrinsic roughness and the unstable flow.

The hydraulic jump in fabric system S-4 was stable with a single roller. The fiber content of the fabric system S-4 was Kevlar®/PBI. Aramid fibers consist of long, highly oriented molecular chains and strong interchain bonding. This fiber structure gives Kevlar®/PBI high tensile strength, high modulus and structural rigidity in comparison to conventional fibers such as cotton and nylon used in fabric system S-8 (Allen & Roche, 1989; Gabara, Hartzler, Lee, Rodini, & Yang, 2007) . As such, it is possible that fabric system S-4's thickness at the stagnation region was less affected by inertial forces compared to fabric S-8. Therefore, a more stable hot water flow was observed on fabric system S-4 compared to fabric system S-8 when the inertial forces are relatively high (Figure 7.7 (a) (b)).

Other physical properties of the fabric such as the fabric's ability to resist water, its surface energy and weave pattern may have influenced the liquid jet's inertial forces and shape of the flow. Fabric system S-8 resisted water penetration which may have affected the velocity of water in the supercritical region compared to fabric system S-4 which did not resist water penetration. The penetration of water through fabric system S-4 may have decreased the velocity of water in the supercritical region and created a more stable hydraulic jump. In addition, fabric system S-8 had excellent hydrophobic surface properties which may have affected the velocity of liquid in the supercritical region. Fabric system S-8's compact twill weave which created ridges on the surface of this fabric also affected the velocity of water in the supercritical region. The interactions of these fabric properties caused the liquid sheet to bounce on the surface of fabric and create instabilities. Some of these properties and their effects on the flow of water on the fabric systems will be discussed later in Chapters 7 and 8.

It was mentioned that the axisymmetric hydraulic jump occurs when the hot water jet hits the surface at the stagnation region. Due to inertial forces, it changes its direction and spreads outwards radially in the form of a thin liquid film. As the thin film spreads and gains potential energy, the thickness of the liquid film abruptly increases and creates a hydraulic jump. However, it was observed that when permeable fabric systems S-4, D-1, D-3 and D-4, which have the same surface properties, were exposed to a jet of hot water at 90°C with 80 mL/s flow rate, the areas of the supercritical region were different (Table 6.13). As such, it can be inferred that impingement of a water jet over the surface of the fabric is not only a

surface phenomenon but also may be influenced by other physical properties of the fabric system as well.

As such, the areas of the supercritical zones of fabric systems S-1, D-1, D-3 and D-4 were compared. Shell fabric A was mounted on the surface of each fabric system and the effect of fabric surface properties such as fabric surface free energy on the inertial forces were kept constant. Fabric systems D-1, D-3 and D-4 are double-layer fabrics constructed from Kevlar®/PBI (Fabric S-4) and thermal liners A, C and D as the underlying layers, respectively. Table 7.10 shows the values of the supercritical zone area of fabric systems S-1, D-1, D-3 and D-4 exposed to a 90°C hot water jet under different experimental settings.

Table 7.10. Supercritical zone area on fabric systems S-1, D-1, D-3 and D-4.

Angle of orientation, β (degrees)	Flow rate, $\dot{m}$ (mL/s)	Liquid temperature T_l (°C)	Dimensionless nozzle-to-sensor board separation (z/d)	Supercritical zone area, A_{sup} (cm^2) (SD)			
				S-4	D-1	D-3	D-4
0	40	60	3	18 (0.66)	17 (0.59)	16 (0.61)	15 (0.85)
		90	3	20 (0.07)	19 (0.39)	17 (0.89)	18 (2.03)
	80	60	3	60 (0.21)	45 (0.67)	38 (0.4)	36 (0.98)
		90	3	83 (0.90)	64 (1.06)	66 (0.88)	64 (1.12)

The boundary conditions on the surface of Kevlar®/PBI were kept constant in each experimental setting (Weber number, Reynolds number, Froude number, $P_{impingement}$=constant) for fabrics S-4, D-1, D-3 and D-4. According to Table 3.6, the thicknesses of fabric system S-4, D-1, D-3 and D-4 are 0.54, 1.43, 2.54, and 3.13 mm and their densities are 0.45, 0.30, 0.20 and 0.18 g/m^2 respectively. It was observed that the area of the supercritical zone for fabric systems D-1, D-3 and D-4 were similar or slightly decreased with an increase in the thickness and a decrease in the density.

Hot liquid impingement on the surface of the fabric is different from the classical hot fluid impingement onto a flat surface where the vertical momentum is

converted into horizontal momentum (Kate et al., 2007b). When a fabric is impinged by a liquid jet, the fabric can be compressed at the stagnation region. In addition, fabric usually has a porous structure and the jet of water can penetrate within and through the fabric. Employing linear momentum conservation principles, the vertical momentum of the liquid jet converts to the horizontal momentum of liquid flow on the surface as well as the vertical momentum of penetration liquid. Therefore, the velocity of the water jet at impingement ($v_{impingement}$) in the vertical direction can be equal to the velocity of the supercritical region on the fabric (v_{sup}) in the horizontal direction and the velocity of the penetrating water through the fabric (v_{pen}). As such, it is expected that the physical properties of the fabric influence the inertial forces on the surface of the fabric, the position of the jump from the stagnation point, as well as the area of supercritical region.

The average value of the supercritical area of Kevlar®/PBI (fabric system S-4) is 83 cm^2 (SD=0.90 cm^2) during the exposure of the fabric to 90°C water (80 mL/s and z/d=3). When fabric system S-4 is impinged by hot water, the fabric is compressed at the stagnation point by the liquid jet and its thickness decreases relative to the thickness of the fabric underneath the wall jet (A_{fab}^{stag}<A_{fab}^{wall}). This phenomenon causes an indention on the surface of the fabric which creates roughness around the stagnation point and can affect the velocity of water in the supercritical region. Once Kevlar®/PBI was placed on top of the permeable nonwoven thermal liner A in fabric system D-1, the area of the supercritical region decreased by almost 23% (A_{sup}^{D-1}= 64.09 cm^2). Thermal liner A has a non-woven structure which entraps a large amount of air within its structure. When this fabric is compressed, the liquid jet can create a deeper indention (Δz) at the fabric in comparison to fabric system S-4 due to the fact that the impinging jet removes the entrapped air within the nonwoven structure of fabric system D-1. This phenomenon can affect the velocity and the area of the water sheet in the supercritical region. Using thermal liners with entrapped air enhances the effect of impinging water which results in a deeper indention (Δz) on the stagnation point (Figure 7.9). The deeper indention may cause more roughness and change in the hydrostatic pressure around the impingement zone which results in decreasing the inertial forces and reducing the area of the supercritical region.

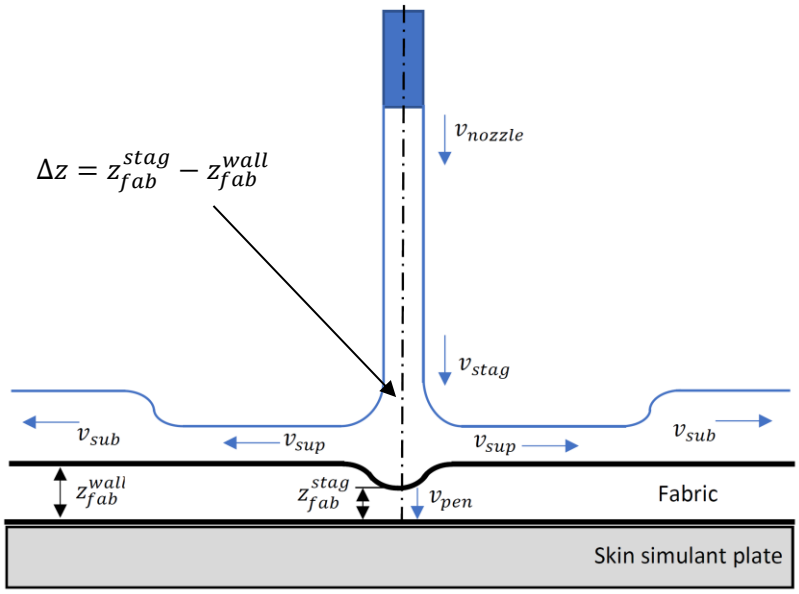

Figure 7.9. Illustration of impinging jet of water on the surface of fabric mounted on skin simulant plate.

The other important factor that may affect the velocity of the liquid sheet in the supercritical region is the increase in the velocity of the penetrating water jet through the fabric structure. Therefore, physical properties of the fabric system can affect the inertial forces of penetrating water through the fabric system. For this purpose, the areas of the supercritical zone on the surface of single layer fabrics exposed to 90°C water (80 mL/s flow rate) were determined and shown in Table 7.11.

Table 7.11. The area of the supercritical zone on single layer fabrics exposed to water at 90°C, 80 mL/s with 3 and 9 nozzle-to-plate separation (z/d=9 and 3).

Assembly code	A_{sup} (cm^2) (SD)	
	90°C, 80 mL/s	
	z/d=9	z/d=3
S-1	71 (0.71)	73 (0.57)
S-2	79 (0.99)	72 (0.60)
S-3	65 (0.69)	64 (1.03)
S-4	87 (0.82)	83 (0.90)
S-5	---	---
S-6	86 (1.54)	76 (0.91)
S-7	51 (0.97	80 (1.30)
S-8	49 (2.39)	54 (0.97)
S-9	263 (2.61)	203 (0.72)

The "---"means that the area was not determined for the fabric.

The supercritical region for fabric system S-5 (Nomex® with no finish) was not determined because the area of the hydraulic jump on this fabric was changing during the exposure. At the beginning of the exposure, a jump with a single roller was created on the surface of fabric (Figure 7.10 (a)). Since water stayed on the surface of the fabric for the first few seconds due to the surface tension forces, the inertial forces in the supercritical region tried to push the water into the subcritical region. A hydraulic jump with a single roller was observed. After 5 s of exposure, water adhered to the surface of fabric system S-5 which had high surface energy ($\theta_{90°C}$=0°) and penetrated through its capillaries (Figure 7.10 (b)). Penetration of water on the surface of the fabric decreased the fluid velocity in both supercritical and subcritical regions. The decrease in the inertial forces resulted in a reduction in the supercritical film Froude number (Equation 2.5 and 2.7) and the ratio of the subcritical region depth to supercritical region depth (Equation 2.9). The decrease in the ratio, changes the jump from a single roller to a very smooth jump with no roller which is illustrated in Figure 7.10 (c) (Liu & Lienhard, 1993). Once the entire fabric is wet, water drips from the sides of the fabric. The flow of water off the surface of the fabric increases the inertial forces in the subcritical region after 30 s of exposure. In addition, taking into account the decreasing trend in inertial forces of the supercritical region, the ratio of the subcritical region depth to supercritical region depth approaches unity (Equation 2.9). As such, the subcritical region depth (s in Figure 7.8) is approximately equal to the supercritical region depth and the hydraulic jump disappears on this fabric after 30 s of exposure (Figure 7.10 (d)). Figure 7.10 shows fabric system S-5 exposed to water at 90°C, 80mL/s and z/d=9 and the schematic illustration of hot water splash phenomenon on fabric system S-5.

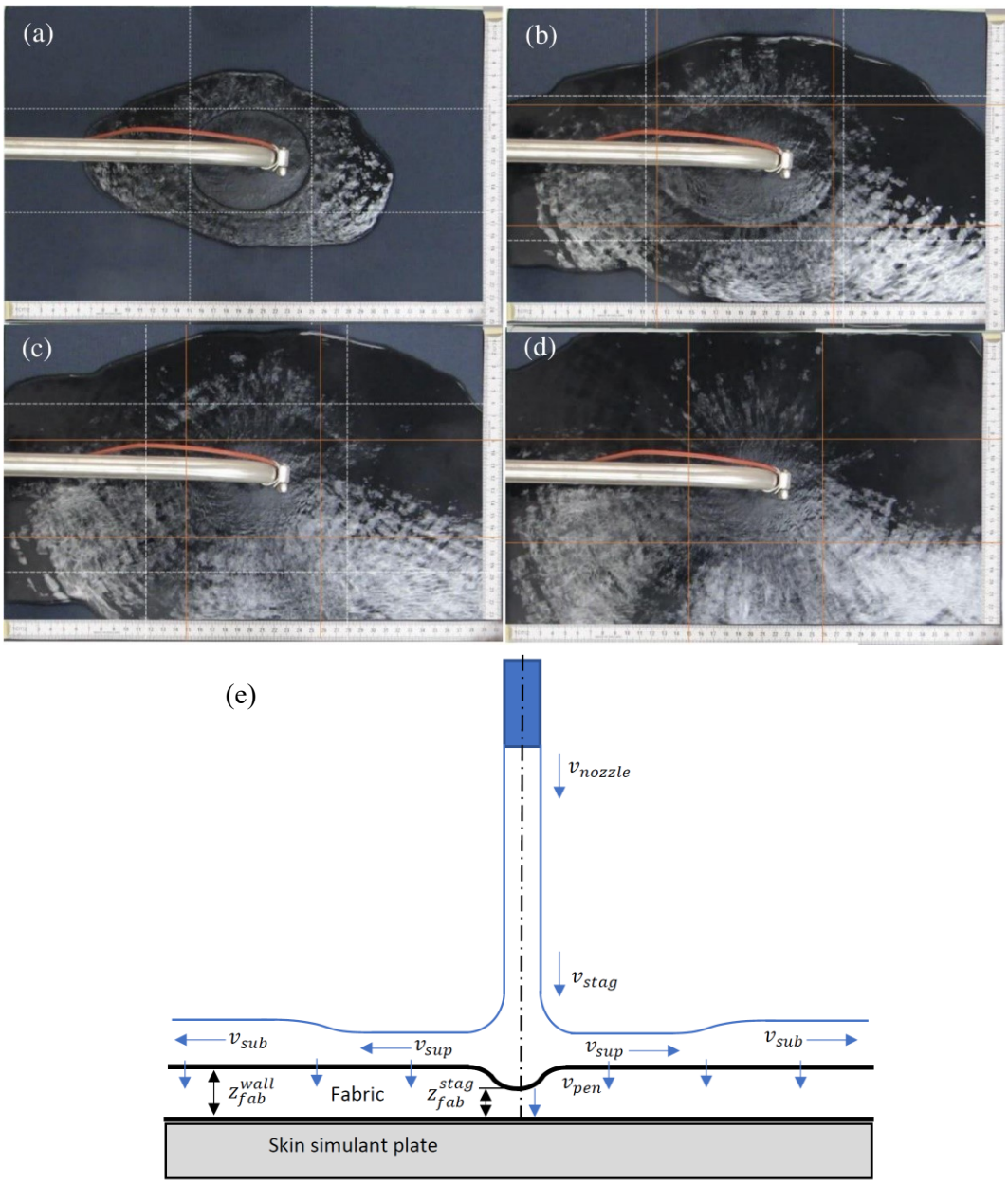

Figure 7.10. fabric system S-5 exposed to hot water: (a) hot water flow pattern after 2 s exposure (developing single roller hydraulic jump), (b) 6 s of exposure (single roller jump), (c)12 s of exposure (jump with no roller) (d) 30 s of exposure (no jump); (e) schematic illustration of hydraulic jump with no roller on hydrophobic fabric.

Contrary to the fabric with no finish, on fabrics with water resistant properties, the area of supercritical region did not change noticeably with time. According to the data presented in Table 7.11, the area of the supercritical region

for single layer fabrics with hydrophobic properties exposed to hot water under the same experimental setting are different. These differences are due to the difference in the physical properties of the fabrics. Correlation coefficients between the area of the supercritical region on the fabrics (dependent variable) and the physical properties of the fabrics such as contact angle at 90°C, mass, thickness, density, air permeability and water vapor diffusion resistance (independent variables) were determined (Table 7.12).

Table 7.12. The correlation coefficients between the area of the supercritical region (A_{sup}^{fab}) and physical properties of fabric system.

	Supercritical region area (A_{sup}^{fab})
Contact angle, $\theta_{90°C}$	-0.90
Mass	0.66
Thickness	-0.45
Density	0.92
Air permeability	-0.09
Water vapor diffusion resistance	0.94

The correlation coefficient for contact angle confirms that it is highly and negatively correlated (correlation coefficient= -0.90) with area of the supercritical region which shows that in fabrics with water resistant surfaces, the area of the supercritical region decreases as the contact angle increases. The decrease in fabric surface energy and increase in hydrophobicity of fabric can reduce the area of hydraulic jump. Therefore, vertical impingement of hot water on the horizontal surface of fabric system S-9, fire-resistant rain wear, results in a significantly larger area of supercritical region. This fabric has a water resistant neoprene coating on its surface. However, the neoprene coating becomes hydrophilic when the temperature of water is 90°C. This means a larger area of hot water can cover this fabric which may enhance heat transfer to its underlying surface in hot water exposure.

Resistance to water vapor diffusion is also highly correlated with the area of supercritical region (correlation coefficient= 0.94). More resistance to water impingement through the structure of the fabric results in a larger area of the supercritical region. According to the earlier discussion, resistance to mass transfer through the structure of the fabric minimizes penetration inertial forces through the fabric and enhances the fluid velocity at the supercritical region.

The effect of fabric density and thickness on the area of the supercritical region were discussed earlier. A dense fabric has less entrapped air within its structure and shows less variation in thickness when it is impinged by a water jet. Therefore, the roughness of fabric at the stagnation area decreases which results in a more stable jump and a large supercritical region area.

Air permeability of the fabric did not seem to influence the area of the supercritical region. The values of air permeability shown in Table 3.6 were obtained under approximately 125 kPa differential pressure (ASTM, 2012a). However, the pressure of water on the surface of the fabric at the stagnation point varies between 417 to 1378 kPa. Therefore, the air permeability of the fabric systems that are used to provide protection against hot water impingement should be determined under a higher differential pressure in order to obtain more realistic data for the evaluation of fabric system.

In summary, it appears that the position of the hydraulic jump on the surface of the fabric and the area of the supercritical region is a function of experimental variables as well as physical properties of the fabric system.

Investigation of hot water jet flow onto inclined fabric system surfaces

In the impingement of a vertical jet of water onto an inclined fabric surface, water spreads out as a thin liquid film and the noncircular hydraulic jump appears as a rim at the outer boundaries of the flow. In the stagnation region, the thin film of water is created on the fabric and radially spreads from the stagnation point. In Figure 7.11 (a), r_j is refers to the radius of the spreading water on the fabric. The radius of the liquid film that expands in the opposite direction of the main flow (r_j at point A) is the smallest. The thin liquid film expands and gains potential energy until the surface tension forces overcome the inertial forces. At this point the thickness of the thin liquid film increases and creates rims at the outer boundaries of the flow due to the effects of the surface tension and the inertial force (Kibar et al., 2010). In order to use the same terminology for circular and noncircular hydraulic jump, the thin liquid film and the rim are referred to supercritical and subcritical regions, respectively. The transition between these two regions is called the position of the jump which occurs at r_j. Therefore, the width of the subcritical region at each point (Δr_{rim}) can be defined as the radius of the outer boundaries of the flow r_s subtracted from the radius of the supercritical region (7.10 (a)). The

width of the rim ($\Delta r_{rim} = r_s - r_j$) grows as the potential energy in the rim transforms to kinetic energy, from point A with maximum potential energy to point C with maximum kinetic energy. The liquid flow expands up to a certain extent which is called the width of the flow (W). At the outer boundaries of the jump, the potential energy in the subcritical region as well as the gravitational forces, accelerate the flow of the liquid in the rim toward the downstream region of the flow. In fabrics with hydrophobic properties, the surface tension forces bring the outer boundaries of the flow back together and create braiding on the surface of the fabric (point C in Figure 7.11 (b)). This type of fabric creates "a closed rim flow pattern". For a fabric with no finish (S-5) or a water resistant fabric with a hydrophilic surface (S-9), the inertial forces overcome the surface tension forces and create "an open rim flow pattern" (Figure 7.11 (a) and (c)).

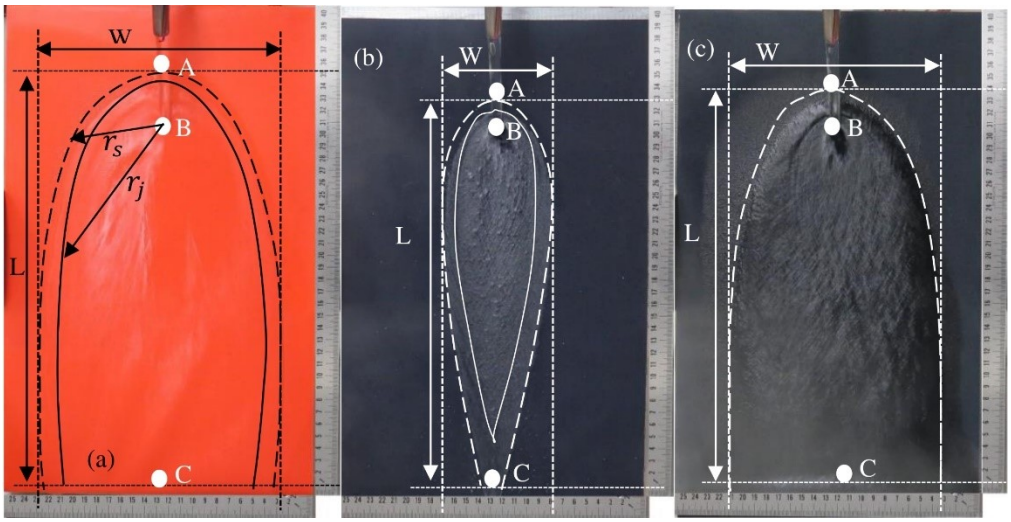

Figure 7.11. Flow pattern on single layer fabrics: (a) water resistant fabric with a hydrophilic surface (S-9), (b) water resistant fabric with a hydrophobic surface (S-6) and (c) fabric with no finish (S-5).

The area of the flow on the surface of the fabric exposed to hot water is very important because a flow pattern that covers a larger area on the fabric with hot water may transfer more thermal energy to the fabric. Figure 7.12 illustrates the infrared images of single layer fabrics exposed to hot water at 90°C (80 mL/s flow rate and z/d=9). The images show that water-resistant fabrics with hydrophobic surfaces, such as moisture barriers (S-1, S-2 and S-3) and shell fabrics (S-4, S-6, S-7 and S-8) have similar closed-rim flow patterns. On the other hand, a fabric with no finish (S-5) and fire resistant rainwear, S-9 (water resistant neoprene laminated

with a hydrophilic surface ($\theta_{90°C}$=81 degrees)) create an open rim flow pattern on the surface when exposed to water at 90°C. However, the rims disappear as the water expands radially from the stagnation point in fabric system S-5 (Figure 7.11 (c)). The component of acceleration due to gravity in the direction of the flow ($g \cos \beta$) enhances the inertial forces as well as the component perpendicular to the direction of the flow ($g \sin \beta$) which enhances water penetration through the capillaries of the unfinished fabric system S-5. The effect of these two components cause the rims to be penetrated through the fabric.

It is evident from the infrared images (Figures 7.12 (a) to (i)) that the temperature of water drops significantly in the subcritical regions (rims). The temperature profiles of the rims in single layer fabrics show that the temperature decreases approximately 10 to 20°C along the width of the rim.

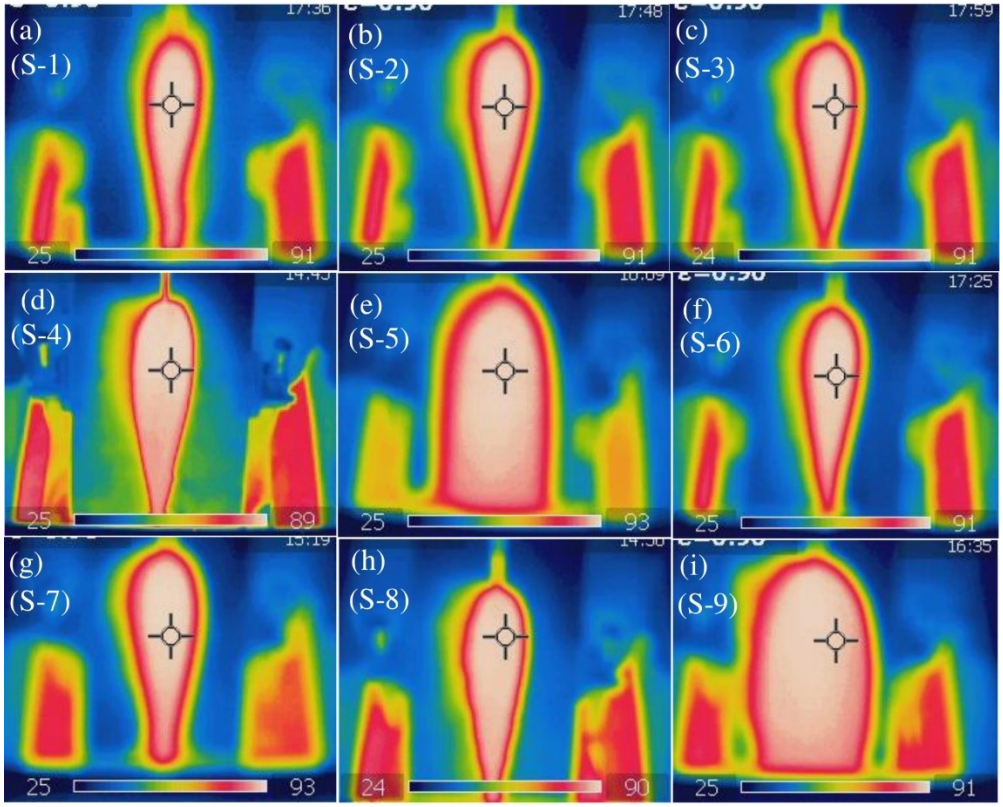

Figure 7.12. Infrared image of single layer fabrics taken 30 s after the onset of exposure (impingement angle 45 degrees): (a) S-1, (b) S-2, (c) S-3, (d) S-4, (e) S-5, (f) S-6, (g) S-7, (h) S-8 and (i) S-9 exposed to 90°C water with 80 mL/s flow rate and 9 nozzles diameter to plater separation.

It can be inferred that a closed rim flow pattern (fabric system S-8 in Figure 7.12 (h)) covers a smaller area of fabric with hot water than an open rim flow pattern (fabric system S-9 in Figure 7.12 (i)). It appears that manipulating hydrophobic surface properties of the fabrics positioned at the outer layer can affect thermal performance of a fabric that may be exposed to hot water.

The change in the experimental parameters such as liquid temperature, liquid flow rate and nozzle-to-plate separation can also affect the shape of the liquid flow pattern on fabrics. Figure 7.13 (a), (b) and (c) illustrate fabric system S-3 (Nomex®IIIA with water resistant finish and polyurethane lamination) exposed to 90°C water and z/d=9 with 20, 40 and 80 mL/s flow rate respectively.

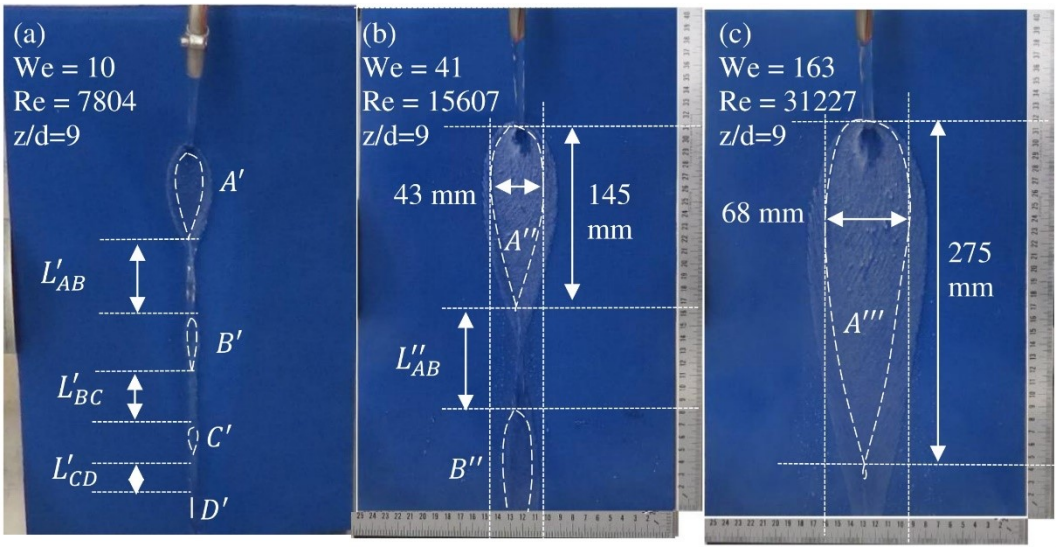

Figure 7.13. Fabric system S-3 (Nomex®IIIA with water resistant finish and polyurethane lamination) exposed to 90°C with 9 nozzle-to-fabric separation with (a) 20, (b) 40 and (c) 80 mL/s flow rate.

Considering the length of the fabrics that were tested in this study (404 mm), decreasing the velocity of the liquid jet changed the hot water flow pattern on the surface of fabric. A closed rim flow pattern with a single supercritical area and single braids formed on the fabric system S-3 exposed to water at 80 mL/s. As the jet velocity was decreased to 40 mL/s, a closed rim flow pattern with two supercritical regions (A'' and B'') and single braiding (L''_{AB}) was formed on the fabric. The length of the supercritical region decreased from 275 to 145 mm and the width of the supercritical region decreased from 68 to 43 mm (Area A''< Area A'''). It was observed that the area of the supercritical region B'' is smaller than the

area of the supercritical region A''. The collision of the rims in braiding did not create any jump from the surface of the fabric and the reflection angle was zero (γ=0 degrees).

Once the velocity of the hot water jet was reduced to 20 mL/s, the closed rim flow pattern resembled a liquid chain which consisted of four supercritical regions (A', B', C' and D') and three braidings (L'_{AB}, L'_{BC} and L'_{CD}). These chains are the result of mutual transformation of potential energy to kinetic energy in the rims. The area of region $A'$was the largest with $A' > B' > C'$. The supercritical region D' was the smallest. The length of braiding L'_{AB} was larger than L'_{BC}, and the length of braiding L'_{BC} was larger than L'_{CD}. The collisions of the rims in braidings L'_{AB}, L'_{BC} and L'_{CD} did not create any jumps from the surface of the fabric and the reflection angle was zero (γ=0 degrees).

For fabrics with a hydrophobic surface, a closed rim flow pattern was observed. In closed rim flow patterns, the rims that are formed on each side collide into each other and release energy which transforms into surface tension energy and enhances the cohesiveness of the molecules in water drops. This phenomenon causes a rise in the fluid and gives height to the braiding effect. The magnitude of the rise due to collision is proportional to the contact angle of the hydrophobic surface (Kibar et al., 2010). Figure 7.14 illustrates fabric system S-3 exposed to water at 60°C and 90°C respectively. In these experiments, the jet flow rate (40 mL/s) and nozzle-to-fabric separation (z/d=9) were kept constant. It was observed that braiding on the fabric exposed to water at 60°C made a reflection with a jump, whereas the reflection on fabric exposed to water at 90°C had no jump.

According to the values of contact angle for fabric systems with surface finish, S-1 to S-4 and S-6 to S-9 in Table 7.5, it was observed that the contact angle between water and the fabrics decreased with an increase in the temperature of the water drop (Table 7.5). The data in Table 7.2 showed that an increase in temperature of the water drop decreased its surface tension. As such, the increase in temperature of the water increased its adhesive property which made it easier for the drop of water to expand on the rough surface of fabrics. A 30°C temperature difference was enough for the water drop to create a reflection with jump on the surface of fabric system S-3. This phenomenon was also observed on fabrics with good hydrophobic surfaces such as fabric systems S-4 and S-6. It was also observed that a decrease in

surface tension of water with a 30°C temperature change enhanced the adhesiveness of water drops to the fabric and increased the areas of the supercritical regions.

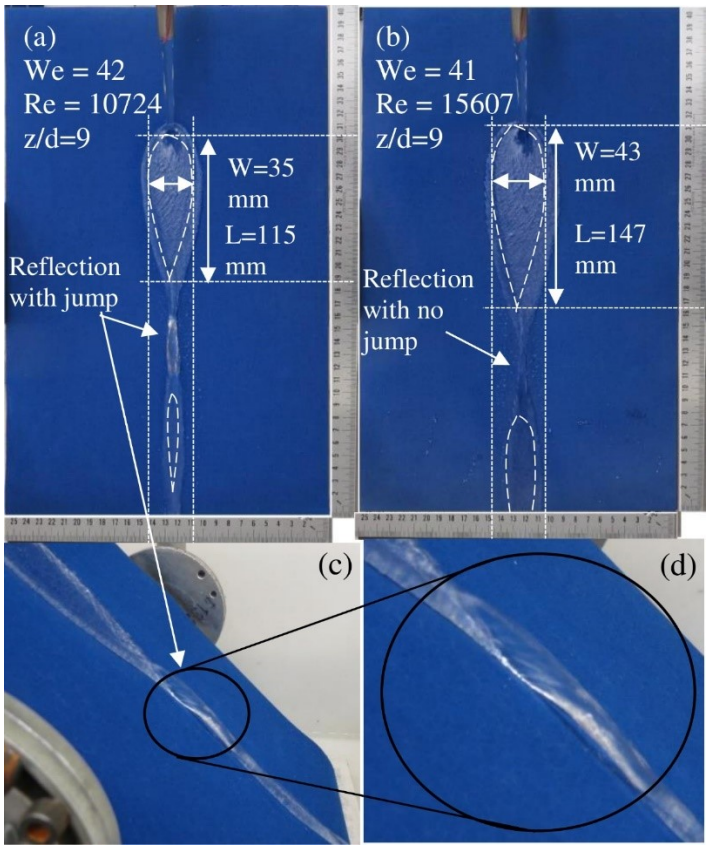

Figure 7.14. Fabric system S-3 (Nomex®IIIA with water resistant finish and polyurethane lamination) exposed to jet of water (40 mL/s flow rate and 9 nozzle-to-fabric separation z/d=9 at temperatures of (a) 60°C and (b) 90°C; (c) and (d) reflection with jump.

Nozzle-to-fabric spacing has an influence on the water flow pattern on fabrics. Figure 7.15 is an illustration of water at 90°C with 40 mL/s flow rate on the inclined (β=45 degrees) surface of fabric system S-3. The width and the length of the supercritical regions increased with an increase in the nozzle-to-fabric spacing. It was also observed that the angle of reflection was not zero on the fabric with smaller nozzle-to-fabric separation (z/d=3). Increasing the momentum of the liquid jet at the stagnation point by increasing nozzle-to-fabric separation caused more adhesiveness of the water drops to the surface of the fabric. As such, larger supercritical regions were created with larger nozzle-to-fabric separation (z/d=9). In addition, the adhesiveness of water molecules to the surface of the fabric caused

the reflection of the colliding rims to stay on the fabric surface (reflection with no jump).

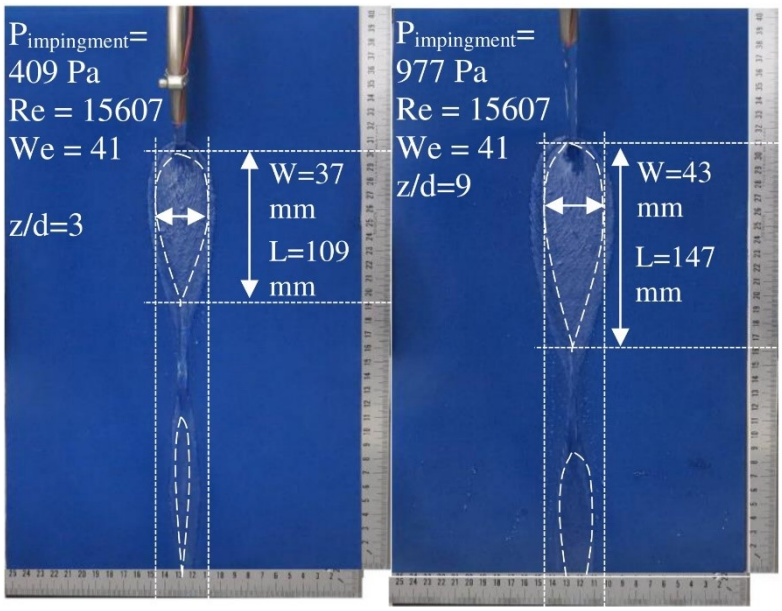

Figure 7.15. Fabric system S-3 (Nomex®IIIA with water resistant finish and polyurethane lamination) exposed to jet of water at 90°C (40 mL/s flow rate and (a) z/d=3 and (b) z/d=9.

Effect of water temperature on contact angle in horizontal flat single layer fabrics

In Chapter 4, it was discussed that the surface energy of fabrics is a factor that affects the thermal performance of protective clothing exposed to hot liquids. Wetting is the main process involved in hot liquid splash, and the contact angle is a direct characterization of the fabric's wettability. In Chapter 4 contact angles of the water drop at room temperature (22± 2°C) for the single layer fabrics were determined and the relation between contact angle and thermal performance of fabrics was determined. In this study, the effect of water temperature on the contact angle between a water drop and the fabric and its relationship to the flow pattern of water on the fabric system were investigated.

Total wetting was observed in the contact angle test of Nomex®IIIA with no finish, fabric system S-5 (see Page 174). The wetting time for fabric system S-5 was 26 s with standard deviation of 1.6 s when the water drop was at 22°C. The wetting time decreased significantly to 7.3 s with standard deviation 1.2 s when the

temperature of the water drop was at 95±5°C. Therefore, the fabric with no finish (S-5) wet almost 19 s faster with a hot water droplet than a water droplet at room temperature (22±2°C). According to Table 7.2, the surface tension of water decreases when the temperature of the drop increases. It is noted that there is a decrease in surface tension of water from room temperature to intermediate temperatures (60°C) and then a more gradual decrease to higher temperatures. The decrease in the surface tension of water causes a decrease in the adhesive forces within the water drop and causes more adhesion between the drop and the fabric. As such, the hydrogen bonds in water molecules at 95± 5°C are not bonded together as tightly as water at 22±2°C temperature and can get through the capillaries of the unfinished fabric system S-5 in a shorter length of time (7.3 s). An increase in the temperature of water can also cause a significant decrease in the dynamic viscosity of water (Table 7.2). Therefore, less viscous water can penetrate faster through the unfinished structure of fabric system S-5. The decrease in viscosity and surface tension of water as its temperature rises, enhances water drop penetration in fabric.

The values of the contact angle in Table 7.5 confirm that they decrease approximately 2 to 25% when the temperature of the droplet increases from 22±2°C to 95±5°C. The relatively larger values of fabric system S-3, S-4, S-6 and S-8 contact angles at 95±5°C state that these fabrics are relatively more hydrophobic than the other fabric systems. In addition, the contact angles of the fabric S-4 and S-6 do not change noticeably (approximately 2%) with the change of water drop temperature showing that the surface property in these fabrics is not affected much by the increase in the water drop temperature.

Fabric system S-9 is made of a neoprene coating with an underlying Nomex®IIIA fabric. This fabric is used in fire-resistant rain wear. In this fabric, the coated side is typically used as the face of the fabric. Figures 7.16 (a) and (b) depict the shapes of water drop at room temperature (20±2°C) and at 95±5°C on the surface of fabric system S-9.

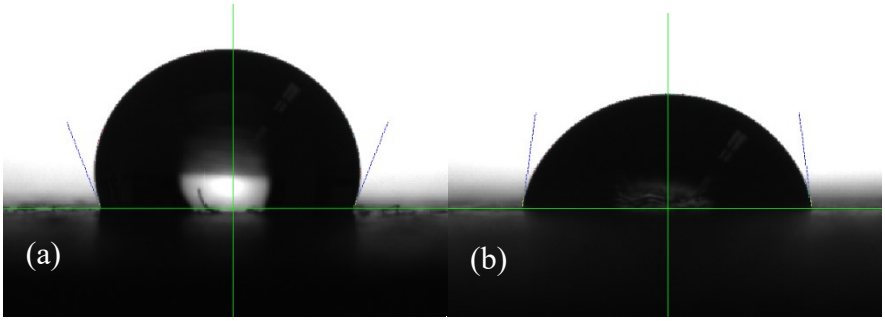

Figures 7.16. Shape of water drop at (a) 20±2°C and (b) 95±5°C on the surface of fabric system S-9.

According to classification of fabrics based on their surface properties, if the water droplet contact angle on solid surface is between 0° and 90°, the surface is defined as hydrophilic. The solid surface with contact angle between 90° and 150° is referred to as hydrophobic. If the contact angle is more than 150°, the surface has superhydrophobic property (Kibar et al., 2010; Nakajima, Fujishima, Hashimoto, & Watanabe, 1999).

Fabric system S-9's contact angle at room temperature (22±2°C) was approximately 107° (Table 7.5) while the value of contact angle with water drop at 90±5°C is 81°. Therefore, fabric system S-1 has a hydrophobic surface when it is exposed to hot water at 95±5°C. The length of the interface of the water drop and the fabric, called the width of the water drop (Figure 7.2), increases from 2.86 mm (SD=0.07) to 3.73 mm (SD=0.33) when the temperature of the water drop increases from 22±2°C to 90±5°C. The water-resistant Neoprene coating on the surface of fabric system S-9 has a very smooth surface in comparison to the other single layer fabrics. In addition, the increase in the temperature of water drop decreases the surface tension significantly. Therefore, this fabric shows hydrophilic behavior when it is tested with water at 95±5°C.

Relation between contact angle and water flow pattern on single layer fabrics

In the next step, a series of experiment were conducted using the hot liquid splash apparatus (Figure 3.1) to investigate the flow pattern of water at 22°C and 90°C on the surface of single layer fabric systems. The hot liquid splash apparatus was set in order to provide a water flow rate of 80 mL/s water flow rate. The nozzle to the fabric spacing was set at 9 cm and the impingement angle was adjusted at 45 degrees. The photographs were taken 60 s after the start of water exposure. The

dashed lines and the solid lines indicate the border of the flow of water at 22°C and 90°C respectively (Figure 7.17).

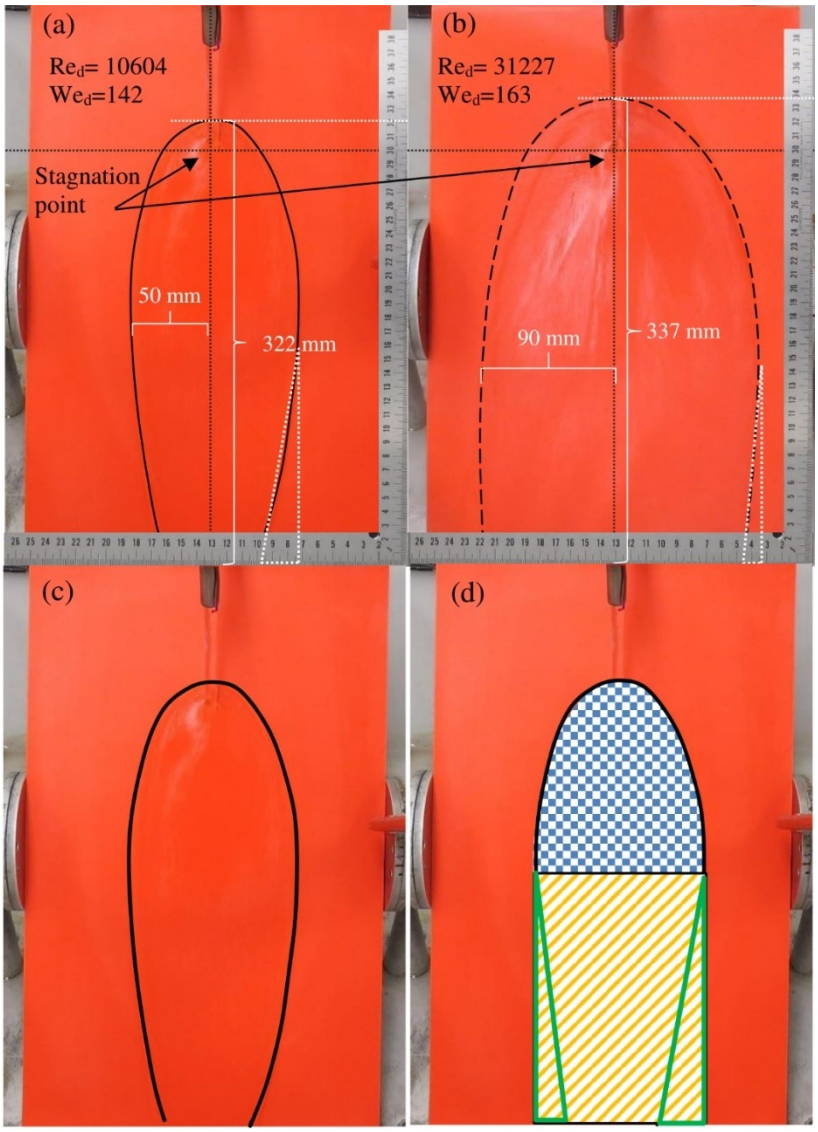

Figures 7.17. Flow pattern of water at (a) 22°C and (b) 90°C on fabric system S-9; (c) the edge of the water flow on fabric system S-9 at 22°C and (d) the geometrical shapes used for the determination of the area of flow pattern on fabric system S-9 at 22°C.

The area of the flow patterns in this study was determined assuming that the flow pattern consists of plane geometrical shapes and the area of the flow pattern can be approximately determined by dividing the shape of the flow pattern into geometrical shapes with known areas. Therefore, the flow patterns shown in Figure

7.17 (a) and (b) resembles half of an elliptical from the stagnation area until the maximum width of the flow pattern (flow width), plus a rectangle minus two triangles on each side of the bottoms of the flow. These geometrical shapes are shown in the Figure 7.17 (d).

The values of the flow pattern area in Figure 7.17 (a) and (b) were calculated as 25 and 52 cm^2 respectively. The flow pattern area increased by a factor of two by increasing the temperature form 22°C to 90°C. In addition, increasing the temperature of the hot water jet (22°C to 90°C) with a constant value flow rate (80 mL/s), increased Reynolds number by three times confirming the significant influence of temperature on inertial and viscous forces. On the other hand, the Weber number grows 15% as the temperature of water increases which explains the effect of the decrease in surface tension forces.

The effect of temperature on flow pattern surface area and the contact angle was observed in all single layer fabric systems with hydrophobic finishes. Figure 7.18 depicts the single layer fabric system flow pattern exposed to water at 22°C and 90°C. The dashed and the solid lines indicate the border of the flow of water at 22°C and 90°C, respectively. The increase in water temperature was observed to create a slight increase in flow pattern area for fabric systems S-4 and S-6 (Figure 7.18 (d) and (f)) and an increase in flow pattern area for the rest of the fabric systems (Figure 7.18). As such, the flow pattern area is inversely related to the contact angle in each fabric. The flow patterns shown in Figure 7.18 reveal that the decrease in the contact angle causes an increase in the area of the flow pattern in each single layer fabric with a hydrophobic finish. However, in the hydrophilic fabric system S-5, it was also observed that the increase in the wetting time increased the area of the flow pattern. Therefore, in a water splash test, the water at 90°C spreads to cover a larger area than water at 22°C. This phenomenon may occur due to the change in viscous and surface tension forces of water with temperature. Water with less viscosity and surface tension tends to spread more on the surface of the fabric.

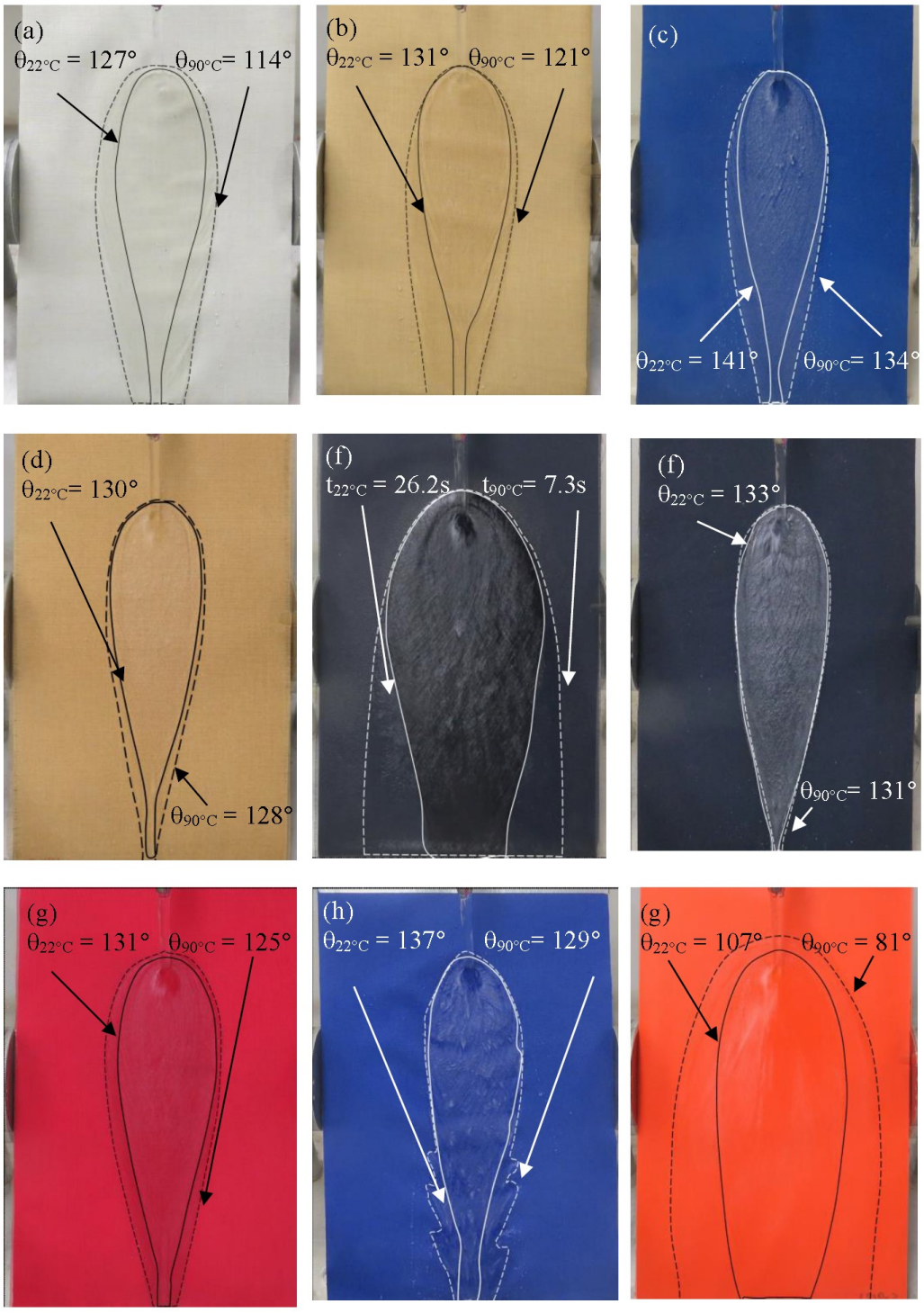

Figure 7.18. Fabric systems (a) S-1, (b) S-2, (c) S-3, (d) S-4, (e) S-5, (f) S-6, (g) S-7, (h) S-8 and (i) S-9 flow pattern exposed to water at 22°C (solid lines) and 90°C (dotted lines). The photographs were taken 30s after the onset of exposure. Wetting time was determined for fabric system S-5 (see page 200).

From the indicated border lines of the single layer fabric systems in Figure 7.18, it is evident that the temperature of the impinging water affects the flow of water. However, the temperature of water did not noticeably affect the flow pattern of fabric system S-4 and S-6 which is also confirmed by the difference in the values of contact angle. The contact angles of fabric systems S-4 and S-6 changed 2.5° and 2.2° degrees respectively when the temperature of the water drop increased to 95±5°C.

Surface *wetting* vs. in-depth wetting

It was discussed earlier in the chapter that exposure of the fabric to hot water jet is a three dimensional phenomenon because fabric has a three-dimensional porous structure. When the three-dimensional structure of the fabric is exposed to a jet of liquid, the surface of the fabric gets wet which is referred to as "surface wetting". In addition, when the structure of the fabric system transfers liquid through its depth, the wetting phenomenon occurs as a result of "in-depth-wetting".

Surface wetting

Analyses of the area of the flow pattern during the exposure of the single layer fabric system to a jet of water and the wetted area on the surface of the fabric after the termination of exposure revealed that water-resistant surface finishing affected surface wetting. In fabrics with no finish (S-5), it was observed that the fabric was wet in a larger area than in cases where the water flowed on the fabric. The comparison was made by looking at the flow pattern area during the exposure and the wetted area after the termination of exposure. The adhesive forces between the water molecules and the surface of the fabric can cause a wicking effect through the capillaries on the surface of the fabric with no finish (fabric system S-5). As such, water is transported farther from the stagnation point and wets a larger area.

Figure 7.19 illustrates the flow pattern of water at (a) 22°C and (b) 90°C on fabric system S-5. According to Figure 7.19 (a) the value of the wetted area and the flow pattern area are 421 and 344 cm^2 respectively, with the wetted area being larger that the flow pattern area by almost 15%. Moreover, the effect of temperature causes the flow pattern area (447 cm^2) to be expanded 55% and wet a larger area (695 cm^2). This can be attributed to the decrease in surface tension of water at 90°C.

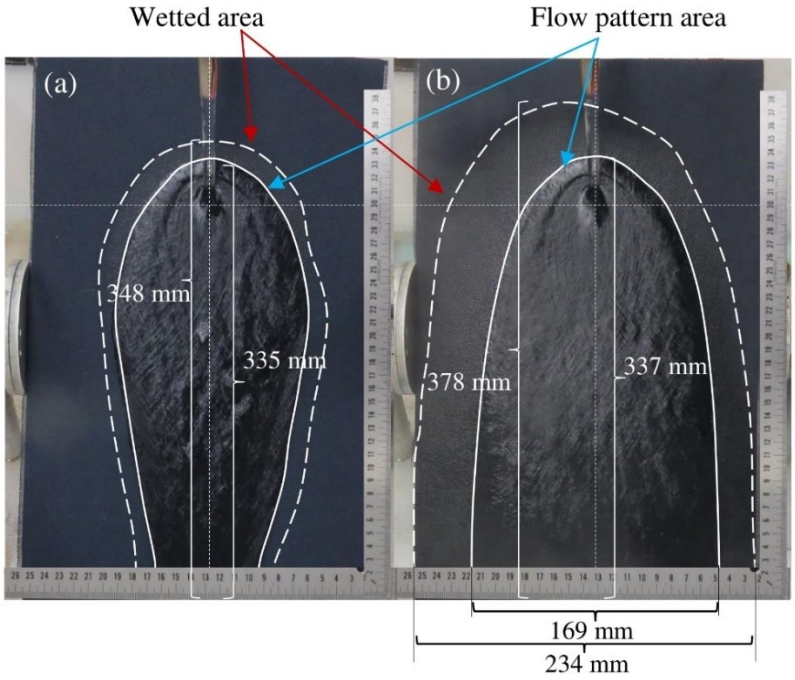

Figures 7.19. Flow pattern of water at (a) 22°C and (b) 90°C on fabric system S-5. The dash boarder lines show the wetted area of fabric system S-5 and the solid lines indicate water flow pattern.

In fabrics with a hydrophobic surface, the flow pattern area (A_{flow}) and the wetted areas (A_{wet}) have relatively close values and the wetted area expands less that 5%. Figure 7.20 shows fabric system S-7, (Nomex®IIIA with a water resistant finish) during the exposure and after the exposure is terminated. The wetted and the areas of the flow pattern were determined as 220 and 212 cm^2 respectively which shows that the wetted area increased by 3.7 %.

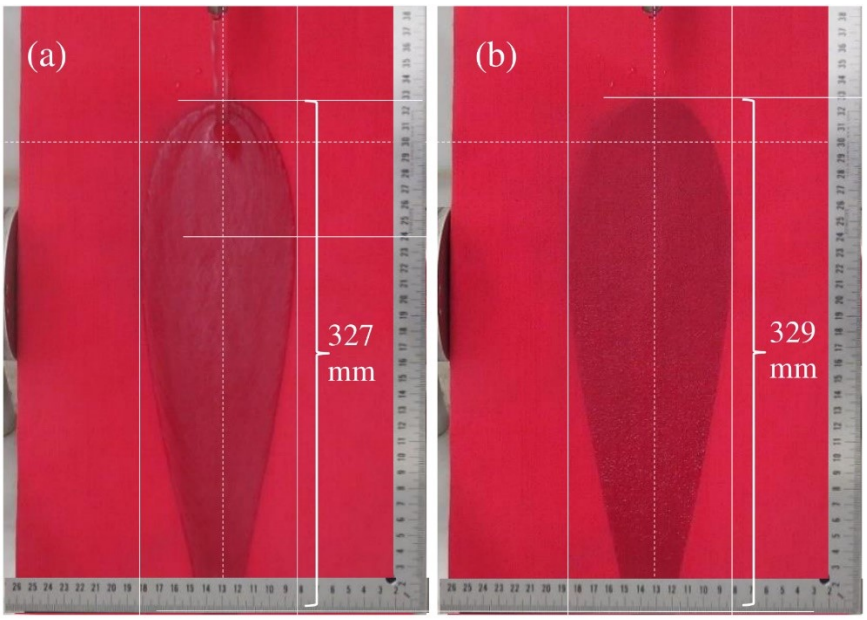

Figures 7.20. Flow pattern of water at 90°C on fabric systems S-7, Nomex®IIIA with water resistant finish (a) during hot water exposure (b) after exposure.

Interestingly, in fabric system S-8 (88% cotton+12% high tenacity nylon with polymer finishing) it was observed that the wetted area was smaller than the flow pattern area (Figures 7.21 (a) and (b)). The fibers in this fabric were treated with a polymer finishing which gives fabric system S-8 an enhanced hydrophobic property. According to Figure 7.21 (a), it was observed that the water had low adhesiveness to the surface of fabric system S-8 and created an unstable flow and many local rims in the supercritical area. The local rims flow back together, collided and created braiding effects. In each braid, the encountered rims rose to a certain height and hit the surface of the fabric and created a reflection. When the rims hit the fabric, they also created unevenness on the surface of the fabric (i.e., extrinsic roughness) in supercritical area, which was introduced in Chapter 7. At the beginning of the exposure, the reflections occurred with no jump on the fabric. As exposure time increased, a large number of reflections occurred. As such, the liquid sheet jumped off the fabric at an angle in a number of locations on the surface of the fabric and created reflections with jumps during exposure. This phenomenon created a wavy liquid flow on the surface of fabric system S-8, which is termed the "cascading effect" in this study (Figure 7.21 (a)).

In the "cascading effect" it was observed that the areas underneath the reflections were not wet ((Figure 7.21 (d) and (e))). The non-wetted areas are shown

with solid lines in Figure 7.21 (b). Figure 7.21 (c) shows an infrared image of fabric system S-8 right after the termination of 90°C water exposure with 80 mL/s flow rate. The infrared image shows the temperature distribution over the wetted surface of the fabric and illustrates the influence of the "cascading effect" on heat transfer from the hot water to the surface of the fabric. According to the infrared image (Figure 7.21 (c)), the areas underneath the jumps had lower surface temperature in comparison to the areas that were contacted by hot water (dotted arrow).

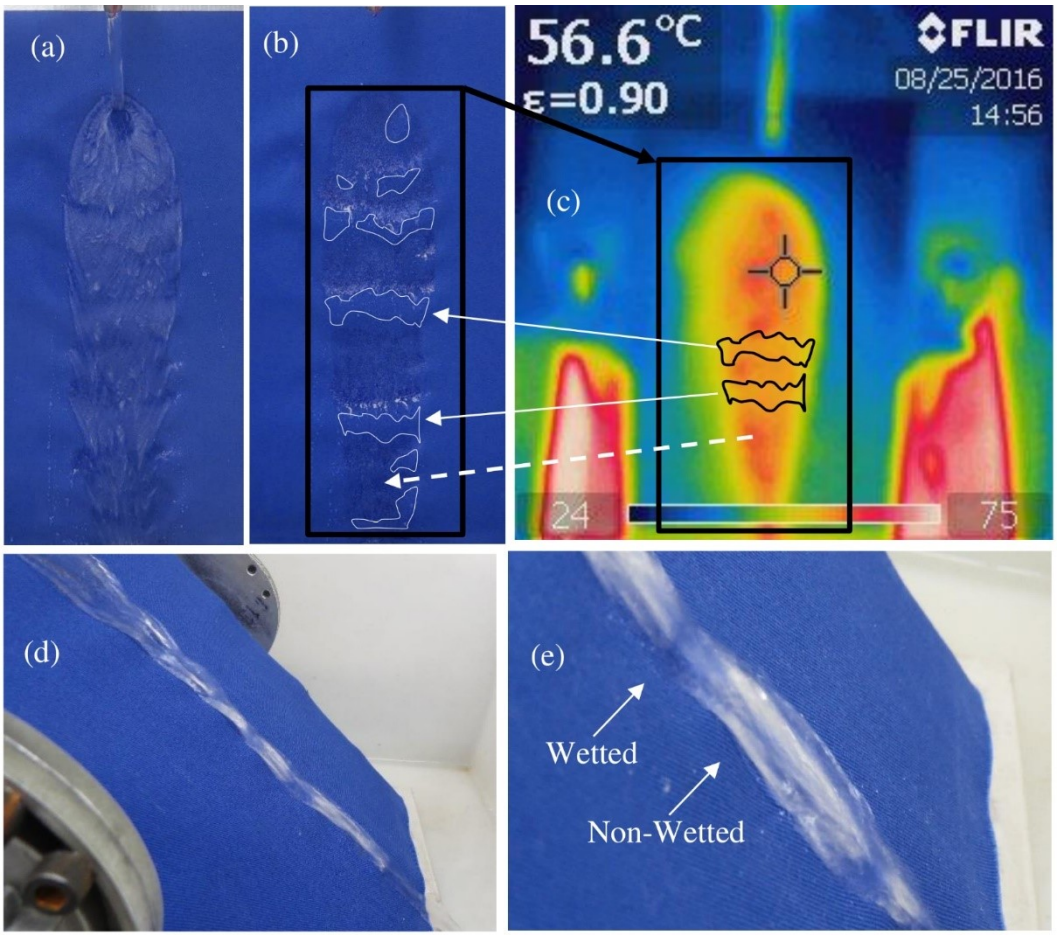

Figures 7.21. (a) Flow pattern and cascading effect of water at 90°C on fabric system S-8 during exposure (b) after hot water exposure. (c) an infrared image of fabric system S-8 after the termination of exposure. (d and e) cascading effect on fabric system S-8, side view.

In conclusion, applying water resistant surface properties to the surface of fabric systems is a crucial factor which is required to be manipulated on thermal protective clothing systems that may be exposed to hot water exposure. A

comparison of the infrared images of fabric systems S-5, S-7 and S-8 confirmed that enhancing the water resistant surface properties of the fabric decreased surface wetting which resulted in lower heat transfer from the hot water to the surface of the fabric. Figure 7.22 (a), (b) and (c) illustrate infrared images of fabric systems S-5, S-7 and S-8 respectively. The images are taken a few seconds after a-60-second exposure of water at 90°C water with an 80 mL/s flow rate on the mentioned fabrics. Hot water covered a larger area of fabric system S-5 while a significantly smaller area of the fabrics with water resistant surface property (S-7 and S-8) was covered with hot water. In addition, the flow of hot water increased the surface temperature of fabric S-5. However, the surface temperature of fabrics with water resistant surface property is lower than S-5. Comparing the range of temperature in fabric systems S-7 and S-8 confirms the effect of the enhanced water resistant surface property with polymer finishing in fabric system S-8. After the termination of exposure, the maximum surface temperature on fabric system S-8 was approximately 55°C which was observed in a few (red) spots (Figure 7.22 (c)). While the maximum surface temperature of fabric system S-7 after the exposure stopped was almost 75°C which covers majority of the areas where hot water flowed.

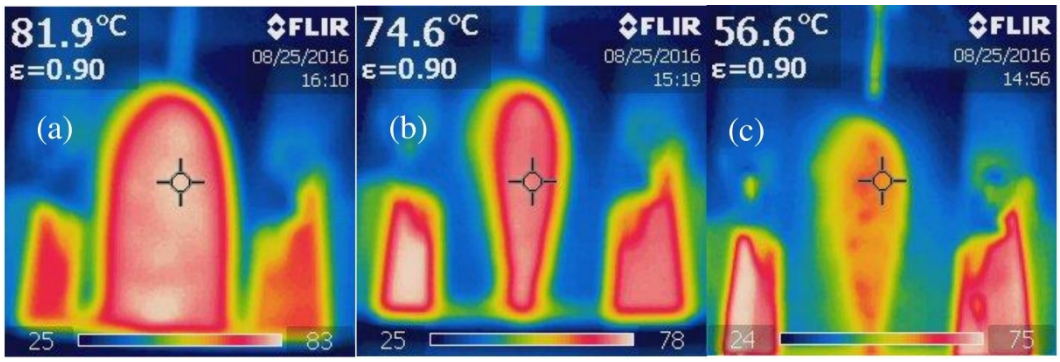

Figures 7.22. Infrared imgaes of fabric systems (a) S-5, (b) S-7 and (c) S-8, after a-60-second exposure of 90°C water with 80 mL/s flow rate.

Surface wetting influences temperature in hot water exposure. An infrared image of the wetted surface after the exposure was terminated showed to be a useful tool in order to identify the boundaries of the wetted areas and the fabric's temperature. The amount of the penetrated liquid as a result of "in-depth penetration" was determined by an impact penetration test which will be descussed later in the chapter.

In depth wetting

A series of experiments was carried out to investigate the effect of the experimental variables and the physical properties of fabrics on the liquid penetration properties of fabric system. The angle of orientation (β), hot water flow rate ($\dot{m}$), temperature of the liquid (T_l) and the dimensionless nozzle-to-sensor board separation (z/d) were adjusted to the desired values according to Table 7.1.

The experiments were performed in two phases. In the first phase, fabric system S-4 (Kevlar®/PBI) was tested during hot water exposures using the test matrix shown in Table 7.1 to investigate the effect of the experimental variables on the liquid penetration properties of the fabric system. In the second phase, all fabric systems listed in Table 3.4 were exposed to the following experimental settings:

- distilled water at 90°C with the flow rate of 80 mL/s and nozzle to fabric separation of 9 nozzle diameters in 45-degree orientation of sensor board (β=45°).
- distilled water at 90°C with the flow rate of 80 mL/s and nozzle-to-fabric separation of 9 nozzle diameters in horizontal orientation of sensor board (β=90°).

According to the preliminary liquid penetration experiments, the two abovementioned settings caused the largest amounts of liquid penetration on the studied fabric systems.

The fabrics were cut to 410 mm by 257 mm to cover the surface of the sensor board. The blotting paper was cut to 400 mm by 250 mm. The blotting paper was cut smaller than the fabric. In this case, hot water was prevented from wicking back underneath the fabric from the sides which could affect the weight of the blotting paper. The weight of the blotting paper was measured and it was mounted on the sensor board. The weight of the fabric was also measured and the fabric was placed on the blotting paper. Hot water was heated to a pre-set temperature. The valve was opened and the fabric was exposed for 60 s. After the exposure was terminated, the weights of the blotter paper and fabric were measured after the test. The difference between the wet and the dry fabric was reported as “stored water in the fabric”. The difference between the wet blotting paper before and after the exposure was reported as “transferred water”. As such, the in-depth water

penetration is divided into two subgroups: the amount of water and water vapour which penetrate through and are transferred to the backside of the fabric (transferred water) and the amount of water and water vapor stored in the fabric (stored water). The "transferred water" and the "stored water" were determined by the average of three test specimens.

The effect of the experimental variables on impact penetration of water

Table 7.13 shows the results of water penetration tests for fabric system S-4 considering different experimental variables.

Table 7.13. The amount of transferred and stored water of fabric system S-4.

Fabric system S-4						
Liquid	β (degrees)	$\dot{m}$ (mL/s)	T_l (°C)	z/d	Transferred water (g) (SD)	Stored Water in fabric (g) (SD)
Distilled water	45	40	60	3	0.2 (0.02)	1.2 (0.30)
				9	0.3 (0.07)	1.4 (0.20)
			90	3	0.8 (0.11)	1.2 (0.22)
				9	1.2 (0.13)	1.5 (0.35)
		80	60	3	0.4 (0.03)	1.8 (0.49)
				9	0.4 (0.09)	2.0 (0.46)
			90	3	2.5 (0.45)	2.4 (0.28)
				9	3.5 (0.74)	2.9 (0.22)
	0	40	60	3	0.8 (0.13)	4.6 (0.94)
				9	0.9 (0.01)	5.0 (0.66)
			90	3	2.3 (0.19)	7.6 (1.28)
				9	3.7 (1.00)	8.0 (0.32)
		80	60	3	1.9 (0.57)	9.4 (0.68)
				9	2.4 (0.85)	10.0 (1.88)
			90	3	6.2 (0.73)	10.0 (1.59)
				9	10.8 (2.26)	10.7 (0.30)

β is the angle of orientation, $\dot{m}$ is the flow rate; T_l is the liquid temperature; z/d is dimension nozzle-to-sensor board separation.

Effect of impingement angle

The range of the amount of transferred water when the angle of orientation is 45° is from 0.2 to 3.5 g, while this range is from 0.8 to 10.8 g of water in horizontal orientation (β=0°). The minimum amount of transferred water in 45-degree orientation of the sensor board is 0.2 g of water when fabric system S-4

is exposed to water at 60°C with a flow rate of 40 mL/s and z/d=3. The amount of transferred water increases almost four times when fabric system S-4 was exposed in the horizontal orientation. The maximum amount of transferred water in the 45-degree orientation of the sensor board was 3.5 g of water when fabric system S-4 was exposed to water at 90°C with a flow rate of 80 mL/s and z/d=9. The amount of transferred water increased approximately three times when fabric system S-4 was exposed when the angle of orientation was 0°. Comparing data for the same values of flow rate, water temperature and nozzle to fabric separation in Table 7.13, it was confirmed that a decrease in the angle of orientation increased the transferred water.

According to Table 7.13, the amount of stored water in fabric system S-4 increased when the angle of orientation decreased from 45° to 0°. A comparison of data for the same values of flow rate, water temperature and nozzle to fabric separation confirmed that a decrease in the angle of orientation increased the amount of stored water in the fabric by 3.8 to 6.2 times. As such, the decrease in the angle of orientation increased the accumulation of hot water within the fabric structure which may contribute to more transmitted and discharged thermal energy to the skin, which will be discussed in the following chapter.

Effect of flow rate

The data shown in Table 7.13 indicates that an increase in hot water flow rate increases the transferred water and stored water in fabric system S-4. For instance, in a 45-degree orientation, fabric system S-4 when was exposed to hot water at 90°C with nozzle-to-plate separation of 9 nozzle diameters, transferred 1.2 g of water for a flow of 40 mL/s and 3.5 g of water for a flow of 80 mL/s flow rate. Once the flow rate of hot water increased from 40 to 80 mL/s, more water (2400 g) was exposed to the fabric in 60 s. On the other hand, an increase in the flow rate caused more pressure at the stagnation region upon the fabric. This phenomenon enhanced water penetration through the permeable structure of fabric system S-4.

In the horizontal orientation, when the flow rate is 80 mL/s, the transferred water increased by 2 to 3 times from when the flow rate was 40 mL/s. In addition, the water in the fabric increased significantly when the flow rate increased from 40 to 80 mL/s. The increase in the transferred water and the stored water in the fabric was mainly due to the increase in the pressure of water jet at the stagnation region.

According to Equation 7.4, the pressure of the water jet at the stagnation point is proportional to water flow rate squared. Once the flow rate is increased by twofold, the pressure increased four times. As such, the increase in the pressure of water flow enhanced water penetration through the permeable structure of fabric system S-4.

Effect of water temperature

The effects of water temperature on the contact angle and the area of flow pattern of the fabric were discussed earlier in this chapter. It was mentioned that an increase in temperature of water decreased the surface tension of water. The decrease in surface tension of water decreased the cohesiveness of the water drop. As such 90°C water can penetrate more easily within the small capillaries of fabric system in comparison to water at 60°C. The data in Table 7.13 confirms that the transferred water and the water in the fabric (stored water) were increased significantly (4 to 5 times) by an increase in water temperature from 60 to 90°C. Therefore, the increase in temperature enhanced in depth water penetration.

Effect of nozzle-to-sensor board separation

According to the data presented in Table 7.13, the change in nozzle-to-fabric separation slightly influenced the impact penetration of hot water. The transferred water was increased 1.2 to 1.7 times when the nozzle-to-fabric separation increased from three to nine nozzle diameters. Stored water in fabric system S-4 did not change significantly (1.1 to 1.2 times) with an increase in the nozzle-to-fabric separation. However, the slight increase in the transferred water can be explained due to the increase in the pressure of the hot water jet in the larger nozzle-to-fabric separation (z/d=9). The pressure of the water jet at the stagnation region was determined and shown in Table 7.4. The pressure of water jet on the fabric increased from 785 to 1353 Pa by increasing z/d, the separation of nozzle-to-fabric, from z/d=3 to z/d=9 nozzle diameters, influenced in depth water penetration.

From the study of the effect of the experimental variables in the hot liquid splash apparatus on water penetration properties of fabric system S-4, it can be inferred that the angle of orientation, flow rate and the temperature of the water significantly affected the transferred water and the stored water in fabric system S-4.

The effect of fabric properties on impact penetration of the liquid

In the second phase of the study, a series of experiments were conducted to investigate the effects of the physical properties of fabrics on liquid penetration in the fabric systems. Three replicates of each fabric system were tested. During the preliminary testing, it was confirmed that when the flow rate is at 80 mL/s, the temperature of hot water is at 90°C and the nozzle-to-fabric separation is nine diameters of the nozzle (z/d=9), the largest amounts of water were transferred and stored in the fabric systems in the horizontal and 45-degree orientations.

Table 7.14 depicts the results of the water penetration test on single layer, double layer and multilayer fabric systems shown in Table 3.4. Table 7.14 also demonstrates the amount of water which remained on the surface of the fabric in the horizontal test (β=0°) after the exposure. The amount of water on the fabric was measured by weighing the pooled water which accumulated on the surface of the fabric after exposure.

Table 7.14. Water penetration test on the fabric system exposed to hot water at 90°C with the flow rate of 80 mL/s and z/d=9.

Fabric system	β=0°			β=45°	
	Transferred water (g) (SD)	Stored Water (g) (SD)	Water on fabric (g) (SD)	Transferred water (g) (SD)	Stored Water (g) (SD)
S-1	0.8 (1.0)	5.3 (0.4)	66.9 (5.8)	0.5 (0.1)	1.7 (0.2)
S-2	1.1 (0.2)	10.6 (0.6)	107.8 (7.9)	1.0 (0.1)	2.5 (0.2)
S-3	1.9 (0.1)	4.1 (1.3)	70.2 (10.6)	1.3 (1.9)	1.3 (1.2)
S-4	10.8 (7.3)	10.7 (2.3)	53.1 (8.9)	6.5 (0.7)	2.2 (0.2)
S-5	208.2 (15.4)	39.5 (1.1)	0.0 (0.0)	98.6 (10.0)	31.1 (0.7)
S-6	60.1 (3.9)	4.8 (1.1)	62.6 (8.9)	38.3 (1.9)	3.0 (0.2)
S-7	7.5 (9.9)	10.0 (5.1)	34.8 (10.2)	5.2 (2.7)	5.5 (0.1)
S-8	2.0 (0.1)	2.0 (0.8)	68.9 (2.8)	1.1 (0.1)	1.4 (0.1)
S-9	0.2 (0.5)	2.1 (0.4)	46.0 (13.3)	0.1 (0.0)	1.4 (0.2)
D-1	18.3 (4.3)	4.3 (0.6)	41.6 (4.2)	4.2 (0.5)	2.7 (0.2)
D-2	16.7 (2.5)	5.9 (3.5)	43.3 (0.5)	3.7 (1.8)	2.3 (0.6)
D-3	14.4 (3.3)	7.2 (1.9)	33.1 (3.6)	3.1 (0.1)	3.8 (0.4)
D-4	9.8 (2.9)	8.0 (1.9)	20.6 (4.8)	2.2 (0.2)	6.6 (4.4)
D-5	1.1 (0.2)	13.9 (1.3)	57.7 (1.2)	0.3 (0.1)	4.7 (0.2)
D-6	0.8 (0.6)	7.4 (1.0)	61.3 (4.8)	0.2 (0.1)	2.3 (0.1)
M-1	0.7 (0.1)	7.5 (0.3)	22.9 (1.0)	0.3 (0.0)	1.2 (0.1)
M-2	0.5 (0.2)	8.0 (0.7)	49.7 (1.3)	0.5 (0.1)	3.4 (1.0)
M-3	0.6 (0.0)	9.1 (0.5)	24.4 (3.3)	0.5 (0.1)	3.0 (0.3)
M-4	0.8 (0.0)	4.4 (0.2)	33.7 (1.0)	0.1 (0.1)	2.0 (0.1)
M-5	0.6 (0.0)	21.4 (6.7)	54.1 (3.3)	0.5 (0.0)	6.4 (0.1)
M-6	0.6 (0.3)	10.6 (0.3)	51.7 (2.6)	0.2 (0.0)	3.5 (0.1)

β is the angle of orientation.

The amounts of the water on the surface of the fabric after the termination of hot water exposure in the horizontal orientation test (β=0°) showed that a considerable amount of hot water stayed on top of the fabrics with water resistant finish. The accumulated hot water on the fabric has the potential to enhance hot water penetration. The range of water on the fabric systems with water resistant surface finish was from 20 to 107 g of water. This amount of hot water on the fabrics can be a potential thermal hazard. The hydrophobic surface of fabric systems S-1, S-2 and S-3 (moisture barriers A, B and C) as well as fabric systems S-6 and S-8 seems to hold more hot water on the fabric after the termination of exposure in comparison to the other single layer fabric systems.

The fabric with the largest amounts of transferred and stored water was the unfinished fabric system S-5. For the water penetration test on this fabric, four sheets of blotting paper were used because the amount of transferred water for fabric system S-5 was very large.

Single layer fabric systems

By comparing the results of the water penetration test and the water diffusion test for single layer fabric systems, it can be inferred that the transferred water increases as diffusion resistance of the single layer fabric decreases. Employing StatCrunch® software, the result from the correlation coefficient between the transferred water and the diffusion resistance shows that they are negatively correlated with a correlation coefficient of -0.27. For single layer fabric systems S-1, S-2, S-3, S-8 and S-9, no water transfer was observed. There was no sign of water absorption by the blotting paper after the exposure of these fabrics to hot water. However, the weight of the paper was slightly more after the exposure showing that water vapor was passed through the structure of these fabrics. The laminations underneath the structure of moisture barriers A (S-1), B (S-2) and C (S-3) as well as Neoprene coating on the surface of the FR rainwear (S-9) provides excellent water penetration resistant properties to these fabric systems.

Among single layer fabric systems that are typically used as a shell fabric in thermal protective clothing (S-4, S-6, S-7 and S-8), fabric system S-8 transferred no water through its structure and passed less than 2 g of water vapor according to Table 7.14. Employing polymer finishing on the fiber content of this fabric (encapsulated fibers) provided superior water penetration resistant properties to fabric system S-8.

Fabric system S-6 (Nomex® IIIA with water resistant finish) passed a large amount of water through its structure. Although this fabric has a hydrophobic surface property, it was observed that the permeable structure of this fabric (air permeability of 33.8 (cm^3 cm^{-2} s^{-1}), Table 3.6) cannot resist water penetration. This phenomenon was also observed in single layer fabrics S-7 (Nomex® IIIA with water resistant surface property) and S-4 (Kevalr®/PBI with water resistant surface property). Therefore, it can be concluded that in spite of good water resistant surface properties, fabric system S-4, S-6 and S-7 provide poor resistance to water penetration.

Among moisture barriers, fabric system S-1 (moisture barrier A, made from Nomex®IIIA with water resistant surface property and underlying expanded polytetrafluoroethylene coating) transferred the least amount of water vapor through its structure. The resistance to water vapor can also be an important property because this fabric can be used in thermal protective clothing that may be exposed to high pressurized water or steam. In this study, the maximum pressure of water at the stagnation point on the surface of the fabric was approximately 1.38 kPa (Table 7.4). On the other hand, the fabrics' physical properties, such as air permeability and water vapor diffusion, were tested under pressures less than approximately 150 Pa (ASTM, 2012a; CGSB, 1999), However, in actual application and during firefighting and industrial operations, workers may be exposed to hot liquid and steam at high pressure (typically 100~4000 kPa) and temperature (100~300^{o}C) (Ackerman et al., 2011). As such, caution needs to be exercised in applying the results of the water penetration, air permeability and water vapor diffusion tests for the evaluation of thermal protective clothing that may be exposed to water and steam at higher pressures.

Double layer fabric system

Double layer fabric systems D-1, D-3 and D-4 consist of shell fabric A, Kevlar®/PBI with underlying thermal liners A, C and D. Thermal liners A, C and D have the same fibrous structure. The combination of shell fabric A with these thermal liners provide three permeable fabric systems with the same fiber contents and fabric structure, but different fabric densities. The densities of fabric systems D-1, D-3 and D-4 are 0.295, 0.197 and 0.176 (g m^{-3}). The decrease in density means more air space within the fabric system. The stored water in the structure of fabric systems D-1, D-3 and D-4 shown in Table 7.14 confirms that there was more stored water within the structure of the fabric systems with more air spaces. Therefore, it is concluded that in permeable fabric systems, the fabric with more air spaces can store more hot water. The stored hot water may increase the discharge of thermal energy to the skin and lower the thermal performance of the fabric.

The change in the structure of the thermal liner affected the liquid penetration properties. Thermal liner B and C have almost the same mass (256 g/m^2). The two thin nonwoven batts of thermal liner B provide a thinner fabric structure (1.3 mm) than thermal liner C (2.0 mm), which has a bulkier structure. As such, thermal liner is able to store more water within its structure.

Fabric systems D-5 and D-6 are switched layer fabric systems with the same fiber content, density, mass, thickness and air permeability, but different configurations. In fabric system D-6, the shell fabric A is switched with its underlying moisture barrier A. Although the configuration of fabric system D-6 is not practical, it helps to understand the effect of the position of the moisture barrier on the transferred and stored hot water in the fabric. According to Table 7.14. it is understood that the amount of transferred water did not change significantly in fabric systems D-5 and D-6. However, the amount of stored water almost doubled when moisture barrier A was positioned underneath shell fabric A (S-5). In fabric system D-6, the moisture barrier was in direct contact with the impinging hot water, so that the accumulation of hot water in the underlying shell fabric was eliminated. On the other hand, in fabric system D-5, hot water penetrated through the permeable structure of shell fabric A and was blocked by the underlying moisture barrier. Therefore, more hot water was stored through the structure of fabric system D-5 in comparison to fabric system D-6.

Multilayer Fabric system

Multilayer fabric systems M-1, M-3 and M-6 consist of shell fabric A, Kevlar®/PBI, and moisture barrier A with thermal liners A, C and D respectively. The construction of these fabrics was indicated in Tables 3.3 and 3.4. Thermal liners A, C and D have the same fibrous structure. The combination of shell fabric A and moisture barrier A with these thermal liners provided three impermeable fabric systems with the same fiber content and fabric structure, but different densities. The densities of fabric systems M-1, M-3 and M-6 are 0.34, 0.24 and 0.21 (g/m^3). Among fabric systems M-1, M-3 and M-6, the fabric with less density had less fibrous material and more air space in a given volume of the fabric system. In the impact penetration test, hot water penetrates through shell fabric A in fabric system M-1, M-3 and M-6. Then, hot water penetration was blocked by the moisture barrier A mounted underneath shell fabric A. As such, hot water did not penetrate into the air spaces in the thermal liners of fabric systems M-1, M-3 and M-6 and the change in the density of these impermeable fabric did not affect transferred water. However, water vapor was condensed in the air spaces of their thermal liners and the amount of water vapor caught by blotting paper is negligible. The values of the stored and transferred water in fabric systems M-1, M-3 and M-6 confirm that there was no significant difference between the transferred water and stored water in fabric systems M-1, M-3 and M-6 (Table 7.14).

In order to investigate the effect of the position of moisture barrier on the impact penetration test in multilayer fabric systems, fabric system M-3 (fabric A+ moisture Barrier A+ thermal Liner C), M-4 (Moisture Barrier A+ Fabric A+ Thermal Liner C) and M-5 (Fabric A+ Thermal Liner C+ Moisture Barrier A) were compared. According to Table 7.14, the amount of transferred water did not change in these impermeable fabrics. Although it is not a practical setting, when the moisture barrier is positioned in the innermost layer (M-5), the amount of stored hot water in the fabric system increased by almost two times in comparison to M-3 and more than three times in comparison to M-4. Therefore, it is concluded that minimizing hot water transfer within the fabric structure in the outer layers decreased hot water accumulation within the fabric structure and enhanced water penetration resistance of the fabric system. Enhancing water penetration resistance of a multilayer fabric system by resisting mass transfer in the outermost fabrics enhanced its thermal performance when exposed to hot water splash which will be discussed in Chapter 8.

Summary

Analyses of the infrared images of circular and non-circular hydraulic jump confirmed that the temperature of water in the supercritical region is higher than in the subcritical region downstream of the flow. It is also confirmed that the area of the supercritical region on the fabric depends on experimental variables and physical properties of the fabric. Therefore, the understanding of the hydrodynamics of the hot liquid flow on the surface of fabrics provides a useful tool in understanding of local heat transfer caused by liquid jet on the surface of fabric.

It is understood that applying efficient water resistant surface finishing and water penetration resistant finishing are crucial factors that should be manipulated in outer layer fabric systems in order to increase protection against hot liquids. It was also realized that the transferred water and diffusion resistance of the single layer fabric are negatively correlated and diffusion resistance of the single layer fabric can be used as approximate estimation of how well the single layer fabric system exposed to hot water is able to resist hot water transfer. In addition, it was understood that the contact angle and the wetting time in the microscopic scale can provide an approximate estimation of the shape of the flow pattern on the surface of the fabric.

CHAPTER 8 EVALUATION OF THE THERMAL PERFORMANCE OF PROTECTIVE FABRIC SYSTEMS EXPOSED TO HOT WATER JET BY TAKING INTO ACCOUNT THE TRANSMITTED AND THERMAL STORED ENERGY DEVELOPED IN THE FABRIC SYSTEM DURING THE EXPOSURE AND COOLING PERIOD OF THE FABRICS[5]

Introduction

In Chapter 3, the thermal performance of fabric systems exposed to hot water, drilling fluid and canola oil was evaluated. The evaluation of the fabric systems was based on the transmitted and the discharged thermal energy received by three sensors in the horizontal and 45-angle orientations. These three sensors were able to measure the transmitted and the discharged energy at the stagnation point as well as the energies at 10 and 20 nozzle diameters from the stagnation point in the 45-degree orientation (β=45°) and 10 nozzle diameters from the stagnation point in the horizontal orientation (β=0°). However, when the water jet hits the surface of the fabric, it spreads on the fabric. In Chapter 7, it was observed that depending on the experimental settings and the physical properties of the fabrics, the size of the "spread area" of hot water may differ. In this chapter, it is intended to investigate the influence of the flow pattern of hot water and liquid transfer properties (water surface resistance and water penetration resistance) of the fabrics on the transmitted and discharged thermal energy received by the skin simulant. The skin simulant board used for the study in this chapter was described in Chapter 3.

Experimental procedure

Nude test

The experimental settings and variables (shown in Chapter 7, Table 7.1) considered were angle of orientation, water temperature, water flow rate, nozzle to skin simulant plate separation as the experimental variables. A total number of 48 experiments were performed for nude tests. Therefore, the orientation of the skin simulant plate (β), hot water flow rate ($\dot{m}$), temperature of the liquid (T_l) and dimensionless nozzle-to-sensor board separation (z/d) were adjusted at the desired settings according to Table 7.1 (Chapter 7, page 171). Hot water was heated to pre-

[5] This chapter is an original work by the author. No part of this chapter has been previously published nor presented at conferences.

set temperature. The data acquisition system was run before the exposure started. The valve was opened and the skin simulant plate were exposed for a fixed duration (30 s). After the exposure was terminated, the data acquisition system continued recording the data during cooling period of the system for 60 s. The measured heat flux and absorbed energy as a function of time for each sensor were obtained. The second and third degree burn time were also determined for each sensor employing the burn evaluation criteria.

Fabric system-skin simulant test

The abovementioned procedures were repeated in the presence of the fabric systems presented in Chapter 3 (Table 3.3 and Table 3.4). The fabric systems were conditioned at 20±2°C with 65% relative humidity for at least 24 hours prior to the testing. The fabric systems were exposed to hot water for a fixed duration of time (60 s). Once the exposure was terminated, data acquisition systems continued recording the discharged energy in the system until the fabric was cooled (60 s). The measured heat flux, temperature and absorbed energy as a function of time for each sensor were obtained. The second and third degree burn time were also determined for each sensor.

Results and discussion

Table 8.1 depicts the thermal performance predictive parameters used in this study. The predictive parameter in Table 8.1 are the summary of the parameters which were introduced in the previous chapters.

Table 8.1. Thermal predictive parameters.

Parameter	Symbol	Definition
Second degree burn time	t_{2nd}	Predicted time required for a complete destruction of the epidermis during and after the termination of thermal energy to the skin; s.
The predicted area of second degree burn	A_{2nd}	the sum of the weighted area corresponds to the heat flux sensors that predicts a second-degree burn.
Third degree burn time	t_{3rd}	the time corresponds to when the thermal energy exceeds the threshold (supra-threshold) and thermal tolerance of epidermis; s.
The predicted area of third degree burn	A_{3rd}	the sum of the weighted area corresponds to the heat flux sensors that predicts a third-degree burn.
Local absorbed energy throughout test	q_{total}	total thermal energy absorbed by each sensor during the exposure and post-exposure; (kJ/m^2).
Total absorbed energy throughout test	TAE	total energy received by all sensors as the average of the weighted total energy transferred to each heat flux sensor over the data sampling period; (kJ/m^2).
Local energy absorbed at onset of second degree burn	q_{2nd}	energy absorbed by each sensor at the time at which second degree burn time is predicted to occur; (kJ/m^2).
Total energy absorbed at onset of second degree burn	TAE_{2nd}	TAE_{2nd} is the total energy received by all heat flux sensors at the time at which second degree burn time is predicted to occur; (kJ/m^2).
Local discharged energy	$q_{cooling}$	energy absorbed by each sensor during cooling period; (kJ/m^2).
Total discharged energy	TDE	the total energy received by all heat flux sensors during cooling period; (kJ/m^2).
Local stored energy coefficient transmitted	ψ	the discharged energy's contribution to total absorbed energy.
Total stored energy coefficient	SEC	the total discharged energy's contribution to total absorbed energy by all heat flux sensors.
Local stored energy rating	---	the energy received by each sensor during cooling period considering the proportion of the discharge energy to the total absorbed energy for the sensor.
Total stored energy rating	$STE\ Rating$	the total energy received by all sensors during cooling period considering the proportion of the discharge energy to the total absorbed energy for the sensor.

An average of a minimum of three tests for each experimental setting for nude and fabric tests was obtained for each of the abovementioned predictive parameters. The coordinates of the skin simulant board in 45-degree and horizontal orientation were shown in Figures 3.4 (a) and (b), respectively. Tables 3.9 and 3.10 also present the location of the thermocouples relative to the stagnation point in the inclined and horizontal orientation of the skin simulant plate, respectively.

Evaluation of thermal performance skin simulant plate alone (nude) in the horizontal orientation exposed to hot water

Figures 8.1 (a) and (b) show the variation of local absorbed energy along the x-axis and y-axis in the horizontal orientation at different flow rate, and z/d respectively. A spline was used to fit the data employing SigmaPlot Version 11.0. The polynomial curves can be fitted up to the 10^{th} order. In the horizontal orientation, mirror images are assumed for the data on the y-axis (y/d). In Figure 8.1 (b), the data for the positive y-axis were mirrored in order to obtain a better illustration of absorbed energy along the width of the skin simulant plate. The plots illustrate the variation of absorbed energy during 30 s of hot water exposure at 90°C, at flow rates of 40 and 80 mL/s and nozzle-to-plate separations of 3 (z/d=3) and 9 (z/d=9) nozzle diameters. According to the figures, it is confirmed that the absorbed energy is a function of position from stagnation point in x (x/d) and y (y/d) direction.

It is evident from the figures that absorbed energy is larger at adjacent locations to the stagnation point. The absorbed energy curve plateaus at a certain distance from the stagnation point and decays as x/d and y/d increase. By analysis of the location of the heat flux sensors and the flow of hot liquid, it is inferred that the relatively flat curve belongs to the absorbed energy received by the sensors in the supercritical region. It is also interesting that the decrease in the absorbed energy occurs at the onset of the hydraulic jump in the horizontal orientation of sensor board. In the supercritical region, the amount of absorbed energy increased when the flow rate was increased from 40 to 80 mL/s. In addition, the absorbed energy curves reach a given level and then stay the same in the higher flow rate. This confirms that as the flow rate increases, the radius of the supercritical region increases and hydraulic jump forms at a larger distance from the stagnation point. As such, the heat flux sensor receives more thermal energy during 30 s of exposure as the flow rate and the hydraulic jump radius increases.

A similar phenomenon was observed when the temperature of water was at 60°C. Figures 8.2 (a) and (b) illustrate the variation in absorbed energy during 30 s of hot water exposure at 60°C, at flow rates of 40 and 80 mL/s and nozzle-to-plate separations of 3 (z/d=3) and 9 (z/d=9) nozzle diameters. It is expected that that the absorbed energy is considerably lower when the water jet temperature decreases by 30°C. It is also observed that the absorbed energy is a function of position from the stagnation point in x (x/d) and y (y/d) directions. However, the absorbed energy curves show that the maximum values of absorbed energy do not vary significantly as the flow rate doubled.

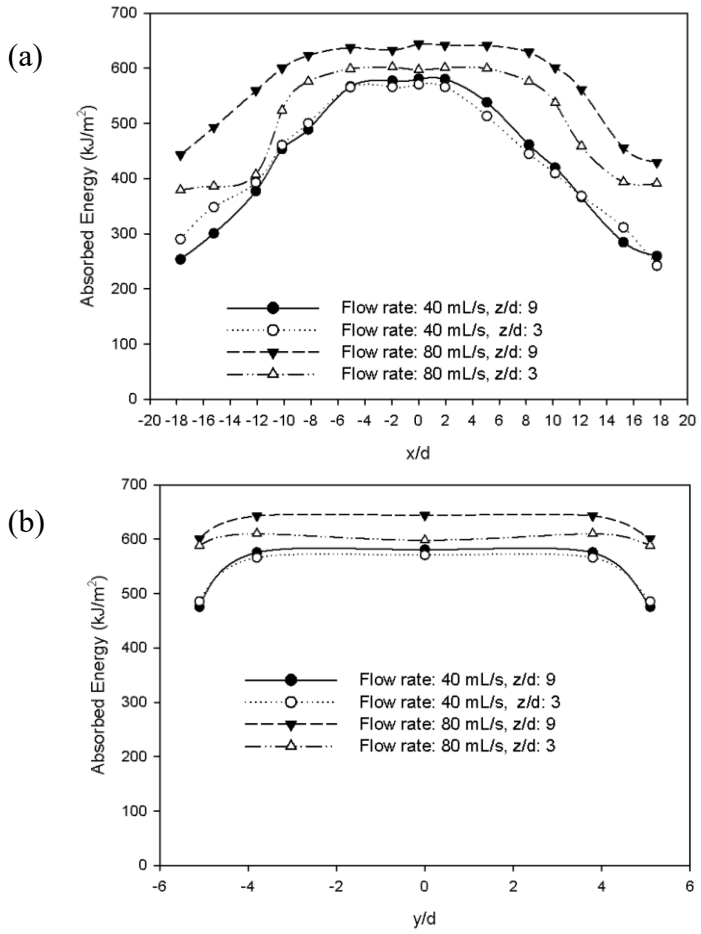

Figure 8.1. Absorbed thermal energy distribution along: (a) x-axis and (b) y-axis for different flow rates and nozzle to skin simulant separations (z/d) in horizontal orientation for 90°C water jet.

(a)

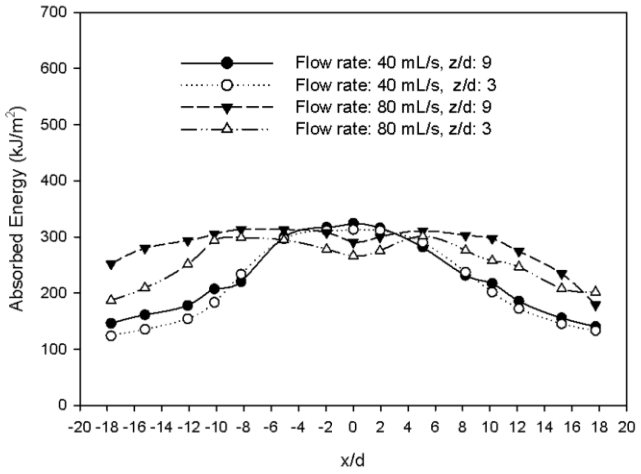

(b)

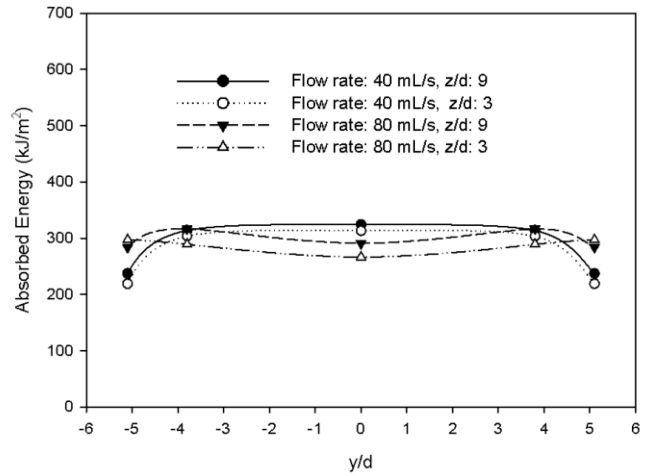

Figure 8.2. Absorbed thermal energy distribution along: (a) x-axis and (b) y-axis for different flow rates and nozzle to skin simulant separations (z/d) in horizontal orientation for 60°C water jet.

It is interesting that the maximum absorbed energy occurs off the stagnation point for high flow rates. This phenomenon may happen due to transition from an accelerating stagnation region flow to decelerating wall jet region (Gardon & Akfirat, 1965). This causes an increase in the heat transfer and absorbed energy in the areas in close proximity to the stagnation region when the liquid jet momentum increases due to an increase in the flow rate. The change in the momentum of the liquid jet due to a change in the nozzle-to-plate spacing does not seem to affect the occurrence of the absorbed energy maxima off the stagnation region. However, nozzle-to-plate spacing may cause an increase in the heat transfer off the stagnation point at higher nozzle-to-plate separation (z/d>9) which needs further

investigations. It can be inferred that depending on the flow rate, the areas in close proximity to the stagnation region may receive a relatively higher amount of thermal energy than the stagnation region. As such, it is crucial to equip the bench-scale apparatus with some heat flux sensors in close proximity to the stagnation area in order to have more realistic data for evaluation of thermal performance of protective clothing exposed to hot water.

In order to show the effect of the position of the hydraulic jump (hydraulic jump radius) and the absorbed energy by the skin simulant plate during exposure, a comparison between the area of the supercritical region area and the amount of absorbed energy by the heat flux sensors within the supercritical area during exposure was made. The areas of the supercritical region for horizontal orientation of the nude sensor board were obtained and shown in Table 7.6. Given the area of the skin simulant board (40.4cm×25.3cm=1022.1cm^2), the ratio of the supercritical region area to the skin simulant area ($\frac{A_{sup}}{A_{total}}$) is obtained and shown in Table 8.2. On the other hand, the ratio of the amount of absorbed energy by the heat flux sensors within the supercritical area during exposure to the absorbed energy by all heat flux sensors during exposure ($\frac{E_{sup}}{E_{total}}$) is also calculated for each experimental setting (Table 8.2).

Considering the range of the ratio of the areas ($\frac{A_{sup}}{A_{total}}$ = 0.06 to 0.26), it can be inferred that a considerable amount of thermal energy ($\frac{E_{sup}}{E_{total}}$= 0.32 to 0.96) is absorbed within the supercritical region. At 40 mL/s flow rate, less than 9% of the total area of the skin simulant plate is covered by the supercritical region, while more than 32% of the thermal energy absorbed by the skin simulant plater is received by the heat flux sensors in the supercritical area. As the area of the supercritical region increases, the radius of the hydraulic jump increases which means the hydraulic jump occurs at a larger distance from the stagnation point (Figure 8.3 (a) to (d)). The occurrence of the hydraulic jump causes a considerable decrease in heat transfer to the skin simulant plate at the onset of the jump. Heat transfer decays as the displacement from the stagnation point increases downstream of the jump in the subcritical area. Nozzle-to-plate spacing has a minor effect on the absorbed energy within the supercritical area for the 40 mL/s flow rate. However, the effect of nozzle-to-plate spacing has a large effect when the flow rate is increased to 80 mL/s.

Table 8.2. The ratio of $\frac{A_{sup}}{A_{total}}$ and $\frac{E_{sup}}{E_{total}}$ in different experimental setting.

Angle of orientation, β (degrees)	Flow rate, $\dot{m}$ (mL/s)	Liquid temperature, T_l (°C)	Dimensionless nozzle-to-sensor board separation (z/d)	$\frac{A_{sup}}{A_{total}}$	$\frac{E_{sup}}{E_{total}}$
0	40	60	3	0.06	0.40
			9	0.06	0.38
		90	3	0.06	0.32
			9	0.09	0.33
	80	60	3	0.22	0.69
			9	0.26	0.93
		90	3	0.21	0.45
			9	0.22	0.50

Contour plots of absorbed thermal energy during 30 s exposures of the skin simulant plate to hot water at 90°C also illustrate the effect of water flow rate and the nozzle-to-plate spacing on the absorbed thermal energy. Comparisons of Figures 8.3 (a) and (c), as well as Figure 8.3 (b) and (d), confirm that the increase in the flow rate caused a larger supercritical zone area to be exposed to hot water and more thermal energy to be received by the heat flux sensors. They also illustrate that the skin simulant plate absorbed more thermal energy downstream of the flow when the 90°C water flow rate is set at 80 ml/s.

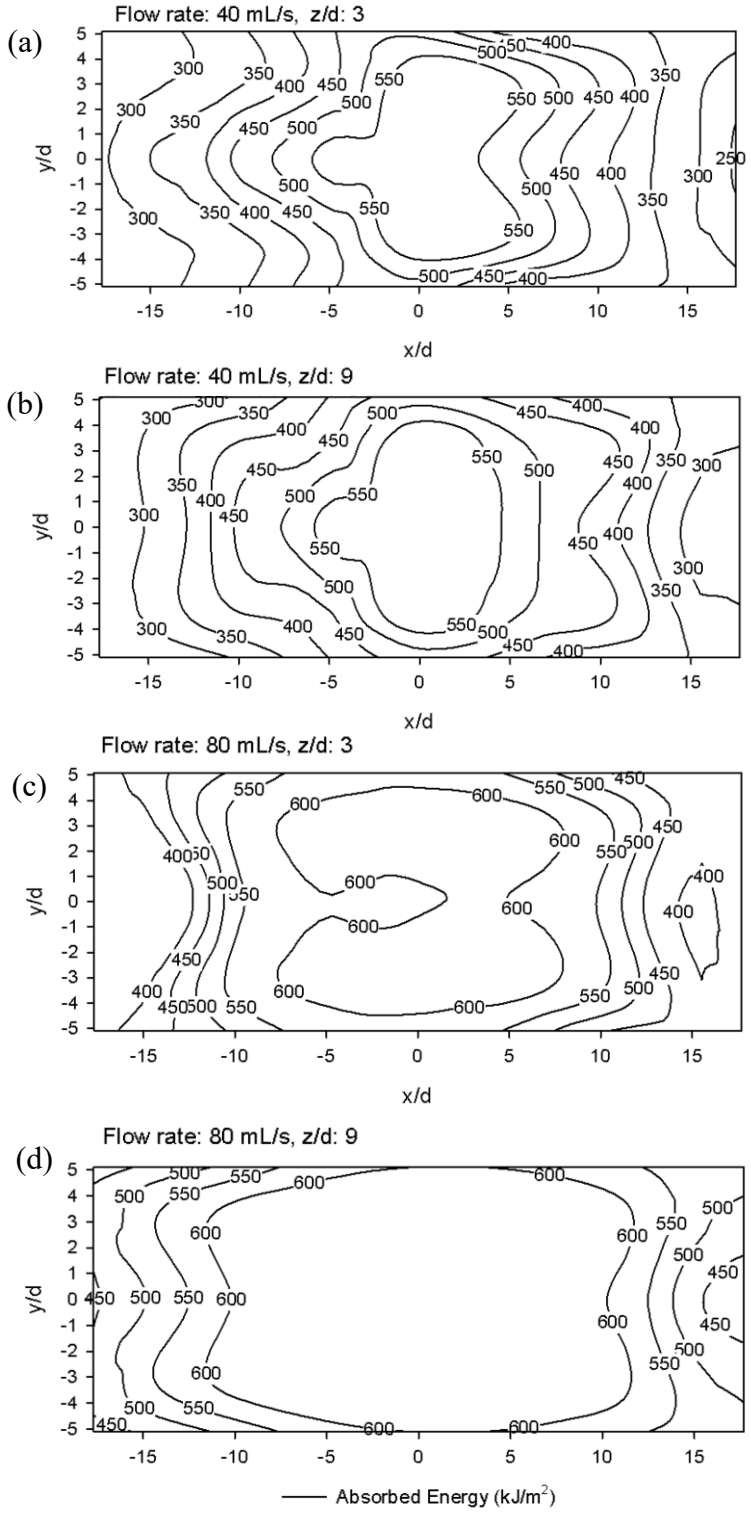

Figure 8.3. Absorbed thermal energy contour plots during 30 s exposure of skin simulant plate to hot water at 90°C: (a) flow rate: 40 mL/s, z/d=3; (b) flow rate: 40 mL/s, z/d=9; (c) flow rate: 80 mL/s, z/d=3 and (d) flow rate: 80 mL/s, z/d=9.

Comparison of the contour plots in Figure 8.3 (c) and (d) shows that nozzle-to-plate separation had an effect on the absorbed thermal energy both upstream and downstream when the flow rate is 80 mL/s. This is due to an increase in the pressure at the stagnation point and the inertial forces in supercritical regions as nozzle-to-plate spacing increases. However, when the flow rate was at 40 mL/s, the effect of nozzle-to-plate spacing was minimal. Total absorbed energy during the entire test presented in Table 8.3 also shows that the increase in the nozzle-to-plate separation increased the total absorbed energy during the exposure and the cooling period by 5 to 14%.

Table 8.3. Thermal performance of the skin simulant exposed to hot water at 45-degree orientation with different liquid temperature, liquid flow rate and z/d.

β (degrees)	$\dot{m}$ (mL/s)	T_l (°C)	(z/d)	2nd degree burn (%) (SD)	3rd degree burn (%) (SD)	TAE (kJ/m^2) (SD)	TDE (kJ/m^2) (SD)
0	40	60	3	100.0 (0.0)	77.6 (17.3)	300.6 (93.5)	93.5 (17.5)
			9	100.0 (0.0)	96.3 (4.3)	338.1 (17.5)	115.2 (8.1)
		90	3	100.0 (0.0)	100.0 (0.0)	541.5 (12.1)	141.5 (5.1)
			9	100.0 (0.0)	100.0 (0.0)	566.8 (5.5)	163.2 (14.3)
	80	60	3	100.0 (0.0)	100.0 (0.0)	325.4 (29.7)	68.3 (11.4)
			9	100.0 (0.0)	99.6 (0.7)	371.6 (8.6)	91.7 (5.3)
		90	3	100.0 (0.0)	100.0 (0.0)	566.2 (19.8)	22.3 (3.1)
			9	100.0 (0.0)	100.0 (0.0)	634.5 (9.3)	31.2 (3.2)

TAE is the total energy received by all sensors throughout the test; TDE is the total energy received by all heat flux sensors during cooling period respectively.

There is a large amount of thermal energy (93.5 to 163.2 kJ/m^2) which is discharged to the skin simulant plate during the cooling period. It was observed that a considerable amount of hot water (a minimum 50 g) stays on the skin simulant plate after the exposure is terminated. The hot sheet of water delivers thermal

energy to the skin simulant during exposure. It is interesting to see that the amount of discharged energy is significantly higher when the flow rate is 40 mL/s. For instance, the discharged energy was 163.2 kJ/m^2 under 40 mL/s flow rate of water at 90°C and z/d of 9, while the discharge energy was 31.20 kJ/m^2 when the flow rate increased to 80 mL/s.

Evaluation of thermal performance of skin simulant plate (nude) in 45-degree orientation exposed to hot water

Sixty eight to eighty seven percent of the skin simulant areas predicted second degree burn (Table 8.4) during 30 s of exposure. This is due to the fact that the flow of hot liquid on the skin simulant plate resembles a bell-shaped open rim flow similar to the shape of the flow of the liquid on a hydrophilic surface (Figure 7.17 (b)). Figure 8.4 illustrates the contour plots for the skin simulant plate in the 45-degree orientation exposed to 90°C water jet at different flow rates and nozzle-to-plate separations. The intersection of the dashed lines indicates the stagnation point on each figure. It is observed that the areas that are located on the y-axis opposite to the main stream of the flow received a large amount of thermal energy between the stagnation point and y/d=+2. When hot water hit the stagnation region, it spread radially in all directions. The liquid film also spread in the opposite direction to the main flow. The flow in this direction is opposite to the component of the acceleration due to gravity in the direction of the accelerating flow ($mg\cos\beta$). The thin liquid film expands upward, decelerates and gains potential energy until the surface tension forces and the gravitational forces overcome the inertial forces and create a rim beyond y/d=+2. This phenomenon occurs for the water that expanded in the opposite direction to the main flow above the x^--x^+ axes shown in Figure 8.4.

Table 8.4. Thermal performance of the skin simulant exposed to hot water at 45-degree orientation with varying water temperature, liquid flow rate and z/d.

β (degrees)	$\dot{m}$ (mL/s)	T_l (°C)	z/d	2nd degree burn (%) (SD)	3rd degree burn (%) (SD)	TAE (kJ/m^2) (SD)	TDE (kJ/m^2) (SD)
45	40	60	3	68.4 (0.0)	67.5 (1.0)	210.0 (8.8)	5.5 (3.0)
			9	74.3 (0.0)	74.3 (0.0)	229.6 (7.5)	4.5 (1.1)
		90	3	80.1 (0.0)	74.3 (0.0)	409.5 (30.4)	6.7 (1.8)
			9	80.1 (0.0)	80.1 (0.0)	410.8 (9.0)	8.5 (2.4)
	80	60	3	80.1 (0.0)	74.3 (1.3)	244.9 (14.2)	3.5 (1.3)
			9	80.1 (0.0)	80.1 (0.0)	258.5 (3.5)	4.5 (1.5)
		90	3	86.0 (0.0)	80.1 (0.0)	467.7 (6.1)	6.7 (1.5)
			9	87.3 (0.0)	83.0 (3.8)	490.2 (23.9)	8.4 (1.1)

TAE is the total energy received by all sensors throughout the test; TDE is the total energy received by all heat flux sensors during cooling period respectively.

Once the rim was created, heat transfer to the skin simulant plate decreased beyond y/d=+2. According to Figure 8.4, the absorbed thermal energy decreased from 550 kJ/m^2 to almost 250 kJ/m^2 between y/d≈+2 and y/d≈+4. However, the increase in the momentum forces due to the increase in the flow rate and nozzle-to-plate separation intensified the inertial forces of the flow in the opposite direction and increased the displacement of the rim from the stagnation point. This phenomenon enhanced heat transfer to the skin simulant plate in supercritical and subcritical regions (rim). Figure 8.4 (d) shows the effect of the increase in the inertial forces due to increase in the flow rate and nozzle-to-plate separation on the absorbed thermal energy by the skin simulant plate.

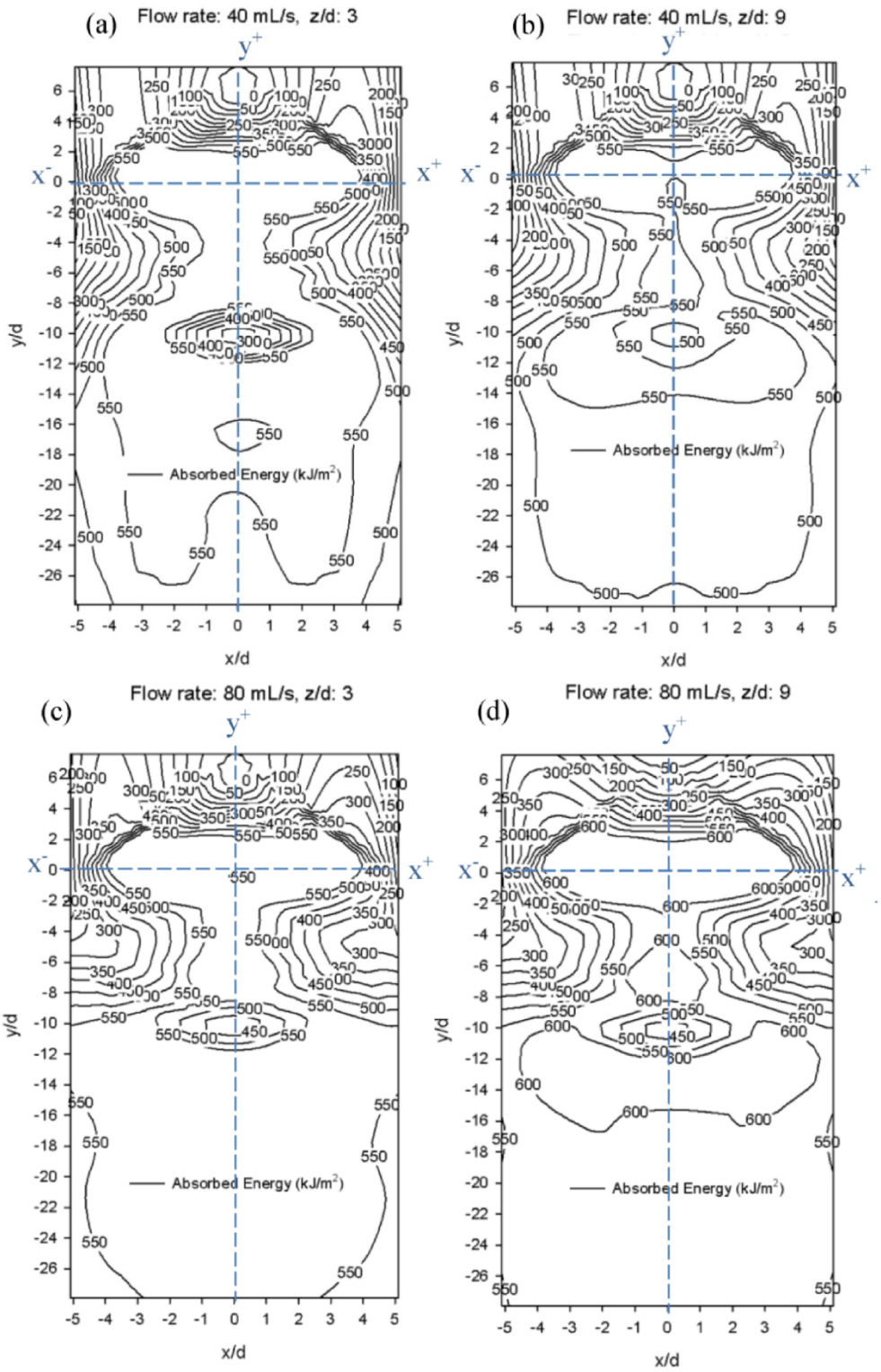

Figure 8.4. Absorbed thermal energy contour plots during 30 s exposure of 45-degree skin simulant plate to hot water at 90°C: (a) flow rate: 40 mL/s, z/d=3; (b) flow rate: 40 mL/s, z/d=9; (c) flow rate: 80 mL/s, z/d=3 and (d) flow rate: 80 mL/s, z/d=9.

In 45-degree impingement of the skin simulant plate, it is realized that the liquid in the supercritical region tends to flow back at y/d≈-8 to -10 and x/d=0 as it was flowing in the negative y-direction, downstream of the flow. This phenomenon was observed during the exposure of the liquid as the liquid at the boundaries of the flow accelerates and tend to move toward y^{-}-y^{+} and causes a very smooth collision. The encounter of the rims (braiding) between y/d≈-8 to -10 and x/d≈-2 to 2, decreased the local heat transfer (Figure 8.4 (a), (b), (c) and (d)).

According to the figures, it can be confirmed that the increase in the inertial forces caused a larger supercritical region to be covered by hot water. This caused an increase in the absorbed thermal energy. However, the increase in the nozzle-to-plate separation slightly affected the inertial forces of the water jet. As such, when the nozzle-to-plate separation increases from 3 to 9, the total absorbed energy received by the skin simulant plate slightly increased in all experimental settings (Table 8.4).

The increase in nozzle-to-plate spacing showed its effect on the predicted skin simulant plate area with predicted second and third degree burn. According to absorbed energy contour plot, the increase in the nozzle-to-plate spacing slightly enhances the heat transfer upstream and downstream of the flow. Therefore, the predicted skin simulant plate area of second and third degree burn increased 3 to 10% with an increase in z/d from 3 to 9.

However, increasing the flow rate can cause a larger area of the skin simulant to be exposed to hot water and therefore, more thermal energy to be received by the sensors. The increase in the inertial forces due to increase in the flow rate from 40 to 80 mL/s increases the absorbed energy to the skin simulant from 15 to 19% during the entire test.

The effect of different experimental settings on thermal performance of thermal protective clothing in the horizontal orientation

While fabric system S-4 is typically used as a shell fabric for thermal protective clothing, fabric system S-8 showed superior thermal performance among single layer fabric systems exposed to hot water in preliminary experiments in Chapter 3. Therefore, permeable fabric system S-4 (Kevlar®/PBI with water resistant finish) and impermeable fabric system S-8 (cotton/nylon with water

resistant finish polymer finishing) were chosen for the analyses of the effects of experimental parameters on thermal performance of the single layer fabric systems.

Tables 8.5 and 8.6 show the thermal performance of fabric systems S-4 and S-8 when exposed to 90°C water with different flow rates and nozzle-to-fabric separations in the horizontal orientation. The comparison between the total transmitted thermal energies for these two fabrics with the total transmitted thermal energy for the nude test (Table 8.3) in each experimental setting, it is inferred that employment of fabric system on the skin simulant decreases heat transfer to the skin simulant plate during the exposure.

In addition, a comparison of the total absorbed energy at the onset of second degree burn between the fabric tests and nude test in the horizontal orientation confirms that thermal protective fabric systems provided protection against hot water splash under various exposure conditions. The predicted area of second degree burn for nude test and fabric system S-4 were 100% when they were exposed to 90°C water with 80 mL/s flow rates and z/d=9. This means all of the heat flux sensors predicted second degree burn during 60 s of exposure in nude and fabric system (S-4) tests. The total absorbed energy at onset of second degree burn is 54.08 kJ/m^2 for skin simulant and 91.2 kJ/m^2 for fabric system S-4. Although, the predicted areas of second degree burn for nude test and fabric system S-4 were 100%, almost 69% less thermal energy was transmitted to the skin simulant in the presence of fabric system S-4.

A comparison of the total absorbed energy at onset of second degree burn between fabric systems S-4 and S-8 in the horizontal orientation confirms that the presence of an efficient water resistant finish enhanced thermal protective performance of these fabric systems. For instance, the predicted skin simulant plate areas of second degree burn for fabric systems S-4 and S-8 were 100% when they were exposed to 90°C water with 80 mL/s flow rates and z/d=3. All of the heat flux sensors predicted burn during 60 s of exposure for these two fabrics. However, the total absorbed energy at onset of second degree burn is 93.5 kJ/m^2 for fabric S-4 and 128.8 kJ/m^2 for fabric system S-8. This means that almost 38% more thermal energy was absorbed by fabric system S-4 to produce 100% second degree burns. Fabric system S-4's poor resistance to water penetration allowed water transfer to the skin simulant during 60 s exposure. The data presented in Table 7.12 in Chapter 7 shows that almost 6 g of hot water was transferred and 10 g of water was stored

within the structure of fabric system S-4, but no water was transferred within the impermeable structure of fabric system S-8.

From this analysis, it can be concluded that the predicted skin simulant plate area of burn cannot completely address the thermal performance of fabric systems in a fixed duration approach. The above example showed that when the plate area of second degree burn is the same for two fabric systems, the total absorbed energy at onset of second degree burn can differentiate the level of performance each fabric system provided. As such, in standard tests such as ISO 13506: 2008, the results of testing based on (1) total surface area of manikin receiving second and third degree burn, (2) the total energy transferred to surface of manikin during testing, cannot differentiate the performance of clothing with the same predicted area of burns.

The total discharged thermal energy during the cooling period of fabric systems S-4 and S-8 varied from 88.3 kJ/m^2 to 160.4 kJ/m^2 given the experimental settings (Tables 8.5 and 8.6). Thus, a considerable amount of thermal energy is discharged to the skin simulant during the cooling period of the fabrics in the horizontal orientation.

Table 8.5 Thermal performance of fabric system S-4 exposed to 90°C water with different flow rates and nozzle to fabric separations in horizontal orientation

Fabric system S-4 (Kevlar®/PBI with water resistant finish)								
β (degrees)	$\dot{m}$ (mL/s)	T_l (°C)	z/d	2nd degree burn (%) (SD)	3rd degree burn (%) (SD)	TAE_{2nd} (kJ/m^2) (SD)	TTE (kJ/m^2) (SD)	TDE (kJ/m^2) (SD)
0	40	90	3	80.7 (6.1)	74.0 (4.8)	89.7 (16.2)	341.0 (30.7)	88.3 (18.9)
			9	76.8 (15.3)	74.8 (14.6)	83.2 (18.4)	379.4 (35.7)	124.4 (39.1)
	80	90	3	100.0 (0.0)	100.0 (0.0)	93.5 (2.3)	515.6 (0.9)	142.1 (20.8)
			9	100.0 (0.0)	100.0 (0.0)	91.2 (4.1)	551.8 (27.8)	132.8 (16.1)

TAE_{2nd} is the total energy received by all heat flux sensors at the time at which second degree burn time is predicted to occur; TTE and TDE are the total energies received by all heat flux sensors during exposure and during cooling period respectively.

Table 8.6 Thermal performance of fabric S-8 exposed to 90°C water with different flow rates and nozzle to fabric separations in horizontal orientation.

Fabric system S-8 (cotton/nylon with water resistant finish polymer finishing)								
β (degrees)	$\dot{m}$ (mL/s)	T_l (°C)	z/d	2nd degree burn (%) (SD)	3rd degree burn (%) (SD)	TAE_{2nd} (kJ/m^2) (SD)	TTE (kJ/m^2) (SD)	TDE (kJ/m^2) (SD)
0	40	90	3	96.1 (6.7)	93.8 (5.2)	129.1 (10.5)	261.2 (7.9)	160.4 (36.9)
			9	82.2 (11.2)	73.2 (18.2)	113.5 (13.9)	232.2 (31.3)	129.5 (26.3)
	80	90	3	100.0 (0.0)	97.7 (3.1)	128.8 (2.7)	312.4 (17.1)	133.1 (12.0)
			9	87.1 (7.1)	85.2 (7.8)	110.9 (10.4)	284.7 (13.6)	121.7 (5.9)

TAE_{2nd} is the total energy received by all heat flux sensors at the time at which second degree burn time is predicted to occur; TTE and TDE are the total energies received by all heat flux sensors during exposure and during cooling period respectively.

Figure 8.5 illustrates the thermal discharged energy distribution along the x-axis for fabric systems S-4 and S-8 exposed to a 90°C water jet at different flow rates and nozzle to skin simulant separations (z/d) in the horizontal orientation. According to the figure, the discharged thermal energy increases as the dimensionless displacement from the stagnation point increases along the x-axis (x/d). During the experiments, it was observed that a considerable amount of water stayed on the fabric in the horizontal orientation during the cooling period. Table 7.13 shows that almost 53 and 68 g of water stayed on fabric systems S-4 and S-8 exposed to 90°C water with 80 mL/s and z/d=9, respectively. The temperature distributions along the x-axis at the onset of the cooling period after exposure to 90°C water with 80 mL/s and z/d=9 are shown in Figure 8.6. The average of temperature of the skin simulant plate on x-axis is approximately 74°C and 55°C for fabric systems S-4 and S-8 respectively at onset of the cooling period. Based on the IR measurements, the temperature difference between fabric S-8 and the skin simulant is more pronounced than the temperature difference between the plate and S-4. Therefore, more thermal energy is discharged from fabric system S-8 to the skin simulant plate. This phenomenon can be observed in all the studied experimental settings shown in Figures 8.5 (a) and (b).

It is observed in Figure 8.5 (a) that there is a sharp increase in the absorbed energy as the displacement from the stagnation point in fabric system S-4 increases. The variation in temperature may be due to mass transfer at the stagnation region and its adjacent area.

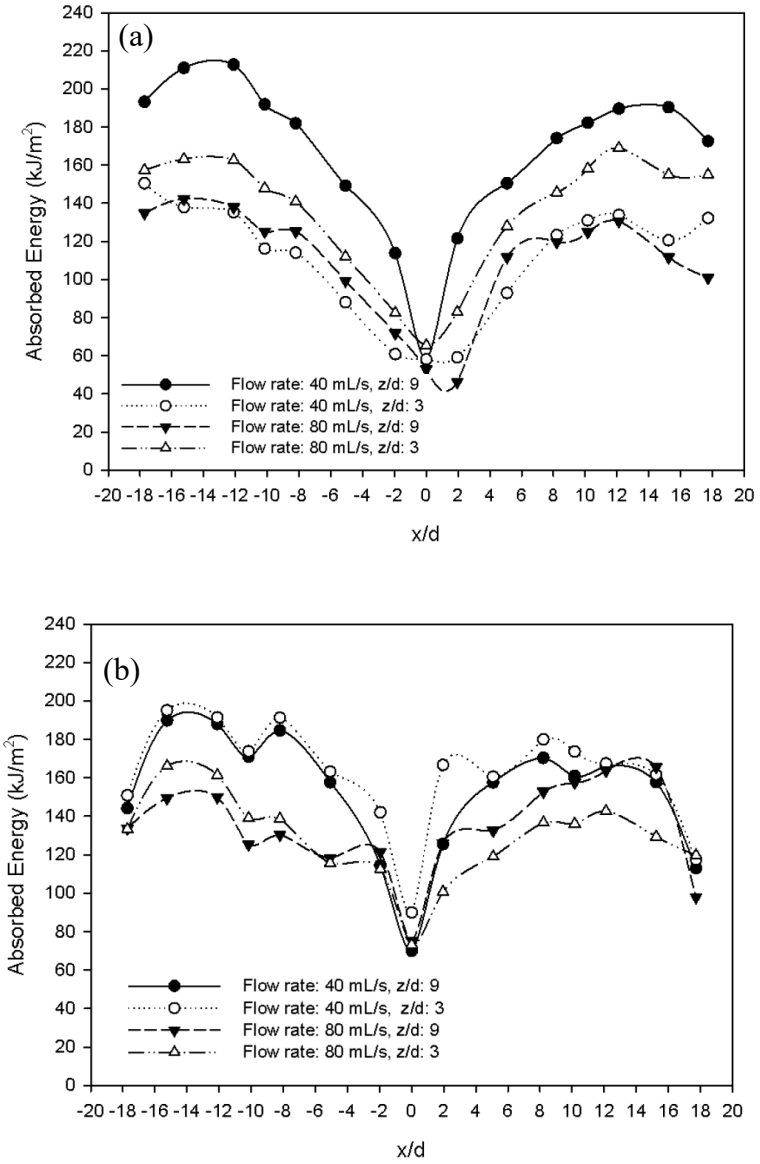

Figures 8.5. Thermal discharged energy distribution along x-axis for horizontal fabric systems (a) S-4 and (b) S-8 exposed to vertical stream of 90°C water jet at different flow rates and nozzle to fabric separation (z/d).

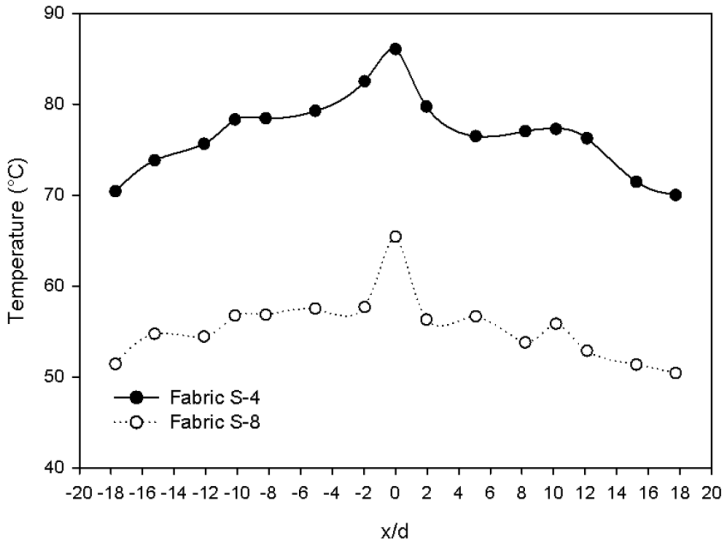

Figures 8.6. Temperature distribution along x-axis for horizontal fabric systems S-4 and S-8 exposed to vertical stream of 90°C water jet at 80 mL/s flow rates and z/d=9.

Figure 8.7 (a) and (b) illustrate the thermal energy absorbed by the skin simulant during 60 s exposure of fabric systems S-4 and S-8 to 90°C water at different flow rates and nozzle to fabric separations. The maximum absorbed energy in both figures is at the stagnation point where the heat transfer is maximum due to inertial forces cause by the impinging hot water at this region. Fabric system S-4 is a permeable fabric with water resistant surface finishing which cannot resist in depth penetration when exposed to the hot water jet. At the stagnation point, hot liquid is transferred through the porous structure of fabric system S-4 to the skin simulant due to the inertial forces caused by the impinging jet. However, for low flow rates at the stagnation point (40 mL/s and z/d=3), the absorbed energy is relatively smaller than for higher flow rates. As radial displacement along the x-axis increases from the stagnation point, the absorbed energy is reduced.

Figure 8.7 (b) depicts the absorbed energy by the skin simulant sensor along the x-axis during the exposure of fabric system S-8 to 90°C water and at different flow rates and nozzle to fabric separations. Fabric system S-8 is an impermeable fabric with polymer finish which encapsulates the fibers. The encapsulation process fills the spaces between the yarns. It has minimized hot water mass transfer. Unlike fabric system S-4, the maxima in Figure 8.7 (b) is not caused by the direct contact of hot water to the skin simulant at the stagnation point. In S-8, the pressure caused by the impinging water jet compressed the fabric and decreased its thickness at the

stagnation point. This enhanced conductive heat transfer to the skin simulant and increased the absorbed thermal energy during 60 s of exposure. As the pressure at the stagnation point significantly increased due to increase in hot water flow rate from 40 to 80 mL/s, the conductive heat transfer was enhanced and the absorbed energy was increased in comparison to the lower flow rate, 40 mL/s.

The absorbed thermal energy suddenly decreases with an increase in radial displacement from the stagnation region along the x-axis at x/d≈±2 (supercritical region). The sudden decrease in the absorbed thermal energy may be caused by the instability in the supercritical area upstream of the flow due to the surface tension forces. Fabric system S-8 has excellent hydrophobic surface properties. In addition, the compact twill weave has ridges on the surface of this fabric. Fabric system S-8 is made of 88% cotton fiber which has poor resistance to compression (compressive strength) (Morton & Hearle, 1975). Therefore, the impinging hot water compressed the fabric and created unevenness on the surface of fabric system S-8. The unevenness cause by the compression on the surface of this fabric may affect the inertial forces as the vertical momentum converts into horizontal momentum which was discussed in Chapter 7.

Consequently, the instability in the upstream region creates minor collisions of thin water sheets, braidings and reflections (Figure 8.8 (a)). These phenomena affect the inertial forces and create an instable hydraulic jump (Liu & Lienhard, 1993). The reflection effects create a large non-wetted area in the supercritical region at x/d≈±2 as the liquid sheet bounces on the surface of fabric. The bounce of the liquid sheet on the fabric decreases heat transfer and the absorbed thermal energy to the skin simulant (Figure 8.8 (b)). Beyond x/d≈±2, the absorbed thermal energy increases and creates secondary peaks at x/d≈±5 as the bounced liquid sheet (reflection with jump, Figure 2) hit the surface of the fabric (Figure 8.8 (a)). The unstable hydraulic jump traps air bubbles as the jump entrains air. A decrease in the trend of absorbed energy is observed downstream of the flow. In the downstream flow, the air bubbles that were trapped stay between the liquid sheet and the fabric downstream of the hydraulic jump. It was observed that some of the air bubbles float to the surface as they get enlarged underneath the flow. Creation of many non-wetted spots in the subcritical region is the result of air bubble formation in the subcritical region. No hot water transfer was observed when fabric system S-8 was exposed to hot water under the studied experimental settings. Only water vapor was

transferred and condensed on the skin simulant plate ((Figure 8.8 (c)). Figures 8.8 (a), (b) and (c) were taken, 30 s, 90 s and 120 s after the start of the hot water exposure.

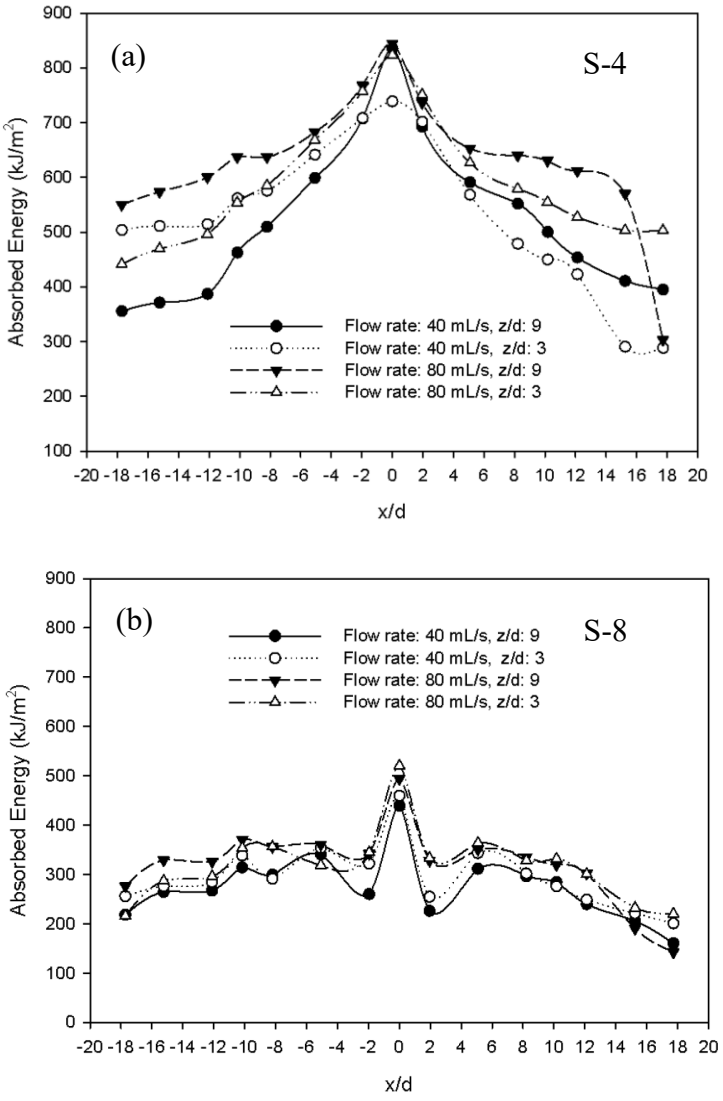

Figures 8.7. Energy absorbed by the skin simulant during 60 s exposure along the x-axis for horizontal fabric systems (a) S-4 and (b) S-8 exposed to vertical water jet at 90°C (80 mL/s flow rates and z/d=9).

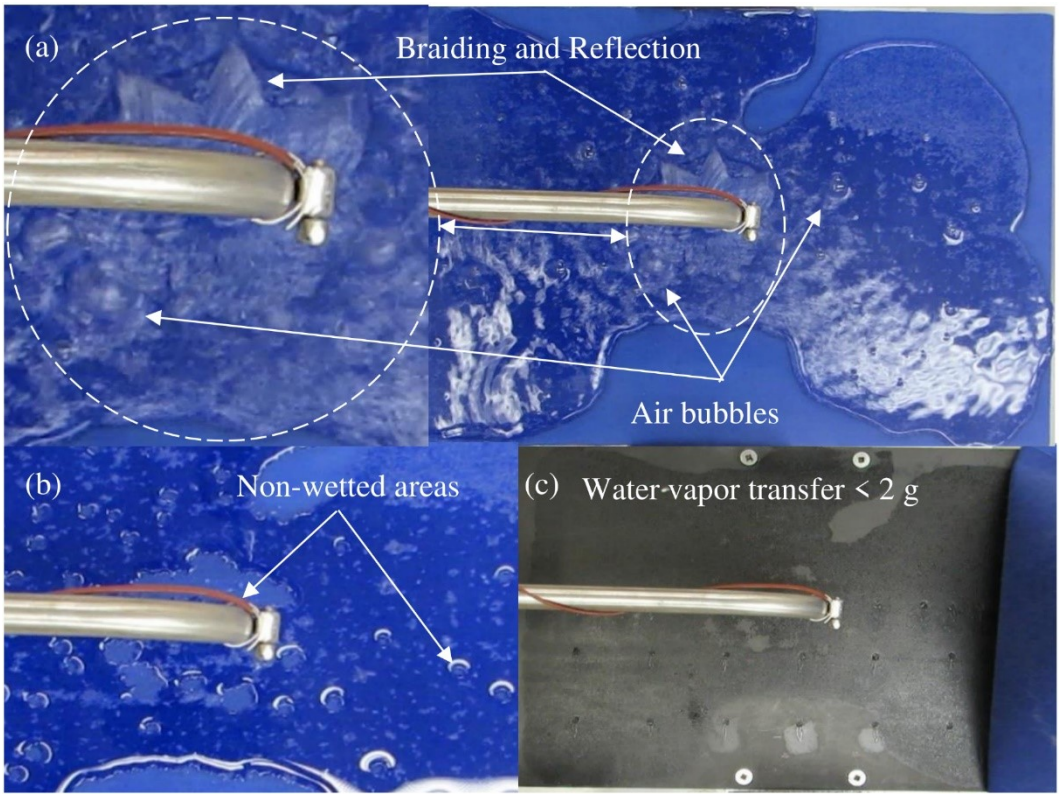

Figure 8.8. Fabric system S-8 during and after exposure to 90C water at 80 mL/s and z/d=9: (a) instable hydraulic jump and creation of local braiding, reflection in supercritical region, (b) non-wetted areas on fabric system S-8 after exposure (c) water vapor transfer.

The effect of different experimental settings on thermal performance of thermal protective clothing at 45-degree orientation

Fabric systems S-4 and S-8 have a hydrophobic surface and hot liquid impingement on the inclined surface of these fabrics creates a closed-rim flow pattern. Comparison between the areas of the predicted second and third degree burn in fabric tests and the nude test confirms that employment of a thermal protective fabric system with a hydrophobic surface reduces the area of the second and third degree burn. In the nude test, 87% second degree burn was predicted during hot water exposure (β=45°, 90°C, 80 mL/s and z/d=9). While the presence of fabric systems S-4 and S-8 reduced the area of second degree burn to 43% and 29% respectively.

In hot water exposure at lower flow rates (40 mL/s), the predicted skin simulant plate area of second and third degree burn decreased significantly. When

fabric system S-4 was subjected to 90°C water at 80 mL/s with 9 nozzle diameters to plate separation, the predicted areas of second and third degree burn were 44 and 43%, respectively. The area of second and third degree burn decreased to 18 to 15%, respectively as the hot liquid flow rate decreased to 40 mL/s. According to the data presented in Table 8.7 and 8.8, the change in nozzle-to-plate separation had minimal effect on the predicted area of second and third degree burn.

Table 8.7 Thermal performance of fabric system S-4 exposed to 90°C water at 45-degree angle and different flow rates and nozzle-to-fabric separations.

S-4								
β (degrees)	$\dot{m}$ (mL/s)	T_l (°C)	z/d	2nd degree burn (%) (SD)	3rd degree burn (%) (SD)	TAE_{2nd} (kJ/m^2) (SD)	TTE (kJ/m^2) (SD)	TDE (kJ/m^2) (SD)
45	40	90	3	14.8 (0.0)	14.8 (0.0)	12.9 (0.2)	98.7 (2.4)	2.1 (0.2)
			9	17.8 (4.13)	14.8 (0.0)	18.2 (5.6)	111.4 (11.9)	6.0 (4.3)
	80	90	3	43.3 (5.8)	41.3 (6.7)	40.8 (7.1)	254.9 (21.4)	14.8 (6.92)
			9	44.3 (6.7)	43.4 (3.3)	38.2 (5.8)	272.4 (5.9)	7.4 (3.3)

TAE_{2nd} is the total energy received by all heat flux sensors at the time at which second degree burn time is predicted to occur; TTE and TDE are the total energies received by all heat flux sensors during exposure and during cooling period respectively.

Table 8.8 Thermal performance of fabric S-8 exposed to 90°C water at 45-degree angle and different flow rates and nozzle-to-fabric separations.

S-8								
β (degrees)	$\dot{m}$ (mL/s)	T_l (°C)	z/d	2nd degree burn (%) (SD)	3rd degree burn (%) (SD)	TAE_{2nd} (kJ/m^2) (SD)	TTE (kJ/m^2) (SD)	TDE (kJ/m^2) (SD)
45	40	90	3	13.8 (0.9)	8.5 (1.3)	20.1 (1.7)	34.6 (1.8)	2.9 (0.2)
			9	12.5 (2.2)	5.8 (2.3)	18.2 (3.2)	32.3 (2.7)	4.3 (1.2)
	80	90	3	30.5 (4.3)	25.4 (3.8)	45.8 (6.1)	104.8 (7.5)	12.0 (0.3)
			9	29.0 (4.6)	21.7 (4.6)	40.5 (7.8)	88.7 (12.2)	11.4 (0.7)

TAE_{2nd} is the total energy received by all heat flux sensors at the time at which second degree burn time is predicted to occur; TTE and TDE are the total energies received by all heat flux sensors during exposure and during cooling period respectively.

Figures 8.9 shows the skin simulant absorbed energy during 60 s exposure of fabric system S-4 to hot water at 90°C with different flow rates and nozzle-to-plate separations. Figure 8.9 depicts the variation in the absorbed energy on the y-axis, as the displacement from the stagnation point (y/d=0) increases toward positive and negative y-axis. The main stream of the flow is along the y-axis.

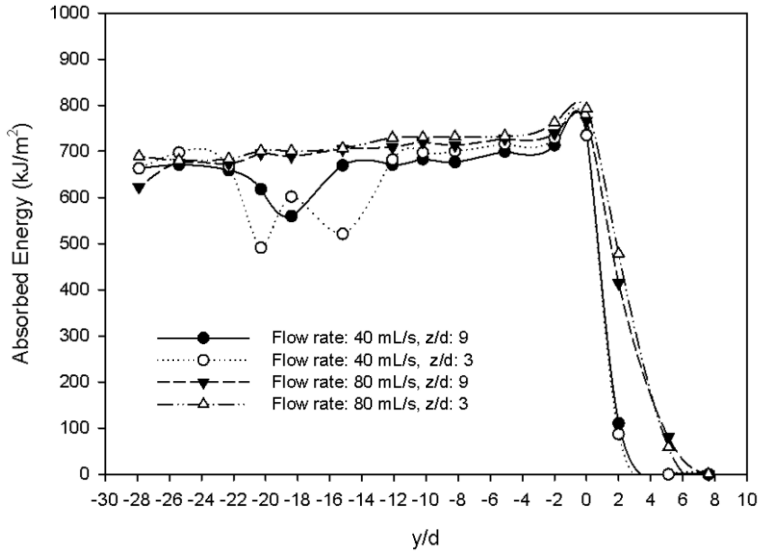

Figure 8.9. Transmitted thermal energy distribution along y-axis for inclined (β=45°) fabric systems S-4 exposed to vertical stream of 90°C water jet at different flow rates and nozzles to fabric separations.

According to the figures, the exposure of hot water on the fabric mounted on the inclined skin simulant plate (β=45°) creates a peak at the stagnation region (y/d=0). Once the hot water jet hits the surface of the permeable Kevlar®/PBI with water resistant finish (S-4) at the stagnation region, the liquid jet also spreads upward in the opposite direction of the main flow toward positive y-axis (Figure 8.10). The liquid sheet expands in this direction, gains potential energy until the component of the acceleration due to gravity in the direction of the flow ($mg\cos(180-\beta)$) equals the component of the acceleration due to gravity in the opposite direction of the flow ($mg\cos(180-\beta)$). At this point, the liquid flow reaches its maximum radial displacement opposite of the main stream of the flow. This point is referred in the chapter as the maximum length point ($B_{L_{max}}$) shown in Figure 8.10. The liquid flow stops at the maximum length point and then the accumulated potential energy in the liquid sheet accelerates the liquid downward toward the main stream of the flow in the negative y direction. However, the liquid is pushed upward again by the ongoing flow of liquid which causes the liquid to be directed to the sides and to accelerate toward the main stream of the flow. At the maximum length point, the liquid flows back and is pushed upward again by the ongoing liquid flow. This phenomenon causes hot water to stagnate in the maximum length region. The complex phenomenon causes heat transfer from the

fabric to the skin simulant to behave differently during the exposure and during cooling period.

According to Figure 8.9, the liquid sheet that travels in the opposite direction of the flow at y/d=2 delivers almost 100 kJ/m^2 at a 40 mL/s flow rate. This is because y/d=+2 lies underneath the rim in the maximum length region and the heat transfer decreases noticeably at the rim. By increasing the flow rate to 80 mL/s, the radius of the hydraulic jump increases and the hydraulic jump occurs closer to y/d=+4. As such, heat flux sensor at y/d=+2 is exposed to hot water in the subcritical region. Therefore, a relatively higher heat transfer (between 400 kJ/m^2 to 500 kJ/m^2) was delivered to the skin simulant at y/d=2.

Increasing the inertial forces due to change in water flow rate causes the liquid sheet to spread wider on the fabric and to cover a larger portion of the fabric surface. Comparing the transmitted thermal energy data in Figures 8.9 and 8.11 as the flow rate increases confirms that the increase in the flow rate lowers the thermal performance of fabric system exposed to hot water. Similar to the horizontal orientation, it can also be inferred that the position of hydraulic jump affects the amount of thermal energy received by the skin simulant during an exposure in the inclined orientation.

In the high flow rate (80 mL/s), the absorbed thermal energy decays as the liquid flows and departs from the stagnation point toward the negative y-axis. However, when the flow rate is 40 mL/s, the accelerating outer boundaries of the flow collide and this creates braiding. The collision of the accelerated rims causes a secondary peak in the absorbed energy curve which can be a result of rising turbulence and falling velocity (Gardon & Akfirat, 1965). The braided liquid flow does not remain confined on the fabric and bounces from the surface and creates reflection. The dimensions of the reflection (width, length and height) were observed to be dependent on the experimental parameters, as was briefly explained in Chapter 7. The jump of the liquid sheet off of the surface (reflection with jump, Figure 8.10) decreases the contact between the liquid sheet and the fabric and reduces heat transfer to the skin simulant. Once the encountered rims rise to a certain height in reflection, the water gains potential energy as it flows on the fabric; it then hits the surface of the fabric and creates a secondary impingement (Figure 8.10). The secondary impingement region enhances heat transfer to its underlying region and creates another peak (y/d<-22, flow rate=40 mL/s) in the absorbed

thermal energy curve (Figure 8.9). Fabric system S-4 does not resist hot water penetration in the secondary stagnation region because it has poor resistance to hot water penetration. This phenomenon was also observed in the impact penetration test of fabric system S-4. The secondary stagnation region enhances heat and mass transfer in fabric system S-4.

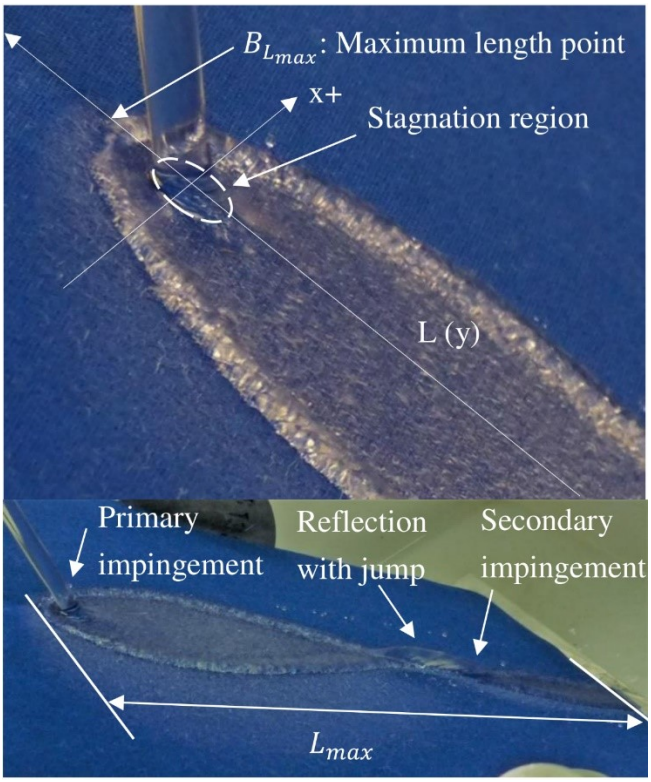

Figure 8.10. Stagnation region and maximum length point and reflection on inclined surface of an inclined fabric.

The bouncing of the liquid sheet causes less contact between the liquid sheet and the surface of the fabric which reduces heat transfer to the fabric significantly. When the bounced off water hits the fabric, it impinges the fabric. The local hot water impingement causes a sudden rise in the absorbed energy curve. This phenomenon is shown in Figure 8.11 where fabric system S-8 was impinged by 90°C water at different flow rates and nozzle-to-fabric surface separations. In fabric system S-8, the bounced off liquid sheet creates a cascading effect which created the wave-like absorbed energy curves in Figure 8.11 (a).

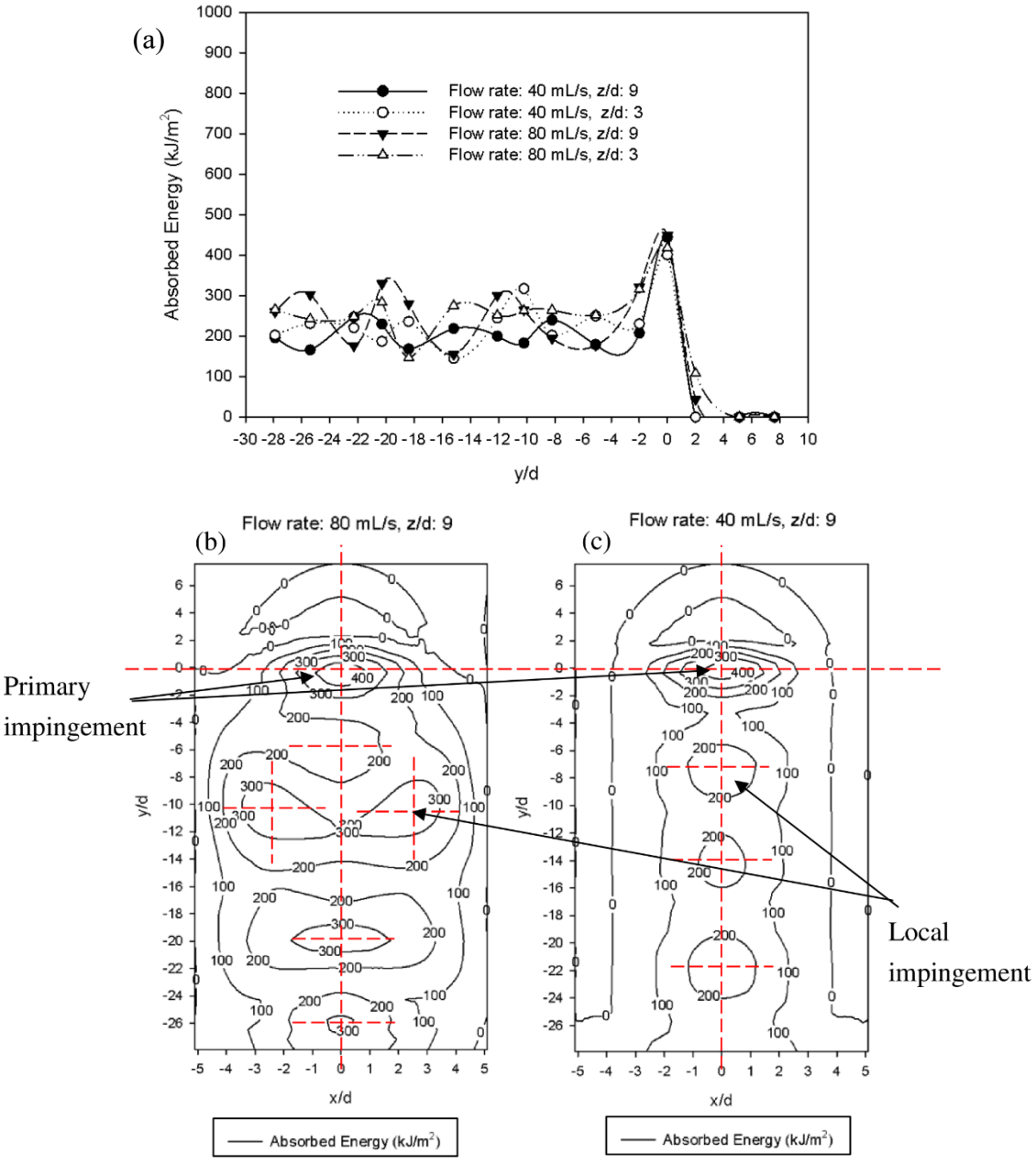

Figure 8.11. (a) Transmitted thermal energy distribution along the y-axis for fabric system S-8 exposed to water jet at 90°C at different flow rates and nozzle to fabric separations (45-degree orientation); (b) Contour plots of transmitted thermal energy distribution for fabric system S-8 exposed to 90°C water jet (b) at 80 mL/s and (c) 40 mL/s flow rates (z/d=9).

In Figure 8.11 (b) and (c), the intersections of dashed lines show the primary impingement point at x/d=0 and y/d=0 and the local impingement points. It can be observed that the decrease in the flow rate from 80 to 40 mL/s decreased the number of the local impingement points as well as the magnitude of the absorbed energy at these regions.

Comparison of the transmitted thermal energy distribution (Figure 8.12 (b)) and the time to second degree burn distribution (Figure 8.12 (a)) for fabric system S-8 exposed to a 90°C water jet (80 mL/s flow rate and z/d=9) reveals that this fabric's water resistant surface property gives it superior thermal performance. Fabric system S-8 has an excellent hydrophobic surface which creates a closed rim flow pattern with many reflections on the surface of the fabric which leave many non-wetted areas on the fabric. The times to second-degree burn for the areas underneath the reflections are considerably higher (40 to 50 s) than the times to second-degree burn for the other areas. In Figures 8.12 (a) and (b), the arrows show the non-wetted areas on the transmitted energy contour plots and the corresponding second degree burn times. In addition, the excellent resistance to water penetration of this fabric minimizes hot water transfer in the water jet impingement zone as well in the local stagnation regions.

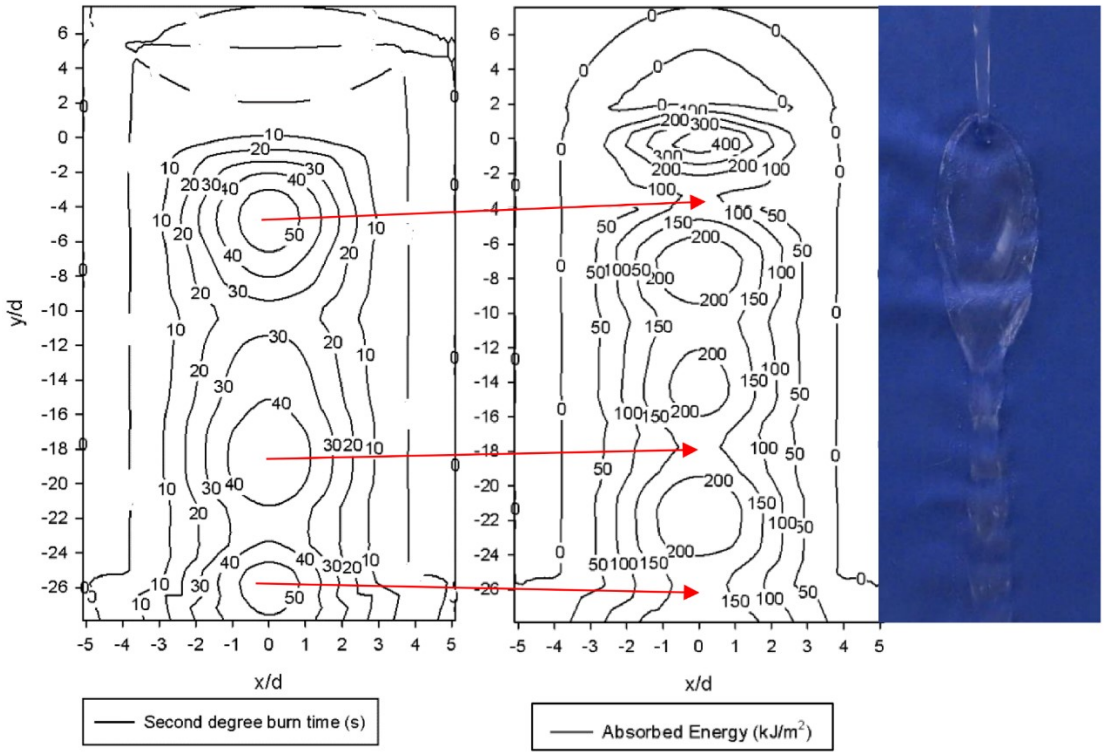

Figure 8.12. (a) The second degree burn distribution and (b) the transmitted thermal energy distribution for fabric system S-8 exposed to 90°C water jet with 40 mL/s flow rate and z/d=9.

From the analysis of absorbed thermal energy and the studies of the hydraulic jump on horizontal fabrics exposed to a vertical stream of hot water, it is understood that heat transfer from the liquid sheet significantly decreases at the location of hydraulic jump, and downstream of the jump. These are the areas where the thickness of the liquid sheet increases and gains potential energy due to interactions between the inertial-gravitational forces and inertial forces-surface tension forces (Kibar et al., 2010; Liu & Lienhard, 1993). Moreover, it was realized that heat transfer from the boundaries of the flow around the maximum length point ($B_{L_{max}}$) and the areas underneath the reflections to the fabric-skin simulant decreases significantly.

Analyses of the absorbed energies during the cooling period of the fabric exposed to hot liquid shows that the fabric areas underneath the reflections and maximum length point discharge a relatively higher amounts of thermal energy to the skin simulant during the cooling period of the fabrics. For instance,

Figure 8.13 (a) and (b) are fabric system S-4's absorbed energy contour plots during the exposure (Figure 8.13 (a)) and cooling period of the fabric (Figure 8.13 (a)) exposed to a 90°C water jet (40 mL/s and z/d=9). The impingement of water forms a flow pattern on the fabric that is shown in Figure 8.13 (c). The horizontal dashed line indicates the impingement points and the dotted lines shows reflection and the maximum length point on the y-axis. It is observed that the maximum length point occurred at y/d<+2 and the areas of the fabric around the maximum length point deliver a significant amount of thermal energy to the skin simulant plate from y/d=+2 to y/d=+4 (Figure 8.13 (b)). While it can be recognized from Figure 8.13 (a) that the area between y/d=+2 and y/d=+4 did not receive significant thermal energy during exposure.

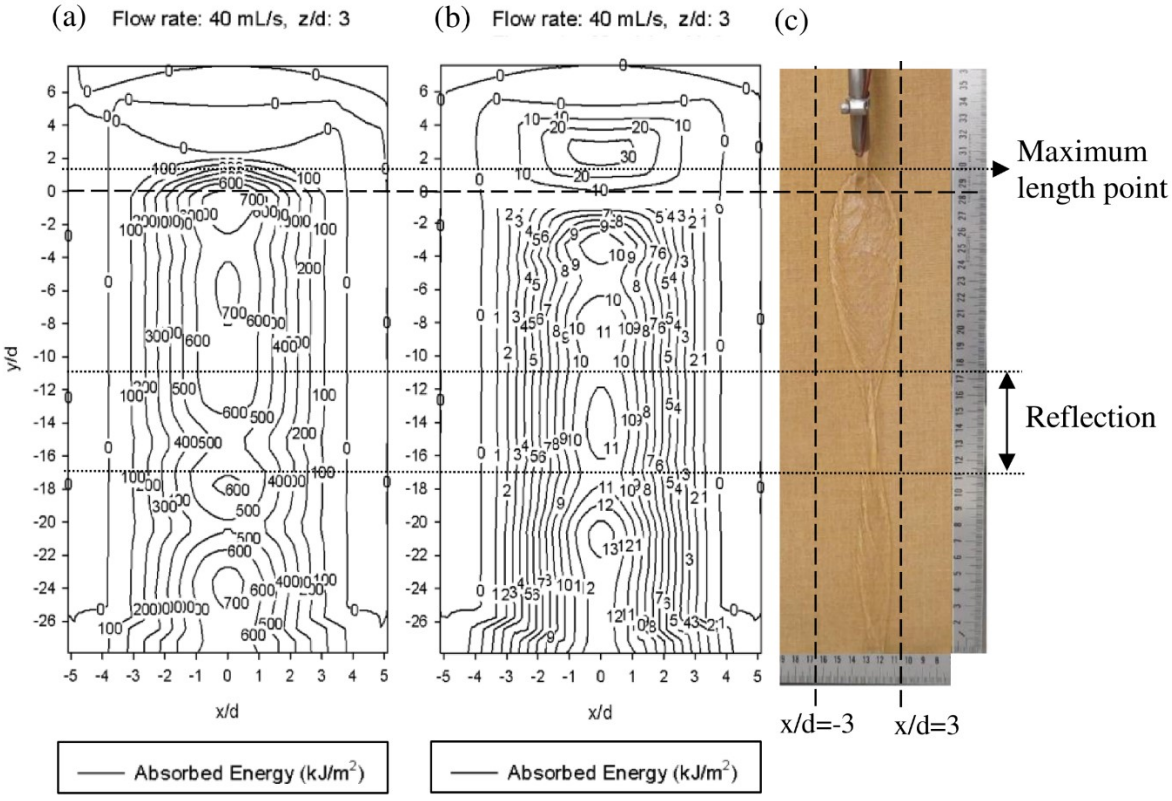

Figure 8.13. Absorbed energy distribution during (a) exposure and (b) cooling period of fabric system S-4 exposed to 90°C water jet at 80 mL/s and 9 nozzle diameters to fabric separation.

The other areas of interest include the area underneath the reflection caused by the encounter of the rims (Figure 8.13 (c). The collision of the rims creates braiding effect which causes a rise in the liquid sheet between y/d=-11 and y/d=-17. In Figure 8.13 (b), it is indicated that the reflection of the liquid sheet influenced the absorbed energies of areas underneath the reflection. The instabilities of the flow on the fabric shown in Figure 8.14 (a) and (c) also affect the absorbed energy to the sensors. The instability of the flow pattern was observed when the flow rate was high (80 mL/s) downstream of the flow where the outer boundaries tend to flow together and create braiding on the fabrics with hydrophobic surfaces such as S-4 and S-8. Because of increased flow rate and inertial forces, hot water tends to slip on the surface of fabric systems S-4 and S-8 which have water-resistant surfaces. Also, the component of the acceleration force due to gravity may cause the liquid in the rim to slip on the surface of the fabric as the rims tend to flow back together. Therefore, the resultant of the surface tension forces and the inertial forces may cause instabilities in the downstream flow of water on the surface of the fabric with a water resistant finish when the liquid flow rate is high.

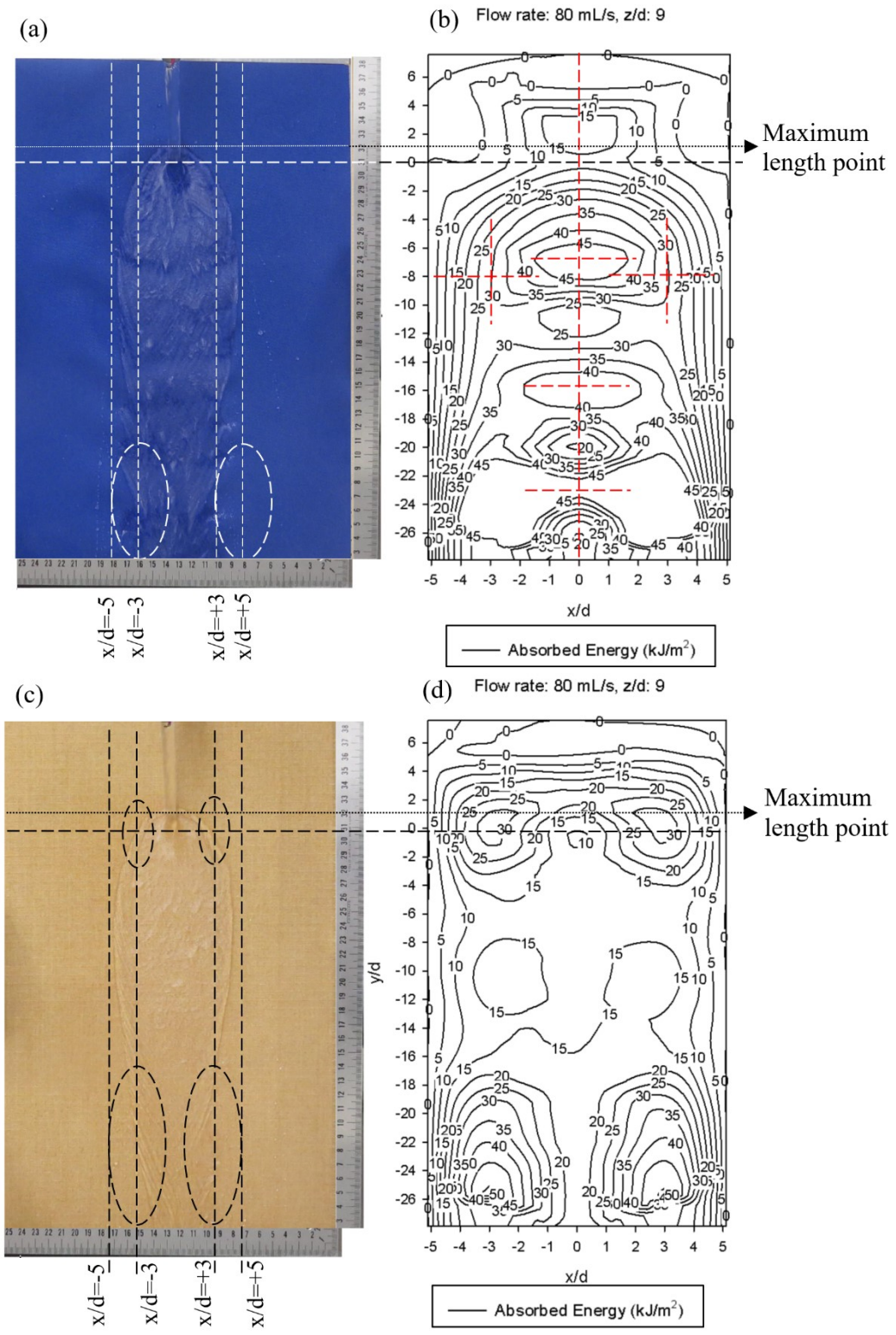

Figure 8.14. Flow pattern and absorbed energy distribution during cooling period of (a) and (b) fabric system S-8 (c) and (d) fabric system S-4 exposed to 90°C water jet at 80 mL/s and 9 nozzle diameters to fabric separation.

Consequently, the slip of flowing water on the surface of fabric causes less contact of hot water. The prolonged exposure of hot water to the fabric underneath the areas may cause a gradual accumulation of thermal energy during exposures. Investigation of the temperature distribution suggests that the temperature of the skin simulant underneath these areas is relatively low at the onset of the cooling period. As such, a relatively higher thermal energy is discharged from the fabric area to the skin simulant during the cooling period.

Comparison of the discharged thermal energy between the maximum length point and y/d=4 in Figures 8.14 (b) and (d) confirms that the impermeable fabric system S-8 with water resistant polymer finish provides a better thermal protection during the cooling period in these areas than in fabric system S-4. The effect of physical properties of fabric on its heat transfer properties during exposure and cooling periods is discussed in the next section.

Evaluation of thermal performance of thermal protective clothing

Analysis of the absorbed thermal energy received by the skin simulant plate during exposure shown in Tables 8.3 and 8.4 confirms that a 90°C water jet (80 mL/s and z/d=9) causes the skin simulant to receive the largest amount of absorbed thermal energy during the entire test. In addition, the values of the transferred water and the stored water obtained for fabric system S-4 shown in Table 7.12 in Chapter 7 suggest that this experimental setting causes the highest amount of hot water transfer in both 45-degree and horizontal orientations of the fabric. Single layer, double layer and multilayer fabric systems shown in Table 3.4, Chapter 3 were exposed to 90°C water jet (80 mL/s and z/d=9) and the thermal performance of the fabric systems was evaluated for this setting.

Evaluation of thermal performance of thermal protective clothing in horizontal orientation exposed to hot water

Single layer fabric systems

The thermal performance of single layer fabric systems in the horizontal orientation is presented in Table 8.9. Almost 85 to 100% of the skin simulant plate area predicted second and third degree burn. The predicted area of second degree burn for fabric system S-5 (Nomex®IIIA with no finish) was 100% and the skin simulant received the largest amount of absorbed energy during the entire test (676.69 kJ/m^2). Total absorbed energy at onset of second degree burn shows that

the exposure of this fabric to almost 62 kJ/m^2 of thermal energy can cause 100% predicted area of second degree burn, while this value for (S-6) Nomex®IIIA with water resistant finish is almost 25% more (82 kJ/m^2). Comparison of the thermal performance of fabric systems S-5 and S-6 shows the importance of water resistant finishes on the thermal performance of fabrics.

Among moisture barriers, fabric system S-3, Moisture barrier C (Nomex®IIIA with water resistant finish and polyurethane lamination) showed an almost 13% lower area of second and third degree burn. The contact angle of 90±5°C water drop on moisture barrier C (fabric system S-3) was 141° which was 10% and 17% more that the contact angles on moisture barriers B (fabric system S-1) and A (fabric system S-2) respectively. As such, moisture barrier C has a surface with a more hydrophobic surface and therefore a much smaller surface of the fabric is covered with hot water.

However, the transmitted energy distribution along the x-axis for horizontal tests of moisture barriers A, B and C shows that moisture barrier C delivers a higher amount of thermal energy to the skin simulant during the exposure, specifically between x/d=-10 to x/d=+10. According to Figure 8.15 (a), moisture barriers A, B and C receive maximum amounts of thermal energy at the stagnation region. The absorbed thermal energy curve drops significantly at x/d=±2. The drop in the heat transfer may be caused by the instability of the flow due to the local reflection after the jet of hot water hits moisture barriers A and B. The local reflections of the flow cause less absorbed thermal energy by the fabric underneath the reflected and decelerated flow regions. The interaction of the bounced-off liquid and the surface of the fabric creates a rise in the absorbed energy curve at x/d=±5. The absorbed energy curve increases until the occurrence of the hydraulic jump between x/d=±5 and x/d=±8. The absorbed energy curve decreases downstream of the hydraulic jump as the displacement from the stagnation region increases.

In single layer fabric systems S-4 to S-9, which are typically used as shell fabrics, similar trends in the absorbed energy curves were observed (see Figure 8.15 (b)). In general, the behavior of the transfer of energy to the skin simulant sensor on single layer fabrics can be divided into three main regions. The first region is the decrease in the absorbed thermal energy between the stagnation region until the onset of the hydraulic jump. Then, the second region is the variation in the absorbed energy at the position of the hydraulic jump. Finally, the decrease

in the absorbed thermal energy downstream of the flow after the height of the liquid sheet increased. The decreasing trend in the absorbed energy curve was observed in all fabric systems tested as the water hits the surface of fabric.

The behavior of the absorbed energy is different between the stagnation point and the hydraulic jump based on the fabric's water resistant properties. In the permeable fabric, where the water penetrates into the fabric at the stagnation point, second peaks are not created because the water sheet does not bounce on the surface of fabric. However, in impermeable fabric, such as fabric system S-8, a similar trend to moisture barrier A (S-1) and B (S-2) was observed. In these fabrics, when the water bounces on the surface of the fabric, the peaks in the supercritical region are created.

Table 8.9. Thermal performance of single layer fabric system exposed to 90°C water jet with 80 mL/s and 9 nozzle diameters to plate separation in horizontal orientation of the fabric.

Fabric system	2^{nd} degree burn (%) (SD)	3^{rd} degree burn (%) (SD)	TAE_{2nd} (kJ/m^2) (SD)	TAE (kJ/m^2) (SD)	TDE (kJ/m^2) (SD)	STE Rating (kJ/m^2) (SD)
S-1	100.0 (0.0)	98.1 (3.36)	99.6 (1.8)	649.8 (31.8)	176.6 (33.8)	50.9 (18.4)
S-2	100.0 (0.0)	100.0 (0.0)	95.5 (0.78)	626.5 (16.9)	119.7 (19.5)	24.5 (7.3)
S-3	87.2 (5.8)	85.2 (3.4)	86.7 (7.03)	602.4 (81.0)	142.9 (47.9)	36.9 (19.2)
S-4	99.6 (0.7)	99.6 (0.7)	91.2 (4.1)	684.6 (18.8)	132.8 (16.1)	29.3 (8.5)
S-5	100.0 (0.0)	100.0 (0.0)	62.1 (1.8)	676.7 (10.4)	74.5 (8.9)	9.0 (2.5)
S-6	100.0 (0.0)	100.0 (0.0)	82.4 (2.9)	719.0 (13.5)	127.9 (10.8)	26.9 (4.3)
S-7	90.4 (6.7)	82.6 (10.0)	96.6 (7.9)	523.3 (48.3)	109.2 (13.0)	30.8 (10.4)
S-8	87.1 (7.1)	85.1 (7.8)	110.9 (10.4)	406.4 (19.4)	121.7 (5.9)	37.1 (1.9)
S-9	98.8 (1.2)	97.5 (0.1)	110.1 (2.1)	478.8 (11.0)	78.6 (8.7)	15.0 (3.5)

TAE_{2nd} is the total energy received by all heat flux sensors at the time at which second degree burn time is predicted to occur; TAE is the total energy received by all sensors throughout the test; TDE is the total energy received by all heat flux sensors during cooling period; STE rating is the total energy received by all sensors during cooling period considering the proportion of the discharge energy to the total absorbed energy.

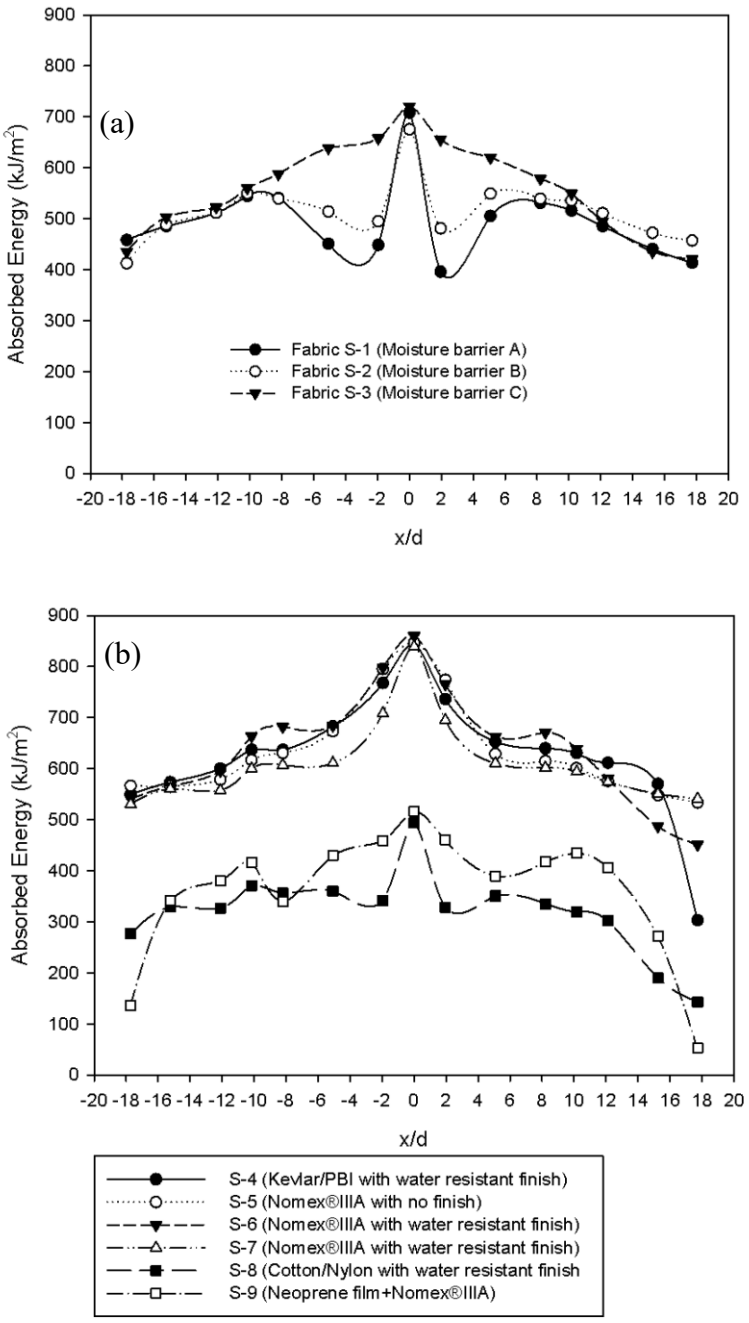

Figure 8.15. The transmitted thermal energy distribution along x-axis for horizontal single layer fabric systems exposed to a 90°C water jet at 80 mL/s and z/d=9: (a) moisture barriers A, B and C (b) shell fabrics A, B, C, D, E ,F and G.

Permeable single layer fabrics with water resistant finishes show very similar thermal energy distributions along the x-axis. Among these fabrics, fabric system S-7 shows slightly better performance during the exposure. The fire-retardant rainwear (S-9) and impermeable fabric system S-8 showed superior

performance among the single layer fabrics. A comparison of Figures 8.15 (a) and (b) confirms that the water resistant structure of a fabric system enhances thermal performance during exposure. Fabric system S-8 transfers the least amount of thermal energy during the exposure in most of the areas along the x-axis. The predicted area of second degree burn is 85% which is the lowest value among the single layer fabric. In addition, the total absorbed energy at the onset of second degree burn indicates that fabric system S-8 provides superior thermal performance among the single layer fabrics tested.

Caution needs to be exercised in using the predicted area of burn to compare thermal performance of fabric systems. According to Table 8.9, fabric systems S-3 and S-8 showed almost the same area of burn (85%). The total absorbed energy at onset of second degree burn suggests that fabric system S-8 received 110.9 kJ/m^2 thermal energy to produce 85% area of second degree burn. However, thermal energy of 86.7 kJ/m^2 was needed to produce 85% area of second degree burn for fabric system S-3. Under constant experimental variables, more thermal energy to predict 85% burn means a longer exposure time. A longer exposure time to produce a prescribed area of burn would imply better thermal performance.

The values of discharged energy for fabrics in the horizontal orientation during the cooling period are affected by the accumulated water on the fabric, within its structure as well as the transferred water shown in Table 7.13. According to the data, a relatively large amount of water created a pooling effect and stayed on the fabric during the cooling period. As such, the range of the discharged energy in the horizontal orientation is relatively higher than in the 45-degree orientation, which is discussed later in the chapter.

The discharged thermal energy distribution along the x-axis shows that as the distance from the stagnation point increases, the discharge of thermal energy from fabric to skin simulant increases (Figure 8.16 (a) and (b)). It is interesting that the stagnation point discharges the smallest amount of energy to the skin simulant except for moisture barrier C (S-3) and Kevlar®/PBI with a water resistant surface finish (S-4). In these two fabrics, the minimum value of the discharged thermal energy is at x/d=2. Taking into account the trend of the absorbed thermal energy during the cooling period, it can be inferred that the areas downstream of the flow are the areas which have more potential to discharge thermal energy to the skin simulant during the cooling period.

The values of stored energy rating shown in Table 8.9 suggest that among moisture barriers, moisture barrier B (fabric system S-2) has the least potential to store thermal energy within its structure during cooling period of the garment. Also, the fire-retardant rainwear (fabric system S-9) has the potential to store a considerably lower thermal energy. Comparing the stored energy rating values of permeable shell fabrics with a water resistant finish (S-4, S-6 and S-7) suggests that these fabrics have a similar ability to store thermal energy within their structure.

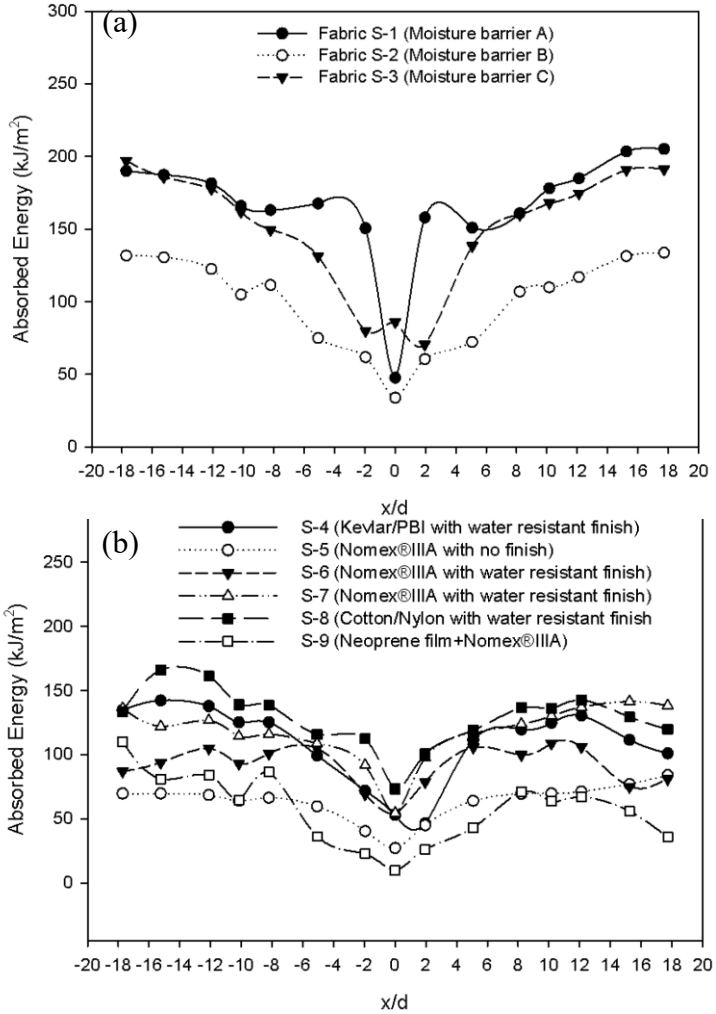

Figure 8.16. The discharged thermal energy distribution along x-axis for horizontal single layer fabric system exposed to a 90°C water jet (80 mL/s and z/d=9): (a) moisture barriers A, B and C (b) shell fabrics A, B, C, D, E ,F and G.

Double layer fabric systems

Double layer fabrics D-1, D-2, D-3 and D-4 were constructed from permeable shell fabric A (Kevlar®/PBI with water resistant finish) with an underlying thermal liner A, B, C and D respectively. Table 8.10 shows each fabric assembly's description, density, thickness, and transferred and stored water obtained from impact penetration test as well as thermal performance exposed to a 90°C water jet (flow rate= 80 mL/s and z/d=9). The predicted area of second degree burn and the transmitted thermal energy to the skin simulant on the x-axis decreases with an increase in fabric thickness and a decrease in fabric density according to Table 8.10 and Figure 8.17, respectively. The predicted areas of second degree burn for fabric systems D-1, D-2, D-3 and D-4 are approximately 65, 64, 60 and 54%, respectively. The improvement in the thermal performance of these fabrics with thickness can be explained as follows.

Table 8.10. Thermal performance of horizontal double layer fabric systems exposed to 90°C water jet (80 mL/s, z/d=9).

Fabric system	Assembly description	Physical property		Penetration property		Thermal performance		
		Fabric thickness (mm)	Fabric density (g/cm^3)	Transferred water (g) (SD)	Stored Water (g) (SD)	2^{nd} degree burn (%) (SD)	TAE_{2nd} (kJ/m^2) (SD)	STE Rating (kJ/m^2) (SD)
D-1	Fabric A+ Thermal Liner A	1.43	0.29	18.3 (4.3)	4.3 (0.6)	65.2 (7.3)	64.0 (3.4)	14.0 (7.4)
D-2	Fabric A+ Thermal Liner B	1.84	0.27	16.7 (2.5)	5.9 (3.5)	63.9 (5.3)	70.3 (9.2)	28.0 (8.7)
D-3	Fabric A+ Thermal Liner C	2.54	0.20	14.4 (3.3)	7.2 (1.9)	60.1 (13.8)	73.9 (18.0)	27.2 (9.1)
D-4	Fabric A+ Thermal Liner D	3.13	0.18	9.8 (2.9)	8.0 (1.9)	53.7 (0.0)	77.7 (12.5)	39.0 (17.3)

Fabric A (60% Kevlar®/ 40% polybenzimidazole); thermal liner A (plain weave, Nomex® layer quilted to a thin Nomex® oriented web); thermal liner B (plain weave, Nomex® layer quilted to two thin Nomex® oriented webs); thermal liner C (plain weave, Nomex® layer quilted to Nomex® needle felted batt); thermal liner D (plain weave, Nomex® layer quilted to Nomex® needle felted batt).

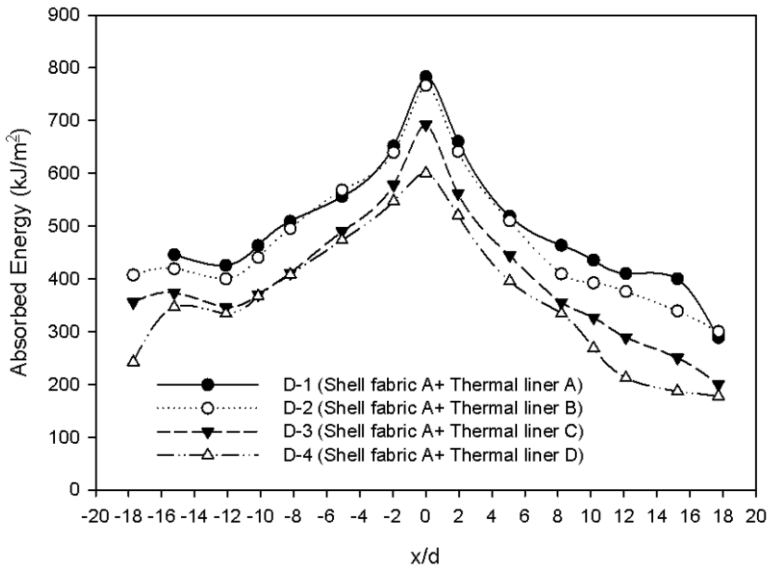

Figure 8.17. The transmitted thermal energy distribution along the x-axis for a horizontal double layer fabric system exposed to a 90°C water jet (flow rate= 80 mL/s and z/d=9).

The absorbed thermal energy curves during 60 s of exposure (transmitted energy) along the x-axis for fabric systems D-1, D-2, D-3 and D-4 are shown in Figure 8.17. These curves follow relatively similar trends with a peak at the stagnation point and a decay as the displacement from the stagnation region increases. In addition, the range of the values of the transmitted thermal energy is between 200 to 800 kJ/m^2 which suggests that these fabric systems do not provide protection against hot water impingement.

Fabric systems D-1, D-2, D-3 and D-4 cannot resist water penetration. The impact penetration test revealed that the transferred water from a 90°C water jet (80 mL/s flow rate, z/d=9) was 18.3 g for D-1, 16.7 g for D-2, 14.4 g for D-3 and 9.8 g for D-4. The transferred water through these permeable fabric systems decreases with increasing thickness. The hot water penetrates the porous fabric structure and is stored in the fabric. The data for the impact penetration test for fabric systems D-1, D-2, D-3 and D-4 show that the stored water within the structure of these fabrics is 4.3, 5.9, 7.2 and 8.0 g of water, respectively. As the density of the fabric decreases, the fabric system with less fiber content and more trapped air stores more hot water within its structure. As such, less hot water is transferred to the back side of the fabric to contact the skin simulant directly (Table 8.10).

The trapped hot water within the structure of the fabric can also increase the effective thermal conductivity of the fabric and may enhance heat transfer to the skin simulant during the cooling period. The values of the stored energy ratings in Table 8.10 and the discharged thermal energy to the skin simulant plate in Figure 8.18 indicate that heat transfer is increased as the amounts of trapped water increase in the fabric system from D-1 to D-4.

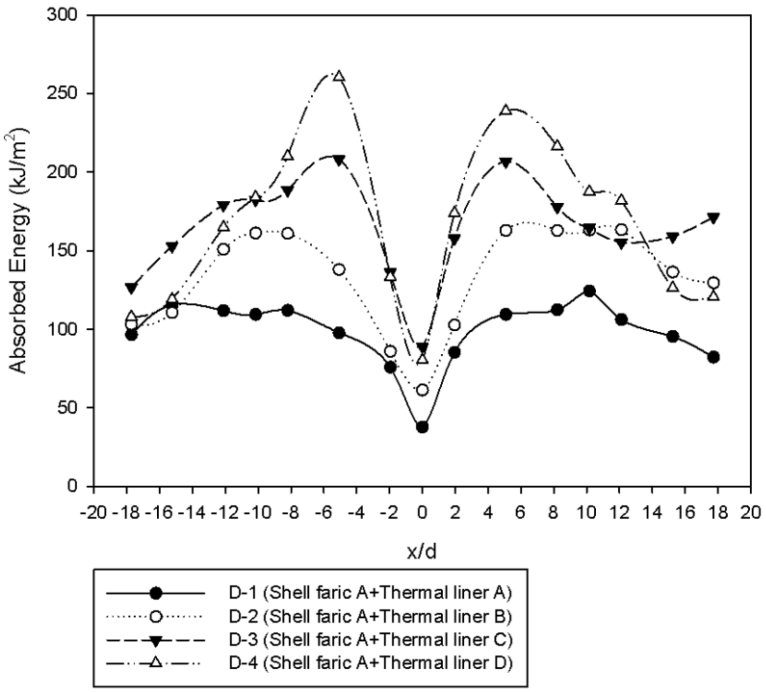

Figure 8.18. the discharged thermal energy distribution along the x-axis for horizontal double layer fabric systems exposed to a 90°C water jet (flow rate= 80 mL/s and z/d=9).

The accumulation of thermal energy in these fabrics creates a potentially hazardous thermal environment close to the skin simulant during the cooling period. In fabric systems D-1 to D-4, larger amounts of thermal energy are discharged during the cooling period of the fabrics in comparison to single layer fabric systems.

In addition, applying compression can cause a secondary penetration, pushing the entrapped hot water within the fabric toward the skin. This phenomenon was named “the wringing effect” in Chapter 4, namely, the discharge of stored liquid in a permeable fabric due to compression. Depending on the position on the x-axis, the thermal energy may be discharged with a different magnitude to the skin simulant plate. For instance, if fabric system D-4 is

compressed to the skin simulant plate at x/d=-5, a large amount of energy would be discharged to the skin simulant, while the impingement of the fabric in the stagnation region may discharge considerably less thermal energy to the skin simulant at x/d=0.

According to Figure 8.18, the maximum values of the discharged energy are in the areas of the fabric that were underneath the hydraulic jump at x/d=±5. At the hydraulic jump and downstream of the flow, heat transfer decreases significantly in comparison to upstream of the flow. Therefore, the areas underneath the jump may gain thermal energy gradually during exposure. When the fabric underneath the hydraulic jump is thick, such as fabric system D-4, more thermal energy can be stored in comparison to thinner fabrics, such as D-1.

The other phenomenon which may contribute to the creation of maximum peaks in the discharge energy curve is the accumulation of stored water in the fabric in these areas. According to Table 7.13 in Chapter 7, the stored water in the fabric increases as the thickness of the fabric increases. The amount of stored water in fabric systems D-1, D-2, D-3 and D-4 exposed to a 90°C water jet (80 mL/s flow rate for 60 s, z/d=9) were 4.3, 5.9, 7.2 and 8.0 g of water, respectively. The impingement of water at the stagnation point caused penetration of water within the fabric. As more water penetrated at this point, water within the fabric structure of the fabric at the stagnation point was pushed by the impinging jet toward the sides of the impingement zone (see x/d=±5 in Figure 8.18).

From Figures 8.16 (a), (b) and 8.18, it was observed that, in most cases, the minimum thermal energy discharge occurs at the stagnation point. However, in bench scale tests, thermal performance of the fabric systems is typically evaluated at the stagnation point. Therefore, modifications need to be made to existing bench top test methods in order to obtain data from the areas off the stagnation point in hot liquid exposures. In addition, more investigations are required in order to study the discharged thermal energy to the areas other than the stagnation point when evaluating the performance of thermal protective clothing exposed to other thermal hazards.

Multilayer fabric systems

An improvement in the thermal performance of fabric systems exposed to hot water was observed in M-2, M-3 and M-6, respectively. In these fabrics,

Kevlar®/PBI with a water resistant finish was placed as a shell fabric with an underlying moisture barrier to improve water penetration resistance of the fabric system as well as thermal insulation. Table 8.10 shows fabric thickness, density and thermal performance of multilayer fabric systems, which were constructed from thermal liners of different thickness and density.

Table 8.11. Thermal performance of multilayer fabric systems exposed to 90°C water jet with 80 mL/s and 9 nozzle diameters to plate separation in horizontal orientation of the fabric.

Fabric system	Assembly description	Fabric thickness (mm)	Fabric density (g/cm^3)	2^{nd} degree burn (%) (SD)	TAE_{2nd} (kJ/m^2) (SD)	TAE (kJ/m^2) (SD)	STE Rating (kJ/m^2) (SD)
M-1	Fabric A+ Moisture Barrier A+ Thermal Liner A	1.88	0.34	20.9 (12.5)	35.3 (20.7)	79.4 (40.9)	30.3 (20.3)
M-2	Fabric A+ Moisture Barrier A+ Thermal Liner B	2.29	0.31	7.6 (2.8)	9.2 (8.2)	18.3 (14.4)	7.7 (5.7)
M-3	Fabric A+ Moisture Barrier A+ Thermal Liner C	3.02	0.24	0.0 (0.0)	0.0 (0.0)	8.3 (0.9)	1.5 (0.5)
M-6	Fabric A+ Moisture Barrier A+ Thermal Liner D	3.62	0.21	0.0 (0.0)	0.0 (0.0)	0.0 (0.0)	0.0 (0.0)

Fabric A (60% Kevlar®/ 40% polybenzimidazole); moisture barrier A (Nomex® +2%carbon+ underlying polytetrafluoroethylene coating); thermal liner A (plain weave, Nomex® layer quilted to a thin Nomex® oriented web); thermal liner B (plain weave, Nomex® layer quilted to two thin Nomex® oriented webs); thermal liner C (plain weave, Nomex® layer quilted to Nomex® needle felted batt); thermal liner D (plain weave, Nomex® layer quilted to Nomex® needle felted batt).

Fabric systems M-1, M-2, M-3 and M-6 resist water penetration. The increase in the thickness of these fabric assemblies decreases the rate of heat transfer to the skin simulant and improves thermal performance of the fabric system (Table 8.11). In addition, the decrease in the density of these fabrics from 0.34 to 0.21 g/cm^3 improves the thermal insulation property of fabric system. A decrease in the density of the fabric systems with resistance to water penetration enhances the thermal insulative property the fabrics. As such, no absorbed thermal energy was received by the skin simulant during the exposure and cooling period of horizontal fabric M-6 to a 90°C water jet (80 mL/s, z/d=9).

The enhancement of the insulative property of a fabric system exposed to hot water also affects the discharge of thermal energy to the skin simulant. The discharge thermal energy decreased significantly from fabric systems M-1 to M-3. The stored thermal energy ratings decreasing trend from 30.3 to 0.0 kJ/m^2 suggests that fabric system M-6 has the lowest ability to store thermal energy in is structure. This is due to use of a thick, low density thermal liner D underneath the moisture barrier A in fabric system M-6's construction.

Fabric systems M-3 and M-6 demonstrated superior thermal performance upon exposure to hot water in this study when considering the transmitted and stored thermal energy developed in the fabric system during the exposure and cooling periods of the fabric.

The effect of water penetration resistance on thermal performance of the fabric system

In this study, the effect of the position of a moisture barrier on thermal performance of the fabric system was investigated in double layer and multilayer fabric systems. In Chapter 3, the effect of the position of a moisture barrier was investigated in double layer fabric systems in the stagnation region. It was realized that minimizing mass transfer in the outermost layer of the fabric improves the thermal performance of the fabric system at the stagnation region. In this chapter, the investigation concerns improving the penetration resistance of the fabric system by positioning the moisture barrier from innermost to outermost layers.

In Chapter 6, it was concluded that minimizing hot water transfer within the fabric structure in the outermost layer decreased hot water accumulation within the fabric structure in multilayer fabrics and enhanced water penetration resistance. According to Table 8.12, enhancing water penetration resistance of multilayer fabric systems by resisting mass transfer in the outermost fabrics enhanced their thermal performance when exposed to a hot water splash. Therefore, rotated layer fabric systems were used in which the moisture barrier (moisture barrier A) was positioned from the outermost position such as fabric systems D-6 and M-4 to the innermost layer, such as fabric system M-5. Although the configuration of these fabrics is not practical, it helps to understand the effect of minimizing mass transfer by improvement in the water penetration resistance of the fabric system.

In Chapter 6, the impact penetration test was run for fabric systems D-6, M-4 and M-5 in order to evaluate the effect of position of moisture barrier on water penetration resistance in the fabrics. Positioning the moisture barrier in the outermost layer of the fabric system decreased the amount of stored water in the fabrics by half in horizontal and 45-degree orientations. Therefore, the thermal performance of the fabric system improved when the penetration of hot water was blocked in the outermost layers. According to Table 8.12, the total absorbed energy at onset of second degree burn increased by 25% from 102.7 to 128.8 kJ/m^2 by switching the moisture barrier to the face of the fabric system.

Table 8.12. Thermal performance of switched double layer and multilayer fabric system exposed horizontally to 90°C water jet (80 mL/s, z/d=9).

Fabric system		Assembly code	2nd degree burn (%) (SD)	TAE_{2nd} (kJ/m^2) (SD)	TAE (kJ/m^2) (SD)	STE Rating (kJ/m^2) (SD)
Double layer	D-5	Fabric A+ Moisture Barrier A	88.0 (6.5)	102.7 (10.0)	484.1 (29.4)	47.8 (11.4)
	D-6	Moisture Barrier A+ Fabric A	87.6 (5.2)	128.8 (7.3)	314.3 (25.6)	47.3 (9.0)
Multilayer	M-3	Fabric A+ Moisture Barrier A+ Thermal Liner C	0.0 (0.0)	0.0 (0.0)	8.3 (0.9)	1.5 (0.5)
	M-4	Moisture Barrier A+ Fabric A+ Thermal Liner C	0.0 (0.0)	0.0 (0.0)	3.0 (1.7)	0.5 (0.5)
	M-5	Fabric A+ Thermal Liner C+ Moisture Barrier A	65.2 (5.8)	80.3 (7.4)	368.1 (39.8)	53.5 (10.6)

The improvement in the water penetration resistance of the fabric systems is more noticeable by comparing the thermal performance of fabric systems M-3 and M-5. The fabric assembly code in Table 8.12 shows the position of the moisture barrier in these fabrics. The amount of stored water in fabric systems M-3 and M-5 is 9.1 g and 21.4 g, respectively (Table 7.13). The thermal performance of fabric system in fabric system M-5 decreased due to the permeable shell fabric A and thermal liner C. These fabrics cannot resist penetration of hot water into the fabric. Once fabric System M-5 is exposed to the hot water jet, hot water penetrates into

the fabric until it is stopped by the moisture barrier in the innermost layer of fabric system M-5. Therefore, hot water transfers thermal energy closer to the skin simulant and causes 65% predicted area of second degree burn in fabric system M-5. In addition, the increased water accumulation in fabric system M-5 increased the thermal energy discharge to the skin simulant plate in comparison to fabric system M-3. The stored thermal energy rating for fabric system M-5 (53.5 kJ/m^2) was higher than for fabric system M-3 (0.5 kJ/m^2).

Evaluation of thermal performance of thermal protective clothing in 45-degree orientation exposed to hot water

Single layer fabric system

The thermal performance of single layer fabrics exposed to 90°C water in a 45-degree orientation is presented in Table 8.13. Almost 22 to 76% of the skin simulant plate area indicated a second and third degree burn. This range is relatively smaller than the range for the predicted area of second and third degree burn in a horizontal hot water flow (85 to 100%). The maximum predicted area of second and third degree burn was for fabric system S-5 (Nomex®IIIA with no finish (76%). Fabric system S-8 (88% cotton+12% HT nylon with water resistant finish) had 29% predicted area of second degree burn and showed superior performance among the fabric systems exposed to hot water at 90°C (flow rate= 80 mL/s and z/d=9). Total discharge energy (TDE) to the skin simulant sensor was from 6.8 kJ/m^2 to 21.6 kJ/m^2. This range is relatively smaller than the range of discharged energy to the skin simulant for water impingement in the horizontal orientation (78.6 to 176.6 kJ/m^2). Therefore, it is concluded that the orientation of the sensor board to water flow significantly affected the transmitted and the discharge thermal energy to the skin simulant.

Table 8.13. Thermal performance of single layer fabric system in 45-degree orientation exposed to 90°C water jet (80 mL/s, z/d=9).

Fabric system	2nd degree burn (%) (SD)	3rd degree burn (%) (SD)	TAE_{2nd} (kJ/m^2) (SD)	TAE (kJ/m^2) (SD)	TDE (kJ/m^2) (SD)	STE Rating (kJ/m^2) (SD)
S-1	41.0 (3.7)	38.2 (5.8)	43.7 (3.0)	200.3 (29.5)	6.8 (2.2)	0.6 (0.5)
S-2	43.3 (3.3)	36.3 (6.7)	43.6 (4.8)	208.8 (9.6)	9.7 (0.7)	1.7 (1.2)
S-3	39.5 (0.0)	34.7 (4.1)	40.9 (1.1)	227.6 (1.6)	13.5 (1.7)	4.9 (2.8)
S-4	43.3 (6.7)	41.4 (3.3)	38.2 (5.8)	269.2 (8.0)	7.4 (3.3)	0.6 (0.7)
S-5	76.2 (3.4)	76.2 (3.4)	54.6 (0.6)	493.9 (22.0)	18.4 (8.1)	1.6 (2.0)
S-6	47.2 (3.3)	43.3 (6.7)	42.6 (3.6)	300.7 (15.2)	12.5 (3.6)	3.1 (2.4)
S-7	47.2 (3.3)	43.4 (3.4)	52.5 (5.1)	246.6 (12.9)	13.1 (6.4)	3.6 (5.3)
S-8	29.0 (4.6)	21.7 (4.6)	40.5 (7.8)	100.1 (12.6)	11.4 (0.7)	2.2 (0.3)
S-9	62.2 (9.2)	57.5 (8.7)	73.8 (7.4)	242.5 (12.0)	21.6 (2.9)	3.8 (0.6)

TAE_{2nd} is the total energy received by all heat flux sensors at the time at which second degree burn time is predicted to occur; TAE is the total energy received by all sensors throughout the test; TDE is the total energy received by all heat flux sensors during cooling period; STE rating is the total energy received by all sensors during cooling period considering the proportion of the discharge energy to the total absorbed energy.

Figure 8.19 (a) and (b) shows the absorbed energy (y-axis) received by the skin simulant during the exposure and cooling periods for the moisture barriers A, B and C. The stagnation region is indicated with dashed lines and the maximum length point is indicated with a solid line. The direction of the main stream of the flow is from the stagnation region toward the negative y-axis. The absorbed energy curve during the exposure shows that the transmitted energy is maximum at the stagnation region and decreases as the displacement from the stagnation region increases. However, it was observed that moisture barrier A, (Fabric system S-1, Nomex® +2%carbon+ underlying polytetrafluoroethylene coating) exhibited uneven surface wrinkles during hot water exposure. The uneven wrinkled surface

remained after the exposure to hot water. Therefore, the transmitted and the discharge thermal energy curves resemble concave- and convex-shaped curves.

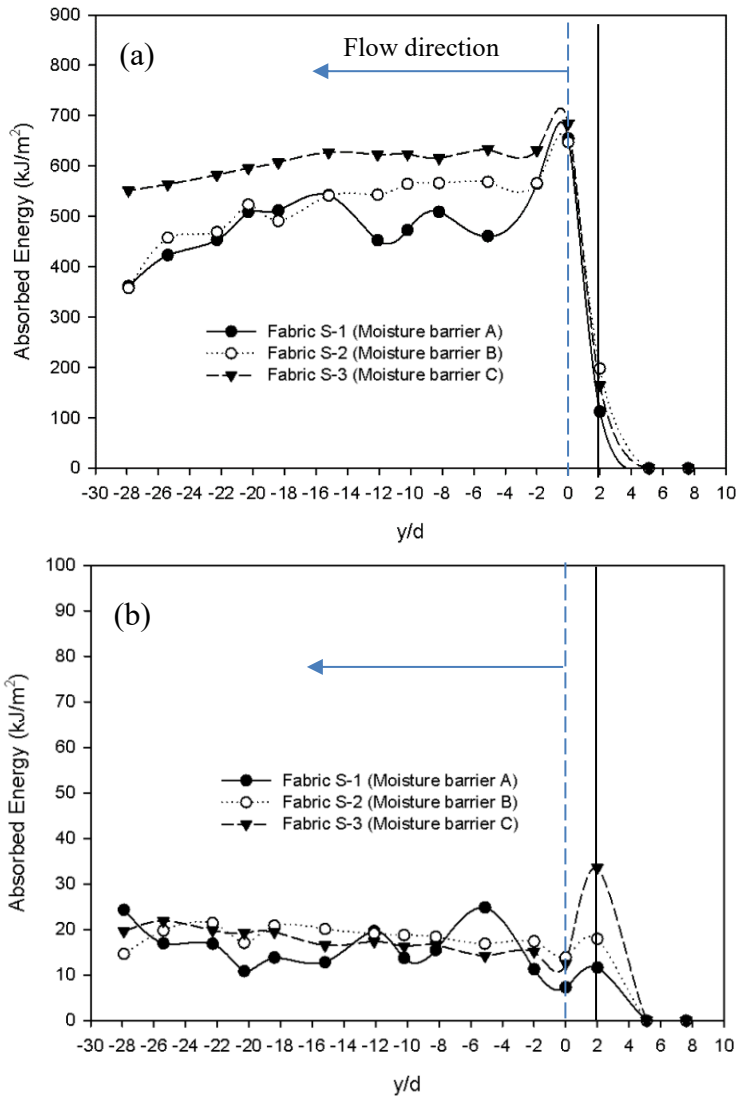

Figure 8.19. (a) The transmitted and (b) discharged thermal energy distribution along y-axis for moisture barriers A, B and C in 45-degree orientation exposed to vertical stream of 90°C water jet at 80 mL/s flow rate and z/d=9. The maximum length and the stagnation points are indicated with solid and dashed-lines.

When the fabric becomes wrinkled, it does not stay flat on the skin simulant surface. As such, some parts rise from the surface and do not contact the skin simulant and some parts stay on the skin simulant. The parts of the fabric that rise from the skin simulant, such as y/d=-5 in fabric system S-1's curve, create a concave-shaped absorbed energy curve showing that the absorbed energy at the

spot is relatively low. However, the spots of the fabric that contact the skin simulant deliver more thermal energy to the skin simulant.

On the contrary, the parts of the fabric that rise from the skin simulant such as y/d=-5 in 7.23 (b), transmit less thermal energy to the skin simulant than the contacted spots such as y/d=-10. Less transmitted thermal energy causes an accumulation in thermal energy at risen parts in the fabric. After termination of exposure, the accumulated thermal energy in the risen parts of the fabric causes thermal energy to be discharged to the skin simulant which causes a rise in the discharge energy curve.

The maximum length points are indicated with solid line at y/d≈+2 in figures 8.19 (a) and (b). The maximum length region receives approximately 100 kJ/m^2 to 200 kJ/m^2 thermal energy during the exposure. As such, the energy in the maximum length region is potentially high enough to cause skin burn injuries. Considering the discharge energy curves, it is understood that the maximum of the discharged energy curve for each moisture barrier is located at the maximum length region at y/d≈+2. Consequently, by taking into account the transmitted and the discharged thermal energy to the skin simulant, as well as the predicted area of second and third degree burn, it appears that moisture barrier A has relatively better performance to hot water among the moisture barriers studied in this thesis.

Figure 8.20 illustrates the thermal energy transmitted to the skin simulant from fabric systems S-4 to S-9 exposed at 45-degree orientation to a 90°C water jet (flow rate= 80 mL/s and z/d=9). The stagnation region is indicated with a dashed line at y/d=0. It is evident that a considerable amount of thermal energy is transmitted to the skin simulant between the stagnation point and the maximum length point.

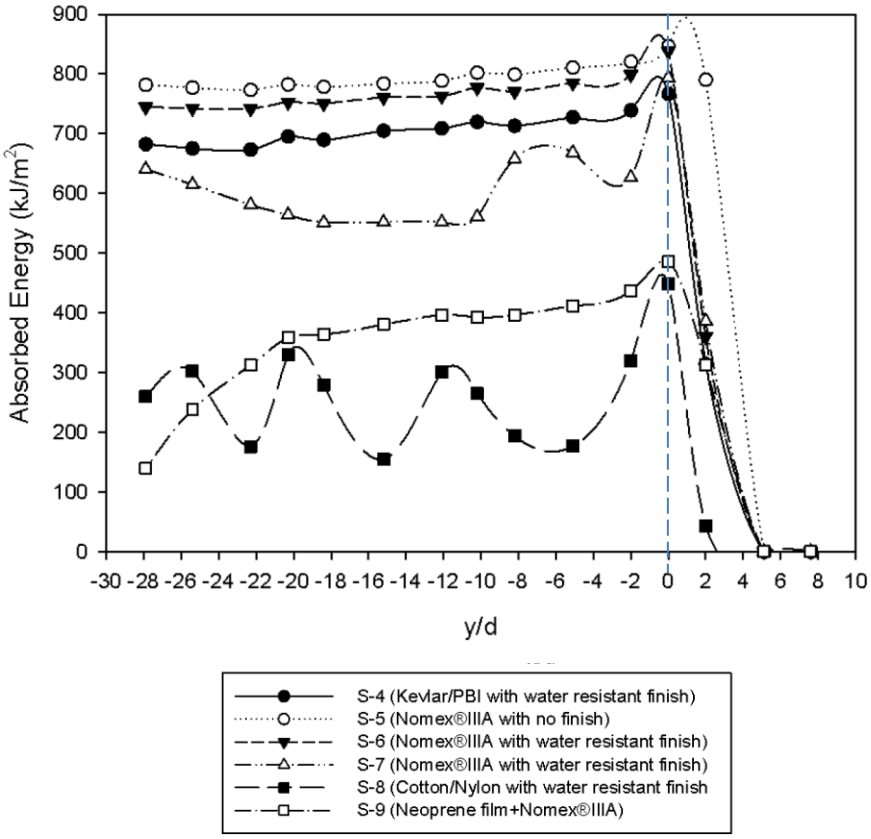

Figure 8.20. (a) The transmitted thermal energy distribution along y-axis for shell fabrics A, B, C, D, E ,F and G at 45-degree orientation exposed to a 90°C water jet (flow rate= 80 mL/s and z/d=9). The maximum length and the stagnation points are indicated with a solid and a dashed-line.

The water resistant finish can be divided in two subgroups: those providing (1) a water resistant (hydrophobic) surface and (2) resistance to water penetration. A hydrophobic surface decreases surface free energy, creates a closed rim flow pattern, repels water off the fabric and reduces its surface wettability. Fabrics with resistance to water penetration, resists in-depth transport of the liquid from the surface to the backside of the fabric. In other words, in a fabric with resistance to water penetration, water does not partially (partial penetration) or completely (total penetration) penetrate through the fabric as discussed in Chapter 6. The analysis of single layer fabric systems that are typically used as shell fabrics in protective clothing is carried out by dividing the studied fabrics into four groups based on their water-resistance.

Fabrics with poor water-resistant surface properties and a poor water resistance to water penetration

According to Figure 8.20, the maximum of the transmitted energy occurs the stagnation point in all single layer fabrics. Fabric system S-5 (Nomex®IIIA with no finish) shows the lowest thermal performance among the fabric systems as expected. The wicking effect caused by the transport of water through the capillaries of fabric system S-5 caused fast penetration and surface wetting of fabric system S-5 which caused a larger area of the fabric to be exposed to the highest level of transmitted thermal energy among the studied fabric systems. As such, inherently fire retardant fabrics with no water resistant finish cannot provide thermal protection under conditions such as hot water exposure.

Fabrics with poor water-resistant surface properties and excellent resistance to water penetration

Among the studied fabrics, the fire-retardant rain wear (Fabric system S-9) belongs to this group of fabrics based on its water-resistant and water penetration characteristics. The Neoprene face film covered a tightly woven underlying Nomex®IIIA (88 × 60) which had an excellent water penetration resistance. The data obtained from the water penetration test and water vapor diffusion test confirmed that this fabric transfers no water and passed the lowest amount of water vapor through its structure. However, the wetting contact angle for this fabric and the water flow pattern on fabric system S-9 revealed that the Neoprene film has a poor water-resistant surface property. The predicted area of second and third degree burn for fabric system S-9 are 62% and 58%, the highest values of burn area after fabric system S-5 (Nomex®IIIA with no finish). Therefore, a water-resistant surface is a crucial factor that should be utilized in shell fabric systems in order to increase its thermal performance against hot liquids.

Fabrics with excellent water-resistant surface properties and poor resistance to water penetration

The predicted area of second degree burn for fabric systems S-4 (60% Kevlar®/ 40% polybenzimidazole with water resistant finish), S-6 (Nomex®IIIA with water resistant finish) and S-7 (Kermel® with water resistant finish) are 43, 47 and 47% respectively. It was observed that the closed rim flow pattern of water covered a relatively small area on these fabrics which had excellent hydrophobic surfaces. The values of the contact angles and the area of the flow pattern for these

fabrics affirmed that fabric systems S-4, S-6 and S-7 had excellent water resistance surface properties. On the contrary, these fabrics had poor resistance to hot water transfer during 60 s of exposure. The values of the transferred water for fabric systems S-4, S-6 and S-7 are 10.8, 60.1 and 7.5 g. These values were relatively higher values of the transferred water among the studied fabrics confirming that they had poor resistance to water penetration.

The poor water penetration resistance of fabric systems S-4, S-6 and S-7 is based on the results from the impact penetration test; 38 g of water was transferred through fabric system S-6 while this value was 6 g for fabric system S-4 and 5 g for S-7. The thermal performance of these fabric systems was affected by water penetration resistance. The total transmitted thermal energy during the exposure for fabric systems S-4 (252.4 kJ/m^2), S-6 (288.2 kJ/m^2) and S-7 (233.5 kJ/m^2) confirms that water penetration resistant property is the other crucial factor that needs to be considered in shell fabric systems in order to increase their thermal performance against hot liquids.

Fabrics with an excellent water-resistant surface properties and excellent resistance to water penetration

Fabric system S-8 (88% cotton+12% HT nylon with water resistant finish) transfers 88.7 kJ/m^2 thermal energy to the skin simulant during the exposure to hot water which is approximately two to five times lower that other single layer fabric system. The water vapor diffusion resistance of fabric system S-8 is 188.6 mm. In addition, no water transfer was observed in the impact penetration test. Only less than 2 g of water vapor was condensed on the blotting paper confirming fabric system S-8's excellent water resistance. In addition, the excellent hydrophobic surface of fabric system S-8 presented low surface energy to the fabric. This creates a closed rim flow pattern on the fabric, and repelled water off the fabric at many locations, and created "cascading effect". The "cascading effect" reduced surface wetting and created concave absorbed energy curves at the position of the fabric where the local reflections occurred (Figure 8.20). The excellent water-resistant surface of fabric system S-8 and its resistance to water penetration resulted in a superior thermal performance against hot liquid. In addition, the thermal stored energy rating for this single layer fabric systems confirmed that it stored a small amount of thermal energy (2.2 kJ/m^2).

Double layer fabric system

In the double layer fabric systems, shell fabric A (60% Kevlar®/ 40% polybenzimidazole with water resistant finish) was positioned as the outer layer (Table 8.14). The excellent water resistance of shell fabric A created a similar closed-rim flow pattern on the surface of each double layer systems (fabric systems D-1, D-2, D-3, D-4 and D-5). The predicted areas of second degree burn are slightly different for each double layer fabric. Fabric systems D-1and D-2 had predicted areas of second degree burn at almost 45% while the use of a thicker thermal liner in fabric system D-2 slightly improved its thermal performance. Comparison of the total absorbed energy at onset of second degree burn of fabric systems D-1 (47.8 kJ/m^2) and D-2 (51.4 kJ/m^2) affirms that the two thin Nomex® oriented webs in thermal liner B, slightly enhanced the thermal performance of permeable fabric system D-2.

Using a thicker thermal liner resulted in smaller predicted areas of second degree burn in fabric systems D-3 (35.6%) and D-4 (33.6%) in comparison to fabric systems D-1 (45.3%) and D-2 (45.3%). Employing thicker thermal liners in fabric systems D-3 and D-4 improved thermal performance of double layer fabrics.

The effect of water penetration properties in a fabric system can be observed in Figure 8.21 where the transmitted energy to the skin simulant of fabric system D-5 is plotted along with fabric systems D-1 to D-4. Fabric system D-5 has a water impermeable structure and can resist water penetration due to an expanded polytetrafluoroethylene coating in moisture barrier A. As such, fabric system D-5 receive significantly less transmitted thermal energy along the y-axis compared to fabric systems D-1 to D-4 which allowed the penetration of 90°C water.

The absorbed energy curve for fabric system D-5 shows some oscillations (Figure 8.21). Similar to the discussions earlier on moisture barrier A, it was also observed in fabric system D-5 that the moisture barrier wrinkled as it wetted in the 45-degree orientation. Although the moisture barrier was mounted underneath shell fabric A in fabric system D-5, it exhibited an uneven surface after hot water penetrated through shell fabric A and contacted the moisture barrier. Therefore, the uneven surface of moisture barrier A formed a wave-like curve.

Table 8.14. Thermal performance of double layer fabric system in 45-degree orientation of the fabrics exposed to a 90°C water jet (flow rate= 80 mL/s and z/d= 9.

Fabric system	Assembly description	Physical property		Penetration property		Thermal performance		
		Fabric thickness (mm)	Fabric density (g/cm^3)	Transferred water (g) (SD)	Stored Water (g) (SD)	2nd degree burn (%) (SD)	TAE_{2nd} (kJ/m^2) (SD)	STE Rating (kJ/m^2) (SD)
D-1	Fabric A+ Thermal Liner A	1.4	0.29	4.2 (0.5)	2.6 (0.2)	45.3 (5.8)	47.8 (7.8)	1.6 (0.8)
D-2	Fabric A+ Thermal Liner B	1.8	0.27	3.7 (1.8)	2.5 (0.6)	45.2 (10.1)	51.4 (13.3)	2.5 (0.8)
D-3	Fabric A+ Thermal Liner C	2.5	0.20	3.1 (0.1)	3.8 (0.4)	35.6 (3.4)	40.7 (6.1)	4.7 (2.2)
D-4	Fabric A+ Thermal Liner D	3.1	0.18	2.2 (0.2)	6.6 (4.4)	33.6 (3.9)	47.2 (13.1)	5.3 (2.3)
D-5	Fabric A+ Moisture Barrier A	0.9	0.50	0.3 (0.1)	4.7 (0.2)	35.6 (3.4)	50.0 (5.1)	2.2 (0.2)

TAE_{2nd} is the total energy received by all heat flux sensors at the time at which second degree burn time is predicted to occur; STE rating is the total energy received by all sensors during cooling period considering the proportion of the discharge energy to the total absorbed energy.

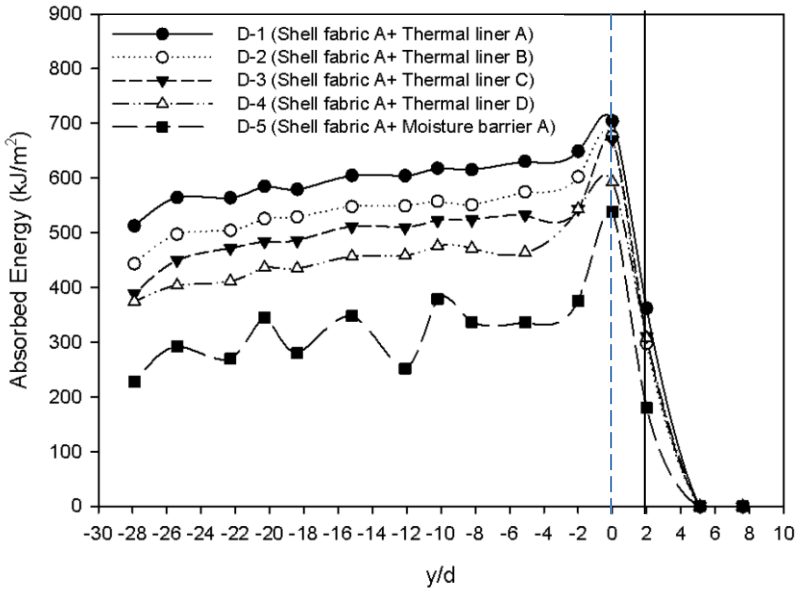

Figure 8.21. The transmitted thermal energy distribution along y-axis for double layer fabric systems at 45-degree orientation exposed to a 90°C water jet (80 mL/s flow rates, z/d=9). The maximum length and the stagnation points are indicated with a solid and a dashed-line.

Figure 8.22 shows the discharged thermal energy curve of the skin simulant for double layer fabrics during the cooling period, after the exposure to 90°C water at 45-degree angle. There is thermal stored energy accumulated in the double layer fabric system. The energy slightly increases as the displacement from the stagnation point increases toward negative y/d. However, the thermal stored energy is significantly lower than that of the same fabric exposed to 90°C in horizontal orientation (Figure 8.18).

The discharged energy curves increase from the stagnation point in the negative y directon until they reached their maxima in close proximity to the stagnation region. The accumulation of water within the structure of the permeable double layer fabrics may have created the maxima on the discharged energy curves. At the beginning of exposure, the impinging water jet at the stagnation region may push hot water into the fabric structure. During the exposure, the ongoing impingement of water within the structure of the fabric may push the accumulated water further in the fabric. As such, more water would be accumulated in the areas in close proximity to the stagnation region and create a maximum.

It was also observed that the maxima at the discharge energy curve decreased with a decrease in the thickness of the fabric. The maximum values of the discharge energy in fabric systems D-4 and D-3 are approximately 85 and 50 kJ/m^2, respectively. The thicker fabric system D-4 structure holds more water and create almost a 40% increase in the maximum value of the discharge energy (Figure 8.22).

The position of the maximum in fabric system D-4's discharge energy curve at $y/d \approx -5$ is also farther from the stagnation point than the position of maximum in fabric D-3's discharged energy curve at $y/d \approx -2$. Fabric system D-4's density is 10% less than the density of the fabric system D-3 (Table 8.14). As such, there are more spaces between the fibers in the nonwoven structure of thermal liner D in fabric system D-4 rather than thermal liner C in fabric system D-3. Therefore, the impinged water may penetrate through the structure of the fabric system D-4 farther from the stagnation point.

The maxima on fabric system D-5's discharged energy curve are caused by the wrinkles on the moisture barrier A caused by the impinging jet of hot water (Figure 8.23). The unevenness of the surface of moisture barrier A on the skin simulant

created some spots with maximum discharge energy on D-5 discharged energy curve shown in Figure 8.22 at y/d=-2, y/d=-8, y/d=-12, y/d=-18 and y/d=-22. These areas belong to the spots in the fabric which did not contact the skin simulant.

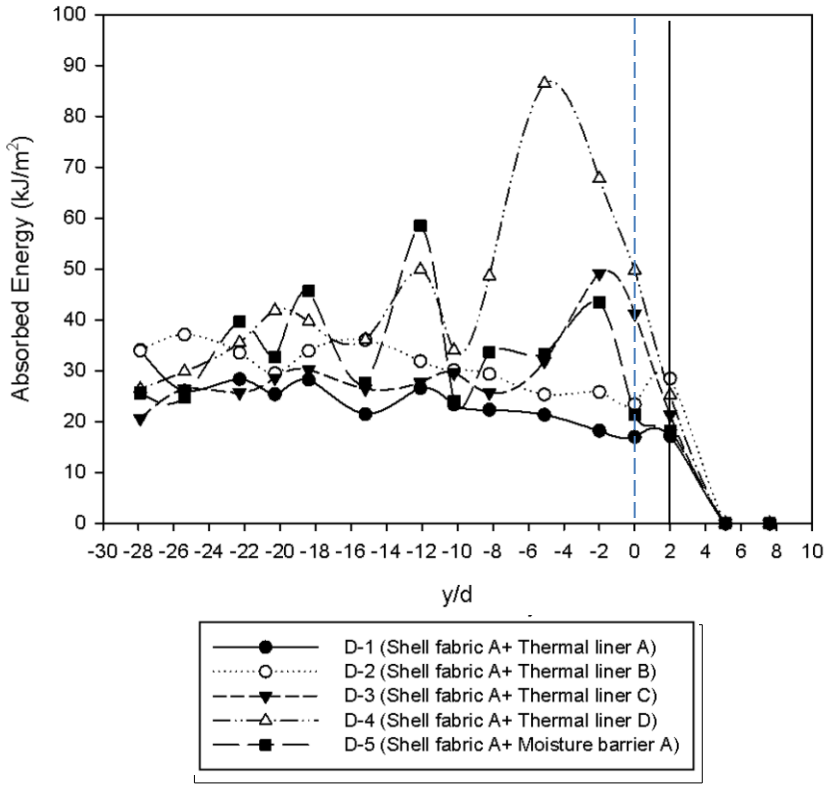

Figure 8.22. (a) The discharged thermal energy distribution along the y-axis for double layer fabric systems at 45-degree orientation exposure to jet of 90°C water (80 mL/s flow rates, z/d=9). The maximum length and the stagnation points are indicated with a solid and a dashed-line.

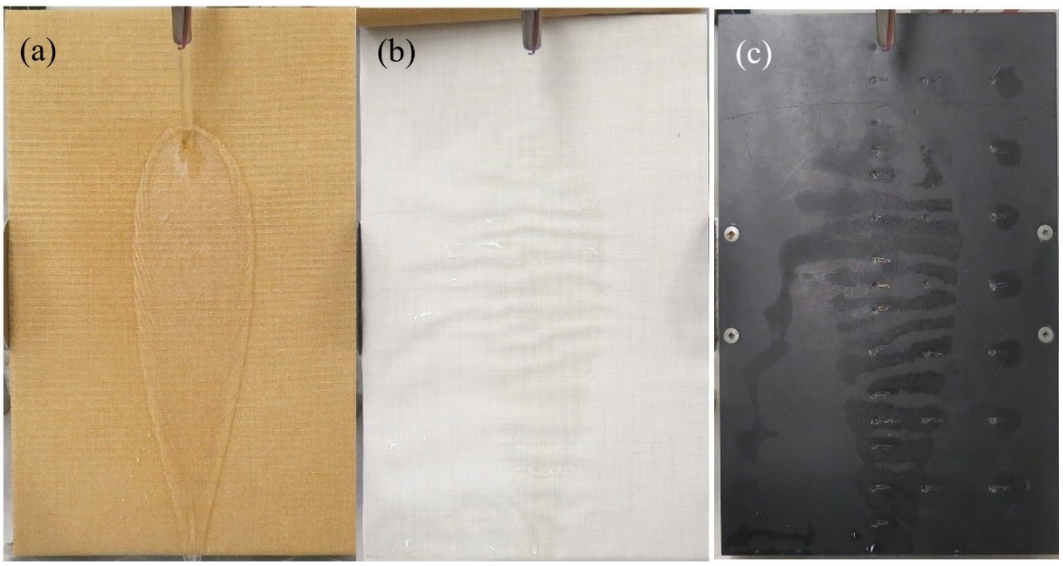

Figure 8.23. Fabric system D-5 exposed to hot water: (a) water flow pattern on shell fabric A, (b) uneven surface of the underlying moisture barrier A and (c) condensed water vapor on the skin simulant caused by the unevenness of moisture barrier A.

Multilayer fabric systems

The data in Table 8.15 confirms that a multilayer fabric system may provide resistance to a 90°C water jet (80 mL/s, z/d=9). In the multilayer fabrics tested, shell fabric A (Kevlar®/PBI with water resistant surface property) was used as a shell fabric. The excellent surface water resistance created a closed-rim flow on its surface resulting in a smaller area covered with hot water. The underlying moisture barrier A improved the resistance to water penetration through the fabric system. The thermal liners in the fabric structures improved thermal insulation. By varying the thermal liner underneath the moisture barrier, the rate of heat transfer from the flow of hot water onto the surface of fabric A could be decreased. This also decreased the rate of heat transfer from the penetrated hot water within the structure of shell fabric A. In addition, the porous structure of thermal liners underneath the moisture barrier trapped the condensed water vapor that was passed through the structure of moisture barrier A. The entrapment of condensed water vapor by the innermost layer in the fabric system, reduced the risk of direct exposure of the skin simulant to the latent heat of condensation released from the condensed water vapor.

Table 8.15. Thermal performance of multilayer fabric system in 45-degree orientation exposed to a 90°C water jet (flow rate= 80 mL/s and z/d= 9).

Fabric system	Assembly description	Fabric thickness (mm)	Fabric density (g/cm^3)	2^{nd} degree burn (%) (SD)	TAE_{2nd} (kJ/m^2) (SD)	TAE (kJ/m^2) (SD)	STE Rating (kJ/m^2) (SD)
M-1	Fabric A+ Moisture Barrier A+ Thermal Liner A	1.88	0.34	0.95 (0.00)	1.06 (0.92)	6.24 (2.05)	0.20 (0.14)
M-2	Fabric A+ Moisture Barrier A+ Thermal Liner B	2.29	0.31	0.00 (0.00)	0.00 (0.00)	1.90 (1.65)	0.06 (0.05)
M-3	Fabric A+ Moisture Barrier A+ Thermal Liner C	3.02	0.24	0.00 (0.00)	0.00 (0.00)	0.00 (0.00)	0.00 (0.00)
M-6	Fabric A+ Moisture Barrier A+ Thermal Liner D	3.62	0.21	0.00 (0.00)	0.00 (0.00)	0.00 (0.00)	0.00 (0.00)

TAE_{2nd} is the total energy received by all heat flux sensors at the time at which second degree burn time is predicted to occur; TAE is the total energy received by all sensors throughout the test; STE rating is the total energy received by all sensors during cooling period considering the proportion of the discharge energy to the total absorbed energy.

Summary

In this study, the thermal energy absorbed during exposure and cooling was obtained for the skin simulant plate (nude) in order to see the effects of experimental settings and water flow patterns on the thermal performance of the skin simulant. The increase in the flow rate and temperature of water significantly affected the position of the hydraulic jump on the skin simulant as well as the local and total transmitted and discharged energy to the skin simulant. It was confirmed that the increase in the nozzle-to-plate separation had minimal effect on the energy absorbed by the skin simulant at the lower flow rates. However, at increased flow rates, the effect of nozzle-to-plate separation was more pronounced.

The analysis of the absorbed energy on the bare skin simulant plate affirmed that the position of hydraulic jump (mainly influenced by the flow rate and orientation of skin simulant plate) affected the local and total absorbed energy to the skin simulant during and after exposure.

When the thermal performance of the nude skin simulant impinged with 90°C water was compared to its performance when covered with fabric, the

presence of thermal protective fabric reduced the predicted area of second degree burn and the thermal energy transmitted to the skin simulant. However, when a fabric system discharged thermal energy that was stored within its structure to the skin simulant, a significant amount of heat transferred was received.

From the analyses of the predicted area of burn for nude and fabric covered tests, it was concluded that the predicted skin simulant plate area of burn cannot completely address the thermal performance of fabric systems in a fixed duration approach. When the predicted skin simulant plate areas of second degree burn are identical, the total absorbed energy at onset of second degree burn can differentiate the level of protection each fabric system provided.

Enhancement of the resistance to water penetration through the fabric system reduces water penetration and water vapor diffusion within the structure of fabric system. This phenomenon caused the thermal energy to be transmitted at a slower rate and delayed heat transfer to the skin simulant during exposure. However, the fabric gains thermal energy during the exposure. After the termination of exposure to hot water, the stored energy in the fabric discharged to the skin simulant and lowered the thermal performance of the fabric system. The discharged thermal energy was observed more on the fabric that was positioned underneath the hydraulic jump and downstream from the flow in horizontal orientation. In a 45-degree orientation, the areas with more discharged thermal energy were observed in areas positioned underneath the maximum length region, with reflections and unstable flow at the outer boundaries of the flow.

Increase in the thickness and decrease in the density of the fabric system may decrease the heat transfer rate to the skin simulant plate during exposure. The behavior of the fabric was different during cooling period based on its resistance to water penetration. In fabric with poor resistance to water penetration, an increase in the thickness and decrease in the density caused the accumulation of thermal energy in the fabric system due to entrapment of hot liquid within the structure of the fabrics. However, the thermal performance of a fabric system with excellent resistance to water penetration is significantly enhanced by an increase in thickness and decrease in density. Resistance to water penetration by the outermost layer in multilayer system improved thermal performance of the fabric.

Analyses of the thermal performance of the fabric systems constructed from thermal liners with the same mass but different structures confirmed that using one thick Nomex® needle felted batt instead of two thin Nomex® oriented webs with the same nominal weight provided better thermal performance for the fabric system exposed to hot water.

For fabrics in a 45-degree orientation, a considerable amount of thermal energy was transmitted and discharged to the skin simulant between the stagnation point and the maximum length point. Also, the energy discharge was minimum at the stagnation region. The areas in closes proximity to the stagnation region received a large amount of thermal energy during cooling period. Therefore, modifications need to be made to existing bench top test methods in order to obtain data of the areas off the stagnation point in hot liquid exposures.

Multilayer fabric systems M-3 (shell fabric A+ moisture barrier A+ thermal liner C) and M-6 (shell fabric A+ moisture barrier A+ thermal liner D) were observed to provide the best thermal protection among the studied fabric systems. Shell fabric A (Kevlar®/PBI with water resistant surface property) provided an excellent water resistant surface and created a closed-rim flow on its surface causing a smaller area to be cover with hot water. The underlying moisture barrier A improved the resistance to water penetration through the fabric system. The thick and low density thermal liners (plain weave, Nomex® layer quilted to Nomex® needle felted batt) improved the fabric systems thermal insulation. Positioning the thermal liner underneath the moisture barrier decreased the rate of heat transfer from the flow of hot water on the surface of fabric A. It also decreased the heat transfer rate from the penetrated hot water within the structure of shell fabric A. Moreover, the porous structure of thermal liner underneath the moisture barrier trapped the condensed water vapor that passed through the structure of moisture barrier A. The entrapment of condensed water vapor by the innermost layer in the fabric system, reduced the risk of direct exposure of the skin simulant to the latent heat of condensation released from the condensed water vapor.

CHAPTER 9 SUMMARY, CONCLUSIONS AND FUTURE WORK

The main objective of this thesis was to gain a fundamental understanding of the heat and mass transfer mechanisms associated with protective clothing systems when exposed to hot water and during the cooling period immediately afterwards. This study mainly involved an experimental evaluation of transient heat transfer in thermal protective fabric systems exposed to a jet of hot water which affects the amount of thermal energy transmitted and discharged to the fabric and the skin simulant.

The study is mainly comprised of the study of the hydrodynamics of the hot water flow on the surface of the fabric and the study of in-depth water penetration through the fabric system as well as the parameters which influence heat and mass transfer through the fabric system and their effects on thermal performance of the fabric.

In addition to hot water, thermal hazards such as exposures to hot drilling fluid and hot canola oil (Chapter 4), and steam (Chapter 5) were used in order to improve the understanding of the amount of thermal energy transmitted and discharged to the skin and the thermal response of fabrics during the exposure and the cooling phase. The abovementioned thermal exposures are unexplored/newly explored hazards that may pose a threat to the health of workers, and the traditional materials used for protection against hydrocarbon flash fire provide little protection upon exposure to them. In Chapter 5, high levels of thermal radiation were also used to compare the results obtained from the unexplored/newly explored hazards with thermal radiation hazards and to gain further understanding of the amount of thermal energy transmitted and discharged to skin upon exposure to various thermal hazards. In Chapter 6, the contribution of stored energy to the thermal performance of the garments was investigated using full-scale spray mannequin tests.

This chapter will summarize the important results presented in this thesis, as well as some topics for future work that may be done in the area of thermal protective clothing. The following conclusions correspond to the main objective of this thesis:

- When hot water splashes on the surface of the fabric, the liquid starts spreading radially from the stagnation point until there is a sudden increase

in the fluid height. This phenomenon is termed a hydraulic jump. The hydraulic jump created on the surface of the fabric is similar to the hydraulic jumps commonly formed on smooth rigid surfaces studied previously (Liu & Lienhard, 1993). In classical hot fluid impingement onto a flat surface, the vertical momentum is converted into horizontal momentum. However, due to the nature of the fabrics in this research, different features were observed due to interactions of water with fabric surfaces and the fact that water could penetrate the fabric structure. The specific structure of the hydraulic jump also depended on whether the fabric was in a horizontal or an inclined orientation.

- Heat transfer decreases significantly at the location of the hydraulic jump and in the flow downstream of the jump. As such, the determination of flow patterns, including the position of hydraulic jump or area of the supercritical zone or the types of hydraulic jump is a crucial factor in the evaluation of thermal performance of the fabric systems exposed to water. The position of the hydraulic jump on the surface of the fabric and the area of the supercritical region are a function of experimental variables as well as physical properties of the fabric system which will be summarized as follows:

    - The area of the flow on the surface of the fabric exposed to hot water is mainly dependant on the water resistant properties of the surface. In fabrics with poor water resistant surfaces, the flow pattern covers a larger area than in the fabrics with excellent water resistant surfaces and transfer more thermal energy to the fabric.

    - The area of the supercritical region is highly and positively correlated with the water jet's Weber number, Reynolds number and Froude number in nude skin simulant plate tests and fabric tests. Therefore, the inertial forces, surface tension and viscous forces of the liquid jet strongly affect the area of the supercritical region and the position of hydraulic jump as noted previously by Liu and Lienhard (1993). The impingement pressure of the liquid jet at the stagnation point is also positively correlated with the area of the supercritical zone. As such, increasing the water temperature, flow rate and nozzle-to-plate separation can increase the area of the

supercritical region on the nude skin simulant plate and the studied fabric systems.

- The contact angle and the wetting time, which were measured in this research, can provide an approximate estimation of the shape of the flow pattern on the surface of the fabric. In fabrics with water resistant surfaces, the area of the supercritical region decreases as the contact angle increases.

- When a fabric is impinged by a liquid jet, the fabric can be compressed at the stagnation region which creates intrinsic roughness in the impingement zone. A dense fabric or a rigid fabric structure shows less variation in thickness when it is impinged by a water jet which results in a more stable jump and a large supercritical region area.

- Depending on the ability of the fabric to resist water penetration, the liquid sheet may transport through the fabric, be stored in the fabric (partial penetration) and/or transfer to the backside of the fabric system (total penetration) during and after the end of the exposure. Resistance to water vapor diffusion affects the area of supercritical region.

Some other important conclusions obtained from this thesis research are also summarized below.

- Among the physical properties of fabrics, air permeability is a dominant factor in the effective protection against hot liquid since resistance to mass transfer is shown to be the key factor for reducing the amount of transmitted and discharged thermal energy to the skin.

- Fabric surface energy is another important factor in the effective performance of fabrics against hot liquid splash. By blocking or reducing the hot liquid's penetration from the outer surface through the fibrous structure, the transmitted and the discharged energy are minimized.

- The introduction of an impermeable membrane into the fabric system proved to be a critical factor to minimize the transmitted and discharged

energy in double and multilayer fabrics by keeping hot liquid flow further from the skin.

- During the cooling period after the exposure, hot liquid may stay at the surface of the fabric and create beading or pooling effects which increase the discharge of thermal energy to the skin.

- Diffusion resistance of the single layer fabric can be used as an approximate estimation of how well the single layer fabric system exposed to hot water is able to resist hot water transfer.

- This research introduces the finding that the combined effect of fabric density and air permeability significantly affects the performance of fabric systems against hot liquid splashes. In an impermeable thick fabric system, the fabric system resists mass transfer and the entrapped air provides thermal insulation and decreases the transmission and discharge of thermal energy to skin. In a permeable thick fabric system, the accumulation of hot water in the fabric system creates a potentially hazardous thermal environment close to the skin during the cooling period. Applying compression to this fabric can cause a secondary penetration, pushing the entrapped hot water within the fabric toward the skin (the wringing effect) and may lower the predicted performance of the fabric system.

- Similar to hot liquid exposures, stored energy in fabrics after exposures to steam and radiant heat could contribute significantly to burn injuries. Minimizing mass transfer could significantly improve the predicted performance of fabric systems upon exposure to steam. The absorptivity of the fabric can be one of the key factors that influences the transmitted and the discharged thermal energy upon radiant heat exposure in all of the fabric systems.

- The results obtained from the full-scale spray mannequin test confirmed the results in bench-scale tests in Chapter 4 and 5, namely, that mass transfer is a critical factor influencing the transmitted and the discharge energy to the skin. The analysis of the thermal energy showed that the discharge of thermal energy is higher in the lower body regions where the thermal energy is stored due to the flow of hot water exposures. In addition, hot water flows

into and remains entrapped in the garment's unflapped side pockets and causes a significant amount of discharged thermal energy to these sensors. The comparison of the values of the stored energy rating for the nude and clothed mannequin reveals that the stored thermal energy in the exposed garment can be a potential hazard for its wearer during the cooling period of the garment.

- Taking into account the analysis of the flow pattern on the surface of the fabric as well as the analysis of the results from the water penetration test, contact angle test and water diffusion test, the water resistant property of the single layer fabric systems in this thesis can be classified into four groups:
    - Water penetration fabric with hydrophilic surface: fabrics with poor water surface resistance and poor water penetration resistance.
    - Water penetration resistant fabric with hydrophilic surface: fabrics with poor water surface resistance and excellent water penetration resistance.
    - Water penetration fabric with hydrophobic surface: fabrics with excellent water surface resistance and poor water penetration resistance.
    - Water penetration resistant fabric with hydrophobic surface: fabrics with excellent water surface resistance and excellent water penetration resistance.

The findings from this study could result in modifications to existing bench top test methods, which will improve the ability of these tests to evaluate the protection fabrics provide over a wider range of hazards. Some of these suggested modifications are summarized as follows:

- The thermal performance of the fabric system exposed to hot liquids cannot be limited to the analyses of the transmitted energy. Stored thermal energy can be discharged to the skin after the termination of the thermal exposure and can contribute to burn injuries.

- In order to address the contribution of the stored energy in a full-scale garment test, new predictive parameters such as total and local thermal discharged energy (TDE) and total and local stored thermal energy rating (STE rating) were introduced. These parameters reveal the thermal response of protective clothing during the cooling period of the garment where heat transfer is influenced by the garment/fabric properties and/or the liquid flow.

- From the analyses of the predicted area of burn for nude and fabric covered tests, it was concluded that the predicted skin simulant plate area of burn cannot completely address the thermal performance of fabric systems in a fixed duration approach. When the predicted skin simulant plate areas of second degree burn are identical, the total absorbed energy at onset of second degree burn (TAE_{2nd}) can differentiate the level of protection each fabric system provided.

- An Effective Thermal Protective Performance (ETPP) was proposed in order to determine and predict the thermal response of protective fabric systems upon exposure to hot liquid splash by taking into account the transmitted and thermal stored energy developed in the fabric system during the exposure and cooling periods. The effective thermal protective performance (ETPP) was quantified which is comprised of two parts: (1) the prediction of the time to second degree burn by continuous heating (TPP approach); (2) the prediction of minimum exposure time that can cause the occurrence of second degree burn by taking to account the transmitted and the discharge energy (MET approach). In addition, the effective Thermal Protective Performance Rating (ETPP rating) is proposed in order to improve the thermal protective performance rating of the current standards.

- A stored energy model and a burn evaluation model were also proposed in order to determine the minimum exposure time for prediction of second degree burn in the cooling period. The proposed stored energy model calls for the use of only one test to predict the minimum exposure time to second degree burn (which could be employed by the existing standards).

- In hot water exposures, it was observed that the maximum absorbed energy occurs off the stagnation point during exposure to high flow rates. This

phenomenon was also observed in another study where a vertical heated air jet impinged horizontal fabrics in large nozzle to fabric separations (Anguiano, 2005). In addition, the areas in close proximity to the stagnation region received a large amount of thermal energy during the cooling period. Therefore, modifications need to be made to existing bench top tests methods in order to obtain data for the areas off the stagnation point.

Future Work

Based on this research, the following future research is suggested.

- The findings of this research could result in the development and redesign of the existing bench top tests and equip the test apparatus with an additional compressor. This would enable the rating of the thermal performance of protective clothing while taking into account the ordinary and compressive discharge.

- The thermal performance of fabric systems needs to be tested at higher pressures (100~4000 kPa) which may represent firefighting and industrial operations in actual applications. The maximum pressure of water at the stagnation point on the surface of the fabric was approximately 0.5 kPa in the bench scale tests and 250 kPa in full-scale tests in this study.

- The structure of thick impermeable fabric systems needs to be investigated from a comfort perspective. The thick impermeable structure of these fabrics may impede moisture and heat transfer from the skin to the environment and disturb thermo-physiological comfort. These particular fabric systems are heavy and lack flexibility due to the use of fibers with high bending rigidity such as Kevlar® and Nomex®.

- Caution needs to be exercised in using the results from this study in order to evaluate thermal protective fabrics. The test results presented in this thesis are based on a limited number of experiments on specimens from a limited number of fabrics and hence may not be representative of other fabric systems. In addition, the specimens were tested under a specific range of exposures. More laboratory work is required in order to evaluate thermal performance of the fabrics under a wider range of exposure conditions.

- Caution needs to be exercised in applying the stored energy model to all situations as a small number and types of exposure conditions were investigated in this thesis. In future studies, it is recommended that additional test procedures such as flame, ISO 9151 (ISO, 2016) and hot surface contact, F 1060-05 (ASTM, 2016) can be combined with the results obtained from this study in order to see if the proposed stored energy and burn evaluation models are able to predict the minimum exposure time close to the minimum exposure time to second degree burn obtained from the iterative tests.

- The stored thermal energy analysis in this study was focused on the ordinary discharge of the thermal energy during the cooling period of the garment for the mannequin in static positions. A new test method should be employed in order to study the effect of the compressive discharge on the effective thermal performance of the garment system.

- More investigation is required in order to study the discharged thermal energy to areas other than the stagnation point. In these areas, there is a possibility that a fabric system stores thermal energy due to the flow of hot liquids and other thermal hazards such as steam and flame tests.

- In this thesis, air permeability is used as an indicator of how well liquid can flow through the fabric structure.The values of air permeability in this study were obtained under approximately 125 kPa differential pressure (ASTM, 2012a). However, the pressure of water on the surface of the fabric at the stagnation point varies between 417 to 1378 kPa. Therefore, the determination of air permeability of the fabric systems in this study should be tested under a higher differential pressure in order to obtain more realistic data for the evaluation of the studied fabric systems.

- The findings from this study can contribute to the improvement of the current standard test methods. Suggestions made in this thesis to improve of the methods used to rate the thermal performance of fabrics in standard tests should be investigated further in order to provide a more realistic system with which to rate the thermal protective performance of the fabric systems.

REFERENCES

AATCC. (2000). 42-2000 water resistance: Impact penetration test. Research Triangle Park, NC: American Association of Textile Chemists and Colorists.

ABA. (2014). National Burn Repository: Report of data from 2004-2013, Version 10. Chicago, IL: American Burn Association, National Burn Repository.

Abramovich, G. N. (1963). *The theory of turbulent Jets*: MIT Press.

Ackerman, M., Crown, E. M., Dale, J. D., Paskaluk, S., & Song, G. (2011). *Project update: Protection from steam and hot water hazards.* Paper presented at the Protective Clothing System for Safety '11, Edmonton, Alberta, Canada.

Allen, J., Corrado, S., Cox, D., & Dale, D. (2008). Thermal capacity of firefighter protective clothing Quincy, MA: The Fire Protection Research Foundation.

Allen, S. R., & Roche, E. J. (1989). Deformation behaviour of Kevlar® aramid fibres. *Polymer, 30*(6), 996-1003.

Anguiano, M. R. (2005). *Transient heat transfer through thin fibrous layers.* (Master of Science), University of Alberta, Edmonton. Available from University of Alberta Database.

Armstrong, C. P., & Harris, W. S. (1966). Temperature distributions in steam and hot water jets simulating leaks. *ASHRAE Transactions, 72*, 147-156.

ASTM. (1999). F 1939-08: Standard test method for radiant heat resistance of flame resistant clothing materials with continuous heating. West Conshohocken: American Society for Testing and Materials.

ASTM. (2008a). F 2701-08: Standard test method for evaluating heat transfer through materials for protective clothing upon contact with a hot liquid splash. West Conshohocken: American Society for Testing and Materials.

ASTM. (2008b). F 2702-08: Standard test method for radiant heat performance of flame resistant clothing materials with burn injury prediction. West Conshohocken, PA: American Society for Testing and Materials.

ASTM. (2010). F 2731-10: Standard test method for measuring the transmitted and stored energy of firefighter protective clothing systems. West Conshohocken: American Society for Testing and Materials.

ASTM. (2011). D 1777-96: Standard test method for thickness of textile materials. West Conshohocken, PA: American Society for Testing and Materials.

ASTM. (2012a). D 737-04: Standard test method for Air permeability of textile fabrics. West Conshohocken, PA: American Society for Testing and Materials.

ASTM. (2016). F1060-16, Standard test method for evaluation of conductive and compressive heat resistance (CCHR). West Conshohocken, PA: ASTM International.

ASTM. (2017). F 1930-17: Standard test method for evaluation of flame resistant clothing for protection against flash fire simulations using an instrumented manikin. West Conshohocken: American Society for Testing and Materials.

ASTM. (2012b). ASTM D3775-12, Standard test Method for warp (end) and filling (pick) count of woven fabrics. West Conshohocken, PA: ASTM International.

Bajaj, P., & Sengupta, A. K. (1992). Protective clothing. *Textile Progress, 22*(2-4), 1-110.

Baonga, J. B., Louahlia-Gualous, H., & Imbert, M. (2006). Experimental study of the hydrodynamic and heat transfer of free liquid jet impinging a flat circular heated disk. *Applied Thermal Engineering, 26*(11-12), 1125-1138.

Barker, R. L., Guerth, C., Behnke, W. P., & Bender, M. (2000). Measuring the thermal energy stored in firefighter protective clothing. In C. N. Nelson & N. W. Henry (Eds.), *Performance of protective clothing: issues and priorities for 21st century* (Vol. 7, pp. 33-44). West Conshohocken, PA: American Society for Testing and Materials.

Behnke, W. P. (1977). Thermal protective performance test for clothing. *Fire Technology, 13*(1), 6-12.

Behnke, W. P., Geshury, A. J., & Barker, R. L. (1992). *Thermo-Man(R) and Thermo-Leg - large scale test methods for evaluating thermal protective*

performance (Vol. 1133). Philadelphia: American Society of Testing and Materials.

Bowles, R. I., & Smith, F. T. (1992). The standing hydraulic jump: theory, computations and comparisons with experiments. *Journal of Fluid Mechanics, 242*, 145-168.

Bush, J. W. M., & Hasha, A. E. (2004). On the collision of laminar jets: fluid chains and fishbones. *Journal of Fluid Mechanics, 511*, 285-310.

Çengel, Y. A. (2005). Fluid mechanics : fundamentals and applications. In J. M. Cimbala (Ed.), (1st ed. ed.). Boston: McGraw-Hill Higher Education.

Cengel, Y. A., & Boles, M. A. (2008). *Thermodynamics: an engineering approach*: Boston: McGraw-Hill Higher Education, 6th ed.

Cengel, Y. A., & Ghajar, A. J. (2011). *Heat and mass transfer: fundamentals & applications*: New York: McGraw-Hill, 2nd ed.

CGSB. (1999). CAN/CGSB-4.2, 49-99: Resistance of materials to water vapour diffusion. *Textile Test Method*. Ottawa, Canada: Canadian General Standards Board.

CGSB. (2004). CAN/CGSB-4.2, No 5.1-M90: Unit mass of fabric. *Textile Test Method*. Ottawa, Canada: Canadian General Standards Board.

Choudhury, A. K., Majumdar, P. K., & Datta, C. (2011). Factors affecting comfort: human physiology and the role of clothing In G. Song (Ed.), *Improving comfort in clothing* (pp. 3-60). Cambridge, UK: Woodhead Publishing Ltd.

Clanet, C. (2007). Waterbells and liquid sheets *Annual Review of Fluid Mechanics* (Vol. 39, pp. 469-496).

Crown, E., & Dale, D. (1992). Evaluation of flash fire potective clothing using an instrumented mannequin: University of Alberta

Crown, E. M., Ackerman, M. Y., Dale, J. D., & Tan, Y. (1998). Design and evaluation of thermal protective flightsuits. part II: instrumented mannequin evaluation. *Clothing and Textiles Research Journal, 16*(2), 79-87.

Crown, E. M., & Dale, J. D. (2005). Protection for workers in the oil and gas industries. In R. A. Scott (Ed.), *Textiles for protection* (pp. 699-713). Cambridge, UK: Woodhead Publishing Ltd.

Crown, E. M., Rigakis, K. B., & Dale, J. D. (1989). Systematic assessment of protective clothing for Alberta workers, *Final research project report prepared for Alberta occupational health and safety* (pp. Appendix 19). Edmonton, AB.

Dale, J. D., Crown, E. M., Ackerman, M. Y., Leung, E., & Rigakis, K. B. (1992). Instrumented mannequin evaluation of thermal protective clothing, *Performance of Protective Clothing : Fourth Volume, ASTM STP* (Vol. 1133, pp. 717-733). West Conshohocken, PA: American Society for Testing and Materials.

Desruelle, A.-V., & Schmid, B. (2004). The steam laboratory of the Institut de Medecine Navale du Service de Sante des Armees: a set of tools in the service of the French Navy. *European Journal of Applied Physiology, 92*(6), 630-635.

Diller, K. (1985). Analysis of skin burns. In A. Shitzer & R. C. Eberhart (Eds.), *Heat transfer in medicine and biology* (Vol. 2, pp. 85-134). New York: Plenum Press.

Enform. (2004). Brass ball valve failure in power boiler service, Information Bulletin No. 1B04-002. Retrieved 2015, September 15, from Canadian Petroleum Safety Council http://www.enform.ca/files/safety-alerts/sa11_23.pdf

Enform. (2006a). Derrickhand receives second degree burns. Retrieved 2015, September 15, from Canadian Petroleum Safety Council http://www.enform.ca/files/safety-alerts/sa06_22.pdf

Enform. (2006b). Worker sustained severe steam-related burns. Retrieved 2015, September 15, from Canadian Petroleum Safety Council http://www.enform.ca/files/safety-alerts/sa06_10.pdf

Enform. (2010). Worker suffers severe burn to foot. Retrieved 2015, September 15, from Canadian Petroleum Safety Council http://www.enform.ca/files/safety-alerts/sa10_28.pdf

Enform. (2011). Worker burned by hot water. Retrieved 2015, September 15, from Canadian Petroleum Safety Council http://www.enform.ca/files/safety-alerts/sa11_23.pdf

Farnworth, B. (1986). A numeral model of the combined diffusion of heat and water vapor through clothing. *Textile Research Journal, 56*(11), 653-665.

Gabara, V., Hartzler, J. D., Lee, K., Rodini, D. J., & Yang, H. H. (2007). Aramid Fibers. In M. Lewin & E. M. Pearce (Eds.), *Handbook of fiber chemistry, Third Edition* (Vol. 8): Boca Raton : CRC/Taylor & Francis, c2007. 3rd ed.

Gardon, R., & Akfirat, J. C. (1965). The role of turbulance in determining the heat transfer charactristics of impinging jets. *International Journal of Heat and Mass Transfer, 8*, 1261-1272.

Glauert, M. B. (1956). The wall jet. *Journal of Fluid Mechanics, 1*(6), 625-643.

Greene, W. H. (2012). Econometric analysis (7th ed.). Boston: Prentice Hall.

Hancock, P. A., & Vasmatzidis, I. (2003). Effects of heat stress on cognitive performance: the current state of knowledge. *International Journal of Hyperthermia, 19*(3), 355-372.

He, J., Chen, Y., Wang, L., & Li, J. (2017). Quantitative assessment of the thermal stored energy in protective clothing under low-level radiant heat exposure. *Textile Research Journal*, 0040517517732084.

He, J., & Li, J. (2016a). Analyzing the transmitted and stored energy through multilayer protective fabric systems with various heat exposure times. *Textile Research Journal, 86*(3), 235-244.

He, J., & Li, J. (2016b). Quantitatively assessing the effect of exposure time and cooling time of fabric assemblies representative of those used in firefighter clothing on the thermal protection. *Fire and Materials, 40*(6), 773-784.

He, J., Lu, Y., Chen, Y., & Li, J. (2017). Investigation of the thermal hazardous effect of protective clothing caused by stored energy discharge. *Journal of Hazardous Materials, 338*, 76-84.

He, J., Wang, M., & Li, J. (2015). Determination of the thermal protective performance of clothing during bench-scale fire test and flame engulfment test: Evidence from a new index. *Journal of Fire Sciences, 33*(3), 218-231.

Henriques, F. C. (1947). Studies of thermal injury: V. The predictability and the significance of thermally induced rate processes leading to irreversible epidermal injury. *Archives of Pathology, 43*(5), 489-502.

Henriques, F. C., & Moritz, A. R. (1947). Studies of thermal injury: I. The conduction of heat to and through skin and the temperatures attained therein. A theoretical and an experimental investigation. *The American Journal of Pathology, 23*(4), 530-549.

Hewes, G. W. (1957). The anthropology of posture. *Scientific American, 196*(2), 122-133.

Holcombe, B. V., & Hoschke, B. N. (1986). Do test methods yield meaningful performance specifications. In R. L. Barker & G. C. Coletta (Eds.), *Performance of Protective Clothing: First Volume ASTM STP 900* (pp. 327-339). West Conshohocken, PA: American Society for Testing and Materials.

Hoschke, B. N. (1981). Standard specifications for firefighters clothing. *Fire Safety Journal, 4*(2), 125-137.

Huyer, D. W., & Corkum, S. H. (1997). Reducing the incidence of tap-water scalds: Strategies for physicians. *Canadian Medical Association Journal, 156*(6), 841-844.

Incropera, F. P., & DeWitt, D. P. (2007). *Introduction to heat transfer* (5th ed.): Hoboken, N.J.: Wiley ; Chichester.

ISO. (2014). ISO 11092: Textile--phsiological effect--measurment of thermal and water-vapour resistance under steady-state conditions (sweating guarded-hotplate test). Geneva, Switzerland: Standard Organization for Standardization.

ISO. (2016). ISO 9151: Protective clothing against heat and flame- determination of heat transmission on exposure to flame. Geneva, Switzerland: International Organization for Standardization.

ISO. (2017). ISO 13506-1: Protective clothing against heat and flame- Test method for complete garments- Prediction of burn injury using an instrumented manikin. Geneva, Switzerland: International Organization for Standardization.

Jalbani, S. H., Ackerman, M. Y., Crown, B. M., van Keulen, M., & Song, G. W. (2011). *Modification of ASTM F 2701-08 apparatus for use in evaluating protection from low pressure hot water jets*. Paper presented at the 9th symposium on performance of protective clothing and equipment: emerging issues and technologies, Anaheim, California.

Johnson, M., Maynes, D., Vanderhoff, J. C., & Webb, B. W. (2012). Hydraulic jump due to jet impingement on micro-patterned surfaces exhibiting ribs and cavities. (45233), 1293-1302.

Kate, P., Das, K., & Chakraborty, S. (2007). Hydraulic jumps due to oblique impingement of circular liquid jets on a flat horizontal surface. *Journal of Fluid Mechanics, 573*, 247-263.

Kate, R. P., Das, P. K., & Chakraborty, S. (2007). Hydraulic jumps with corners due to obliquely inclined circular liquid jets. *Physical Review E, 75*(5), 6.

Kibar, A., Karabay, H., Yiğit, K. S., Ucar, I. O., & Erbil, H. Y. (2010). Experimental investigation of inclined liquid water jet flow onto vertically located superhydrophobic surfaces. *Experiments in Fluids, 49*(5), 1135-1145.

Kiling-Balci, F. S. (2011). How consumers perceive comfort in apparel. In G. Song (Ed.), *Improving comfort in clothing* (pp. 97-113). Oxford; Philadelphia: Woodhead Publishing.

Kim, I. Y., Lee, C., Li, P., Corner, B. D., & Paquette, S. (2002). Investigation of air gaps entrapped in protective clothing systems. *Fire and Materials, 26*(3), 121-126.

Kirkpatrick, A. T., Curtis, H., & Adelgren, A. (1982). Experimental measurements of the thermal effectiveness of two types of protective clothing for fire fighters. *Fire Technology, 18*(3), 259-267.

Kirsner, W. (1999). Surviving a steam rupture in an enclosed space. Retrieved 2015, October 17 http://www.kirsner.org/kce/media/pdfs/KirsnerSurvive.pdf

Lawton, B. (1996). Transient temperature in engineering and science. In G. Klingenberg (Ed.). New York: Oxford University Press.

Li, R., & Shan, Y. (2013). Local wetting at contact line on textured hydrophobic surfaces. In K. L. Mittal (Ed.), *Advances in contact angle, wettability and adhesion*. Salem, Mass.: Scrivener/Wiley.

Lipkin, M., & Hardy, J. D. (1954). Measurement of some thermal properties of human tissues. *Journal of Applied Physiology, 7*, 212-217.

Liu, X., & Lienhard, J. H. (1993). The hydraulic jump in circular jet impingment and in other thin liquid films. *Experiments in Fluids, 15*(2), 108-116.

Lu, Y., Song, G., Ackerman, M., Paskaluk, S., & Li, J. (2013). A new protocol to characterize thermal protective performance of fabrics against hot liquid splash. *Experimental Thermal and Fluid Science, 46*, 37-45.

Lu, Y., Song, G., & Li, J. (2013). Analysing performance of protective clothing upon hot liquid exposure using instrumented spray manikin. *Annals of Occupational Hygiene, 57*(6), 793-804.

Lu, Y., Song, G., Li, J., & Paskaluk, S. (2013). Effect of an air gap on the heat transfer of protective materials upon hot liquid splashes. *Textile Research Journal, 83*(11), 1156-1168.

Lu, Y. H., Song, G., Zeng, H. B., Zhang, L., & Li, J. (2014). Characterizing factors affecting the hot liquid penetration performance of fabrics for protective clothing. *Textile Research Journal, 84*(2), 174-186.

Mah, T., & Song, G. (2010a). Investigation of the contribution of garment design to thermal protection. Part 1: characterizing air gaps using three-dimensional body scanning for women's protective clothing. *Textile Research Journal, 80*(13), 1317-1329.

Mah, T., & Song, G. (2010b). Investigation of the contribution of garment design to thermal protection. Part 2: Instrumented female mannequin flash-fire evaluation system. *Textile Research Journal, 80*(14), 1473-1487.

Mandal, S., Song, G., Ackerman, M., Paskaluk, S., & Gholamreza, F. (2013). Characterization of textile fabrics under various thermal exposures. *Textile Research Journal, 83*(10), 1005-1019.

Mertens, K., Putkaradze, V., & Vorobieff, P. (2005). Morphology of a stream flowing down an inclined plane. Part 1. Braiding. *Journal of Fluid Mechanics, 531*, 49-58.

Metha, A. K., & Wong, F. (1973). Measurement of flammability and burn potevtial of fabrics Fuels Research Laboratory, Massachusetts Institute of Technology, Cambridge, Massachusetts.

Mikielewicz, J., & Mikielewicz, D. (2009). A simple dissipation model of circular hydraulic jump. *International Journal of Heat and Mass Transfer, 52*(1–2), 17-21.

Moritz, A. R. (1947). Studies of thermal injury III. The pathology and pathogenesis of cutaneous burns an experimental study. *American Journal of Pathology, 23*(6), 915-941.

Moritz, A. R., & Henriques, F. C. (1947). Study of thermal injury II. The relative importance of time and surface temperature in the causation of cutaneous burns. *American Journal of Pathology, 23*(5), 695-720.

Moritz, A. R., Henriques, F. C., Dutra, F. R., & Weisiger, J. R. (1947). Study of thermal injury IV. An exploration of the casualty-producing attributes of conflagration- local and systemic of general cutaneous exposure to excessive circumambient (air) and circumradiant heat of varying duration and intensity. *Archives of Pathology, 43*(5), 466-488.

Morse, H., Ticker, G., & Brown, R. (1975). Burn damage and burn depth criteria: Aerotherm Report TN-75-26.

Morton, W. E., & Hearle, J. W. S. (1975). *Physical properties of textile fibres [By] W.E. Morton and J.W.S. Hearle*: London, Heinemann, 1975. 2d ed.

Murtaza, G. (2012). *Development of fabrics for steam and hot water protection.* (Master of Science), University of Alberta, Edmonton. Available from University of Alberta Database

Nakajima, A., Fujishima, A., Hashimoto, K., & Watanabe, T. (1999). Preparation of transparent superhydrophobic boehmite and silica films by sublimation of aluminum acetylacetonate. *Advanced Materials, 11*(16), 1365-1368.

NFPA. (2012). NFPA 2112: Standard on flame-resistant garments for protection of industrial personnel against flash fire. Quincy, MA: National Fire Protection Association.

NFPA. (2013). NFPA 1971: Standard on protective clothing for structural firefighting and proximity fire fighting. Quincy, MA: National Fire Protection Association.

Olderman, G. M. (1984). Liquid repellency and surgical fabric barrier properties. *Engineering in Medicine 13*(1), 35-43.

Passandideh-Fard, M., Teymourtash, A. R., & Khavari, M. (2011). Numerical study of circular hydraulic jump using volume-of-fluid method. *Journal of Fluids Engineering, 133*(1), 1-11.

Pause, B. (1996). Measuring the water vapor permeability of coated fabrics and laminates. *Journal of Industrial Textiles, 25*(4), 311-320.

Rayleigh, L. (1914). On the theory of long waves and bores. *Proceedings of the Royal Society of London. Series A, Containing Papers of a Mathematical and Physical Character, 90*(619), 324-328.

Rezazadeh, M. (2013). *Evaluation of performance of in-use firefighters' protective clothing using non-destructive tests.* (Doctor of Philosophy), University of Saskatchewan, Saskatoon, SK.

Rossi, R. (2005). Interactions between protection and thermal comfort. In R. A. Scott (Ed.), *Textiles for protection* (pp. 261-292). Cambridge, UK: Woodhead Publishing Ltd.

Rossi, R., Indelicato, E., & Bolli, W. (2004). Hot steam transfer through heat protective clothing layers. *International Journal of Occupational Safety and Ergonomics, 10*(3), 239-245.

Sati, R., Crown, E. M., Ackerman, M., Gonzalez, J., & Dale, D. (2008). Protection from steam at high pressures: Development of a test device and protocol. *International Journal of Occupational Safety and Ergonomics, 14*(1), 29-41.

Shitzer, A., Eberhart, R., & Diller, K. (1985). Analysis of skin burns: heat transfer in medicine and biology (pp. 85-134): Springer, US.

Song, G. (Ed.). (2011). *Improving comfort in clothing*. Oxford ; Philadelphia: Woodhead Publishing.

Song, G., Cao, W., & Gholamreza, F. (2011). Analyzing stored thermal energy and thermal protective performance of clothing. *Textile Research Journal, 81*(11), 1124-1138.

Song, G., Paskaluk, S., Sati, R., Crown, E., Dale, D., & Ackerman, M. (2011). Thermal protective performance of protective clothing used for low radiant heat protection. *Textile Research Journal, 81*(3), 311-323.

Stevens, J., & Webb, B. W. (1991). Local heat transfer coefficients under an axisymmetric, single-phase liquid jet. *Journal of Heat Transfer, 113*(1), 71-78.

Stoll, A. M., & Chianta, M. A. (1969). Method and rating system for evaluation of thermal protection. *Aerospace Medicine, 40*(11), 1232-&.

Stoll, A. M., & Greene, L. C. (1959). Relationship between pain and tissue damage due to thermal radiation. *Journal of Applied Physiology, 14*(3), 373-382.

Su, Y., He, J., & Li, J. (2016). Modeling the transmitted and stored energy in multilayer protective clothing under low-level radiant exposure. *Applied Thermal Engineering, 93*, 1295-1303.

Takata, A., Rouse, J., & Stanley, T. (1973). Thermal analysis program: I.I.T. Research Institute Report, IITRI-J6286.

Taylor, A. J., McGwin, G., Cross, J. M., Smith, D. R., Birmingham, B. R., & Rue, L. W. (2002). Serious occupational burn injuries treated at a regional burn center. *Journal of Burn Care & Rehabilitation, 23*(4), 244-248.

Torvi, D. (1997). *Heat transfer in thin fibrous materials under high heat flux conditions.* (Doctoral Dissertation), University of Alberta, Edmonton. Available from University of Alberta Database

Torvi, D., & Threlfall, T. (2006). Heat transfer model of flame resistant fabrics during cooling after exposure to fire. *Fire Technology, 42*(1), 27-48.

Torvi, D. A., Dale, D., & Faulkner, B. (1999). Influence of air gaps on bench-top test results of flame ressistant fabrics. *Journal of Fire Protection Engineering, 10*(1), 1-12.

Watson, E. J. (1964). The radial spread of a liquid jet over a horizontal plane. *Journal of Fluid Mechanics, 20*(3), 481-499.

Weaver, J. A., & Stoll, A. M. (1969). Mathematical model of skin exposed to thermal radiation. *Aerospace Medicine, 40*(1), 1-24.

Weinbaum, S., Jiji, L. M., & Lemons, D. E. (1984). Theory and experiment for the effect of vascular microstructure on surface tissue heat transfer. Part I: Anatomical foundation and model conceptualization. *Journal of Biomechanical Engineering, 106*(4), 321-330.

Wen, S., Petersen, S., McQueen, R., & Batcheller, J. (2015). Modelling the physiological strain and physical burden of chemical protective coveralls. *Ergonomics, 58*(12), 2016-2031.

Zhang, H., Song, G., Gu, Y., Ren, H., & Cao, J. (2017). Effect of moisture content on thermal protective performance of fabric assemblies by a stored energy approach under flash exposure. *Textile Research Journal*, 0040517517712097.

APPENDIX A: FABRIC SYSTEMS

The fabric systems used in Chapters 4 and 5 as well as the fabric systems used in Chapters 7 and 8 are described in this section. The photographs and the infrared images were taken 30s after the onset of exposure.

Table A.1. Physical properties of fabric system SS-1.

Assembly code		**SS-1**
Chapter		4 & 5
Description		Fabric AA
Fiber content		60% Kevlar®/ 40% polybenzimidazole
Weave Structure		Plain weave, rip-stop
Surface Property		Water resistant surface, breathable coating
Mass		211 g/m^2
Thickness	Pressure: 1 (kPa)	0.51 mm
	Pressure: 13.8 (kPa)	0.48 mm
Density	Pressure: 1 (kPa)	0.41 g/cm^3
	Pressure: 13.8 (kPa)	0.44 g/cm^3
Air permeability		17.1 cm^3/cm^2/s
Rct		0.070 m^{2}C/W
Contact Angle θ (Degree), water at 22°C		127± 1.48°

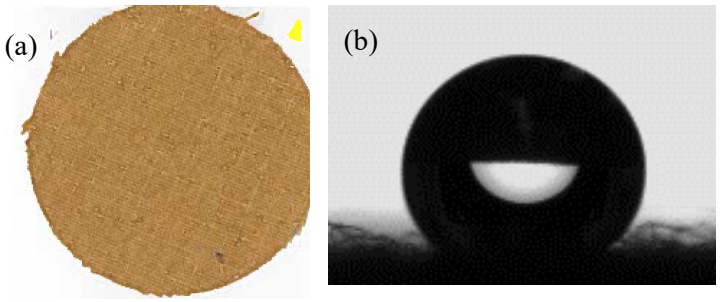

Figure A.1. Fabric system SS-1 (a) fabric swatch (b) contact angle at 20±2°C.

Table A.2. Physical properties of fabric system SS-2.

Assembly code		**SS-2**
Chapter		4
Description		Fabric BB
Fiber content		100% Nomex®aramid
Weave Structure		Plain weave
Surface Property		No finish
Mass		255 g/m^2
Thickness	Pressure: 1 (kPa)	0.66 mm
	Pressure: 13.8 (kPa)	---
Density	Pressure: 1 (kPa)	0.39 g/cm^3
	Pressure: 13.8 (kPa)	---
Air permeability		14.1 cm^3/cm^2/s
Rct		0.075 m^{2}C/W
Wetting time (22±2°C)		25 s

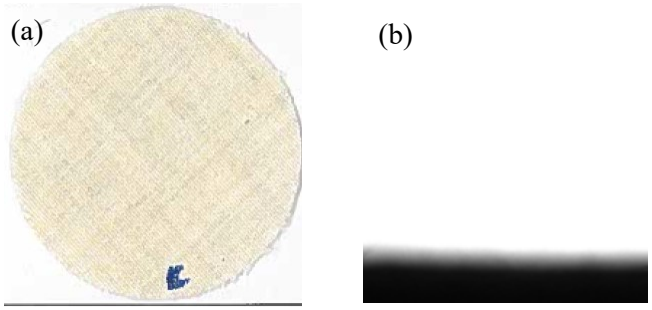

Figure A.2. Fabric system SS-1 (a) fabric swatch (b) contact angle at 20±2°C

Table A.3. Physical properties of fabric system SS-3.

Assembly code		**SS-3**
Chapter		4
Description		Fabric CC
Fiber content		Kermel® (polyamide-imide)
Weave Structure		Plain
Surface Property		Water resistant surface
Mass		229 g/m^2
Thickness	Pressure: 1 (kPa)	0.51 mm
	Pressure: 13.8 (kPa)	---
Density	Pressure: 1 (kPa)	0.45 g/cm^3
	Pressure: 13.8 (kPa)	---
Air permeability		1.65 cm^3/cm^2/s
Rct		0.076 m^{2}C/W
Contact Angle θ (Degree), water at 22°C		130± 1.35°

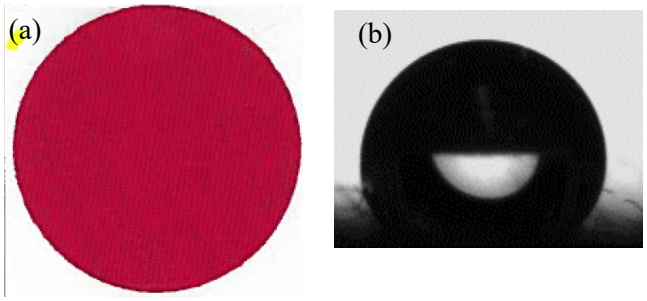

Figure A.3. Fabric system SS-3 (a) fabric swatch (b) contact angle at 20±2°C

Table A.4. Physical properties of fabric system SS-4.

Assembly code		**SS-4**
Chapter		4 & 5
Description		Fabric DD
Fiber content		88% cotton+12% HT* nylon
Weave Structure		Twill
Surface Property		Water resistant surface (encapsulated fibers)
Mass		412 g/m^2
Thickness	Pressure: 1 (kPa)	0.67 mm
	Pressure: 13.8 (kPa)	0.57 mm
Density	Pressure: 1 (kPa)	0.61 g/cm^3
	Pressure: 13.8 (kPa)	0.72 g/cm^3
Air permeability		0 cm^3/cm^2/s
Rct		0.074 m^{2}C/W
Contact Angle θ (Degree), water at 22°C		137± 0.61°

* HT-high tenacity

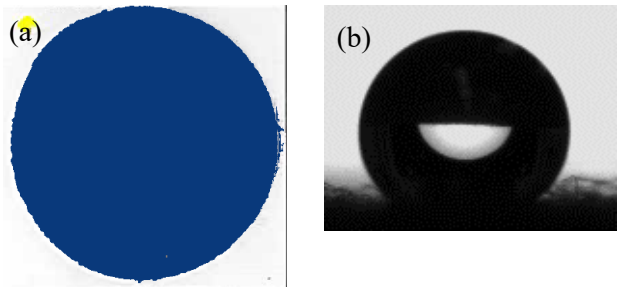

Figure A.4. Fabric system SS-4 (a) fabric swatch (b) contact angle at 20±2°C

Table A.5. Physical properties of fabric system S-1.

Assembly code		**S-1**
Chapter		7 & 8
Description		Moisture Barrier A
Fiber content		Nomex® +2%carbon+ underlying polytetrafluoroethylene coating
Weave Structure		Plain weave, rip-stop
Surface Property		Water resistant surface, breathable coating
Mass		214 g/m^2
Thickness	Pressure: 1 (kPa)	0.41 mm
Density	Pressure: 1 (kPa)	0.52 g/cm^3
Air permeability		0 cm^3/cm^2/s
Rct		0.074 m^{2}C/W
Diffusion resistance		92.00 mm
Fabric count (warp×weft) yarns/cm		(85 × 70) yarns/cm
Contact Angle θ (Degree) (SD)	water at 22±2°C	127 (5.02)°
	water at 90±5°C	114 (5.20)°

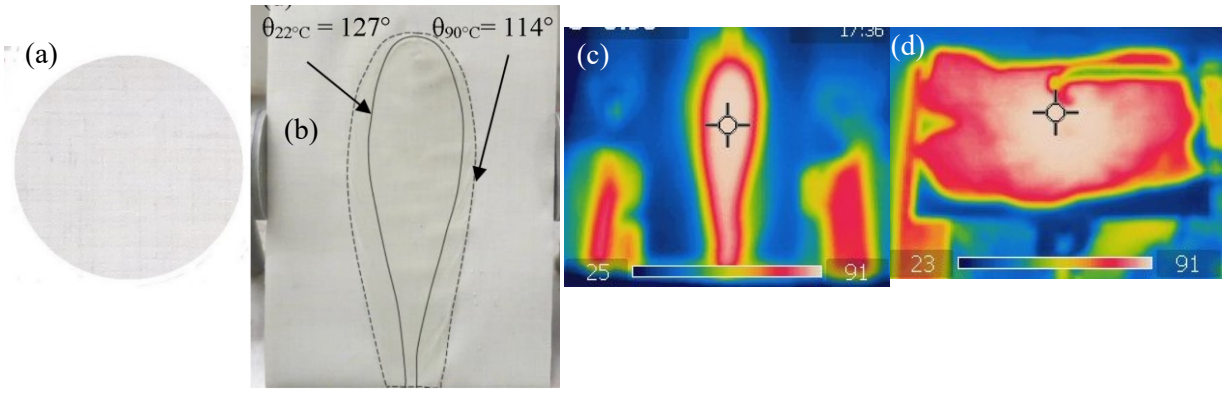

Figure A.5. Fabric system S-1 (a) fabric swatch; (b) flow patterns exposed to water at 22°C (solid lines) and 90°C (dotted lines); Infrared images in (c) 45-degree and (d) horizontal orientation (water at 90°, flow rate: 80 mL/s, z/d=9).

Table A.6. Physical properties of fabric system S-2.

Assembly code		S-2
Chapter		7 & 8
Description		Moisture Barrier B
Fiber content		Kevalr®/PBI +2%carbon+ underlying polytetrafluoroethylene coating
Weave Structure		Plain weave, rip-stop
Surface Property		Water resistant surface, breathable coating
Mass		188 g/m^2
Thickness	Pressure: 1 (kPa)	0.31 mm
Density	Pressure: 1 (kPa)	0.61 g/cm^3
Air permeability		0 cm^3/cm^2/s
Rct		0.074 m^{2}C/W
Diffusion resistance		62.66 mm
Fabric count (warp×weft) yarns/cm		(80 × 74) yarns/cm
Contact Angle θ (Degree) (SD)	water at 22±2°C	131 (4.10)°
	water at 90±5°C	121 (5.46)°

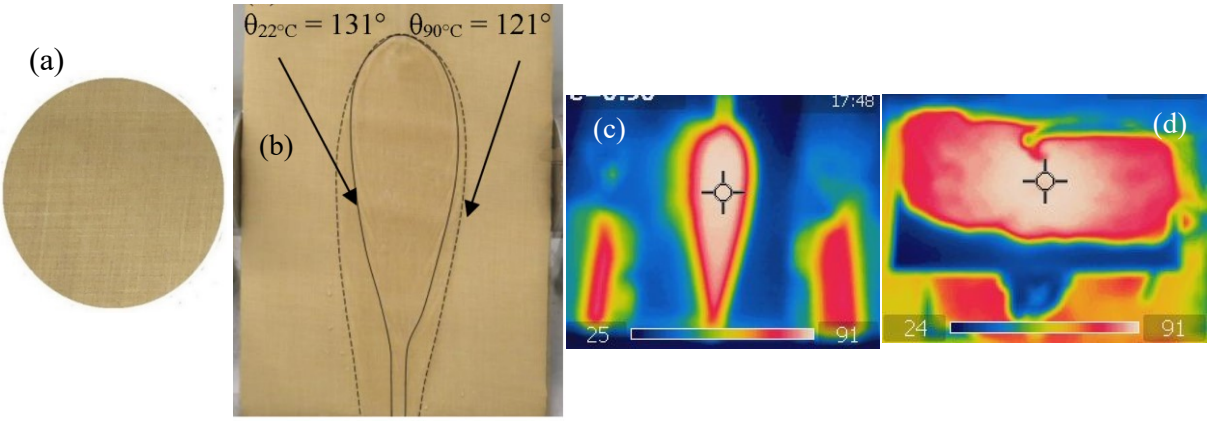

Figure A.6. Fabric system S-2 (a) fabric swatch; (b) flow patterns exposed to water at 22°C (solid lines) and 90°C (dotted lines); Infrared images in (c) 45-degree and (d) horizontal orientation (water at 90°, flow rate: 80 mL/s, z/d=9).

Table A.7. Physical properties of fabric system S-3.

Assembly code		**S-3**
Chapter		7 & 8
Description		Moisture Barrier C
Fiber content		85% Nomex®+ 15% underlying polyurethane coating
Weave Structure		Plain
Surface Property		Water resistant surface, breathable coating
Mass		272 g/m^2
Thickness	Pressure: 1 (kPa)	0.63 mm
Density	Pressure: 1 (kPa)	0.43 g/cm^3
Air permeability		0 cm^3/cm^2/s
Rct		0.084 (m^{2}C/W)
Diffusion resistance		38.04 mm
Fabric count (warp×weft) yarns/cm		(66 × 45) yarns/cm
Contact Angle θ (Degree) (SD)	water at 22±2°C	141 (4.45)°
	water at 90±5°C	134 (2.47)°

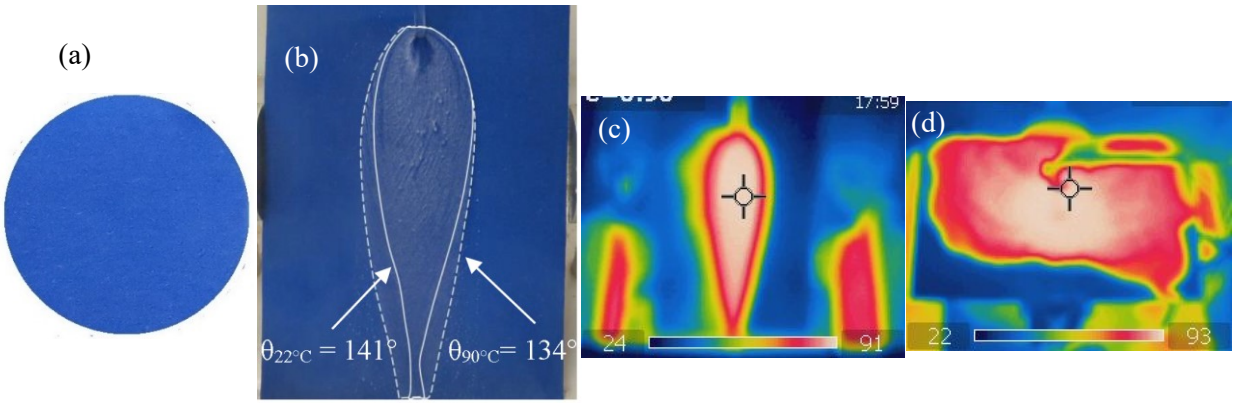

Figure A.7. Fabric system S-3 (a) fabric swatch; (b) flow patterns exposed to water at 22°C (solid lines) and 90°C (dotted lines); Infrared images in (c) 45-degree and (d) horizontal orientation (water at 90°, flow rate: 80 mL/s, z/d=9).

Table A.8. Physical properties of fabric system S-4.

Assembly code		**S-4**
Chapter		7 & 8
Description		Fabric A
Fiber content		60% Kevlar®/ 40% polybenzimidazole
Weave Structure		Plain weave, rip-stop
Surface Property		Water resistant surface, breathable coating
Mass		246 g/m^2
Thickness	Pressure: 1 (kPa)	0.54 mm
Density	Pressure: 1 (kPa)	0.45 g/cm^3
Air permeability		10.06 cm^3/cm^2/s
Rct		0.077 (m^{2}C/W)
Diffusion resistance		6.06 mm
Fabric count (warp×weft) yarns/cm		(43 × 37) yarns/cm
Contact Angle θ (Degree) (SD)	water at 22±2°C	131 (1.27)°
	water at 90±5°C	128 (3.84)°

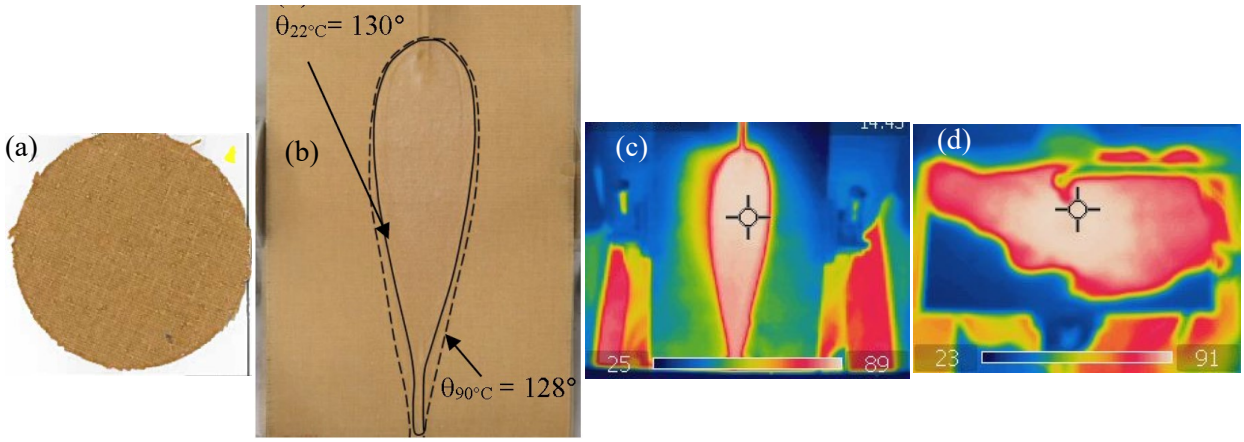

Figure A.8. Fabric system S-4 (a) fabric swatch; (b) flow patterns exposed to water at 22°C (solid lines) and 90°C (dotted lines); Infrared images in (c) 45-degree and (d) horizontal orientation (water at 90°, flow rate: 80 mL/s, z/d=9).

Table A.9. Physical properties of fabric system S-5.

Assembly code		**S-5**
Chapter		7 & 8
Description		Fabric B
Fiber content		Nomex®IIIA (93% Nomex®, 5% Kevlar®, and 2% anti-static)
Weave Structure		Plain weave
Surface Property		No finish
Mass		213 g/m^2
Thickness	Pressure: 1 (kPa)	0.61 mm
Density	Pressure: 1 (kPa)	0.35 g/cm^3
Air permeability		25.62 cm^3/cm^2/s
Rct		0.080 m^{2}C/W
Diffusion resistance		3.47 mm
Fabric count (warp×weft) yarns/cm		(68 × 44) yarns/cm
Wetting time (s) (SD)	water at 22±2°C	26 (1.6) s
	water at 90±5°C	7 (1.2) s

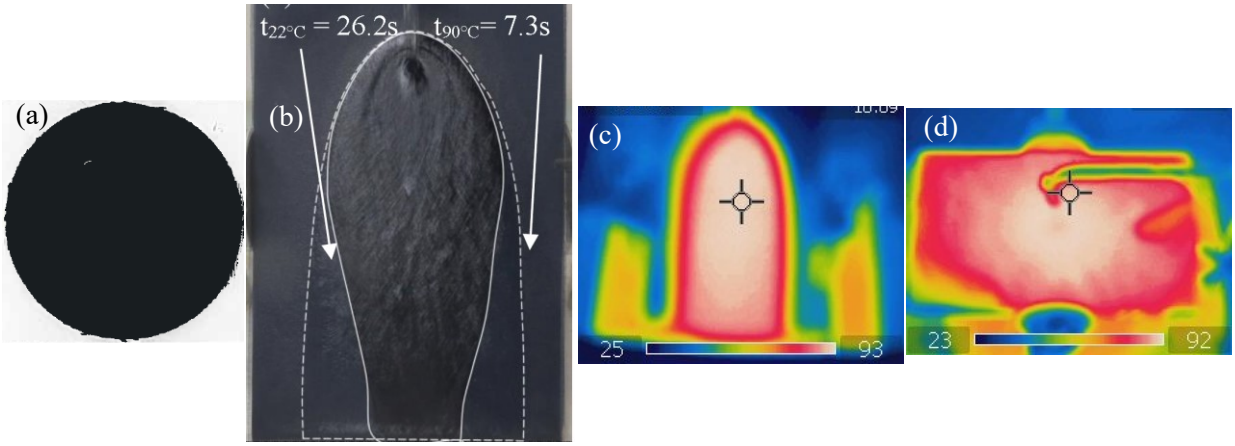

Figure A.9. Fabric system S-5 (a) fabric swatch; (b) flow patterns exposed to water at 22°C (solid lines) and 90°C (dotted lines); Infrared images in (c) 45-degree and (d) horizontal orientation (water at 90°, flow rate: 80 mL/s, z/d=9).

Table A.10. Physical properties of fabric system S-6.

Assembly code		**S-6**
Chapter		7 & 8
Description		Fabric C
Fiber content		Nomex®IIIA
Weave Structure		Plain weave
Surface Property		Water resistant surface
Mass		204 g/m^2
Thickness	Pressure: 1 (kPa)	0.55 mm
Density	Pressure: 1 (kPa)	0.37 g/cm^3
Air permeability		33.80 cm^3/cm^2/s
Rct		0.074 m^{2}C/W
Diffusion resistance		3.61 mm
Fabric count (warp×weft) yarns/cm		(68 × 40) yarns/cm
Contact Angle θ (Degree) (SD)	water at 22±2°C	133 (1.21)°
	water at 90±5°C	130 (1.30)°

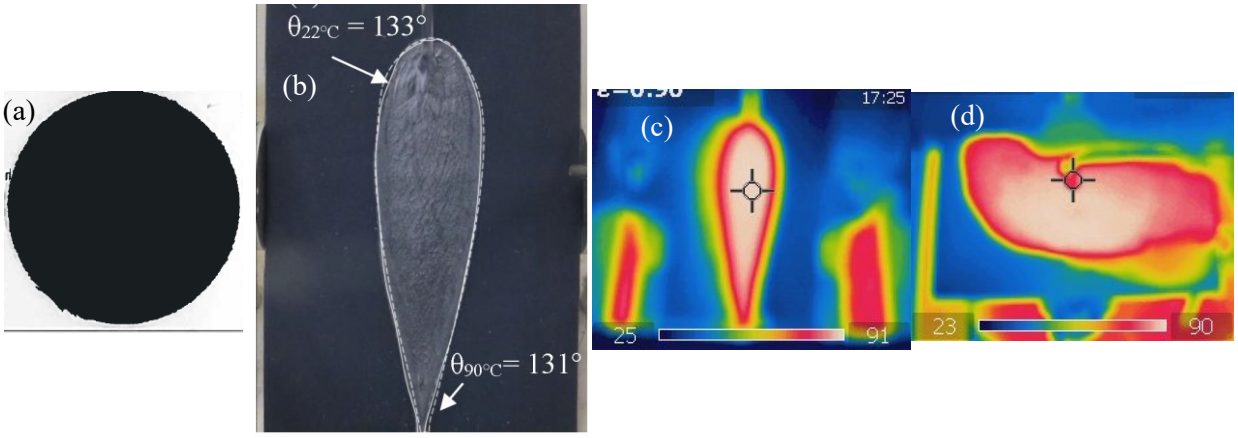

Figure A.10. Fabric system S-6 (a) fabric swatch; (b) flow patterns exposed to water at 22°C (solid lines) and 90°C (dotted lines); Infrared images in (c) 45-degree and (d) horizontal orientation (water at 90°, flow rate: 80 mL/s, z/d=9).

Table A.11. Physical properties of fabric system S-7.

Assembly code		**S-7**
Chapter		7 & 8
Description		Fabric D
Fiber content		Kermel® (polyamide-imide)
Weave Structure		Plain weave
Surface Property		Water resistant surface
Mass		229 g/m^2
Thickness	Pressure: 1 (kPa)	0.51 mm
Density	Pressure: 1 (kPa)	0.45 g/cm^3
Air permeability		0.98 cm^3/cm^2/s
Rct		0.076 m^{2}C/W
Diffusion resistance		22.15 mm
Fabric count (warp×weft) yarns/cm		(70 × 50) yarns/cm
Contact Angle θ (Degree) (SD)	water at 22±2°C	132 (2.12)°
	water at 90±5°C	124 (0.92)°

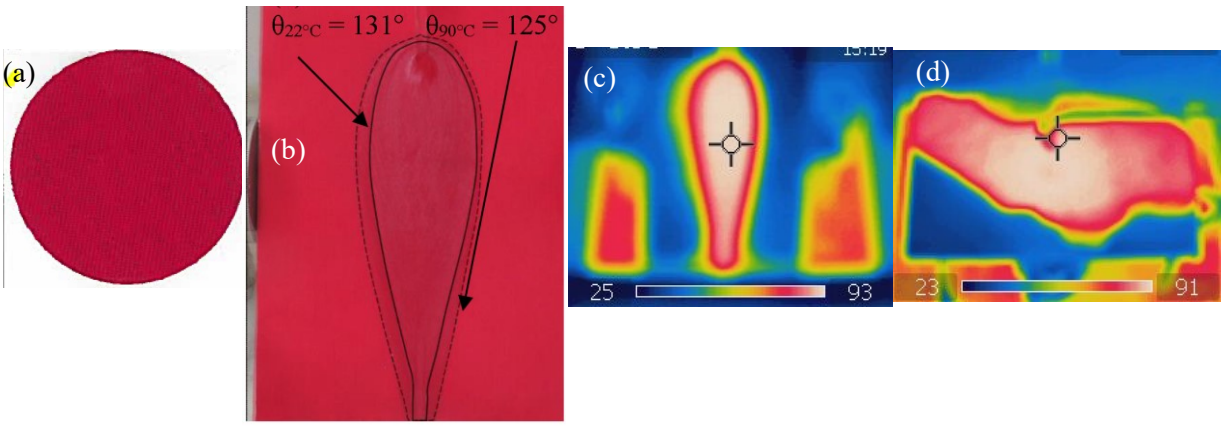

Figure A.11. Fabric system S-7 (a) fabric swatch; (b) flow patterns exposed to water at 22°C (solid lines) and 90°C (dotted lines); Infrared images in (c) 45-degree and (d) horizontal orientation (water at 90°, flow rate: 80 mL/s, z/d=9).

Table A.12. Physical properties of fabric system S-8.

Assembly code		S-8
Chapter		7 & 8
Description		Fabric E
Fiber content		88% cotton+12% HT* nylon
Weave Structure		Twill
Surface Property		Water resistant surface (encapsulated fibers)
Mass		412 g/m^2
Thickness	Pressure: 1 (kPa)	0.67 mm
Density	Pressure: 1 (kPa)	0.61 g/cm^3
Air permeability		0 cm^3/cm^2/s
Rct		0.073 m^{2}C/W
Diffusion resistance		118.57 mm
Fabric count (warp×weft) yarns/cm		(98 × 48) yarns/cm
Contact Angle θ (Degree) (SD)	water at 22±2°C	137 (0.49)°
	water at 90±5°C	129 (1.03)°

* HT-high tenacity

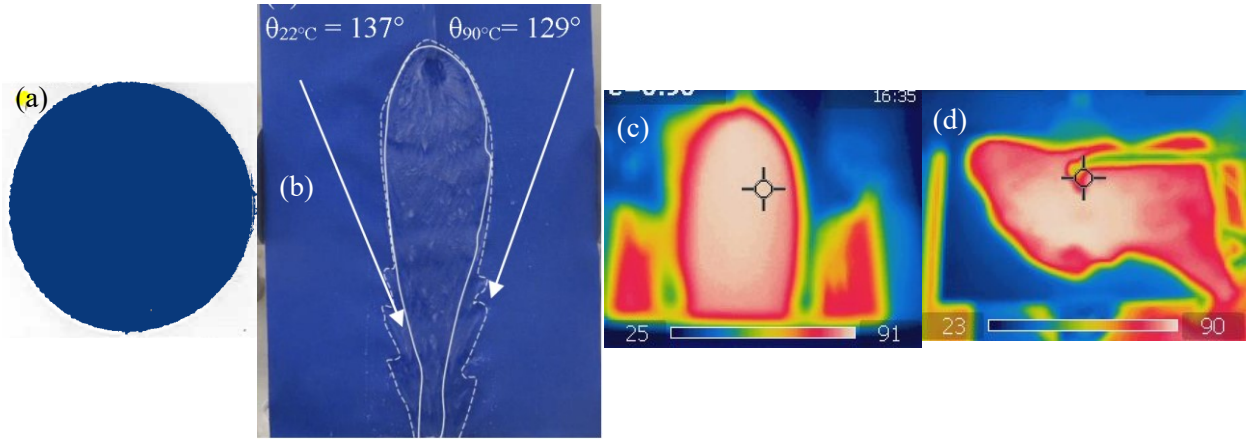

Figure A.12. Fabric system S-8 (a) fabric swatch; (b) flow patterns exposed to water at 22°C (solid lines) and 90°C (dotted lines); Infrared images in (c) 45-degree and (d) horizontal orientation (water at 90°, flow rate: 80 mL/s, z/d=9).

Table A.13. Physical properties of fabric system S-9.

Assembly code		S-9
Chapter		7 & 8
Description		Fabric F
Fiber content		Nomex®IIIA (93% Nomex®, 5% Kevlar®, and 2% anti-stat)+Neoprene coating
Weave Structure		Plain weave, rip-stop
Surface Property		Water resistant surface
Mass		503 g/m^2
Thickness	Pressure: 1 (kPa)	0.38 mm
Density	Pressure: 1 (kPa)	1.32 g/cm^3
Air permeability		0 cm^3/cm^2/s
Rct		0.062 m^{2}C/W
Diffusion resistance		938.03 mm
Fabric count (warp×weft) yarns/cm		(88 × 60) yarns/cm
Contact Angle θ (Degree) (SD)	water at 22±2°C	107 (6.58)°
	water at 90±5°C	81 (1.41)°

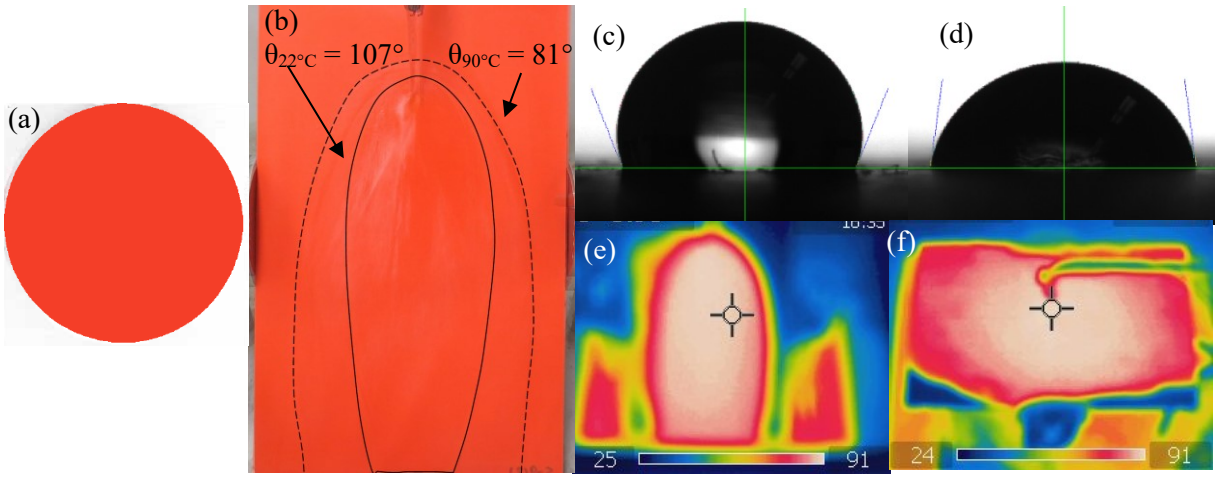

Figure A.13. Fabric system S-8 (a) fabric swatch; (b) flow patterns exposed to water at 22°C (solid lines) and 90°C (dotted lines); (c) contact angle at 20±2°C; (d) contact angle at 95±5°C; Infrared images in (e) 45-degree and (f) horizontal orientation (water at 90°, flow rate: 80 mL/s, z/d=9).

APPENDIX B INSTRUMENTED MANIKIN (SENSOR NUMBER, LOCATION AND WEIGHTED AREA)

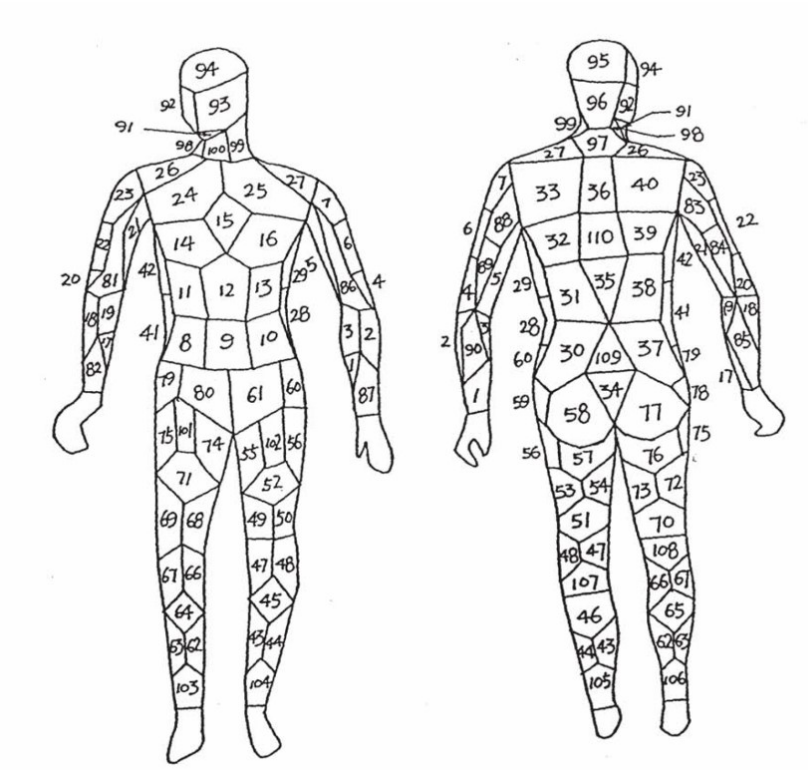

Figure B.1. Sensor areas on the manikin and the corresponding heat flux sensor numbers (Crown & Dale, 1992). Reprinted with permission.

Table B.1. sensor number, sensor location and the weighted area of the sensors used in the manikin.

Sensor number	Sensor location	Sensor weighting (based on area (A_i))		Sensor number	Sensor location	Sensor weighting (based on area (A_i))
1	Left lower arm	0.5		13	Abdomen, upper left	0.95
2	Left lower arm	0.5		14	Chest, lower right	0.95
3	Left lower arm	0.5		15	Chest, center	0.95
4	Left upper arm	0.5		16	Chest, lower left	0.95
5	Left upper arm	1		17	Right lower arm	0.45
6	Left upper arm	0.5		18	Right lower arm	0.45
7	Left upper arm	0.5		19	Right lower arm	0.45
8	Abdomen, lower right	0.95		20	Right upper arm	0.5
9	Abdomen, lower center	0.95		21	Right upper arm	1
10	Abdomen, lower left	0.95		22	Right upper arm	0.5
11	Abdomen, upper right	0.95		23	Right upper arm	0.5
12	Abdomen, upper center	0.95		24	Chest, upper right	0.95

Table B.1. sensor number, sensor location and the weighted area of the sensors used in the manikin, continued.

Sensor number	Sensor location	Sensor weighting (based on area (A_i))		Sensor number	Sensor location	Sensor weighting (based on area (A_i))
25	Chest, upper left	0.95		61	Left pelvis, front	0.95
26	Right shoulder	0.95		62	Right lower leg, inner	1
27	Left shoulder	0.95		63	Right lower leg, outer	1
28	Side of trunk, lower left	0.95		64	Right shin	0.8
29	Side of trunk, upper left	0.95		65	Right calf	0.8
30	Lower back, lower left	0.95		66	Right mid leg, inner	0.6
31	Lower back, upper left	0.95		67	Right mid leg, outer	0.6
32	Upper back, lower left	0.95		68	Right lower thigh, inner	0.9
33	Upper back, upper left	0.95		69	Right lower thigh, front outer	0.9
34	Pelvis, rear center	0.4		70	Right lower thigh, rear	0.9
35	Back, mid center	0.55		71	Right mid thigh, front	0.95
36	Back, upper center	0.7		72	Right mid thigh, rear outer	0.95
37	Lower back, lower right	0.95		73	Right mid thigh, rear inner	0.95
38	Lower back, upper right	0.95		74	Right upper thigh, front inner	1
39	Upper back, lower right	0.95		75	Right upper thigh, front outer	1.2
40	Upper back, upper right	0.95		76	Right upper thigh, rear	0.9
41	Side of trunk, lower right	0.95		77	Right buttock	1.1
42	Side of trunk, upper right	0.95		78	Right buttock, side	0.4
43	Left lower leg, inner	1		79	Right hip	0.4
44	Left lower leg, outer	1		80	Right pelvis, front	0.95
45	Left shin	0.8		81	Right upper arm	1
46	Left calf	0.8		82	Right lower arm	0.5
47	Left mid leg, inner	0.6		83	Right upper arm	0.5
48	Left mid leg, outer	0.6		84	Right upper arm	0.5
49	Left lower thigh, front inner	0.9		85	Right lower arm	0.65
50	Left lower thigh, front outer	0.9		86	Left upper arm	1
51	Left lower thigh, rear	0.9		87	Left lower arm	0.5
52	Left mid thigh, front	0.95		88	Left upper arm	0.5
53	Left mid thigh, outer	0.95		89	Left upper arm	0.5
54	Left mid thigh, rear inner	0.95		90	Left lower arm	0.5
55	Left upper thigh, front inner	1		91	Lower jaw	0.5
56	Left upper thigh, front outer	1.2		92	Right cheek	1
57	Left upper thigh, rear	0.9		93	Left cheek	1
58	Left buttock	1.1		94	Forehead	1.5
59	Left buttock, side	0.4		95	Head, upper back	1.5
60	Left hip	0.4		96	Head, lower back	1.5

Table B.1. sensor number, sensor location and the weighted area of the sensors used in the manikin, continued.

Sensor number	Sensor location	Sensor weighting (based on area (A_i))		Sensor number	Sensor location	Sensor weighting (based on area (A_i))
97	Back, right under rear neck	0.7		104	Left lower leg, front	0.6
98	Neck, right side	0.65		105	Left lower leg, back	0.6
99	Neck, left side	0.65		106	Right lower leg, back	0.6
100	Neck, front	0.65		107	Left mid leg, back	0.5
101	Right upper thigh, front center	0.85		108	Right mid leg, back	0.5
102	Left upper thigh, front center	0.85		109	Lower back, lower center	0.55
103	Right lower leg, front	0.6		110	Upper back, lower center	0.7

APPENDIX C: TABLES OF THERMAL PERFORMANCE OF FABRIC SYSTEMS EXPOSED TO HOT LIQUIDS IN CHAPTER FOUR

Table C.1. Thermal performance of single layer fabric systems exposed to distilled water at 85°C an angle of inclination of 45 degrees.

Distilled Water

Fabric System	Fabric Assembly	Sensor	t_{2nd}	t_{3rd}	q_{2nd}	$q_{cooling}$	Ψ	Φ
SS-1	Fabric AA	Upper	3.2 (0.2)	18.5 (1.1)	65.0 (0.8)	6.0 (1.8)	0.08 (0.02)	0.09 (0.03)
		Middle	4.1 (0.2)	22.6 (0.4)	68.4 (2.6)	18.2 (4.8)	0.21 (0.04)	0.26 (0.06)
		Lower	15.1 (3.5)	22.6 (2.7)	99.7 (4.7)	38.2 (4.8)	0.27 (0.02)	0.38 (0.03)
SS-2	Fabric BB	Upper	1.6 (0.2)	16.3 (1.2)	51.6 (1.5)	17.3 (2.3)	0.25 (0.02)	0.33 (0.03)
		Middle	3.6 (0.4)	21.3 (1.2)	64.6 (3.7)	34.7 (3.6)	0.35 (0.01)	0.54 (0.03)
		Lower	4.4 (0.34)	23.4 (1.0)	65.8 (0.7)	43.5 (4.5)	0.40 (0.02)	0.66 (0.06)
SS-3	Fabric CC	Upper	6.0 (0.6)	22.2 (0.7)	79.8 (5.8)	6.7 (0.6)	0.09 (0.00)	0.09 (0.00)
		Middle	14.4 (2.1)	34.2 (2.4)	112.2 (4.8)	12.9 (5.2)	0.10 (0.03)	0.11 (0.04)
		Lower	21.8 (0.4)	37.7 (1.8)	115.0 (6.4)	23.2 (4.0)	0.17 (0.02)	0.20 (0.02)
SS-4	Fabric DD	Upper	16.6 (1.1)	52.4 (1.8)	118.3 (2.6)	2.2 (0.2)	0.02 (0.00)	0.02 (0.00)
		Middle	43.8 (1.9)	No Burn	112.8 (29.1)	12.1 (5.1)	0.12 (0.02)	0.13 (0.02)
		Lower	42.2 (1.0)	No Burn	112.8 (53.9)	12.1 (3.0)	0.11 (0.03)	0.13 (0.03)

Table C.2. Thermal performance of double-layer fabric systems exposed to distilled water at 85°C an angle of inclination of 45 degrees.

Distilled Water

Fabric System	Fabric Assembly	Sensor	t_{2nd}	t_{3rd}	q_{2nd}	$q_{cooling}$	Ψ	Φ
DD-1	Fabric AA+ Thermal Liner AA	Upper	4.4 (0.4)	19.7 (0.2)	69.5 (4.0)	29.9 (4.2)	0.30 (0.02)	0.43 (0.04)
		Middle	8.7 (0.1)	27.8 (1.2)	92.6 (1.6)	45.2 (6.9)	0.32 (0.03)	0.49 (0.07)
		Lower	14.2 (1.7)	34.2 (2.8)	83.6 (2.1)	64.6 (3.3)	0.42 (0.01)	0.77 (0.02)
DD-2	Fabric AA+ Thermal Liner BB	Upper	8.0 (0.5)	23.1 (0.3)	76.2 (3.8)	97.9 (7.4)	0.54 (0.01)	1.37 (0.03)
		Middle	16.8 (0.7)	33.1 (0.3)	109.2 (6.2)	133.2 (30.8)	0.58 (0.04)	1.21 (0.21)
		Lower	23.1 (2.4)	44.0 (0.5)	96.6 (4.7)	205.7 (21.2)	0.68 (0.01)	2.14 (0.12)
DD-3	Fabric AA+ Moisture Barrier AA	Upper	60.6 (1.7)	No Burn	166.4 (1.94)	10.0 (1.1)	0.06 (0.01)	0.06 (0.01)
		Middle	66.4 (0.5)	No Burn	168.3 (0.9)	16.7 (1.9)	0.09 (0.00)	0.10 (0.00)
		Lower	68.6 (2.9)	No Burn	167.3 (1.5)	19.7 (1.3)	0.11 (0.01)	0.12 (0.01)
DD-4	Moisture Barrier AA+ Fabric AA	Upper	61.5 (1.2)	No Burn	164.6 (0.7)	7.8 (1.0)	0.04 (0.01)	0.05 (0.01)
		Middle	67.5 (2.4)	No Burn	169.4 (1.0)	9.9 (0.4)	0.05 (0.00)	0.06 (0.00)
		Lower	68.3 (3.5)	No Burn	169.1 (1.0)	13.0 (1.6)	0.07 (0.01)	0.08 (0.01)

Table C.3. Thermal performance of multilayer fabric systems exposed to distilled water at 85°C an angle of inclination of 45 degrees.

Distilled Water

Fabric System	Fabric Assembly	Sensor	t_{2nd}	t_{3rd}	q_{2nd}	$q_{cooling}$	Ψ	φ
MM-1	Fabric AA+ Moisture Barrier A+ Thermal Liner AA	Upper	78.5 (3.2)	No Burn	175.9 (1.7)	18.2 (3.1)	0.09 (0.01)	0.10 (0.02)
		Middle	91.8 (4.5)	No Burn	178.3 (1.3)	26.4 (4.1)	0.13 (0.02)	0.15 (0.02)
		Lower	107.4 (9.8)	No Burn	184.1 (4.0)	32.2 (5.8)	0.15 (0.02)	0.17 (0.03)
MM-2	Fabric AA+ Moisture Barrier AA+ Thermal Liner BB	Upper	131.1 (7.2)	No Burn	198.3 (2.9)	24.4 (1.6)	0.11 (0.01)	0.12 (0.01)
		Middle	134.9 (7.8)	No Burn	198.0 (3.5)	31.7 (2.5)	0.14 (0.01)	0.16 (0.01)
		Lower	154.7 (3.8)	No Burn	201.6 (1.2)	36.8 (0.6)	0.16 (0.00)	0.18 (0.00)

Table C.4. Thermal performance of fabric systems exposed to drilling fluid at 85°C an angle of inclination of 45 degrees.

Drilling Mud

Fabric		Sensor	t_{2nd}	t_{3rd}	q_{2nd}	$q_{cooling}$	Ψ	φ
SS-1	Fabric AA	Upper	2.2 (0.4)	17.5 (0.5)	60.4 (2.6)	37.9 (8.3)	0.39 (0.04)	0.63 (0.11)
		Middle	3.6 (0.2)	23.1 (0.8)	68.4 (1.2)	66.2 (10.4)	0.49 (0.04)	0.97 (0.14)
		Lower	5.0 (0.8)	26.0 (1.1)	79.4 (2.8)	82.2 (9.1)	0.51 (0.02)	1.04 (0.08)
SS-2	Fabric BB	Upper	1.9 (0.1)	20.5 (4.6)	49.7 (3.9)	51.1 (4.0)	0.51 (0.00)	1.04 (0.00)
		Middle	2.4 (0.31)	20.9 (2.8)	53.2 (3.0)	81.1 (6.4)	0.60 (0.01)	1.53 (0.03)
		Lower	4.0 (1.4)	25.3 (1.4)	66.1 (13.75)	98.1 (7.7)	0.60 (0.03)	1.51 (0.20)
SS-3	Fabric CC	Upper	9.0 (0.5)	28.3 (1.8)	95.4 (1.3)	51.9 (18.1)	0.35 (0.08)	0.54 (0.18)
		Middle	12.6 (0.6)	46.0 (2.2)	106.3 (1.1)	83.1 (9.3)	0.44 (0.03)	0.78 (0.08)
		Lower	15.5 (0.3)	50.9 (1.0)	112.5 (1.4)	93.6 (32.1)	0.45 (0.10)	0.83 (0.28)
SS-4	Fabric DD	Upper	23.1 (4.0)	61.3 (7.5)	127.2 (6.1)	89.2 (4.2)	0.41 (0.01)	0.70 (0.01)
		Middle	31.7 (5.5)	78.3 (12.8)	140.0 (6.7)	76.6 (7.9)	0.35 (0.01)	0.55 (0.03)
		Lower	30.1 (4.0)	75.5 (5.1)	137.2 (4.6)	80.3 (9.8)	0.37 (0.02)	0.58 (0.05)
DD-3	Fabric AA+ Moisture Barrier AA	Upper	45.5 (3.4)	106.2 (10.6)	154.5 (3.1)	38.8 (1.8)	0.20 (0.01)	0.25 (0.01)
		Middle	45.1 (5.8)	104.0 (8.7)	153.8 (4.8)	53.7 (4.4)	0.25 (0.01)	0.35 (0.02)
		Lower	48.3 (0.4)	107.2 (1.5)	156.1 (0.3)	66.3 (4.3)	0.30 (0.01)	0.42 (0.03)
MM-1	Fabric AA+ Moisture Barrier A+ Thermal Liner AA	Upper	No Burn	No Burn	0	0	-	-
		Middle	No Burn	No Burn	0	0	-	-
		Lower	No Burn	No Burn	0	0	-	-
MM-2	Fabric AA+ Moisture Barrier AA+ Thermal Liner BB	Upper	No Burn	No Burn	0	0	-	-
		Middle	No Burn	No Burn	0	0	-	-
		Lower	No Burn	No Burn	0	0	-	-

Table C.5. Thermal performance of fabric systems exposed to canola oil at 85°C an angle of inclination of 45 degrees.

Canola Oil

Fabric		Sensor	t_{2nd}	t_{3rd}	q_{2nd}	$q_{cooling}$	Ψ	φ
SS-1	Fabric AA	Upper	9.2 (0.6)	29.1 (0.9)	95.1 (1.5)	32.5 (13.6)	0.25 (0.09)	0.34 (0.14)
		Middle	29.4 (2.0)	66.8 (2.6)	138.5 (5.2)	73.9 (8.8)	0.35 (0.03)	0.53 (0.04)
		Lower	34.7 (2.0)	98.5 (15.3)	144.3 (1.9)	57.3 (8.8)	0.28 (0.03)	0.40 (0.06)
SS-2	Fabric BB	Upper	5.8 (0.5)	28.3 (1.0)	85.2 (2.4)	68.2 (7.3)	0.44 (0.02)	0.80 (0.06)
		Middle	11.3 (2.8)	54.3 (6.2)	102.4 (8.6)	77.3 (1.9)	0.43 (0.02)	0.76 (0.05)
		Lower	15.9 (1.7)	No Burn	115.3 (3.9)	89.0 (5.3)	0.44 (0.01)	0.77 (0.02)
SS-3	Fabric CC	Upper	13.5 (1.9)	38.6 (1.7)	103.9 (6.0)	44.8 (13.0)	0.30 (0.05)	0.43 (0.10)
		Middle	48.8 (11.4)	No Burn	154.2 (7.3)	56.8 (4.6)	0.28 (0.02)	0.37 (0.01)
		Lower	45.0 (2.1)	No Burn	153.4 (0.9)	58.0 (2.8)	0.28 (0.01)	0.38 (0.01)
SS-4	Fabric DD	Upper	22.7 (0.73)	64.5 (3.3)	127.6 (1.3)	37.6 (3.0)	0.23 (0.01)	0.29 (0.02)
		Middle	40.5 (7.1)	No Burn	148.5 (6.0)	54.2 (1.6)	0.27 (0.01)	0.37 (0.01)
		Lower	44.3 (3.5)	No Burn	151.7 (3.1)	60.1 (5.6)	0.28 (0.02)	0.40 (0.03)
DD-3	Fabric AA+ Moisture Barrier AA	Upper	78.6 (4.6)	No Burn	177.1 (2.7)	49.7 (6.4)	0.22 (0.02)	0.28 (0.03)
		Middle	92.1 (5.7)	No Burn	181.6 (2.5)	60.8 (2.1)	0.26 (0.01)	0.34 (0.01)
		Lower	112.1 (4.0)	No Burn	178.6 (5.2)	69.1 (3.1)	0.33 (0.01)	0.39 (0.01)
MM-1	Fabric AA+ Moisture Barrier A+ Thermal Liner AA	Upper	No Burn	No Burn	0	0	-	-
		Middle	No Burn	No Burn	0	0	-	-
		Lower	No Burn	No Burn	0	0	-	-
MM-2	Fabric AA+ Moisture Barrier AA+ Thermal Liner BB	Upper	No Burn	No Burn	0	0	-	-
		Middle	No Burn	No Burn	0	0	-	-
		Lower	No Burn	No Burn	0	0	-	-

Table C.6. Thermal performance of single layer fabric systems exposed to distilled water horizontally at 85°C.

Distilled Water

Fabric System	Fabric Assembly	Sensor	t_{2nd}	t_{3rd}	q_{2nd}	$q_{cooling}$	Ψ	φ
SS-1	Fabric AA	Side	11.5 (1.6)	35.3 (3.0)	86.4 (4.5)	142.0 (19.8)	0.62 (0.04)	1.65 (0.14)
		Middle	2.0 (0.3)	15.9 (0.3)	59.4 (2.5)	71.3 (16.9)	0.54 (0.06)	1.20 (0.23)
		Side	8.2 (1.1)	31.1 (2.8)	83.5 (4.5)	148.1 (24.3)	0.64 (0.04)	1.77 (0.20)
SS-2	Fabric BB	Side	5.7 (0.9)	27.9 (2.1)	78.3 (4.7)	103.9 (7.0)	0.63 (0.01)	1.33 (0.01)
		Middle	0.8 (0.0)	14.7 (0.2)	47.1 (3.0)	54.9 (14.3)	0.60 (0.05)	1.18 (0.23)
		Side	6.8 (0.3)	37.5 (2.8)	83.6 (4.0)	137.4 (13.8)	0.66 (0. 01)	1.65 (0.09)
SS-3	Fabric CC	Side	16.4 (2.1)	44.5 (7.4)	111.4 (4.1)	175.5 (19.6)	0.61 (0.02)	1.58 (0.12)
		Middle	2.9 (0.8)	18.3 (1.3)	59.8 (3.7)	77.0 (10.8)	0.56 (0.03)	1.29 (0.10)
		Side	17.6 (2.3)	42.7 (3.5)	110.9 (7.2)	168.9 (21.4)	0.60 (0.01)	1.53 (0.09)
SS-4	Fabric DD	Side	35.2 (9.9)	86.9 (18.3)	133.4 (1.3)	106.9 (29.6)	0.49 (0.08)	0.81 (0.21)
		Middle	10.9 (0.4)	42.6 (0.6)	102.3 (0.93)	71.8 (9.8)	0.41 (0.03)	0.70 (0.09)
		Side	29.9 (4.0)	66.1 (5.3)	134.9 (11.4)	119.8 (14.2)	0.49 (0.01)	0.89 (0.03)

Table C.7. Thermal performance of double layer fabric systems exposed to distilled water horizontally at 85°C.

Distilled Water

Fabric System	Fabric Assembly	Sensor	t_{2nd}	t_{3rd}	q_{2nd}	$q_{cooling}$	Ψ	φ
DD-1	Fabric AA+ Thermal Liner AA	Side	16.4 (2.9)	41.4 (5.7)	107.5 (5.7)	155.1 (10.7)	0.59 (0.01)	1.45 (0.02)
		Middle	2.1 (0.3)	16.8 (0.4)	49.5 (0.3)	86.8 (6.6)	0.63 (0.01)	1.75 (0.12)
		Side	17.5 (0.7)	46.5 (3.7)	111.1 (1.1)	152.4 (4.2)	0.58 (0.01)	1.37 (0.02)
DD-2	Fabric AA+ Thermal Liner BB	Side	29.6 (4.4)	62.6 (4.8)	126.2 (7.0)	178.9 (25.8)	0.58 (0.04)	1.43 (0.12)
		Middle	7.1 (1.0)	23.2 (0.2)	63.0 (1.5)	77.4 (11.4)	0.55 (0.03)	1.23 (0.15)
		Side	33.7 (3.5)	80.8 (1.1)	137.8 (9.3)	194.4 (10.8)	0.58 (0.01)	1.41 (0.01)
DD-3	Fabric AA+ Moisture Barrier AA	Side	66.9 (2.8)	145.0 (2.4)	168.4 (1.5)	84.8 (9.9)	0.33 (0.02)	0.50 (0.05)
		Middle	53.2 (9.2)	106.7 (4.3)	161.0 (7.1)	84.4 (3.6)	0.34 (0.01)	0.53 (0.01)
		Side	67.9 (3.9)	145.8 (5.2)	169.2 (3.2)	93.4 (7.8)	0.36 (0.01)	0.55 (0.04)
DD-4	Moisture Barrier AA+ Fabric AA	Side	84.7 (4.9)	No Burn	177.9 (2.2)	66.3 (3.0)	0.27 (0.01)	0.37 (0.01)
		Middle	70.1 (1.6)	No Burn	171.9 (0.9)	56.7 (4.6)	0.24 (0.03)	0.33 (0.03)
		Side	88.1 (7.2)	No Burn	178.3 (0.8)	96.0 (10.2)	0.35 (0.01)	0.54 (0.05)

Table C.8. Thermal performance of multilayer fabric systems exposed to distilled water horizontally at 85°C.

Distilled Water

Fabric System	Fabric Assembly	Sensor	t_{2nd}	t_{3rd}	q_{2nd}	$q_{cooling}$	Ψ	Φ
MM-1	Fabric AA+ Moisture Barrier A+ Thermal Liner AA	Side	88.0 (5.9)	140.9 (9.7)	178.1 (5.8)	96.0 (3.6)	0.35 (0.01)	0.54 (0.01)
		Middle	74.5 (1.0)	No Burn	178.6 (3.7)	88.4 (4.0)	0.33 (0.01)	0.49 (0.01)
		Side	91.7 (4.8)	No Burn	178.0 (3.7)	107.7 (24.2)	0.37 (0.05)	0.60 (0.11)
MM-2	Fabric AA+ Moisture Barrier AA+ Thermal Liner BB	Side	137.1 (20.9)	No Burn	194.6 (12.5)	102.2 (17.8)	0.35 (0.04)	0.53 (0.06)
		Middle	128.9 (10.4)	No Burn	199.9 (5.2)	95.8 (20.8)	0.32 (0.03)	0.48 (0.07)
		Side	139.1 (10.7)	No Burn	191.2 (11.1)	113.3 (19.4)	0.37 (0.09)	0.60 (0.07)

APPENDIX D: EFFECTIVE THERMAL CONDUCTIVITY OF FABRIC SYSTEMS

In a hot liquid splash phenomenon, the presence of hot liquid within the fabric may affect the effective thermal conductivity of the fabric system and therefore, enhance the overall heat transfer to the skin. Effective thermal conductivity was studied by Farnworth (1986), Torvi (1997) and others. The effective thermal conductivity of the fabric system is influenced by fabric packing factor, φ (a higher factor meaning fewer channels and less space between fibers), the thermal conductivity of the air volume fraction in the fabric (k_{air}), the thermal conductivity of the fibrous component (k_{fiber}) (Equation D.1).

$$k_{eff} = (1 - P_{\varphi})k_{air} + P_{\varphi}k_{fiber} \qquad \text{(D.1)}$$

Torvi (1997) used a model to weigh the contribution of the solid fibers, air and the radiation heat transfer between the fibers (Equation D.2). More details on the radiation thermal conductivity (k_{rad}) can be found in Torvi (1997).

$$k_{eff}(T) = \left[v_{air}k_{air}(T) + (1 - v_{air})k_{fiber}(T)\right] + k_{rad} \qquad \text{(D.2)}$$

However, in hot liquid exposures, the liquids may penetrate and store within the fabric system. As such, Equation D.2 has limitations since the effect of the thermal conductivity of the trapped hot liquid within the fibrous structure (k_{liquid}) was not considered for the determination of the effective thermal conductivity of the fabric system.

In this study, it was proposed that the effective thermal conductivity can be written as the fraction of the thermal conductivity of fibrous component of the fabric system (k_{fiber}), a fraction of the thermal conductivity of the trapped air within the fabric structure (k_{air}), a fraction of the thermal conductivity of the entrapped penetrated fluid within the fibrous structure of the fabric (k_{liquid}) and the thermal conductivity due to the radiation heat transfer between the fibers k_{rad} (Equation D.3). In equation D.3, α is the weighted fraction of the trapped air, β is the weighted fraction of the fibrous material in the fabric and γ is the weighted fraction of the penetrated fluid in the fabric.

$$k_{eff} = \alpha k_{air} + \beta k_{fiber} + \gamma k_{liquid} + k_{rad} \qquad \text{(D.3)}$$